

**MATHEMATICAL DESCRIPTION OF IN-VIVO  
MUSCLE FUNCTION**

by

**Dimitrios Voukelatos**

**A Doctoral Thesis**

**Submitted in partial fulfilment of the requirements for the  
award of Doctor of Philosophy of Loughborough University**

**September 2015**

**© by Dimitrios Voukelatos, 2015**

## Abstract

Mathematical relationships have long been used to describe many aspects of muscle function such as the relationship between muscle force and muscle length, muscle force and velocity of contraction or the degree of muscle activation during a contraction. During this work various mathematical expressions have been employed in order to gain an insight into different aspects of muscle activity.

The first part of the work examined whether performing a strength protocol on a dynamometer can lead to an increase in eccentric strength output as well as in the neuromuscular activation of the quadriceps group of muscles that appears inhibited during slow concentric and fast eccentric contractions. Neuromuscular activation was modelled via a three-parameter sigmoid function that was also tested for robustness to perturbations in the maximum activation values.

During the second part of the study the “functional” hamstrings to quadriceps ratio  $H:Q_{fun}$  was expressed as a function of two variables i.e., angular velocity and joint angle. Initially nine-parameter torque-angular velocity-angle profiles were obtained for the knee extensors and flexors from a group of participants. A theoretical 17-parameter  $H:Q_{fun}$  function was then derived for each dataset. Subsequently, a simpler, 6-parameter function was derived,  $R_E = a \exp(b\omega^n + c\theta^m) - d\omega^{\frac{1}{2}}\theta^2$  that best reproduced the original 17-parameter fit.

Finally, a six-segment subject specific torque-driven model of the Snatch lift was developed in order to investigate the optimal mechanics of the lift. The model simulated the lift from its initiation until the end of the second pull when the feet of the athlete momentarily leave the platform. The six-segment model comprised of foot, shank, thigh, torso (head + trunk), arm and forearm segments with torque generators at the ankle, knee, hip and shoulder joints respectively. The torque profiles were obtained using an isokinetic dynamometer.

Keywords: Muscle function, quadriceps, hamstrings, simulation model, torque

# Publications

## Refereed abstracts

Voukelatos, D., and Pain, M. T. G. 2012. Changes in quadriceps activation during maximal eccentric contractions following short term training. In: *Proceedings of Biomechanics Interest Group, BASES conference*, University of Ulster, Belfast, 4th of April, pp 38.

Voukelatos, D., and Pain, M. T. G. 2012. Training induced changes in quadriceps activation during maximal eccentric contractions. In: *Book of Abstracts. The American Society of Biomechanics conference*, Gainesville, Florida, USA, August 15th-18th.

Voukelatos, D., and Pain, M. T. G. 2014. Hamstrings:Quadriceps strength ratio as a function of angular velocity and angle. In: *Proceedings of the 7th World Congress of Biomechanics*, Boston, MA, USA, July 6th-11th.

Voukelatos, D., and Pain, M. T. G. 2015. A three dimensional description of the hamstrings-quadriceps ratio from a minimal data set. *MathSport International Conference*, Loughborough, June 29th - July 1st.

## Peer reviewed journal articles

Voukelatos, D., and Pain, M. T. G. 2015. Modelling suppressed muscle activation by means of an exponential sigmoid function: Validation and bounds. *Journal of Biomechanics*, 48, 712-715.

## Acknowledgments

First of all I would like to thank my supervisor Dr Matthew Pain for accepting to supervise me and for all his help and guidance throughout the course of my studies. Secondly, I would like to thank my family for their unwavering support and for always believing in me.

I would like to express my gratitude to all the people that took part in the studies while they could be doing something more pleasant instead and to Pavlos Evangelidis and Fraser Young for providing me with data from their research. Special mention should go to Glen Blenkinsop for his help with all things VICON and the many interesting and stimulating discussions we had. I would also like to thank everyone in the Sports Biomechanics and Motor Control research group (Fred, Sam, Mark, Mike, Martin, Paul, Stuart, Dave, Ravina, Aodhan, Erin, Mohsen, Fearghal, Riyadh, Romanda, Ben, Nuridayah and everyone whose name I managed to forget) for their friendship that made life so much easier.

Finally, last (and certainly not least) I would like to thank my wife Evi for all the love and support she has given me and for putting up with me for so many years.

# Contents

<b>Abstract</b>	<b>i</b>
<b>Publications</b>	<b>ii</b>
<b>Acknowledgements</b>	<b>iii</b>
<b>Contents</b>	<b>iv</b>
<b>List of Figures</b>	<b>xi</b>
<b>List of Tables</b>	<b>xvi</b>
<b>1 Introduction</b>	<b>1</b>
1.1 Modelling muscle function . . . . .	1
1.2 Statement of purpose . . . . .	8
1.3 Research Objectives . . . . .	9
<b>2 Quadriceps activation obtained by theoretical and experimental means</b>	<b>12</b>
2.1 Introduction . . . . .	12
2.1.1 Tension-limiting mechanism . . . . .	12
2.1.1.1 Studies performed <i>in vitro</i> . . . . .	12
2.1.1.2 Studies performed <i>in vivo</i> . . . . .	13
2.1.1.3 Alternative hypotheses . . . . .	17
2.1.1.4 Training studies . . . . .	19
2.1.2 Theoretical representation of muscle activation . . . . .	22
2.1.3 Objectives . . . . .	22

2.2	Methods . . . . .	23
2.2.1	Outline of data collection process . . . . .	23
2.2.2	Data collection . . . . .	24
2.2.2.1	Testing and Training protocols . . . . .	24
2.2.2.2	Stimulation . . . . .	25
2.2.2.3	Determination of Voluntary Activation . . . . .	26
2.2.3	Assessment of training intervention effects . . . . .	26
2.2.4	Evaluation of the sigmoid function . . . . .	28
2.3	Results . . . . .	30
2.3.1	Training Study . . . . .	30
2.3.2	Evaluation of sigmoid function . . . . .	33
2.4	Discussion . . . . .	36
2.4.1	Training Study . . . . .	36
2.4.1.1	Conclusion . . . . .	39
2.4.1.2	Limitations and future work . . . . .	39
2.4.2	Evaluation of sigmoid function . . . . .	40
<b>3</b>	<b>Hamstrings–Quadriceps ratio</b>	<b>42</b>
3.1	Introduction . . . . .	42
3.1.1	Hamstring strain injuries . . . . .	42
3.1.2	Mechanism of hamstring injury . . . . .	43
3.1.3	Risk factors . . . . .	44
3.1.4	Conventional and Functional H:Q Ratios . . . . .	45
3.1.5	H:Q <sub>con</sub> and H:Q <sub>fun</sub> as injury indicators . . . . .	46
3.2	Method . . . . .	50

3.2.1	Derivation of $R_T(\omega, \theta)$ . . . . .	50
3.2.2	Derivation of the experimental $R_E(\omega, \theta)$ function . . . . .	54
3.2.3	Testing the $R_E(\omega, \theta)$ function on raw ratio values . . . . .	56
3.3	Results . . . . .	60
3.3.1	Fit of $R_E(\omega, \theta)$ function on $R_T(\omega, \theta)$ . . . . .	60
3.3.2	Fit of $R_E(\omega, \theta)$ function on raw H:Q <sub>fun</sub> points . . . . .	62
3.3.2.1	11, 14, and 17 point fits . . . . .	62
3.3.2.2	8 point fits . . . . .	63
3.4	Discussion . . . . .	69
3.4.1	Co-activation of quadriceps and hamstrings . . . . .	70
3.4.2	Implications of the $R_E(\omega, \theta)$ fit . . . . .	73
3.4.3	Conclusions . . . . .	74
3.4.4	Limitations and future work . . . . .	75
<b>4</b>	<b>Introduction to computer simulation of a sporting activity</b>	<b>76</b>
4.1	Model actuation . . . . .	77
4.1.1	Angle driven models . . . . .	77
4.1.2	Muscle driven models . . . . .	78
4.1.3	Torque driven models . . . . .	79
4.2	Model activation and control . . . . .	80
4.2.1	Ground contact . . . . .	81
4.3	Model optimisation and evaluation . . . . .	82
4.3.1	Optimisation . . . . .	82
4.3.2	Evaluation . . . . .	84

<b>5</b>	<b>The Snatch</b>	<b>85</b>
5.1	Literature Review . . . . .	85
5.1.1	Quantitative analysis . . . . .	88
5.1.2	Bar Kinematics . . . . .	89
5.1.2.1	Vertical displacement of the bar . . . . .	89
5.1.2.2	Bar Trajectory . . . . .	89
5.1.2.3	Bar Velocity . . . . .	90
5.1.3	Joint Kinematics . . . . .	90
5.1.3.1	The double knee bend . . . . .	91
5.1.3.2	The Barbell-Cervical-Hip Angle (BCH) . . . . .	91
5.2	Data Collection . . . . .	91
5.2.1	Motion Capture . . . . .	92
5.2.1.1	Kinematic Data collection . . . . .	94
5.2.1.2	Marker reconstruction . . . . .	95
5.2.1.3	Kinetic Data collection . . . . .	96
5.3	Anthropometry . . . . .	100
5.3.1	Inertia parameters . . . . .	100
5.3.1.1	Anthropometric measurements . . . . .	102
5.3.2	Derivation of <i>torso</i> segmental inertia parameters . . . . .	102
5.3.3	Derivation of the moments of inertia for the barbell & weights system . . . . .	104
5.4	Data Analysis . . . . .	105
5.4.1	Filtering Kinematic data . . . . .	107
5.4.2	Torque–angular velocity–angle profiles . . . . .	108

<b>6</b>	<b>A simulation model for the Snatch</b>	<b>111</b>
6.1	Construction of the six segment model . . . . .	111
6.1.1	Structure . . . . .	111
6.1.2	Building a model in SimMechanics . . . . .	112
6.2	Angle driven model . . . . .	114
6.2.1	Actuating the model . . . . .	114
6.2.2	Ground contact . . . . .	115
6.3	Torque driven model . . . . .	120
6.3.1	Torque generators . . . . .	120
6.3.2	Activation functions . . . . .	122
6.4	Model Evaluation . . . . .	125
6.4.1	Matching optimisation . . . . .	125
6.4.1.1	Objective function . . . . .	128
6.4.2	The first pull phase . . . . .	129
6.4.3	The transition and second pull phase . . . . .	133
6.4.4	The second pull phase . . . . .	138
6.5	Optimisation of the second pull . . . . .	144
6.5.1	Joint angles . . . . .	144
6.5.2	Joint torques . . . . .	144
6.5.3	Activation timings . . . . .	146
6.5.4	Barbell velocity . . . . .	149
6.6	Discussion . . . . .	150
6.6.1	Limitations and future work . . . . .	154
<b>7</b>	<b>Summary and Conclusion</b>	<b>156</b>

7.1	Summary . . . . .	156
7.1.1	Quadriceps activation obtained by theoretical and experimental means . . . . .	156
7.1.2	The H:Q ratio as a function of $\omega$ and $\theta$ . . . . .	157
7.1.3	A six-segment, torque-driven simulation model of the Snatch . . . . .	158
7.1.3.1	Collection and analysis of kinematic data . . . . .	158
7.1.3.2	Collection and analysis of kinetic data . . . . .	158
7.1.3.3	Anthropometric measurements . . . . .	159
7.1.3.4	Ground contact . . . . .	159
7.1.3.5	Model evaluation . . . . .	159
7.2	Research questions . . . . .	159
	<b>References</b>	<b>162</b>
	<b>Appendix A</b>	<b>182</b>
	<b>Appendix B</b>	<b>183</b>
	<b>Appendix C</b>	<b>186</b>
	<b>Appendix D</b>	<b>189</b>
	<b>Appendix E</b>	<b>193</b>
	<b>Appendix F</b>	<b>196</b>
	<b>Appendix G</b>	<b>198</b>
	<b>Appendix H</b>	<b>200</b>

Appendix I	204
Appendix J	209
Appendix K	211
Appendix L	213
Appendix M	216
Appendix N	218

# List of Figures

1.1	The rectangular hyperbola of equation (1.10) for $C = 1$ with asymptotes $y = -\beta$ and $x = -\alpha$ . The third quadrant has been omitted . . . . .	4
2.1	Position of subject and dynamometre for knee extension . . . . .	25
2.2	Plot of average peak torque outputs per angular velocity . . . . .	30
2.3	Example plots from Subject 5 of the pre- and post-training $T-\omega$ raw data and separately fitted function for each data set. . . . .	32
2.4	Example plots from Subject 5 of the combined pre- and post-training $\%VA-\omega$ data and the fitted 3rd degree polynomial. . . . .	32
2.5	The four graphs show how the DIFACT function compares with the raw $\%VA-\omega$ data set for $\alpha_{max} = 100\%$ , $95\%$ , $90\%$ for Subjects 2 (top) and 4 (bottom). Graphs on the left correspond to the pre-training values and on the right to the post-training ones. The top two graphs, per subject, show the DIFACT function from the seven parameter fit superimposed on the $\%VA-\omega$ data set. In the bottom two graphs the DIFACT function has been fitted to the $\%VA-\omega$ data set directly and again plotted against the respective $\%VA-\omega$ values. . . . .	35
3.1	The function $T^{MVC}(\omega, \theta)$ of equation (3.1). Red area corresponds to the concentric part of the surface and green to the eccentric . . . . .	51
3.2	$T_{eccH}^{MVC}(\omega, \theta)$ for hamstrings and $T_{concQ}^{MVC}(\omega, \theta)$ for quadriceps shown separately . . . . .	53
3.3	$T_{eccH}^{MVC}(\omega, \theta)$ for hamstrings (green) overlaid on $T_{concQ}^{MVC}(\omega, \theta)$ for quadriceps (red) . . . . .	53
3.4	The theoretical $H:Q_{fun}$ ratio function, $R_T(\omega, \theta)$ . . . . .	54
3.5	Derivation of $R_E(\theta)$ and $R_E(\omega)$ by fitting 3- and 4-parameter functions on the plane curves $R_T(c, \theta)$ and $R_T(\omega, c)$ of the $R_T(\omega, \theta)$ function . . .	55

3.6	Example of fitting $R_E(\omega, \theta)$ on the whole $R_T(\omega, \theta)$ surface and on $(\omega, \theta, R_T(\omega, \theta))$ points. . . . .	61
3.7	Fit of the $R_E(\omega, \theta)$ function on 11, 14 and 17 $(\omega, \theta, R_{\text{exp}})$ points of the raw H:Q surface for Subject 4 . . . . .	65
3.8	Fit of the $R_E(\omega, \theta)$ function on 14 and 17 $(\omega, \theta, R_{\text{exp}})$ points of the experimental H:Q surface for Subject 2. The ratio values of the 14–point fit fail to increase with increasing $\omega$ and $\theta$ values due to an abnormally high ratio value at $(400^\circ/s, 107^\circ) \equiv (6.98 \text{ rad/s}, 1.87 \text{ rad})$ indicating a possible sub–maximal effort and increasing the likelihood of underestimating the ratio value near full extension of the knee joint. Adding 3 extra points eliminates the skewness of the graph . . . . .	67
5.1	First pull . . . . .	86
5.2	Transition phase and second pull . . . . .	86
5.3	Turn over and catch . . . . .	87
5.4	Recovery . . . . .	87
5.5	Marker placement on the athlete . . . . .	94
5.6	Five–segment marker model consisting of foot, shank, thigh, trunk and arms . . . . .	97
5.7	Dynamometer set up for ankle plantar flexion measurement . . . . .	97
5.8	Dynamometer set up for hip flexion measurement . . . . .	98
5.9	Dynamometer set up for shoulder flexion/external rotation measurement . . . . .	98
5.10	Filtered vs unfiltered linear velocity plots of the thigh . . . . .	107
5.11	Filtered vs unfiltered linear acceleration plots of the thigh . . . . .	108
5.12	Filtered vs unfiltered angular velocity plots of the knee joint . . . . .	108
5.13	Filtered vs unfiltered angular acceleration plots of the knee joint . . . . .	109
5.14	3–d T– $\omega$ – $\theta$ surface plot for knee extension . . . . .	110

6.1	Stick model figure, showing the model configuration at the start of the lift. The circular arrows indicate rotating joints with angle drivers and the double arrow the sliding angle driven elbow joint . . . . .	112
6.2	Structure of the six segment model of a Snatch athlete in the SimMechanics notation. Joint, body and ground blocks are illustrated . . . . .	113
6.3	Combined athlete + barbell COM trajectories in the horizontal (x) and vertical (z) directions from VICON and full angle driven models for the first 3 phases of the lift . . . . .	115
6.4	Combined athlete + barbell COM trajectories in the horizontal (x) and vertical (z) directions from VICON and angle driven with springs models for the first 3 phases of the lift . . . . .	117
6.5	Combined athlete + barbell COM trajectories in the horizontal (x) and vertical (z) directions from full angle driven and angle driven with springs models for the first 3 phases of the lift . . . . .	118
6.6	Horizontal (top) and vertical GRFs for a simulation of the initial 0.7 s of the Snatch . . . . .	119
6.7	Change in the value of the knee joint angle, $\theta$ , during the first 3 phases (1st pull, transition and 2nd pull) of the snatch lift . . . . .	121
6.8	Example of activation function $a(t)$ . . . . .	122
6.9	Example of a single upward activation profile $ACT_u(t)$ of equation (6.5), $n = 0.1, p = 0.9$ . . . . .	123
6.10	Example of an activation profile $ACT_d(t)$ of equation (6.10) with upward and downward slopes, $n = 0.1, p = 0.9, n2 = 0.1$ . . . . .	125
6.11	Example of an activation profile with two full activation curves both of which have an upward and downward slope. The second profile ramps up to a higher peak activation value, $p1 = 0.9, p2 = 0.95$ . . . . .	126
6.12	Knee joint angle from the start of the lift until the end of the second pull. The three phases of the lift are defined in terms of knee extension and flexion of the joint and marked on the graph . . . . .	127

6.13	Joint angle time histories from performance (solid line) and matched simulation (dashed line) for the first pull phase . . . . .	130
6.14	Joint torque time histories from performance, $T_{\text{per}}$ , (blue) and matched simulation, $T_{\text{sim}}$ , (red) for the first pull phase . . . . .	131
6.15	Joint activation time histories from performance (solid line) and matched simulation (dashed line) for the first pull phase . . . . .	132
6.16	Joint angle time histories from performance (solid line) and matched simulation (dashed line) for the transition and second pull phases . . .	134
6.17	Joint torque time histories from performance, $T_{\text{per}}$ , (blue) and matched simulation, $T_{\text{sim}}$ , (red) for the transition and second pull phases . . . .	136
6.18	Joint activation time histories from performance (solid line) and matched simulation (dashed line) for the transition and second pull phases . . .	137
6.19	Joint angle time histories from performance (solid line) and matched simulation (dashed line) for the second pull . . . . .	139
6.20	Joint torque time histories from performance, $T_{\text{per}}$ , (blue) and matched simulation, $T_{\text{sim}}$ , (red) for the second pull phase . . . . .	140
6.21	Joint activation time histories from performance (solid line) and matched simulation (dashed line) for the second pull . . . . .	142
6.22	Joint angle time histories from optimised (solid line) and matched simulation (dashed line) . . . . .	145
6.23	Joint torque time histories from optimised (solid line) and matched simulation (dashed line) . . . . .	146
6.24	Joint activation time histories from optimised (solid line) and matched simulation (dashed line) . . . . .	148
6.25	Vertical velocity, $v_z$ , from optimised and matched simulations during the second pull phase . . . . .	149
6.26	Torque vs angle values for ankle plantar flexion obtained from the study participant during dynamometer testing . . . . .	151

6.27 Ankle, knee and hip joint torques for the first three phases of the Snatch calculated using inverse dynamics for a single lift . . . . .	152
--	-----

# List of Tables

2.1	Testing protocol per session for each of the 10 testing and training sessions. Angular velocities and mode of contraction as well as contraction stimulus are reported . . . . .	23
2.2	Mean peak torque values obtained at 150 and 350°/s during pre- and post-training sessions for both contraction modes. . . . .	31
2.3	Results obtained from fitting the MVC torque function and a 3rd degree polynomial to the raw $T-\omega$ and %VA- $\omega$ data sets respectively. . . . .	31
2.4	RMS differences for the 7-parameter torque function fit to the $T-\omega$ data for $\alpha_{\max} = 100\%, 95\%, 90\%$ , . . . . .	33
2.5	Mean %VA values and standard deviations (SD), pre- and post-training, for each angular velocity (deg/sec). . . . .	34
2.6	Mean $\alpha_{\min}$ values in % and SD, pre- and post-training, for each value of $\alpha_{\max}$ . . . . .	34
3.1	$R^2$ and RMSE values for the fit of equations (3.5), (3.6) on $R_T^c(\theta)$ and $R_T^c(\omega)$ respectively . . . . .	56
3.2	Synopsis of the different $R_{\text{exp}}$ ratio points used in the 6 fits. Number of $R_{\text{exp}}$ points calculated during isometric ( $\omega = 0$ ) and isovelocitry trials ( $\omega \neq 0$ ), number of different isovelocities employed, $\kappa$ , and number of different joint angles per isovelocitry, $n$ . . . . .	58
3.3	$R^2$ and RMSE values for the fit of the $R_E(\omega, \theta)$ function on the theoretical ratio surface and on 17 points of that surface . . . . .	60
3.4	$R^2$ and RMSE values for the fit of the $R_E(\omega, \theta)$ function on 11, 14, and 17 $(\omega, \theta, R_{\text{exp}})$ points of the raw H:Q surface . . . . .	62
3.5	Normalised RMSE values for the fit of the $R_E(\omega, \theta)$ function on 11, 14, and 17 $(\omega, \theta, R_{\text{exp}})$ points of the raw H:Q surface . . . . .	63

3.6	$R^2$ , RMSE and NRMSE values for the fit of the $R_E(\omega, \theta)$ function on 8 $(\omega, \theta_{max}, R_{exp})$ , $(\omega_{max}, \theta, R_{exp})$ and 17 $(\omega, \theta_{varied}, R_{exp})$ points of the raw H:Q surface . . . . .	64
3.7	Normalised RMSE values for the fit of the $R_E(\omega, \theta)$ function on 11, 14, and 17 $(\omega, \theta_{max}, R_{exp})$ points of the experimental H:Q surface . . . . .	66
3.8	Mean $R_2$ , RMSE and NRMSE values for all fits with Subjects 2, 8, 9, 10 excluded . . . . .	66
3.9	$R_E(\omega, \theta)$ values evaluated at $(400^\circ/s, 172^\circ)$ for the 17 $(\omega, \theta, R_{exp})$ points fit. Mean value was 2.73 . . . . .	68
5.1	Joint centre locations . . . . .	96
5.2	ROM, angles where isometric contractions took place, angular velocities of CON–ECC contractions and number of cycles for CON–ECC contractions. Angles are in degrees ( $^\circ$ ) and angular velocities in ( $^\circ/s$ ). . . . .	99
5.3	Segment, mass, length, centre of mass (COM) measured from proximal joint for the head and trunk of the athlete . . . . .	103
5.4	Moments of inertia expressed in $kg \times m^2$ for the head and trunk of the athlete written in simmechanics convention where $x$ is the frontal axis, $y$ the longitudinal axis and $z$ the transverse axis . . . . .	103
5.5	Centre of mass locations, %S, expressed as percentage of segment lengths from the proximal joint centre. Values were derived from inertia parameters with the exception of the value for the forearm that was taken from the Dempster dataset (Dempster, 1955) . . . . .	106
5.6	Torque parameters. Ext. = Extension, Flex.= Flexion . . . . .	110
6.1	Stiffness and damping coefficients for vertical ( $z$ ) and horizontal ( $x$ ) springs	116
6.2	Maximum joint angles . . . . .	128
6.3	RMS and normalized difference scores between matched and performance angle time histories per joint for the first pull phase . . . . .	129

6.4	RMS and normalized difference scores between matched and performance angle time histories per joint for the transition and second pull phases . . . . .	133
6.5	RMS and normalized difference scores between matched and performance angle time histories per joint for the second pull . . . . .	138
6.6	Maximum (MAX) and minimum (MIN) torque values from inverse dynamics and matching simulations for the shoulder, hip, knee and ankle joints . . . . .	147
6.7	Vertical velocity at the end of the second pull for performance, matching simulation and optimised simulation . . . . .	149

# 1 Introduction

## 1.1 Modelling muscle function

Muscle function can be summarized as a change in the configuration of the muscle in response to a nervous signal that allows the muscle to produce force. The force that a muscle can exert depends mainly on its length,  $l$  and also on the rate of change (velocity) of that length  $dl/dt$ . Hill (1938) developed a relatively simple model that was very successful in describing the ability of muscle to produce force when contracting concentrically as a function of the velocity of contraction. Hill was studying the thermodynamics of muscle work when he determined the mechanical concentric force–velocity relationship of muscle. First he measured the heat emitted during isotonic contractions of frog sartorii muscles that had been electrically stimulated to a tetanic state. He observed that a) the amount of heat emitted during isotonic muscle contractions was proportional to the shortening distance and b) the rate of heat emission was proportional to the load used. Assuming that the work done by the muscle is converted into heat he expressed the amount of energy liberated during isotonic contraction as

$$E = (P + a)x \quad (1.1)$$

where  $a$  is a constant with the dimensions of force that depends on the size of the contracting muscle,  $P$  the load lifted and  $x$  the distance travelled. It follows that the rate of energy liberation is

$$\begin{aligned} \frac{dE}{dt} &= (P + a) \frac{dx}{dt} \\ &= (P + a)v \end{aligned} \quad (1.2)$$

where  $v$  is the velocity of muscle shortening. Since  $\frac{dE}{dt}$  was inversely proportional to  $P$ , it obtained its maximum value for  $P = 0$  and was zero during isometric contractions,  $P = P_0$ . Equation (1.2) was rewritten in the form

$$\frac{dE}{dt} = (P + a) = b(P_0 - P) \quad (1.3)$$

where  $b$  was the increase of energy rate per gram decrease in load. Equation (1.3) was then re-arranged to

$$(P + a)(v + b) = b(P_0 + a) \quad (1.4)$$

which has come to be known as “*Hill’s equation of muscle contraction*”. Equation (1.4) is an example of a *rectangular hyperbola* a special case of a family of conic sections. Since this family of functions features throughout this work a short derivation of some important properties is given below.

### Rectangular Hyperbolas

Rectangular hyperbolas are a family of conic sections that are described by the following quadratic equation

$$\frac{(x - \alpha)^2}{a^2} - \frac{(y - \beta)^2}{b^2} = c \quad (1.5)$$

that corresponds to a hyperbola centred at the point  $(\alpha, \beta)$ . If  $a = b$  in (1.5) then it becomes

$$\begin{aligned} \frac{(x - \alpha)^2}{a^2} - \frac{(y - \beta)^2}{a^2} &= c \\ \Rightarrow (x - \alpha)^2 - (y - \beta)^2 &= a^2 c \\ \Rightarrow (x - \alpha)^2 - (y - \beta)^2 &= C \end{aligned} \quad (1.6)$$

The hyperbolas of equation (1.6) are called *rectangular* hyperbolas as their asymptotes meet at right angles. By applying the following transformation

$$\begin{aligned} x &= x' - \alpha \\ y &= y' - \beta \end{aligned} \quad (1.7)$$

the centre of the hyperbola of (1.6) is shifted to the origin.

$$x^2 - y^2 = C \quad (1.8)$$

The hyperbola can now be rotated clockwise  $45^\circ$  with respect to the origin using the rotation matrix

$$\begin{aligned} \begin{bmatrix} x \\ y \end{bmatrix} &= \begin{bmatrix} \cos 45 & -\sin 45 \\ \sin 45 & \cos 45 \end{bmatrix} \begin{bmatrix} x' \\ y' \end{bmatrix} \\ &= \begin{bmatrix} \frac{\sqrt{2}}{2} & -\frac{\sqrt{2}}{2} \\ \frac{\sqrt{2}}{2} & \frac{\sqrt{2}}{2} \end{bmatrix} \begin{bmatrix} x' \\ y' \end{bmatrix} \\ \Rightarrow \begin{aligned} x &= \frac{\sqrt{2}}{2} (x' - y') \\ y &= \frac{\sqrt{2}}{2} (x' + y') \end{aligned} \end{aligned}$$

that gives

$$x'y' = C' \quad (1.9)$$

Dropping the dashes and using the inverse transformation of (1.7) on (1.9) this becomes

$$(x + \alpha)(y + \beta) = C \quad (1.10)$$

which is a special case of equation (1.5) the asymptotes of which are both orthogonal to each other and parallel to the cartesian axes  $x$  and  $y$ . The horizontal and vertical asymptotes of (1.10) can be determined as follows:

- **Horizontal**

$$\begin{aligned} (y + \beta) &= \frac{C}{(x + \alpha)} \\ \Rightarrow \lim_{x \rightarrow \infty} (y) &= \lim_{x \rightarrow \infty} \left( \frac{C}{(x + \alpha)} \right) - \lim_{x \rightarrow \infty} (\beta) \\ \Rightarrow \lim_{x \rightarrow \infty} (y) &= -\beta \end{aligned}$$

- **Vertical**

$$\begin{aligned} (y + \beta) &= \frac{C}{(x + \alpha)} \\ \Rightarrow \lim_{x \rightarrow -\alpha} (y) &= \lim_{x \rightarrow -\alpha} \left( \frac{C}{(x + \alpha)} \right) - \lim_{x \rightarrow -\alpha} (\beta) \\ \Rightarrow \lim_{x \rightarrow -\alpha} (y) &= \infty \end{aligned}$$

therefore as  $x \rightarrow \infty$ ,  $y \rightarrow -\beta$  i.e. the horizontal asymptote of (1.10) is  $y = -\beta$  and  $y = \infty$  as  $x \rightarrow -\alpha$  i.e. the vertical asymptote of (1.10) is  $x = -\alpha$ . Consequently, if  $P = y$  and  $v = x$  then the horizontal and vertical asymptotes of Hill's equation are, respectively,  $P = -a$  and  $v = -b$ .

Hill's equation is very successful in describing the relation between load and velocity of contraction during muscle shortening (concentric), however, it fails to do the same when the muscle is lengthening under load. The reason for this is illustrated in Figure (1.1) where it can be seen that for negative values of  $v$ ,  $P$  increases very quickly. Therefore, (1.4) had to be modified however, this, proved difficult to do as during

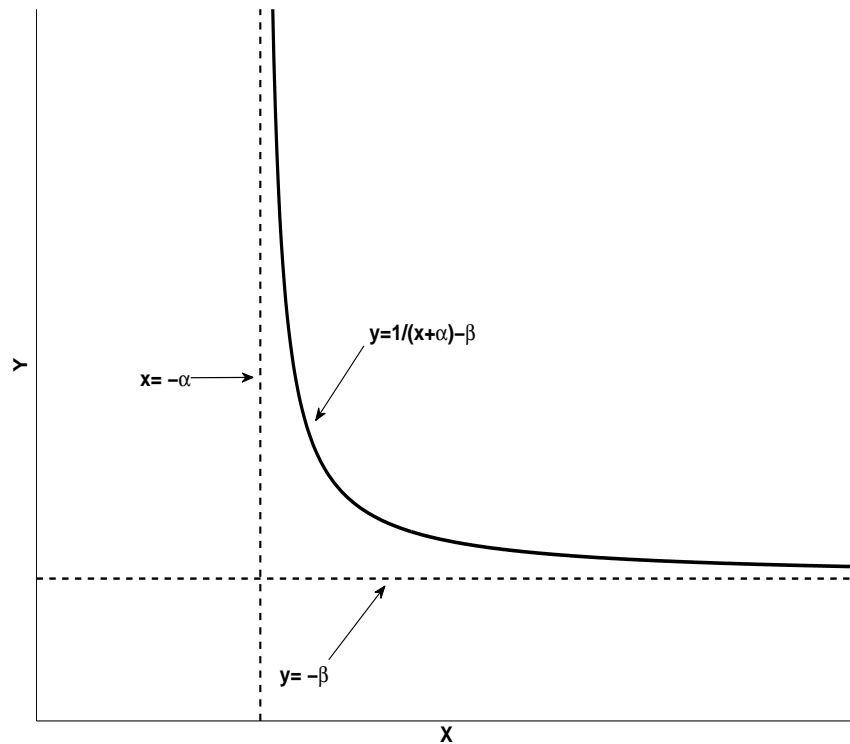


Figure 1.1: The rectangular hyperbola of equation (1.10) for  $C = 1$  with asymptotes  $y = -\beta$  and  $x = -\alpha$ . The third quadrant has been omitted

lengthening work is done on the muscle therefore instead of emitting heat the muscle was absorbing it resulting in a “negative heat of lengthening” that was impossible to measure (Hill, 1938).

Katz (1939) revisited Hill’s work and tried to investigate further the mechanical effects on the muscle when forces greater than isometric,  $P > P_0$  were applied. He ran a series of experiments where the muscle was first maximally stimulated and then made to eccentrically contract under a load  $P$  that was a multiple of  $P_0$ . Loads were applied either in a controlled manner or under an initial velocity. It was found that when load was applied in a controlled manner the velocities of lengthening under a load  $P$  were several times smaller than what was predicted by Hill’s equation. i.e. the rate of change of tension with respect to velocity  $dP/dv$  was approximately 6 times higher for eccentric contractions than concentric. It was also established that for  $P \approx 2P_0$  the muscle relaxed completely, i.e. could not withstand loads twice the isometric force.

Although equation (1.4) successfully described the force–velocity relationship in muscle

it could not provide any insight of the underlying mechanism governing that relationship as no theory successfully could explain this mechanism. Huxley (1957) proposed a new method that was based on his sliding filament hypothesis. He hypothesized that the interaction between actin and myosin filament in the muscle A band was governed by two rate constants,  $f$  and  $g$ , that determined whether actin would bind on ( $f > g$ ) or detach ( $f < g$ ) from myosin. He further assumed that the proportion of sites where actin was bound to myosin in the muscle was  $n$ . Then the rate of change of  $n$  would be given by

$$\begin{aligned}\frac{\partial n}{\partial t} &= f - (f + g)n \\ \Rightarrow -\frac{\partial x}{\partial t} \frac{\partial n}{\partial x} &= f - (f + g)n \\ \Rightarrow -v \frac{\partial n}{\partial x} &= f - (f + g)n\end{aligned}\tag{1.11}$$

where  $-v$  is the velocity with which the actin filament is moving with respect to myosin as muscle shortens. From (1.11), Huxley derived an expression for the total muscle tension in the muscle with respect to velocity of shortening

$$P = \frac{msw}{2l} \frac{f1}{f1 + g1} \left[ 1 - \frac{V}{\phi} \left( 1 - e^{-\frac{\phi}{V}} \right) \left( 1 + \frac{1}{2} \left( \frac{f1 + g1}{g2} \right)^2 \frac{V}{\phi} \right) \right]\tag{1.12}$$

where

- $w$  is the maximum work done in one actin–myosin site during a cycle
- $m$  is the number of myosin sites per  $\text{cm}^3$  of muscle
- $l$  is the distance between actin sites
- $V$  is rate of muscle shortening in muscle lengths /s
- $\phi = \frac{(f1+g1)h}{s}$  with  $h$  being the maximum distance at which a myosin site can become attached to an actin filament
- $f1, f2, g1, g2$  are values of  $f$  and  $s$  that depend on the distance between myosin and actin

The agreement between (1.4) and (1.12) was found by Huxley to be excellent and very close to the experimental error of the observations that Hill's equation was based on. This was significant as on one hand it provided experimental validation to a theoretically derived relationship (and thus to the underlying theory) and on the other established a mechanism for the force–velocity interaction. Moreover, Huxley's hypothesis ascertained the discontinuity in the rate of change of tension with velocity at

zero velocity that Hill and Katz had observed with the value of  $dP/dv$  being 4.33 times higher for slow muscle lengthening. However, Huxley too, stopped short of providing an explicit relationship for the force–velocity interaction during eccentric contraction.

Edman *et al.* (1978) studied the interaction between muscle stretch and tension using maximally stimulated single muscle fibres. They found that the magnitude of the force attained during eccentric contraction depended on the velocity of contraction as the force recorded was approximately proportional to the velocity of stretch. Specifically, after an initial sharp increase during the onset of stretch the force tended to remain constant (plateaued) until the end of the contraction. This was observed for all velocities tested and led the investigators to suggest that the whole force–velocity curve in the “negative” (eccentric) region would have a shape similar to an inverted rectangular hyperbola, however they did not attempt to define it in a quantitative manner. Interestingly, the ratio between maximum force developed during stretch and isometric force ( $P_0$ ) appeared to be independent of the velocity of contraction and was approximately equal to 1.8–1.9  $P_0$ . In a latter paper, Edman (1988) performed further experiments where loads, ranging from 0.1  $P_0$  to 1.8  $P_0$ , were applied on maximally stimulated single muscle fibres. He found that the force–velocity relationship followed a smooth sigmoid trajectory with an inflexion point at  $P_0$ . Contrary to the findings of Katz (1939) and Huxley (1957) no discontinuity appeared to exist at zero velocity however he, too, observed that the rate of change of force with respect to velocity  $dP/dv$  rose very quickly until 1.2  $P_0$  after which it noticeably fell and appeared to tend towards zero.

However, those results could not be quantitatively reproduced *in vivo*. Studies involving the human quadriceps group of muscles performed on isokinetic dynamometers showed little difference in force values produced during eccentric contractions at increasing angular velocities (Westing, 1988) and were more than 50% lower than the values observed *in vitro* during tetanic contractions of single muscle fibres. Moreover, during some subsequent studies eccentric torque values tended to decline with increasing velocity of contraction (Westing *et al.*, 1991; Dudley *et al.*, 1990; Pain & Forrester, 2009). It was hypothesized that this could be due to the existence of a neural, tension-limiting, mechanism that only becomes active during maximal voluntary contractions (henceforth MVC) of skeletal muscle and restricts maximal tension in it. The phe-

nomenon of neural inhibition will be discussed in more detail in the next chapter. For the purposes of the current discussion however, it is noted that due to its existence it became necessary to develop a mathematical function that would incorporate the effect of neural inhibition on muscle performance in order to produce a realistic description of muscle function for use in muscle models.

King & Yeadon (2002) expressed the Torque–angular velocity relationship for both, eccentric and concentric contractions, by means of a 6–parameter exponential function

$$T(\omega) = \frac{a + be^{p\omega}}{(1 + ce^{p\omega})(1 + de^{q\omega})} \quad (1.13)$$

where  $a, b, c, d, p, q > 0$  were the six–parameters that were determined by fitting the function to a torque–angular velocity dataset that had been obtained from a knee extension protocol performed on an isokinetic dynamometer. The function reached a plateau at high eccentric velocities and approached zero asymptotically. In order to establish the accuracy of (1.13) it was fitted to the complete force–velocity dataset of Edman (1988) producing a percentage RMS difference of 2.4% which showed that the function followed experimental data well. Although equation (1.13) was able to successfully reproduce the raw torque–angular velocity datasets it was fitted on it could not differentiate between torque produced during MVC contractions and from tetanic contractions that were not neurally inhibited.

Yeadon *et al.* (2006) addressed this by developing a mathematical function capable of expressing both maximum voluntary and tetanic torque as a function of angular velocity,  $\omega$  and joint angle,  $\theta$ . First the maximum joint torque at full activation was defined as a function of angular velocity,  $\omega$ . The function consisted of two rectangular hyperbolas of the form of (1.10) that represented both the concentric,  $\omega \geq 0$ , and eccentric,  $\omega < 0$ , phase of tetanic contraction and is expressed below in piecewise form.

$$T = \begin{cases} \frac{C}{(\omega_c + \omega)} - T_c, & \omega \geq 0 \\ \frac{E}{(\omega_e - \omega)} + T_{max}, & \omega < 0 \end{cases} \quad (1.14)$$

where

$$T_c = \frac{T_0 \omega_c}{\omega_{max}}, \quad C = T_c(\omega_{max} + \omega_c) \quad (1.15)$$

$$\omega_e = \frac{(T_{max} - T_0)}{\kappa T_0} \frac{\omega_{max} \omega_c}{(\omega_{max} + \omega_c)}, \quad E = -(T_{max} - T_0) \omega_e$$

The functions of (1.14) and (1.15) are defined by four parameters:

- $T_{max}$  is the maximum torque produced during eccentric contraction.
- $T_0$  is the maximum torque produced during isometric contraction.
- $\omega_{max}$  the value of the angular velocity where the torque curve reaches zero on the  $T$  vs  $\omega$  graph.
- $\omega_c$  is defined by the vertical asymptote  $\omega = -\omega_c$  of equation (1.14).

and  $\kappa$  is the value of the ratio of the slopes  $dP/dv$  of the eccentric and concentric functions at  $\omega = 0$  set equal to 4.3 as established by Huxley (1957).

The effect of neural inhibition was initially expressed using a quadratic three-parameter differential activation function (Yeadon *et al.*, 2006). Subsequently, Pain & Forrester (2009) introduced a sigmoid exponential differential activation function (DIFACT) that was shown to follow well the *in vivo* voluntary neural activation-angular velocity profile (Voukelatos & Pain, 2015).

$$DIFACT = \alpha(\omega) = \alpha_{min} + \frac{\alpha_{max} - \alpha_{min}}{1 + e^{\left(-\frac{\omega - \omega_1}{\omega_r}\right)}} \quad (1.16)$$

where  $\omega_r$  is the angular velocity range over which the ramp up in differential activation takes place,  $\alpha_{min}$  is the low plateau activation level and  $\omega_1$  is the angular velocity at the midpoint of the  $\alpha(\omega)$  vs  $\omega$  ramp (Pain & Forrester, 2009). Finally, the relation between torque and angle of contraction was introduced using the following two-parameter normal distribution function.

$$T_\theta = e^{\left(-\frac{1}{2}\right) \left[\frac{(\theta - \theta_{opt})^2}{W^2}\right]} \quad (1.17)$$

where  $\theta_{opt}$  is the optimal angle for torque production and  $W$  is the width of the curve.

## 1.2 Statement of purpose

Equations (1.14), (1.16) and (1.17) are employed throughout the work presented here with the aim of obtaining a mathematical description of muscle function during different activities and for various muscle groups and of answering a number of research questions that will be outlined shortly. First, the effect of a short training intervention, performed on an isokinetic dynamometer, on the neural inhibition during fast eccentric and slow

concentric contractions of the quadriceps will be quantified and assessed by means of the twitch interpolation technique (Merton, 1954) and equations (1.14)–(1.17). Following this, the torque profiles for both knee extensors and flexors will be obtained for two groups of participants and the respective theoretical hamstrings to quadriceps torque ratios will be expressed as functions of two variables, namely angular velocity and angle. Subsequently, a simpler function of the hamstrings to quadriceps surface ratio, representing the full angle–angular velocity range, will be derived and its accuracy assessed by comparing it to both the theoretical torque ratios and also to experimentally obtained raw ratio values. Finally, a simulation model of the Snatch Olympic lift will be developed in order to investigate optimum technique. Using anthropometric, kinetic and kinematic data from a competitive Olympic weightlifter a subject–specific simulation model will be constructed. The action of muscles on the joints will be represented by torque generator functions that will be again based on equations (1.14)–(1.17). The torque–driven model will be evaluated against the performance of the athlete in order to establish its level of accuracy. The lift will be split into phases and the model will be evaluated individually in each phase, consequently only those optimal technique components that pertain to each phase will be examined.

### 1.3 Research Objectives

*Is it possible to reduce the neural inhibition during fast eccentric contractions by means of eccentric strength training?*

Eight sessions of a high velocity eccentric/concentric training protocol on an isokinetic dynamometer will be performed by participants over a period of 3 weeks. Quadriceps strength levels and percentage of voluntary neural activation (henceforth %VA) pre– and post– training will be tested via a testing protocol consisting of maximum voluntary and supra-maximally electrically stimulated isometric and isovelocity contractions at various crank angles and angular velocities. Changes in performance will be assessed by means of Student’s t–tests, repeated measures factorial ANOVA and by application of the extra–sum–of squares F-Test to non–linear regression fits of equation (1.14) to the Torque–angular velocity (henceforth T– $\omega$ ) datasets.

*How well does the sigmoid DIFACT function of (1.16) represent the in vivo neural activation profile during voluntary contractions and can it cope with perturbed levels of maximum activation?*

Voluntary neural drive–angular velocity (henceforth %VA– $\omega$ ) and T– $\omega$  datasets obtained via the interpolated twitch technique will be determined from the pre– and post–training testing sessions. Non–linear regression fits of equations (1.14) and (1.16) will be performed on the pre– and post–training T– $\omega$  and %VA– $\omega$  datasets respectively for three different values of the DIFACT upper bound,  $\alpha_{max}$ , 100%, 95% and 90%. The determination coefficients,  $R^2$ , and the root mean square error (RMSE) of the fits will be derived and statistically compared.

*Is it possible to obtain a mathematical description of the functional H:Q ratio with respect to both angle,  $\theta$  and angular velocity  $\omega$  of contraction?*

Initially, a theoretical, 3–dimensional description for the functional H:Q ratio will be obtained algebraically using equations (1.14)–(1.17) and subsequently will be used to obtain the respective ratios for each one of the 11 participants of a group that performed a protocol of knee extensions and flexions on an isokinetic dynamometer. Since the number of parameters is expected to be high, a simpler expression (containing fewer parameters) in angular velocity and angle will be sought. To establish the level of accuracy this new function will be fitted to a second group of 14 experimental torque–angular velocity–angle (T– $\omega$ – $\theta$ ) datasets obtained again from isokinetic extensions and flexions of the quadriceps and hamstrings muscle groups to produce T– $\omega$ – $\theta$  surfaces.

*How close to optimum was the technique of the Olympic weightlifter that performed the Snatch lift?*

A computer simulation model based on the anthropometry, kinetics and kinematics of the athlete will be used to assess the effectiveness of the technique of the subject from which the data were collected. First a subject–specific simulation model will be constructed using the segmental inertia and mass parameters of the athlete performing the lift. Next, the activation timings of the torque generators will be optimised so as for the simulation model to match, as close as possible, the kinematics of the actual lift. Finally, the activation timings will be re–optimised with the aim to maximise the vertical velocity reached by the barbell during the first 3 phases of the lift. The

difference in bar vertical velocity between the two optimisations will be used to quantify the difference between optimal and “employed” techniques.

# 2 Quadriceps activation obtained by theoretical and experimental means

## 2.1 Introduction

### 2.1.1 Tension-limiting mechanism

#### 2.1.1.1 Studies performed *in vitro*

As was discussed in the previous chapter *in vitro* experiments are usually performed using either isolated animal muscle fibres or whole muscles in solution. For example, Hill (1938) and Katz (1939) used whole sartorii muscles taken from english or hungarian frogs whereas Edman *et al.* (1978); Edman (1988) studied skeletal frog muscles using separated muscle fibres that were placed in a chemical solution and stretched under tetanic contractions. Both Katz (1939) and Edman *et al.* (1978); Edman (1988), determined that the magnitude of the force recorded during stretch was dependent upon the velocity of stretch i.e. the higher the stretch velocity the higher the recorded force. The force developed during stretch was approximately 1.6–2.0 times higher than the isometric tension,  $P_0$ . These findings have been ascertained by various others studies a number of which will be summarized next.

Harry *et al.* (1990) studied the force-velocity relationship during eccentric contractions of whole sartorii muscles taken from frogs that were immersed in solution and tetanically stimulated. The muscles were first stimulated to isometric length and subsequently eccentrically contracted under constant velocity until they reached a specific length. The process was repeated for different stretching velocities. As in previous studies it was established that during lengthening force remained well above  $P_0$  however, the  $P/P_0$  ratio was not as high, as previously observed, as it reached a value of approximately 1.5. Lombardi & Piazzesi (1990) examined the mechanical behaviour of muscle during stretch using single frog muscle fibres. The fibres were electrically stimulated until the tetanus plateau was reached and forcibly stretched at a pre-set

velocity. As was found by Huxley (1957) the force values rose sharply for low stretching velocities and as the latter increased the force tended towards a limiting value of  $2 P_0$ . Krylow & Sandercock (1997) also measured the eccentric, force–velocity relationship using surgically removed soleus muscles taken from male rats. Again the muscle was electrically stimulated at isometric length and, once full tension had been achieved, was stretched at a constant velocity for approximately 3 mm. It was found that force increased monotonically with stretching velocity and approached asymptotically  $1.7 P_0$ .

In all those studies the eccentric, “negative”, region of the force–velocity relationship exhibits two very similar characteristics: a) the rate of change of force with respect to velocity rises very quickly for low stretching velocities and b) as the muscle stretching velocity increases its tension approaches asymptotically a value that is usually between 1.5 and 2.0 times larger than  $P_0$ . It would not be unreasonable to assume that the *in vivo* force–velocity relationship would be qualitatively, if not quantitatively, similar to what had been established *in vitro*. This, however, would prove not to be the case.

#### **2.1.1.2 Studies performed *in vivo***

Westing (1988) studied the eccentric and concentric force–velocity characteristics of the rectus femoris muscle in man, *in vivo*, using a dynamometer. They measured the force developed at preselected angles of extension, both, isometrically and isokinetically, at concentric and eccentric phases of contraction. They concluded that in almost all cases eccentric force did not alter significantly with increasing velocity and it was significantly lower in the region of eccentric contractions than the values observed by Edman *in vitro*, a reduction of 50% or more. Moreover, during some subsequent studies eccentric torque values tended to decline with increasing velocity of contraction (Westing, 1988; Westing *et al.*, 1990; Dudley *et al.*, 1990; Pain & Forrester, 2009). They hypothesized that this could be due to the existence of a neural, tension–limiting, mechanism that only becomes active during maximal contractions of skeletal muscle and restricts maximal tension in it.

However, it was not clear neither whether this proposed neural inhibitory mechanism was the sole cause for the observed disagreement between *in vitro* and *in vivo* results nor

researchers understood its exact nature. As a result a number of studies were performed in order to provide an answer to those two questions. Westing *et al.* (1991) examined the discrepancy between the torque developed during concentric and eccentric contractions of maximally stimulated animal muscle, *in vitro*, and maximal voluntary contractions of skeletal muscle in man. To investigate the relationship between torque and velocity of contraction they studied agonist EMG activity during maximal voluntary eccentric and concentric contractions. The participants performed a number of maximal concentric and eccentric contractions on a dynamometer at various angular velocities. EMG recordings were taken from the vastus medialis, vastus lateralis and rectus femoris muscles. The results showed that:

- Eccentric torque was significantly greater than corresponding concentric for all test velocities and did not change significantly with increasing angular velocities of contraction.
- EMG activity levels were significantly lower for all three extensors during eccentric contractions compared to concentric contractions and remained constant irrespective of contraction velocities whereas they decreased significantly with decreasing contraction velocity during concentric contractions.

These findings support the notion of non-maximal activation of the knee extensors under high-tension conditions. A possible explanation proposed by the authors was a reduction in the neural drive resulting in the aforementioned limiting of tension. It is noted that despite the apparent reduced EMG activity of the knee extensors during eccentric contraction the forces exerted by the muscles are considerably higher than those developed during concentric contractions (Enoka, 1996b).

Dudley *et al.* (1990) examined the hypothesis that artificial activation of the knee extensor group across a range of concentric and eccentric angular velocities, would result in greater changes in force production than what the muscle could achieve under maximal voluntary contraction. To test this they used two levels of transcutaneous tetanic electrical stimulation of the knee extensors to achieve their artificial activation. They found that:

- During eccentric contractions torque tended to decrease with increasing angular

velocities during maximal voluntary contraction (MVC).

- Torque was much less dependent on the speed and type of muscle action with voluntary than with artificial activation as it increased approximately 1.4 times above isometric under artificial activation, irrespective of the level of activation, as eccentric velocity increased. This was not observed during maximal voluntary eccentric contractions.

This lesser change in torque with MVC suggested that the activation of the knee extensors group by the central nervous system during maximal effort depends upon the speed and type of action performed.

A similar study was done by Babault *et al.* (2001) who employed the twitch interpolation technique (Merton, 1954) in order to investigate whether the level of voluntary activation of the human quadriceps femoris muscle depends upon the contractile conditions during concentric, eccentric as well as isometric contractions. The assumption was that if any motor units were not recruited or not discharging at their maximal capacity they would produce a force increase when under electrical stimulation. Their results indicated that during maximal eccentric and concentric contractions voluntary activation was lower than isometric contraction corroborating the hypothesis of a neural tension-limiting mechanism that had been proposed with different approaches such as those based on EMG described earlier.

Amiridis (1996) sought to examine the isokinetic torque produced by highly skilled and sedentary human subjects during maximal voluntary and electrically stimulated knee extensions in order to establish whether the superimposed electrical stimulus would lead to an increase of the produced torque compared to torque produced by MVC only and whether this was dependent on the fitness level of participants. An equal number of sedentary and highly skilled subjects performed voluntary and electrically stimulated isometric and isokinetic contractions of the knee at different angular velocities. No significant difference in torque values were found between electrically stimulated and voluntary contractions in the highly skilled group. In the sedentary group the torque values obtained from electrically stimulated contractions were significantly higher than those obtained from voluntary contractions. Their findings corroborated the existence of a tension-limiting neural mechanism; however this seemed to be dependent upon

the fitness level of the participants.

Aagard *et al.* (2000) sought to compare neural activation during maximal concentric and eccentric quadriceps contraction before and after a period of heavy resistance training. The hypothesis was that the training would help the neuromuscular activation to adapt and diminish the inhibitive effects of the tension-limiting neural mechanism. In full agreement with the previous studies they reported significantly lower neuromuscular activation, established with the use of EMG, during maximal eccentric and slow concentric contractions compared to fast concentric in the pre-training phase. The significantly higher EMG amplitudes recorded during the same motions post-training were indicative of increased neuromuscular activation. Moreover, the inhibition was reduced after the 14-week training regime was over, both for slow concentric and fast eccentric contractions. Their work demonstrated that the inhibition in neuromuscular quadriceps activation can be reduced as a result of a resistance training program.

Although the appearance of reduced neural drive during eccentric contractions had been established at this point using a variety of experimental techniques, a question arose regarding the process under which this mechanism is manifested onto specific fibre types. For example, Enoka (1996a) suggested that the reduction in the neural drive could be caused either by a lower activation of all recruited fibres as a consequence of inhibition or, due to activation of selective fibre populations, accompanied by inhibition of other fibre populations.

Beltman (2004) studied the level of activation during maximal isometric, eccentric and concentric contractions using the ratio of phosphocreatine to creatine (PCr/Cr) which was measured in single characterized fibre fragments isolated from needle biopsies of the vastus lateralis quadriceps muscle. The method allowed them to assess whether type II fibres had been selectively activated or whether all fibres were activated at a lower level during eccentric contractions. They found that the PCr/Cr ratio values obtained from needle biopsies were decreased in all fibre types and there was no evidence for a selective activation of type II fibres during eccentric contractions. They also used the superimposed nerve stimulation technique in order to determine the voluntary activation level of the muscle. As in previous studies they found that the voluntary activation level during eccentric contractions was significantly lower than during isometric and concentric (contractions).

Reduced muscle activation during eccentric contractions was not restricted only to quadriceps despite the bulk of experiments involving that muscle group. Lee & Herzog (2002) investigated the effect of electrical stimulation on the force output of the adductor pollicis muscle during both maximal voluntary and electrically induced contractions. They found that peak forces increased with increasing velocity of stretching for both MVC and electrically induced contractions however, the force output during the latter was significantly higher, approximately 1.5 times the isometric force value, indicating possible reduced muscle activation during MVC contractions. Similar findings were reported by Ruiter *et al.* (2000) who sought to examine the stretch response of the adductor pollicis during electrically stimulated contractions only. They too reported that the force value produced during eccentric contractions of the muscle was approximately 1.4 times higher than the isometric value.

### **2.1.1.3 Alternative hypotheses**

At this point research had well documented the existence and modes of action of the neural tension-limiting mechanism acting during fast concentric and eccentric contractions. Some authors, however, have suggested that factors other than neural should be considered.

In a follow-up study, Aagard *et al.* (2001) examined the physiological adaptations that take place in the vastus lateralis muscle during a heavy training regime. They studied the relationship between the physiological cross sectional area (PCSA) of individual muscle fibres and fibre pennation angles as well as the relationship between anatomical cross sectional area (ACSA) and volume. They hypothesized that heavy weight training would cause muscle fibre pennation angle to increase. After a 14-week intensive strength training programme they reported increased vastus lateralis pennation angles and significantly increased PCSA (+ 16%) than ACSA (+ 10%). These findings suggest that morphology, architecture and a contractile capacity of human pennate muscle are interrelated and that any changes in the size of the quadriceps muscle are associated with changes in single muscle fibre size therefore changes in the pennation angle of the quadriceps muscles may affect the torque produced.

The relation between pennation angle and the state of the muscle fibres of the vastus

lateralis muscle had been studied previously, albeit in a different manner, by Fukunaga (1997). Using ultrasonic muscle imaging they established that muscle fibre and pennation angle depended on the level of tension of the muscle. More specifically, during active contraction of the muscle the fibre shortening was significantly larger than what was observed during passive contraction. Pennation angles increased with increased activation.

However it is not clear from these studies whether the observed changes in pennation angles of the quadriceps is a contributing factor to the reduced action of the tension-limiting neural mechanism or a consequence of it. More recently, Pain & Forrester (2009) sought to provide further insight into the nature of the tension-limiting mechanism of motor units and also to determine whether a synchronous measurement of surface EMG, torque, angle and angular velocities of maximal voluntary eccentric and concentric contractions of the knee extensors could be used to reproduce the classical *in vitro* force-velocity relationship. They obtained maximal voluntary force and EMG amplitude throughout the force-velocity phase space. Normalising the EMG amplitudes and globally mapping them onto maximal voluntary force values the EMG corrected force was obtained representing the force that would have been achieved with maximal amplitude at any fibre length and velocity combination. This EMG corrected force was very close to the classical *in vitro* tetanic velocity curve (Dudley *et al.*, 1990; Westing *et al.*, 1990). Moreover, since a linear EMG amplitude-force relationship was assumed, the closeness of EMG corrected force-velocity shape to the *in vitro* tetanic one points to neural factors as the cause of the tension-limiting mechanism. In a following paper Pain *et al.* (2013) compared the  $P/P_0$  ratios and the low plateau activation levels,  $\alpha_{min}$ , of equation (1.16), from MVC and submaximally stimulated (STIM) eccentric contractions of the knee extensors and flexors. The raw  $P/P_0$  values from the stimulated contractions were significantly higher than the MVC (1.79 vs 0.93) and (1.44 vs 1.00) for knee extensors and flexors respectively. Likewise the  $\alpha_{min}$  values from stimulated trials were also significantly higher during the electrically stimulated trials for both extensors (0.921 vs 0.804) and flexors (0.877 vs 0.764). The  $P/P_0$  values from the STIM trials were very close to the *in vitro* tetanic pattern, especially for the knee extensors, indicating that neural inhibition is responsible for the difference in  $P/P_0$  and activation values between the STIM and MVC conditions.

So on the assumption that the involuntary change of neural factors is largely responsible for the depression in eccentric strength, researchers attempted to establish whether it would be possible to achieve a change in the neural activation action using various strength protocols.

#### **2.1.1.4 Training studies**

Caiozzo *et al.* (1981) examined changes in the *in vivo* force–velocity relationship using two groups of individuals that were trained over a period of 4 weeks on an isokinetic dynamometer on two different angular velocities, 1.68 rads/s and 4.19 rads/s (96°/s and 240°/s respectively). They established that the group of individuals that had trained at the slower angular velocity of 1.68 rads/s exhibited the greatest gains in the slow velocity–high force region of the force–velocity relationship. They hypothesized that this increase might reflect an adjustment of the neural tension–limiting mechanism operating in this region of high tension.

Coyle *et al.* (1981) compared the training induced changes in maximal quadriceps torque at specific isokinetic velocities in groups of individuals performing only slow (60°/s), only fast (300°/s), or a mixture of slow and fast maximal concentric contractions. They found that the training effect on the group that trained with 300°/s was less specific than the other two groups as they exhibited significant post–training increases in peak torques at all three isovelocities and not just at the one they had trained at. Post–training muscle biopsies showed the isokinetic training at 300°/s had induced a significant enlargement (+ 11%) of type II fibers, something that was not observed for the other two groups and it was hypothesized that type II hypertrophy was an additional reason for the improvement exhibited by the group trained at high isokinetic velocities. The authors also hypothesized that increased neural activation may have been partly responsible for the observed increase in torque output although those were not quantified.

Higbie *et al.* (1996) studied the effects of isokinetic training on quadriceps muscle strength, cross sectional area (CSA) and muscle activation (by means of EMG) after a 30 session training intervention, spread over 10 weeks, that had two groups of participants training with either concentric or eccentric contractions. Contrary to Coyle

*et al.* (1981) they reported mode specific strength increases and neural activation for both groups, however, the testing protocol consisted of only one isovelocity at  $60^\circ/\text{s}$ . They also reported significant increases in CSA for both groups post-training with the eccentrically trained group exhibiting significant higher CSA than the concentrically trained. Seger & Thorstensson (2004) compared the effects of pure concentric or eccentric training on the decreased inhibition during maximal voluntary eccentric actions using a similar training protocol. They reported mode-specific strength increases post-training, particularly for the eccentrically trained group, but they did not observe any increase in muscle activation or disinhibition despite the significant increases in raw torque outputs post-training. Tesch *et al.* (2004) assessed force, neural activity and volume of the knee extensors after a 5 week training intervention performed on a gravity-independent, resistance exercise flywheel system. Subjects accelerated the flywheel by concentrically contracting the knee extensors and then decelerated to a full stop via eccentric contraction. After 12 training sessions concentric and eccentric torque outputs increased by 11% and quadriceps muscle volume by 6.1% but, as in Seger & Thorstensson (2004), EMG showed no increase in neural output. The absence of neural effects in the latter two studies is rather perplexing, however, there were some issues which may account for it. In Seger & Thorstensson (2004) the sample size was rather small as there were 5 participants for each of the two training groups and testing was performed at  $60^\circ/\text{s}$  (whilst neural inhibition is thought to manifest at higher contraction velocities). In Tesch *et al.* (2004) on the other hand, EMG was recorded during isometric contractions despite the fact that no isometric training had taken place.

Indeed in other studies an increase in torque output post-training was accompanied by increased neural activation. Aagaard *et al.* (2002) found increased V-wave and Hoffman (H)-reflex responses in the soleus muscle after a 14-week, 38-session, training programme consisting of weight training. Krentz & Farthing (2010) observed increased neural activity, measured by EMG, of the biceps brachii after 7 training sessions consisting of eccentric only contractions performed isokinetically at  $90^\circ/\text{s}$ . Notably, despite the increase in neural output and muscle thickness (measured with ultrasound) the strength output of the participants decreased after the fourth training session and remained reduced until the end of the programme which was attributed by the authors

to the negative impact of the protocol on the surrounding joints and muscles and the high training frequency. More recently, Baroni *et al.* (2013) monitored the progress of twenty participants throughout a 12-week eccentric training isokinetic programme. Subjects performed eccentric only contractions at  $60^\circ/\text{s}$ . Knee extensor peak torque, EMG activity and CSA were assessed every four weeks. Peak torque and CSA increased significantly in the first four weeks and kept increasing as the programme progressed however, neural output remained unchanged after the first four weeks of training indicating that neural adaptations predominantly occur during that period.

Caution has to be exercised when results from the above studies are compared as there are quite a few differences among them. For example, some training programmes were performed using free weights (Aagaard *et al.*, 2000; Aagaard *et al.*, 2002) whereas others on a dynamometer (Coyle *et al.*, 1981; Higbie *et al.*, 1996; Seger & Thorstensson, 2004). Moreover even when the same apparatus was employed the contraction mode was different as some included only concentric (Caiozzo *et al.*, 1981; Coyle *et al.*, 1981) or eccentric contractions (Baroni *et al.*, 2013). The testing protocols were also different in terms of isovelocities used and of course, the muscle groups studied were not always the same (Aagaard *et al.*, 2002; Krentz & Farthing, 2010). Significantly though, no intervention considered the effect of utilizing both concentric and eccentric contractions at fast angular isovelocities (over  $350^\circ/\text{s}$ ) on the post-training raw torque output and the neural inhibition. This approach would appear reasonable as neural inhibition appears to be inversely proportional to the velocity of eccentric contraction (Dudley *et al.*, 1990; Westing *et al.*, 1991) and moreover takes into account the role of powerful eccentric contractions during the stretch shortening (SSC) cycle which is to enable subsequent concentric contractions within the SSC cycle to generate greater outputs of force compared with concentric contractions that do not follow pre-stretch (Komi, 1984). This is very important for the execution of fast powerful movements that employ the SSC cycle. Using exclusively, eccentric or concentric contractions in training fails to utilize the SSC effect and does not allow the muscle to attain the highest possible level of activation.

## 2.1.2 Theoretical representation of muscle activation

At this point it has been established that *in vivo* measurements of the maximum voluntary force–velocity relationship show differences to the *in vitro* tetanic profile, with eccentric forces not increasing much above isometric and tending to decline with increasing lengthening velocity (Westing, 1988; Dudley *et al.*, 1990; Weber & Kriellaars, 1997), probably due to the action of a neural, tension–limiting mechanism that reduces maximal neural drive at high levels of muscular tension (Westing *et al.*, 1991; Pain & Forrester, 2009; Pain *et al.*, 2013). Yeadon *et al.* (2006) represented the *in vivo* maximum voluntary torque–velocity relationship as a product of a theoretical four parameter Hill–type tetanic torque function, and a three parameter differential activation function (DIFACT). The latter representing the net reduction in neural drive to the muscle with low neural activation at high eccentric velocities to full activation at high concentric velocities. However, the DIFACT function was not explicitly based on measured neural changes and its validity was implicitly assumed through the ability of the combined seven parameter function to reproduce the *in vivo* torque–velocity profiles. Furthermore, due to its quadratic form, the DIFACT function had multiple equivalent solutions and is difficult to manipulate algebraically. Pain & Forrester (2009) used a sigmoid exponential function to represent the DIFACT function in order to simplify mathematical manipulation when finding solutions for the seven parameter MVC torque function (MVC). Again the function was only implicitly shown to be successful through scaling of voluntary EMG signals. Therefore, although now used repeatedly (Lewis *et al.*, 2012; Forrester *et al.*, 2011; Tillin *et al.*, 2012; Pain *et al.*, 2013) in the literature the DIFACT function has yet to be verified in an explicit way.

## 2.1.3 Objectives

The objectives of this study were two–fold. The main objective was to investigate whether a training intervention consisting of performing high velocity concentric–eccentric cycles on an isovelocity dynamometer could induce a decrease in the inhibitive action of the neural factors and increase the force output during fast eccentric and slow concentric MVC contractions. The protocol was specifically geared to high velocity eccentric / concentric training on an isovelocity dynamometer over a period of 3 weeks

to limit adaptations to predominately neural changes. It was hypothesized that at the end of the training cycle subjects would exhibit significantly higher torque outputs and a possible reduction in neural inhibition.

The second objective was (i) to establish experimentally how well the DIFACT function follows the in vivo voluntary neural activation–angular velocity profiles in a group of subjects; and (ii) to test the robustness of the exponential DIFACT function to perturbed upper levels of maximal activation.

## 2.2 Methods

### 2.2.1 Outline of data collection process

In this section a brief outline of the data collection sessions and procedures will be given for clarity. The testing protocols followed in each session are summarized in Table 2.1 and in Appendix A

**Session 1:** Familiarisation session

**Session 2:** Pre–training testing session

**Sessions 3–10 :** Training sessions that took place over a three–week period

**Session 11:** Post–training testing session

Table 2.1: Testing protocol per session for each of the 10 testing and training sessions. Angular velocities and mode of contraction as well as contraction stimulus are reported

Session	Angular velocity $\omega$ ( $^{\circ}$ /s)	Contraction Mode	Stimulus
1	0, 50, 150, 250	ISOM, CON, ECC	VOL, STIM
2	0, 50, 100, 150, 250, 350	ISOM, CON, ECC	VOL, STIM
3–10	50–400*	CON, ECC	VOL
11	0, 50, 100, 150, 250, 350	ISOM, CON, ECC	VOL, STIM

\* depending on session

ISOM=Isometric, CON=Concentric, ECC=Eccentric

VOL=Voluntary, STIM=Electrically stimulated

## 2.2.2 Data collection

Six male volunteers, who had not previously engaged in any systematic form of strength training or high level sports practice, took part in the study (age  $26.3 \pm 2.7$  years, body mass  $72.9 \pm 11.7$  kg, height,  $172.2 \pm 8.4$  cm; mean  $\pm$  standard deviation). They all gave written, informed consent and the study was conducted in accordance with the approval given by the Loughborough University Ethical Advisory Committee.

### 2.2.2.1 Testing and Training protocols

The training consisted of 8 sessions over a 3 week period (Appendix A). Sessions lasted no more than 30 minutes, where subjects performed up to 10 sets of isovelocity concentric-eccentric (CON-ECC) knee extension cycles at velocities ranging between 50 and 350°/s. The number of cycles and velocities increased as subjects adapted to the velocities and training load. Since the intensity of the training could not be quantified by counting the number of repetitions and loads, sets were time-matched. All training sessions were supervised by the investigators. The testing protocol took place on an isovelocity dynamometer with built-in gravitational torque correction (Con-Trex, CMV AG, Switzerland) over three sessions: a familiarisation session, and pre- and post-training testing sessions. In each session subjects were seated on the dynamometer with their dominant leg strapped tightly to the unpadded crank arm directly above the ankle joint using a protective moulded plastic shin guard. The anterior hip angle was set at 100° (seat was set at 80° incline). To minimise differences between the crank and joint kinematics, the rotational axis of the crank arm was aligned with the centre of the knee joint during near-maximal efforts, Figure 2.1. The familiarisation session lasted approximately 45 minutes and involved isometric and isovelocity contractions. During the testing sessions a warm up of three isometric contractions, each lasting 5 seconds, and six separate isovelocity concentric-eccentric contractions consisting of three cycles, two at each of 50, 150 and 250°/s, was performed at sub-maxima levels. This was followed by the testing protocol which consisted of maximal voluntary and supra-maximally electrically stimulated isometric and isovelocity contractions. The isometric contractions were performed at crank angles of 15° through to 75° in 15° steps (with 0° corresponding to full extension). Maximum, concentric-eccentric contractions



Figure 2.1: Position of subject and dynamometre for knee extension

were measured at 5 angular velocities: 50, 100, 150, 250 and 350°/s, according to the protocol of Yeadon *et al.* (2006) with two minutes rest intervals between trials. For the maximal isometric contractions subjects were given 5 seconds to achieve and maintain maximal torque. The same process was repeated for the electrically stimulated trials. Finally, an extra isometric trial was performed at an intermediate angle, to provide a measure of reliability and fatigue.

#### 2.2.2.2 Stimulation

Dynamometer data were sampled and recorded with Spike2 (Spike 2, CED, Cambridge, UK) software through an analogue to digital converter (CED micro 1401, CED, Cambridge, UK). The stimulator output was recorded in real time along with the torque and angle through the same ADC and software, enabling the identification of the superimposed twitches. Knee joint angles were measured with a mechanical goniometer during four isometric trials and the instantaneous crank arm angle was converted to joint angle using a linear regression equation (Pain & Forrester, 2009) (Appendix B). For each isovelocity trial the maximum eccentric and concentric isovelocity phases were

identified and the isovelocitv plateau was defined as the region where the angular velocity was within 5% of the peak value. Transcutaneous electrical stimulation of the quadriceps for the interpolated twitch technique (ITT) was achieved using a stimulator (DS7AH, Digitimer Ltd., UK) controlled by Spike 2 software. Two electrodes, a ball probe cathode of 10 mm in diameter, and a rectangular anode (90×50 mm) coated with a thin layer of conductive gel were placed at the femoral nerve and the gluteal fold respectively. The individual stimulation intensity was determined by sending single rectangular pulses (0.2 ms) of increasing strength starting from a current intensity of 30 mA, in 30 mA steps, until the twitch response plateaued. A supra-maximal stimulation level was set at 20% above this intensity and maintained for the entire session. During the electrically stimulated isometric and isovelocitv contractions a doublet supramaximal pulse was sent through the femoral nerve. For isovelocitv contractions the pulse was sent so that the twitch coincided with the optimal knee joint angle, determined from the isometric trials, and this was done for one concentric and one eccentric contraction. The timing of the pulse was regulated by Spike 2.

### 2.2.2.3 Determination of Voluntary Activation

The percentage of voluntary activation (%VA) of the quadriceps muscle was expressed by the following formula:

$$\%VA = \left( 1 - \frac{\text{superimposed twitch}}{\text{controlled twitch evoked at rest}} \right) \times 100$$

where the superimposed twitch is the torque increment noted during a maximal contraction at the time of stimulation and the control twitch is that evoked in the relaxed muscle (Shield & Zhou, 2004; Folland & Williams, 2007b). This resulted in: measured torque–angular velocity data, level of neural drive, and the determination of the three parameters associated with the DIFACT function.

### 2.2.3 Assessment of training intervention effects

In order to assess possible group changes in performance due to the training intervention the torque (T) vs. angular velocity ( $\omega$ ) curves were plotted for every subject pre- and

post-training. These were subsequently numerically integrated and the eccentric and concentric areas under the curves were compared at group level using a one-tailed Students paired t-test, as the torque output was expected to increase post-training. A repeated measures, factorial ANOVA was also used to determine the effects of velocity and training on the neural inhibition during eccentric contractions. Due to difficulties in eliciting stimulated contractions at the predetermined angles during efforts at high isovelocities it was not possible to repeat the t-test comparison for the ITT dataset due to the small number of data points obtained.

Torque vs. Angular velocity ( $T-\omega$ ) and percentage voluntary activation vs angular velocity ( $\%VA-\omega$ ) data sets per subject were obtained in both testing sessions and used in the following analysis in order to assess the training effect for every subject. The individual pre- and post-training  $T-\omega$  data sets for each subject were statistically compared by performing a nonlinear regression fit of the 7-parameter MVC torque function defined in Forrester *et al.* (2011) to each data set, first separately and subsequently to the combined pre- and post-training data sets. The fits for each profile were statistically compared using the extra-sum-of-squares F-test (equation 2.1)

$$F = \frac{(SS_{null} - SS_{alt})/SS_{alt}}{(DF_{null} - DF_{alt})/DF_{alt}} \quad (2.1)$$

where  $DF_{null}$  are the degrees of freedom for the combined pre- and post-training data set and  $DF_{alt}$  the sum of degrees of freedom from the two separate fits.  $SS_{null}$  and  $SS_{alt}$  defined as

$$SS_{null} = \sum_i^n (T_i^{combined} - T_i^{fit})^2$$

$$SS_{alt} = \sum_i^n (T_i^{pre} - T_i^{fit})^2 + \sum_i^n (T_i^{post} - T_i^{fit})^2$$

are the sum of squares for the null hypothesis, i.e. one curve fits both pre- and post-training datasets, and the respective sum of squares for the alternative hypothesis, i.e. one distinct curve per dataset. Once the F-value was obtained, the p statistic was calculated. A value of  $p \geq 0.05$  implied that the two curves were identical as there was no difference in the torque outputs between pre- and post-training sessions. On the other hand, if  $p < 0.05$  then the null hypothesis was rejected as the separate fits were significantly better hence there was significant increase in the torque output post-training (Motulski & Christopoulos, 2004). The statistical process was repeated

for the %VA- data set to establish the training effect on voluntary activation .

Normal distribution of all data sets was checked using a Shapiro–Wilk test of normality. Analysis of the Con-Trex data was performed using Matlab (The MathWorks Inc., Natick, MA, USA) and statistical analysis was performed using SPSS (SPSS Inc., Chicago, Illinois, USA). A statistical level of significance,  $p < 0.05$ , was used throughout. As the small sample size may confound the significance of the test statistic Cohens,  $d$ , was used as an effect size measure where necessary considering 0.2, 0.5, 0.8 as small, medium and large effect sizes, respectively (Cohen, 1992). Data are reported as mean  $\pm$  SD unless otherwise stated.

## 2.2.4 Evaluation of the sigmoid function

In order to establish: a) how well the DIFACT function follows the *in vivo* voluntary neural activation-angular velocity profiles and b) whether different values of the DIFACT upper bound,  $\alpha_{\max}$ , affect the statistical comparison between pre- and post-training results a non-linear regression fit of the seven parameter MVC torque function was performed to each Torque vs. Angular velocity ( $T-\omega$ ) dataset. This was done first to the individual subject results and subsequently to the combined datasets, with the DIFACT upper bound,  $\alpha_{\max}$ , set successively at 100%, 95% and 90%. This range was chosen as %VA has been shown to be as low as around 89% during slow isokinetic concentric contractions of the quadriceps and increase with increasing angular velocity (Babault *et al.*, 2001, 2002; Paillard *et al.*, 2005). The fits for each subject were again statistically compared using the extra-sum-of-squares F-test to establish whether the training intervention had a statistically significant effect on any of the subjects.

The goodness of fit of the resulting maximal voluntary torque-velocity curves was assessed: The values of the determination coefficient,  $R^2$ , and RMS difference scores from each fit were calculated for every  $\alpha_{\max}$  value. A mixed two-way ANOVA was used to assess any differences in the  $R^2$  and RMS scores per  $\alpha_{\max}$  value both within and between the two testing sessions. The same process was repeated for fitting the DIFACT function to the %VA values of both testing sessions. The  $R^2$  values obtained from the two fits are indicative of how well the fitted functions reproduce the raw  $T-\omega$  and %VA- $\omega$  profiles and show whether or not the DIFACT function successfully

follows the *in vivo* voluntary neural activation-angular velocity profiles. The degree that the RMS and  $R^2$  values change for different values of  $\alpha_{\max}$  is a measure of the robustness of the DIFACT function. In order for the DIFACT function to be robust no significant differences between the results of the fits with the different  $\alpha_{\max}$  values should be observed within the pre-training data, or in the post-training data.

The curve fit and statistical analysis was performed using Matlab (The MathWorks Inc., Natick, MA, USA). A statistical level of significance,  $p < 0.05$ , was used throughout.

## 2.3 Results

### 2.3.1 Training Study

The comparison of the numerically integrated  $T-\omega$  plots using the Students paired  $t$ -test (one-tailed) showed significant increase ( $t = 3.2$ ,  $p < 0.05$ ,  $d = 1.3$ ) between pre- and post-training data (Figure 2.2). Dividing the curve into eccentric and con-

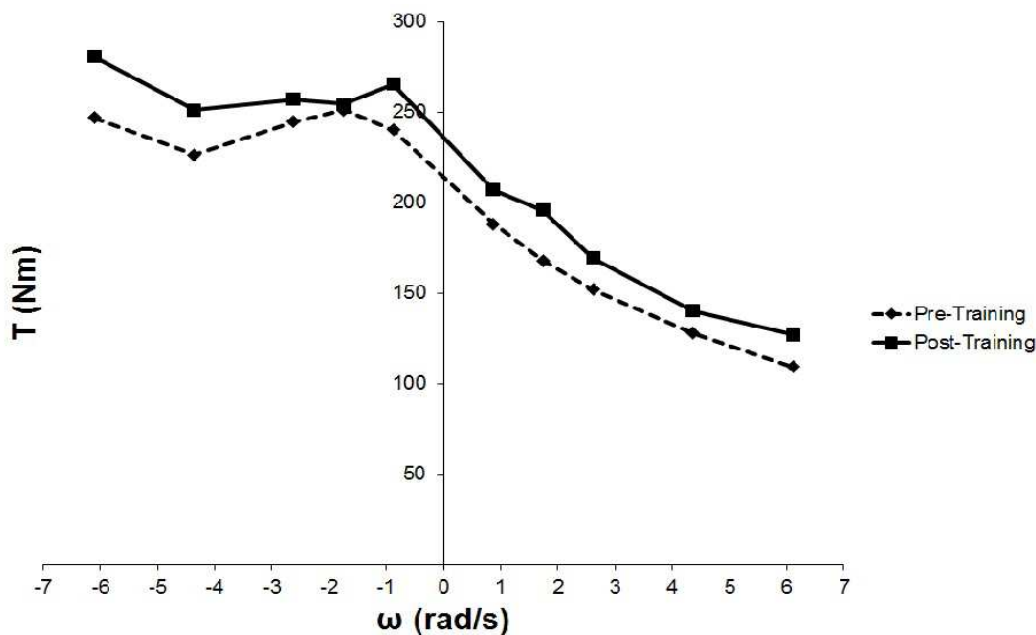


Figure 2.2: Plot of average peak torque outputs per angular velocity

centric quadrants revealed that there was significant increase in the area under the  $T-\omega$  curve post training for both the eccentric quadrant,  $t = 2.0$ ,  $p < 0.05$ ,  $d = 0.82$  and the concentric quadrant,  $t = 2.3$ ,  $p < 0.05$ ,  $d = 0.93$ . In terms of the repeated measures, factorial ANOVA there was a significant main effect for time ( $F = 6.6$ ,  $p < 0.05$ ). There was no significant,  $p \geq 0.05$ , time  $\times$  velocity interaction. Contrasts were performed comparing all isovelocities to a baseline isovelocity ( $350^\circ/\text{s}$ ) during eccentric contractions. These revealed a significant,  $p < 0.05$ , increase in peak torque output obtained post-training, at  $350^\circ/\text{s}$  during eccentric contractions with respect to torque output from  $150^\circ/\text{s}$  (Table 2.1).

The results of the MVC torque function fit to the individual raw  $T-\omega$  datasets are

Table 2.2: Mean peak torque values obtained at 150 and 350°/s during pre- and post-training sessions for both contraction modes.

$\omega(^{\circ}/s)$	Pre-Training Torque (Nm)		Post-Training Torque (Nm)	
	ECC	CONC	ECC	CONC
<b>50</b>	240	188	265	207
<b>100</b>	245	168	254	196
<b>150</b>	245	152	257*	169
<b>250</b>	226	128	251	140
<b>350</b>	247	109	280*	127

\*Significant difference ( $p < 0.05$ ) in torque output between 150 and 350/s post-training

Table 2.3: Results obtained from fitting the MVC torque function and a 3rd degree polynomial to the raw T- $\omega$  and %VA- $\omega$  data sets respectively.

	MVC fit		%VA fit	
	F-ratio	p-statistic	F-ratio	p-statistic
<b>Subject 1</b>	0.92	0.54	1.35	0.33
<b>Subject 2</b>	5.91	0.01	1.93	0.19
<b>Subject 3</b>	1.58	0.27	0.67	0.63
<b>Subject 4</b>	4.95	0.02	4.2	0.024
<b>Subject 5</b>	12.9	<0.001	3.8	0.07
<b>Subject 6</b>	2.62	0.1	0.94	0.48

summarized in Table 2.3. Applying the extra-sum-of-squares F-Test on the seven parameter MVC function fit to the torque-angular velocity dataset, for  $\alpha_{\max} = 100\%$ , showed that 3 out of 6 subjects had a significant ( $p < 0.05$ ) higher torque output post-training. The same outcome was obtained when the  $\alpha_{\max}$  values were set equal to 95% and 90%. The fits of the MVC torque function to the T- $\omega$  data set of a subject are illustrated in Figure 2.3. The respective global fit of the MVC function to the combined pre- and post-training data sets of all subjects showed a significant increase

in the torque output post-training ( $F = 2.06$ ,  $p < 0.05$ ). The global fit of a 3rd degree

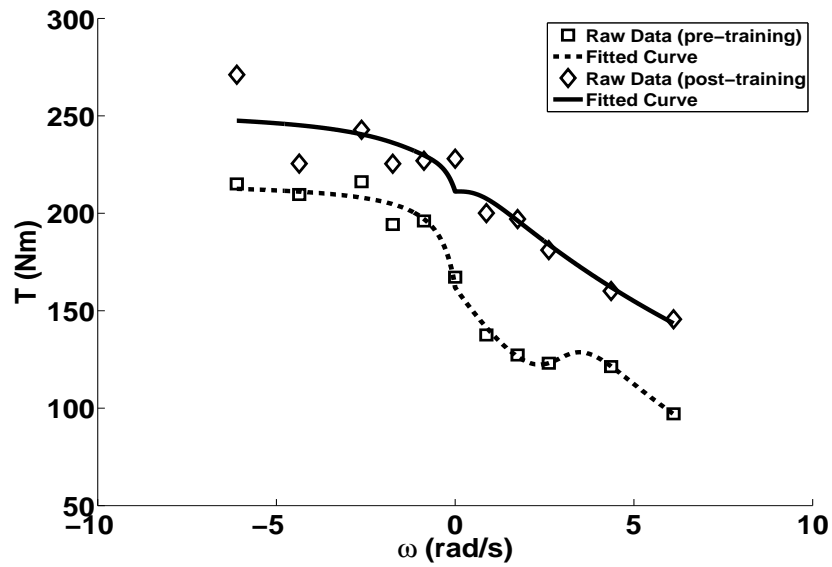


Figure 2.3: Example plots from Subject 5 of the pre- and post-training  $T-\omega$  raw data and separately fitted function for each data set.

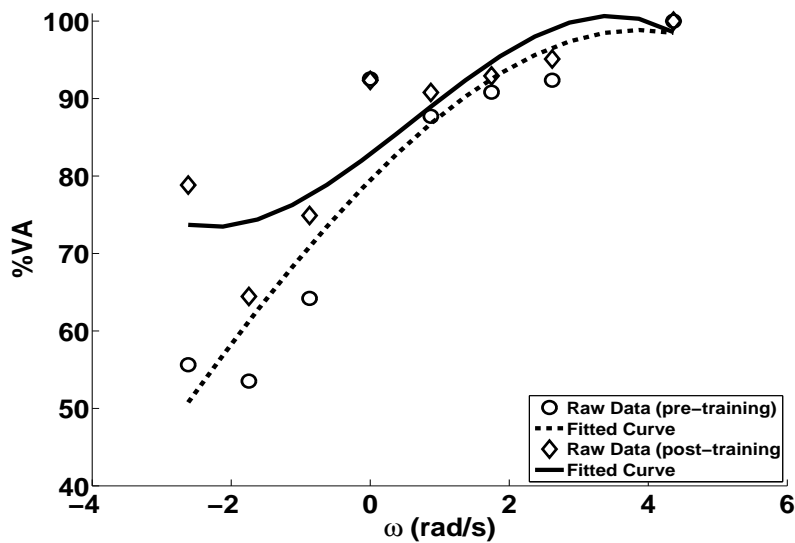


Figure 2.4: Example plots from Subject 5 of the combined pre- and post-training  $\%VA-\omega$  data and the fitted 3rd degree polynomial.

polynomial (Figure 2.4) to the  $\%VA-\omega$  datasets of every subject (Table 2.3) revealed only one significant difference in the  $\%VA$  values pre- and post-training. However, the combined global curve fit showed a significant increase in the  $\%VA$  post-training ( $F =$

3.3,  $p < 0.05$ ). The fits of the MVC torque function and the 3rd degree polynomial on the  $T-\omega$  and  $\%VA-\omega$  datasets, for all subjects, are illustrated in Appendices K and L respectively.

### 2.3.2 Evaluation of sigmoid function

There was no significant difference between the  $R^2$  values of the three fits with different  $\alpha_{\max}$  values for both pre- and post-training datasets ( $p = 0.95$  &  $p = 0.99$  respectively) for any of the six subjects. The mean  $R^2$  values across all subjects (group mean) were 0.95 for pre-training (range 0.84 to 0.99) and 0.96 for post-training (range 0.89–0.99). Additionally, there was no significant difference ( $p \geq 0.05$ ) in the group mean  $R^2$  scores

Table 2.4: RMS differences for the 7-parameter torque function fit to the  $T-\omega$  data for  $\alpha_{\max} = 100\%$ ,  $95\%$ ,  $90\%$ ,

$\alpha_{\max}(\%)$	Pre training			Post training		
	100%	95%	90%	100%	95%	90%
<b>Subject 1</b>	41.2	45.7	45.6	8.8	8.5	8.5
<b>Subject 2</b>	11.2	13.8	11.3	4.7	5.3	5.3
<b>Subject 3</b>	14.5	17.2	14.4	26.6	27.2	26.7
<b>Subject 4</b>	8.0	8.0	8.0	7.0	7.0	7.0
<b>Subject 5</b>	7.6	7.7	12.1	15.1	15.1	15.1
<b>Subject 6</b>	17.5	24.4	16.0	20.5	20.5	20.5

between sessions. Similarly, there was no significant difference between the RMS scores of the three fits with different  $\alpha_{\max}$  values for any of the six subjects (Table 2.4) either pre- or post-training ( $p = 0.92$  &  $0.96$  respectively). The RMS score variation was much greater between subjects than any variation due to changing  $\alpha_{\max}$  within subjects. Group mean RMS scores were 18 (range 7.6–45.7) and 13.9 (range 5.3–26.7) for pre- and post-training sessions respectively. There was no significant difference ( $p \geq 0.05$ ) in the group mean RMS scores between the two sessions.

When the DIFACT function was fitted on the  $\%VA$  dataset the  $R^2$  values per testing

Table 2.5: Mean %VA values and standard deviations (SD), pre- and post-training, for each angular velocity (deg/sec).

<b>Angular Velocity</b>	<b>Mean %VA <math>\pm</math> SD</b>	
	<b>Pre training</b>	<b>Post training</b>
<b>-250</b>	67.4 $\pm$ 12.60	68.5 $\pm$ 11.90
<b>-150</b>	63.6 $\pm$ 12.60	72.0 $\pm$ 7.50
<b>-100</b>	64.8 $\pm$ 20.30	69.7 $\pm$ 11.70
<b>-50</b>	67.1 $\pm$ 10.36	76.1 $\pm$ 4.36
<b>0</b>	86.3 $\pm$ 9.15	89.2 $\pm$ 3.49
<b>50</b>	85.5 $\pm$ 5.17	88.7 $\pm$ 3.93
<b>100</b>	88.6 $\pm$ 7.88	94.1 $\pm$ 2.58
<b>150</b>	91.3 $\pm$ 4.24	94.7 $\pm$ 1.33

Table 2.6: Mean  $\alpha_{\min}$  values in % and SD, pre- and post-training, for each value of  $\alpha_{\max}$

$\alpha_{\max}$ (%)	<b>Mean %VA <math>\pm</math> SD</b>	
	<b>Pre training</b>	<b>Post training</b>
<b>100</b>	62 $\pm$ 0.04	67 $\pm$ 0.05
<b>95</b>	60 $\pm$ 0.02	64 $\pm$ 0.04
<b>90</b>	61 $\pm$ 0.02	63 $\pm$ 0.05

session were not significantly different ( $p \geq 0.05$ ), however, the post-training group mean  $R^2$  score, 0.68, was significantly ( $p < 0.05$ ) higher than the pre-training value, 0.57. The respective ranges were 0.32–0.84 and 0.32–0.89. Again the  $R^2$  score variation was much greater between subjects than any variation due to changing  $\alpha_{\max}$  within subjects. Similarly, there was no significant difference between the RMS scores of the three fits, with different  $\alpha_{\max}$  values, to the %VA– $\omega$  profiles for either pre- or post-training ( $p = 0.98$  &  $0.63$  respectively).

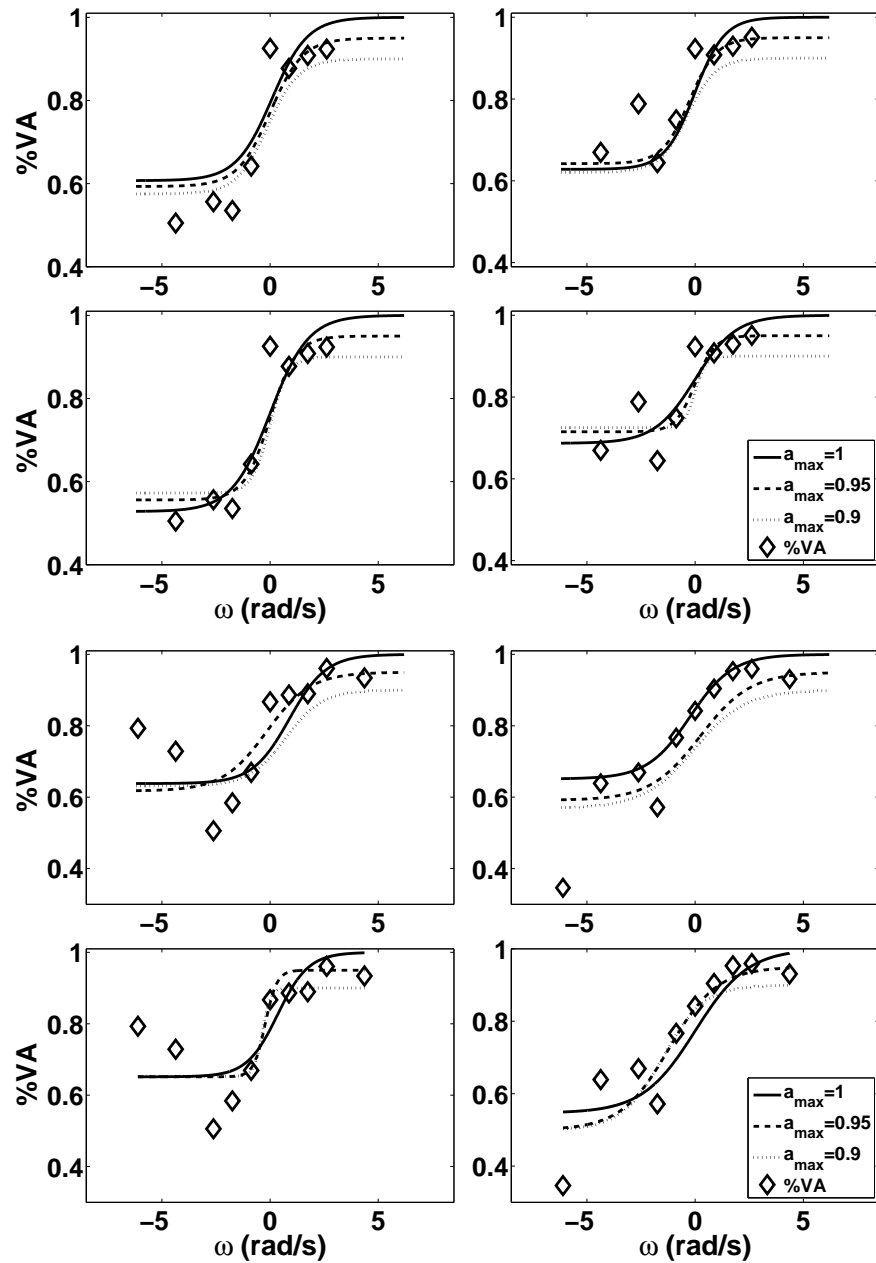


Figure 2.5: The four graphs show how the DIFACT function compares with the raw %VA- $\omega$  data set for  $\alpha_{\max} = 100\%$ ,  $95\%$ ,  $90\%$  for Subjects 2 (top) and 4 (bottom). Graphs on the left correspond to the pre-training values and on the right to the post-training ones. The top two graphs, per subject, show the DIFACT function from the seven parameter fit superimposed on the %VA- $\omega$  data set. In the bottom two graphs the DIFACT function has been fitted to the %VA- $\omega$  data set directly and again plotted against the respective %VA- $\omega$  values.

The RMS score variation was greater between subjects than any variation due to changing  $\alpha_{\max}$  within subjects. The group mean RMS post-training score, 0.09 (range 0.04–0.15) was significantly ( $p < 0.05$ ) lower than the respective pre-training mean RMS score (0.11, range 0.062–0.182). Mean %VA values across eight different isoveLOCITIES showed a general rise from mid 60s to low 90s but with post-training generally being 5% higher (Table 2.5). Mean  $\alpha_{\min}$  was similar to the lowest %VA values at around 60% for pre-training and 64% for post training (Table 2.6).

Figure 2.5 illustrates how the DIFACT function obtained from fitting the seven parameter function to the torque-angular velocity dataset of Subjects 2 and 4 follows the raw ITT-angular velocity dataset for the three  $\alpha_{\max}$  values and how this compares against the DIFACT function fit to the ITT-angular velocity dataset.

## 2.4 Discussion

### 2.4.1 Training Study

This study aimed to determine whether short term high velocity eccentric strength training of the quadriceps would lead to an increase in torque and a concurrent decrease in the inhibitive action of the tension limiting mechanism observed during maximal eccentric contractions of skeletal muscle (Westing, 1988; Westing *et al.*, 1990; Dudley *et al.*, 1990; Pain & Forrester, 2009). At the end of the training protocol subjects achieved a significant,  $p < 0.05$ , increase in overall torque output during both, concentric and eccentric contractions; a result that was established using two different statistical approaches, namely the Student's *t*-test and the extra-sum-of-squares *F*-test. Large effect sizes were found for all comparisons made by Students *t*-test. A subject specific comparison showed that three out of the six subjects demonstrated a significant increase,  $p < 0.05$ , in the torque output produced across the range of angular velocities (Table 2.3). These results indicate that the training protocol was successful in improving the torque output of the subjects during MVC contractions. Regarding the effect of the training protocol on neural activation and the action of the tension limiting mechanism, a significant increase,  $p < 0.05$ , in the %VA post-training was achieved as well as a significant,  $p < 0.05$ , increase in the peak torque outputs dur-

ing eccentric contractions at 350°/s with respect to torque outputs from 150°/s. The latter results are indicative of increased neural activation post-training and a possible reduction in the inhibitive action of the tension limiting mechanism.

These results are in, at least partial, agreement with previous isovelocity training studies. Specifically, Caiozzo *et al.* (1981) and Coyle *et al.* (1981) also reported significant increases in the torque output during concentric contractions of the quadriceps after following isovelocity strength protocols that included 2 different isovelocities. Contrary to the current study, however, neither the training nor the testing protocols included eccentric contractions therefore their training effect was not quantified. Hortobagyi *et al.* (1996), Higbie *et al.* (1996) and Seger & Thorstensson (2004) compared the effects of pure concentric and eccentric isovelocity strength training on torque output whereas Tesch *et al.* (2004) assessed the force output of the knee extensors after a five-week training programme performed on an inertia-based apparatus. All reported significant,  $p < 0.05$ , torque increases post-training in agreement with the current study. Similar findings were reported by Krentz & Farthing (2010) and Baroni *et al.* (2013) who observed significant increase in torque output of the biceps brachii and quadriceps after two and four weeks eccentric isokinetic training respectively. Therefore, with respect to the effect of isovelocity training on the torque output, the results presented here confirm previous observations.

The next question the current study sought to answer regarded the nature of the underlying reason behind the increase in the torque output post-training, and more specifically whether this was due to an increase in neural activation and a possible concomitant decrease in neural inhibition. The significant increase in the %VA value post-training suggests an increase in the neural activation of the quadriceps muscle. This is in line with findings by Hortobagyi *et al.* (1996), Higbie *et al.* (1996) who reported increased EMG activity of the quadriceps muscle post-training. Aagaard *et al.* (2000); Aagaard *et al.* (2002) also reported an increase in the neural activation and strength levels after a 14-week strength training regime with free weights focusing on the quadriceps and soleus muscles respectively. However, the aforementioned training interventions lasted for 10 weeks or more and included a minimum of 30 training sessions. Consequently, they also elicited a number of physiological changes on the quadriceps muscle such as an increase in the cross-sectional area of the muscle (Higbie

*et al.*, 1996) or increased number of type II fibres Hortobagyi *et al.* (1996). Aagard *et al.* (2000) did not test for physiological changes post-training but the duration and nature of training made their occurrence very likely (Staron *et al.*, 1994). Therefore, it is not clear whether the observed increases in EMG values were only due to increased neural activation and reduction of neural inhibition but also due to increased muscle hypertrophy.

More recently, Krentz & Farthing (2010) and Baroni *et al.* (2013) reported significant increases in the neural activity, quantified by EMG measurements, of the biceps brachii and quadriceps within the first two and four weeks respectively of eccentric isokinetic training. They also reported increased muscle thickness and cross-sectional area of the respective muscle groups which raises the question whether the observed torque increase in the current study was predominantly due to increased neural input or there were training-elicited morphological changes of the knee extensors that also contributed to the torque output. This is a question that cannot be answered definitively as the study did not quantify the training effect on muscle morphology. However, when considering the various issues with measurement of muscle CSA (Folland & Williams, 2007a), the prevalent concept in the literature that neural adaptations are dominant during the first 6–8 weeks of training (Staron *et al.*, 1994; Corriander & Tesch, 1990) and the fact that in the current study only 8 training sessions in three weeks took place, it is rather likely that the observed increase in the torque output post-training can be attributed almost exclusively to neural factors such as increased muscle neural activation, more efficient recruitment and, decreased neural inhibition .

The latter effect would manifest itself on one hand through a greater increase in torque output during eccentric contractions compared to concentric post-training and also a reversal of the observed torque plateau during eccentric contractions at high velocities *in vivo* (Westing, 1988; Westing *et al.*, 1990, 1991; Dudley *et al.*, 1990; Weber & Kriellaars, 1997; Seger & Thorstensson, 2004). The observed torque increase in this study was not higher post-training during eccentric contractions compared to concentric. However the results of the repeated measures ANOVA showed that whereas the subjects torque outputs tended to plateau at 150°/s during eccentric contractions pre-training they do not appear to do so post-training. This is possibly a significant finding as it offers an indication that the neural inhibition may, indeed be reversible.

However, marked changes in neural inhibition may need longer periods of training to appear if the neural factors are present to act against overloading the musculoskeletal system as to safely increase eccentric strength concomitant increases in resistance to loading of the tendons, bones, and other structural tissues would be necessary.

#### **2.4.1.1 Conclusion**

Concluding, it has been shown that performing an 8-session, strength training protocol on an isovelocity dynamometer, consisting of fast eccentric and concentric contractions performed at isovelocities of up to  $350^\circ/\text{s}$ , produced notable increases in torque output for angular velocities all velocities and both modes of contraction. This is mainly attributed to an increase in muscle activation and, a decrease in the inhibitive action of the tension-limiting mechanism observed during fast eccentric and slow concentric contractions of the quadriceps group of muscles.

#### **2.4.1.2 Limitations and future work**

Limitations of this study include, the low subject numbers, the difficulty of eliciting consistent electrical pulses at high isovelocities during stimulated contractions and possible learning effects from the repeated use of the dynamometer by the subjects. The low number of subjects was partly addressed by doing both group by group and subject by subject comparisons. Since the familiarization session protocol was designed so as to minimize learning effects and their confounding influence (Madsen, 1996; Lund *et al.*, 2005) they should not be a contributing factor in the performance of the subjects.

Future work should sought to address the main limitations of the current study specifically the relatively small sample size and the non-quantification of training-induced morphological changes to the knee extensors, such as the cross sectional area of the muscle, by means of ultrasound or MRI techniques. EMG recordings of the muscle activity during stimulated and MVC contractions could be taken in order to obtain additional experimental information on the muscle activity other than the %VA measured by means of the ITT. The latter should be also expanded, if possible, to include the entire span of isovelocities. This will allow muscle activity to be assessed via two experimental (EMG, ITT) and one theoretical ( $\alpha_{min}$ ) methods. Finally the training

protocol can also be expanded to other muscle groups that have shown reduced activation during fast eccentric contractions such as the knee flexors (Pain *et al.*, 2013) or biceps brachii.

## 2.4.2 Evaluation of sigmoid function

The aim of this work was to determine how well the three-parameter exponential differential activation function DIFACT reproduces the in-vivo  $T-\omega$  and  $\%VA-\omega$  profiles and whether changing the value of the maximum activation level,  $\alpha_{max}$ , in DIFACT would affect its robustness Pain & Forrester (2009). Results show that the MVC torque function reproduces the  $T-\omega$  raw data set very well irrespective of the  $a_{max}$  value. The DIFACT function is also successful in reproducing the raw  $\%VA-\omega$  data set albeit not to the same extent as the torque function. This is, probably, due to the increased variability in the  $\%VA$  values of some subjects obtained from eccentric contractions, mainly during the pre-training session. A number of factors may have been the cause of the observed variability such as the expectation of noxious stimuli Shield & Zhou (2004) or a possible variation between trials in the joint angle where the stimulus was applied (Tillin *et al.*, 2012). However, the DIFACT function appears to behave consistently irrespective of the range of  $\%VA$  values or the presence of outlier points (Figure 2.5).

In previous studies (Yeadon *et al.*, 2006; Pain & Forrester, 2009; Forrester *et al.*, 2011), the maximum activation level of DIFACT,  $\alpha_{max}$ , was assumed to be equal to 100%, corresponding to full activation, 100%, of the muscles at high concentric velocities. However, activation deficits of 5-30% have been reported during high concentric contractions (Babault *et al.*, 2001, 2002; Paillard *et al.*, 2005) in agreement with the results of this study showing that the muscles do not attain full activation. Using  $\alpha_{max}$  values between 90% and 95% might be a better representation of the maximum activation of muscles during voluntary efforts. In the current study an  $\alpha_{max}$  value of 100% appears to be the appropriate value to use for the post-training as four subjects achieved the lowest RMS scores for that value post-training and there are strong indications of increased neuromuscular activation, due to the training protocol (Table 2.4). For the pre-training datasets an  $\alpha_{max}$  value of 95% seems to be more suitable as the over-

all activation is lower, suggesting that setting the  $\alpha_{\max}$  at 100% may be excessive. However, setting  $\alpha_{\max} = 90\%$  is likely too low to account for fast concentric contractions where the muscle activation appears to be enhanced compared to other types of contraction (Tillin *et al.*, 2012) and surpassed the values reported here (Table 2.3). Given this and the robustness of the fitting methods, setting  $\alpha_{\max}$  to 100% in most cases is likely an assumption that will not introduce any meaningful errors. Indeed, when the mean raw torque outputs at  $350^\circ/\text{s}$  are compared against the mean values of the 7-parameter MVC function fits, at  $350^\circ/\text{s}$ , with  $\alpha_{\max}$  set at 100% and 95%, the differences were 3.7% and 1.3% respectively for the pre-training results and 0.9% and 0.8% post-training. Moreover, the mean  $\alpha_{\min}$  value of 67% compares very well with the mean %VA value of 69% at  $-250^\circ/\text{s}$  (a velocity where the inhibition would be significant) post-training suggesting the use of a higher  $\alpha_{\max}$  value for analysing post-training datasets. The higher post-training  $R^2$  values imply an improved fit in line with the expectation of a more consistent activation pattern and activation profile, with respect to angular velocities, post-training.

Overall the mean  $R^2$  values of the DIFACT fit to the %VA- $\omega$  pre- and post-training (0.57 v 0.68), the agreement between the  $\alpha_{\min}$  and %VA values at  $-250^\circ/\text{s}$ , the qualitative agreement between the fitted DIFACT function and the raw datasets observed in Figure 2.5 suggest that the neural inhibition (Westing, 1988; Dudley *et al.*, 1990; Weber & Kriellaars, 1997) may be represented by means of an S-shaped function such as the DIFACT function. Concluding, it has been shown that the exponential DIFACT function remains robust for various values of the maximum level of activation value,  $\alpha_{\max}$ , and it represents well the neural inhibition of the knee extensors during fast eccentric and slow concentric contractions.

# 3 Hamstrings–Quadriceps ratio

## 3.1 Introduction

### 3.1.1 Hamstring strain injuries

Hamstring strain injuries (henceforth HSIs) are common in a number of sports such as Australian and American football, rugby, soccer and track and field. Woods *et al.* (2004) in a study that involved 91 professional clubs from the English Premier and Football leagues and lasted over a period of two seasons (1997–1999) reported that on average 90 days and 15 matches were missed per club per season due to hamstring injuries whereas (Ekstrand *et al.*, 2011a,b) found that they accounted for 37% of all muscle injuries and 12% of all injuries. In Rugby Football Union HSIs resulted in 17 days of missed time per athlete (Brooks *et al.*, 2005, 2006) whereas 21 matches were lost per season for each club in Australian Football League (Bennel *et al.*, 1998; Orchard & Stewart, 2002; Opar *et al.*, 2012). Similar findings were reported by Feeley *et al.* (2008) in the case of American Football league where hamstring injuries had the highest occurrence rate of all strain injuries resulting on 8.3 days lost on average over a period of 10 seasons. In track and field HSIs accounted for 23.3% of all injuries during the Daegu 2011 IAAF World Championships (Alonso *et al.*, 2012) and were the most occurring in the competition. A similar value, 26% was reported by Drezner *et al.* (2005).

These findings suggest that HSIs are a cause of significant financial loss to clubs and sponsors, with Woods *et al.* (2002) reporting an average loss of 74 million pounds to English Premiership and Championship clubs for the 1999–2000 season alone, and of course are detrimental to players' and athletes' performance and career. Therefore it is important that preventive measures are taken that will enable trainers and coaches to identify potential risk factors for HSIs and apply suitable interventions that will prevent the injury from occurring. Yet, despite the number of studies on the problem and the plethora of potential risk factors suggested the number of HSIs has not declined in recent decades (Opar *et al.*, 2012; Orchard & Stewart, 2002; Brooks *et al.*, 2006;

Alonso *et al.*, 2010, 2012; Elliott *et al.*, 2011; Ekstrand *et al.*, 2011b; Woods *et al.*, 2004; Freckleton & Pizzari, 2013) indicating a possible lack of understanding of the root causes of the injury.

### 3.1.2 Mechanism of hamstring injury

However, the mechanism of hamstrings injury is not yet clear. There is an ongoing debate on whether hamstring injuries occur during the swing or the stance phase of the gait cycle and whether muscle strain or the magnitude of the eccentric force is the causative factor in hamstring strain injuries (Chumanov *et al.*, 2011; Yu *et al.*, 2008).

Initially it was hypothesized that the hamstrings were more susceptible to injury during the early stance phase where they act concentrically to resist the high hip extension forces and decrease the horizontal braking GRFs (Mann, 1981; Orchard, 2012). However, this was contrary to the later assertion that muscle injuries are caused when muscles are under excess strain during contraction and are not a function of muscle force (Lieber & Fridén (1993); Garrett (1990)). Subsequently, a number of studies identified the late swing phase as the likely period where HSIs are likely to occur (Chumanov *et al.*, 2007, 2011; Thelen *et al.*, 2005b,a; Heiderscheit *et al.*, 2005). During that period the hamstrings are eccentrically contracting in order to decelerate the swinging lower limb (Novacheck, 1998). This creates a high tensile force on the highly strained muscle that increases the risk of injury (Lieber & Fridén, 1993). Schache *et al.* (2013) and Higashihara *et al.* (2014) showed that peak musculotendon length of the long head of the biceps femoris muscle coincided with its peak EMG activation and that the magnitude of activation increased with sprinting speed (Schache *et al.*, 2013) a finding supported by Thelen *et al.* (2005b). Chumanov *et al.* (2007) used a forward dynamics sprinting simulation to show that the observed increase in muscle activation with increasing speed was likely due to the increased negative work the muscles produced. They hypothesized that the large amounts of negative work done repeatedly could induce micro-damage to the muscle tissue that under conditions of excessive stretch may induce a strain injury. The same group extended their model analysis to include the stance phase in a subsequent study Chumanov *et al.* (2011). Their analysis showed that although the hamstrings are substantially loaded during both the stance and swing

phases the muscle load did not increase with speed during the stance phase nor any negative work produced.

However, although most findings seem to support the hypothesis that HSIs are more likely to occur during late swing they are either based on models or on biomechanical analyses of running trials from asymptomatic subjects. The deviations from normal stride pattern or muscle function that lead to injury can only be hypothesized unless an actual *in-vivo* strain injury is captured and recorded. Heiderscheit *et al.* (2005) and Schache *et al.* (2009) serendipitously captured an acute HSI during sprinting trials on a treadmill. By analysing the biomechanical data produced during the trial they concluded that the injury most likely occurred during the late swing phase. Those studies came the closest to providing direct evidence about the pathomechanics of HSI.

Yet, despite the bulk of evidence pointing the swing phase as the most likely time of injury Yu *et al.* (2008) suggested that it would be possible for HSI to happen during late stance phase when, according to their findings, the hamstrings undergo an additional eccentric contraction where the maximum musculotendon length was reached at a higher elongation velocity than during the swing phase, thus inducing excessive strain on the muscle. A similar injury mechanism was proposed by Orchard *et al.* (2002) for a calf strain. However, Orchard himself strongly argued in favour of the early stance phase (Orchard, 2012) as the highest risk period arguing that there is little risk of muscle strains during open chain activities which involve stretch and high angular velocities joint extension.

### **3.1.3 Risk factors**

It seems therefore that a consensus regarding the exact moment of injury is unlikely to be reached in the near future and it seems that the disagreement extends to the factors that may place an individual at risk of such an injury. A number of both modifiable and non-modifiable risk factors have been proposed for hamstrings strain injuries including age, previous injury, ethnicity, flexibility, fatigue and strength (Opar *et al.*, 2012). Despite the plethora of risk factors proposed only age and previous injury have shown high correlation with hamstrings injuries (Freckleton & Pizzari, 2013).

Flexibility, fatigue and ethnicity have been correlated to HSIs however, the evidence is inconclusive either due to the small number of studies done on the subject, in the case of ethnicity and fatigue (Woods *et al.*, 2004; Brooks *et al.*, 2006), or due to the variety of protocols employed that make interpretation and comparison of results across studies difficult (Freckleton & Pizzari, 2013; Foreman *et al.*, 2006). Finally strength, or the lack of it, has long been considered a risk factor for HSIs (Burkett, 1969) and most evidence agrees with that assertion (Prior *et al.*, 2009; Foreman *et al.*, 2006) however, there is still some controversy on the issue. Most of this controversy stems from some of the methods employed to assess hamstring strength imbalances and specifically those that express it relative to the strength of its antagonist, the quadriceps. A variety of hamstring to quadriceps strength ratios (Opar *et al.*, 2012) have been proposed and employed to assess hamstring's relative strength at various velocities, angles and modes of contraction with, often, conflicting results as will be discussed in the next section.

### 3.1.4 Conventional and Functional H:Q Ratios

The H:Q ratio was first used to assess the strength of the hamstrings muscle relative to the quadriceps (Heiser *et al.*, 1984) and to identify strength imbalances between the two muscle groups. The rationale was that a lower H:Q ratio suggested that the hamstrings muscles are not strong enough to counteract, by contracting eccentrically, powerful extensions of the knee joint during concentric contractions of the quadriceps, thus, being susceptible to injury (Osternig *et al.*, 1986; Baratta *et al.*, 1988).

Initially, the H:Q ratio was calculated by dividing the peak torque developed during concentric contraction of both the hamstrings and the quadriceps, known as the conventional H:Q ratio,  $H:Q_{con}$ , (Heiser *et al.*, 1984), however, such an approach has two significant limitations. Firstly, the maximum torque attained during hamstring concentric contraction is compared to the maximum torque attained during quadriceps concentric contraction. This may not reflect the functional role of the hamstrings during knee extension which is to resist the motions produced due to the concentric agonist contraction of the quadriceps via eccentric co-activation and development of serial elastic tension (Osternig *et al.*, 1986; Coombs & Garbutt, 2002). Secondly, in most cases the hamstring and quadriceps maximum torque values either are not measured at the

same angle of knee joint extension/flexion (angle-specificity) thus failing to account for changes in muscle length (Tourny-Chollet & Leroy, 2002; Ergun *et al.*, 2004; Iga *et al.*, 2009) or when they are the respective ratio values are insensitive to changes in angular velocity and angle of contraction (Aagard *et al.*, 1998; Coombs & Garbutt, 2002; Croisier, 2004). To better represent the eccentric action of the antagonist, hamstring, muscle during knee extension the “functional” H:Q<sub>fun</sub> ratio was proposed which is calculated by dividing the peak torque developed during the eccentric contraction of the hamstrings with the peak torque developed during the concentric contraction of the quadriceps at the same angular velocity of contraction (Aagard *et al.*, 1995, 1998).

Contrary to H:Q<sub>con</sub>, the H:Q<sub>fun</sub> ratio changes throughout the range of motion (ROM) during knee extension. As the knee joint moves through its ROM from full flexion to extension there is an observed decrease in the concentric torque output of the quadriceps with increasing angle and angular velocity of extension whereas the respective eccentric torque output of the hamstrings remains relatively stable thus producing H:Q<sub>fun</sub> values that increase with increasing angular velocity and angle of extension (henceforth expressed as  $\omega$  and  $\theta$  respectively)(Aagard *et al.*, 1995, 1998; Evangelidis *et al.*, 2015). This in agreement with the integrated electromyographic (iEMG) activity results of Osternig *et al.* (1986) that showed a higher degree of hamstring’s co-activation in comparison to the quadriceps (8–58% vs 5–8% respectively) that increased with increasing  $\omega$  and  $\theta$ .

### 3.1.5 H:Q<sub>con</sub> and H:Q<sub>fun</sub> as injury indicators

Both, the functional and conventional ratios have been used as indicators of potential HSI however with conflicting results. More specifically whereas a number of studies have shown the existence of a correlation between H:Q ratios and injury risk others have come to contrary conclusions. In order to simplify the following discussion the ratio *cut-off value* is defined at this point as the value of the H:Q ratio below which the risk of hamstring injury increases significantly.

In studies on Australian rules football Orchard *et al.* (1997) determined the H:Q<sub>con</sub> ratios of 37 professional Australian rules football players at 60, 180 and 300°/s before the start of the competitive season. Six athletes sustained HSIs during the course of the

season and t-tests showed that those athletes had significantly lower ( $p < 0.05$ ) H:Q<sub>con</sub> values at 60°/s on the injured limb than on the uninjured (mean  $\pm$  SD:  $0.55 \pm 0.065$  vs  $0.662 \pm 0.071$  respectively). In a similar prospective study Cameron *et al.* (2003) followed the progress of a group of 20 professional Australian rules footballers for two seasons. Six subjects sustained one or more significant HSIs and again it was found that those athletes had significantly lower H:Q<sub>con</sub> ratios at 60°/s than uninjured athletes ( $0.59 \pm 0.03$  vs  $0.69 \pm 0.09$  respectively) suggesting a strong association between low H:Q<sub>con</sub> values and subsequent hamstring injury. However, no such association was found by Bennel *et al.* (1998) in their prospective study of 102 professional and amateur Australian rules footballers that included pre-season measurements of H:Q<sub>con</sub> and H:Q<sub>fun</sub> ratios at 60 and 180°/s as there were no significant differences between injured and uninjured players for any of the measured variables.

Similar studies in other sports also confounded the issue. Yeung *et al.* (2009) obtained H:Q<sub>con</sub> and H:Q<sub>fun</sub> ratio values of 44 sprinters at 60, 180 and 240°/s during pre-season training for the 2004–05 season. Twelve athletes sustained HSIs during the season. There were no significant differences between injured and uninjured groups in any of the ratio or peak torque values however, when a Cox regression analysis was performed it was found that a H:Q<sub>con</sub> value of 0.6 or lower, measured at 180°/s, increased the risk of HSI by 17 times. It was also noted that had the authors chosen a slightly higher cut-off value for the H:Q<sub>fun</sub> ratio (0.98 instead of 0.96) then the difference in the H:Q<sub>fun</sub> ratio values, at 180°/s, between injured and uninjured athletes would have been significant.

In one of the largest prospective studies that have been done Croisier *et al.* (2008) followed the injury history of 462 professional football players over a 5 year period. During pre-season testing they established peak torque values for hamstrings and quadriceps, H:Q<sub>con</sub> values at 60 and 240 °/s and a mixed H:Q<sub>fun</sub> where hamstring peak torque obtained during eccentric contractions at 30°/s was divided by quadriceps peak torque produced by concentric contractions at 240°/s. They showed that subjects with a H:Q<sub>fun</sub> ratio value of 0.98 or lower had 4.66 times greater risk of sustaining a HSI than subjects with no strength imbalances and also that the mixed H:Q<sub>fun</sub> ratio was more sensitive to muscle imbalance as it picked up 87% of the players with imbalance compared to the H:Q<sub>con</sub> ratio that picked up 30%.

Therefore, although there exists significant evidence supporting a correlation between low H:Q values and HSI this is not conclusive (Foreman *et al.*, 2006; Freckleton & Pizzari, 2013; Opar *et al.*, 2012; Coombs & Garbutt, 2002). Surprisingly, the correlation becomes weaker when the H:Q<sub>fun</sub> ratio alone is considered as a risk indicator despite the fact that theoretically it describes the eccentric braking action of the hamstrings at the end of the swing phase of the gait cycle Yeung *et al.* (2009); Chumanov *et al.* (2007, 2011); Thelen *et al.* (2005b). Various reasons have been suggested for the observed discrepancies. For example, Orchard *et al.* (1997), Cameron *et al.* (2003) and Bennel *et al.* (1998) studied Australian Rules footballers whereas Croisier *et al.* (2008) studied soccer players and Yeung *et al.* (2009) sprinters. If the cut-off value of the H:Q ratio was sport specific it would confound inter-sport analysis. Intra-sport groups also varied. In the 3 studies that involved Australian rules footballers two studies involved only elite players (Orchard *et al.*, 1997; Cameron *et al.*, 2003) whereas the third of Bennel *et al.* (1998) involved a combination of professional and amateur athletes thus findings may not be directly comparable (Foreman *et al.*, 2006). Additionally, there is not a universally followed assessment protocol. For example, in Bennel *et al.* (1998) testing was performed at 60 and 180°/s and the calculated H:Q<sub>fun</sub> ratios were not angle specific. On the other hand, in Yeung *et al.* (2009) testing was performed at 60, 180 and 240°/s (again not angle-specific) whereas Croisier *et al.* (2008) used a mixed functional ratio where the peak torque during hamstring eccentric contraction at 30°/s was divided by the quadriceps peak torque during concentric contraction at 240°/s, their reasoning being that most hamstring injuries occur in the decelerating phase of the eccentric contraction.

Another confounding factor is the variability in sample size between groups (Murphy *et al.*, 2003). According to Bahr & Holme (2003) a sample of 22–52 injured participants is needed in order to detect a significant association between a risk factor, i.e. an H:Q value, and HSI depending on the injury frequency of the study and the true association between risk factor and injury risk. This would require a sample group of at least 230 participants which was exceeded only by Croisier *et al.* (2008) in the aforementioned studies. This lack of statistical power likely has made a conclusive association between H:Q ratio values and HSIs harder to achieve.

The protocol variability that was discussed earlier indicates that the choice of isoveloc-

ities at which the H:Q ratios are obtained is somewhat arbitrary and is based more on an educated guess from the researcher rather than on a methodologically based choice. Additionally, there is often no information on the angle where the peak torque is produced during muscular contraction, i.e. the H:Q torque ratio is given as a function of  $\omega$  only whereas the effect of  $\theta$  on its value is neglected thus ignoring any effects due to changing muscle length. Even in studies where the angle of extension is taken into account such as in Aagard *et al.* (1998) the angle range is small (30-50°) and does not include the optimum angles for knee extension and flexion (60-70° and 20-30° respectively) (Westing, 1988; Coombs & Garbutt, 2002) or obtuse, near full extension, angles where the hamstrings undergo the greatest biomechanical load during knee extension (Chumanov *et al.*, 2007; Higashihara *et al.*, 2014; Novacheck, 1998) and thus they are the most susceptible to injury. Only recently, Evangelidis *et al.* (2015) produced angle-specific H:Q<sub>fun</sub> ratios, at longer angle ranges, in a study that compared H:Q ratios between football players and recreationally active controls. Although no significant differences in the H:Q<sub>fun</sub> values were found between the two groups the study ascertained that the ratio values tend to increase with both angle and angular velocity of contraction. A possible explanation for the general lack of angle-specific measurements is the great difficulty in obtaining reliable torque data at those angle ranges, and especially at high values of  $\omega$ , using an isokinetic dynamometer (Batzopoulos & Brodie, 1989). Another limitation of using such devices is that they are capable of producing angular velocities that fall well short of achieving angular velocities such as those observed during high intensity athletic activities, e.g. kicking a ball in soccer or sprinting, that can reach values over 1200°/s (Kellis & Katis, 2007; Higashihara *et al.*, 2010)

As it was mentioned above, in order for the hamstrings-quadiceps interaction during knee extension to be fully described the H:Q<sub>fun</sub> ratio needs to be expressed as a function of both  $\omega$  and  $\theta$ . Ideally, this function should be capable of giving the value of H:Q<sub>fun</sub> at high extension angles and angular velocities of contraction. Since those values may exceed the capabilities of an isokinetic device a model equation with the above characteristics would be a very useful tool in the study of the H:Q<sub>fun</sub> ratio and its correlation to hamstrings' pathology.

The aim of this work is to derive an equation that will describe the functional H:Q

torque ratio as a function of two variables, namely angular velocity  $\omega$  and angle  $\theta$ . Ideally, this function (henceforth termed  $R_E(\omega, \theta)$ ) should have a small enough number of parameters to be determined quickly and efficiently thus requiring few  $(\omega, \theta)$  points whilst at the same time it should be accurate enough to provide a sufficient qualitative and quantitative description of the functional H:Q ratio at knee joint angles that cannot, normally, be attained during isokinetic contractions of the hamstrings and quadriceps muscles especially at angular velocities of over 300 °/s.

## 3.2 Method

The first step in the derivation of  $R_E(\omega, \theta)$  was to obtain a description of the behaviour of the H:Q<sub>fun</sub> ratio with concurrently varying  $\theta$  and  $\omega$  by means of a theoretical three-dimensional H:Q ratio function termed  $R_T(\omega, \theta)$ . The purpose of  $R_T(\omega, \theta)$  was to function as a benchmark for  $R_E(\omega, \theta)$ , providing information on its mathematical properties and behaviour. Since the terms *parameters* and *variables* will be used frequently through this chapter henceforth *parameters* will be called the variable coefficients of  $R_T(\omega, \theta)$  and  $R_E(\omega, \theta)$  that are determined by fitting the function to a set of the *dependent variables*  $\omega$  and  $\theta$ .

### 3.2.1 Derivation of $R_T(\omega, \theta)$

The theoretical H:Q<sub>fun</sub> ratio function,  $R_T(\omega, \theta)$ , was based on the product of equations (1.14), (1.16) and (1.17) expressed in piecewise form as

$$T^{MVC}(\omega, \theta) = \begin{cases} T_{conc}^{tet}(\omega)\alpha(\omega)T(\theta), & \omega \geq 0 \\ T_{ecc}^{tet}(\omega)\alpha(\omega)T(\theta), & \omega < 0 \end{cases} \quad (3.1)$$

and expanded below separately for the concentric and eccentric phases of contraction.

- $\omega \geq 0$

$$T_{conc}^{tet}(\omega, \theta) = \left[ \frac{T_0 w_c (w_{max} + w_c)}{w_{max} (w_c + w)} - \frac{T_0 w_c}{w_{max}} \right] \times \left( \alpha_{min} + \frac{\alpha_{max} - \alpha_{min}}{1 + e^{\left(-\frac{w - w_1}{\omega_r}\right)}} \right) e^{\left(-\frac{1}{2}\right) \left[ \frac{(\theta - \theta_{opt})^2}{W^2} \right]} \quad (3.2)$$

- $\omega < 0$

$$T_{ecc}^{tet}(\omega, \theta) = - \left[ \frac{(T_{max} - T_0)^2 \omega_{max} \omega_c}{\kappa T_0 (\omega_{max} + \omega_c) \left[ \frac{(T_{max} - T_0) \omega_{max} + \omega_c}{\kappa T_0 (\omega_{max} + \omega_c)} - \omega \right]} + T_{max} \right] \times \left( \alpha_{min} + \frac{\alpha_{max} - \alpha_{min}}{1 + e^{\left(-\frac{\omega - \omega_1}{\omega_r}\right)}} \right) e^{\left(-\frac{1}{2}\right) \left[ \frac{(\theta - \theta_{opt})^2}{W^2} \right]} \quad (3.3)$$

Equation (3.1) is a 9-parameter function that expresses the maximum voluntary muscle torque as a function of  $\omega$  and  $\theta$  (Forrester *et al.*, 2011) and can be used to provide a 3-dimensional description of the theoretical torque profile for any participant provided that the torque-angular velocity ( $T-\omega$ ) and torque-angle ( $T-\theta$ ) profiles of the participant are known (Figure 3.1).

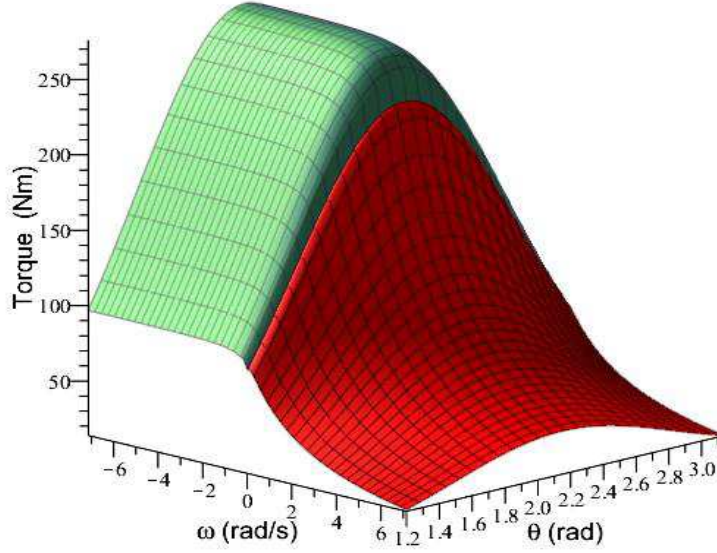


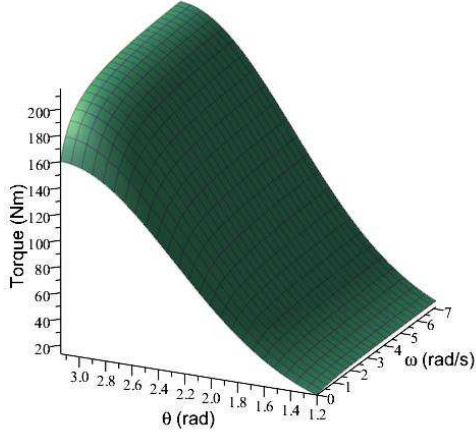
Figure 3.1: The function  $T^{MVC}(\omega, \theta)$  of equation (3.1). Red area corresponds to the concentric part of the surface and green to the eccentric

Eleven such profiles were selected from a previously conducted study (Pain *et al.*, 2013). Participants completed a set protocol on an isokinetic dynamometer that included maximum voluntary contractions (henceforth MVC) isometric, concentric and eccentric knee extensions and flexions. Each muscle group was tested on a separate session. Subjects were seated on the dynamometer with their dominant leg strapped

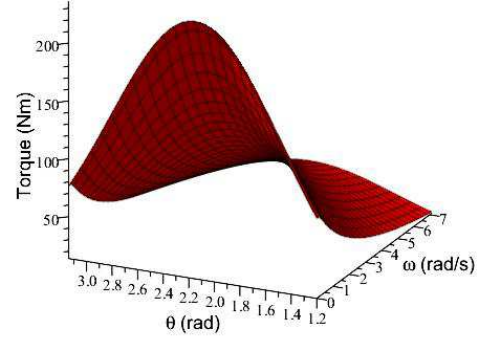
tightly to the unpadded crank arm directly above the ankle joint using a protective moulded plastic shin guard. To account for the difference between crank and joint angles (Batzopoulos & Brodie, 1989) the rotational axis of the crank arm was aligned with the centre of the knee joint during near-maximal efforts for both knee extensors and flexors. First, maximum voluntary isometric torque values were obtained at 5 angles of joint flexion that spanned the participant’s joint range of motion (henceforth ROM). Isokinetic maximum voluntary eccentric-concentric contractions were performed at ten different angular velocities,  $\pm 50, 100, 200, 300, 400^\circ/\text{s}$  according to the protocol of Yeadon *et al.* (2006). In order to determine accurate joint kinematics the MVC trials at 200 and  $400^\circ/\text{s}$  were recorded for each subject at 200 Hz with a high-speed camera (Phantom V4, Vision Research, Inc., Wayne, NJ) and the video images were manually digitised using hip, knee and ankle joint centres that had been marked up at the beginning of the session to determine knee joint angles. Crank angles and angular velocities were then converted to joint angles and angular velocities using a linear regression equation derived from the digitised joint and crank angle data.

Dynamometer data were sampled at 512 Hz and subsequently they were filtered using a low pass 4th order Butterworth filter at 8 Hz and combined with the angle and angular velocity data to obtain torque-angular velocity-angle profiles ( $T-\omega-\theta$ ) for the hamstrings and quadriceps of each subject. For each isovelocity trial the maximum eccentric and concentric isovelocity phases were identified and the isovelocity plateau was defined as the region where the angular velocity was within 10% of the peak value. Since the isovelocity plateaus tend to become smaller with increasing angular velocity, isovelocity torques were interpolated using quintic splines (Wood & Jennings, 1979) to obtain equal number of torque points per isovelocity (Forrester *et al.*, 2011). A more detailed description of the experimental protocol and methods by which the  $T-\omega-\theta$  datasets were obtained is given in Pain *et al.* (2013).

The nine-parameter torque function,  $T^{\text{MVC}}(\omega, \theta)$ , defined in equations (3.1), (3.2), (3.3) was then fitted to the experimental  $T-\omega-\theta$  datasets. The 9-parameters were optimised using a Simulated Annealing algorithm of Corana *et al.* (1987) where the parameter values are varied within bounds in order to minimise the root mean square difference between  $T^{\text{MVC}}(\omega, \theta)$  and experimental torques Forrester *et al.* (2011).



(a) Hamstrings



(b) Quadriceps

Figure 3.2:  $T_{eccH}^{MVC}(\omega, \theta)$  for hamstrings and  $T_{concQ}^{MVC}(\omega, \theta)$  for quadriceps shown separately

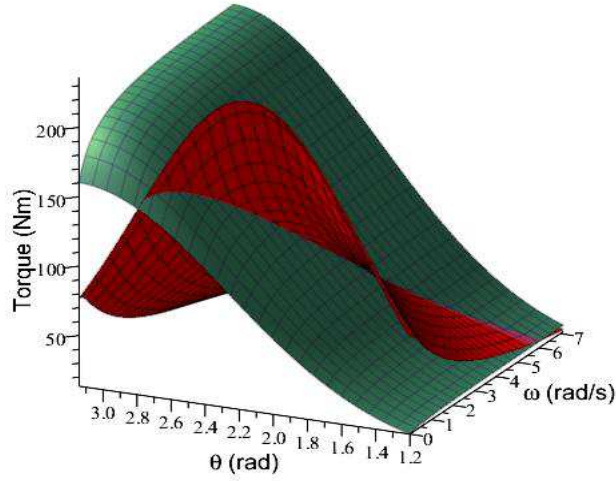


Figure 3.3:  $T_{eccH}^{MVC}(\omega, \theta)$  for hamstrings (green) overlaid on  $T_{concQ}^{MVC}(\omega, \theta)$  for quadriceps (red)

Following the determination of a  $T^{MVC}(\omega, \theta)$  function from the hamstrings and quadriceps  $T-\omega-\theta$  datasets of each participant the theoretical H:Q<sub>fun</sub> ratio function,  $R_T(\omega, \theta)$  was obtained using the equation

$$R_T(\omega, \theta) = \frac{T_{eccH}^{MVC}(\omega, \theta)}{T_{concQ}^{MVC}(\omega, \theta)} \quad (3.4)$$

where  $T_{eccH}^{MVC}(\omega, \theta)$  obtained from hamstrings eccentric and  $T_{concQ}^{MVC}(\omega, \theta)$  obtained from quadriceps concentric contraction respectively (Figures 3.2, 3.3). This is an 17-parameter

function as there are 9 parameters for the eccentric mode of contraction and 8 for the concentric one Figure (3.4).

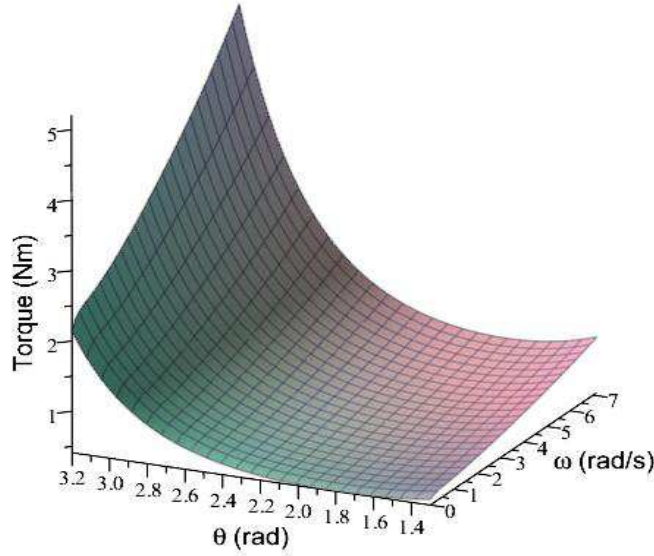


Figure 3.4: The theoretical H:Q<sub>fun</sub> ratio function,  $R_T(\omega, \theta)$

### 3.2.2 Derivation of the experimental $R_E(\omega, \theta)$ function

Having obtained the theoretical ratio surfaces given by  $R_T(\omega, \theta)$  the next step was the determination of a second ratio function that would have the ability to accurately reproduce  $R_T(\omega, \theta)$  using a significantly smaller number of parameters. This new ratio function was termed  $R_E(\omega, \theta)$ . The first step in the derivation of  $R_E(\omega, \theta)$  function was to create plane curves of  $R_T(\omega, \theta)$  by setting first  $\omega$  and then  $\theta$  equal to a constant value  $c$  from the ratio surface of a single subject.

$$R_T^c(\theta) = R_T(c, \theta) \quad (3.5)$$

$$R_T^c(\omega) = R_T(\omega, c)$$

Subsequently different functions, or linear combinations of them, were fitted to the plane curves using MATLAB (The MathWorks Inc., Natick, MA, USA) for different values of  $c$  to determine the one that gave the best fit. Goodness of fit was measured via the coefficient of determination,  $R^2$ , and the root mean square error (henceforth RMSE). It was found that  $R_T^c(\theta)$  and  $R_T^c(\omega)$  were best described by the following 3–

and 4-parameter functions,  $R_E(\theta)$  and  $R_E(\omega)$  respectively (Figure 3.5).

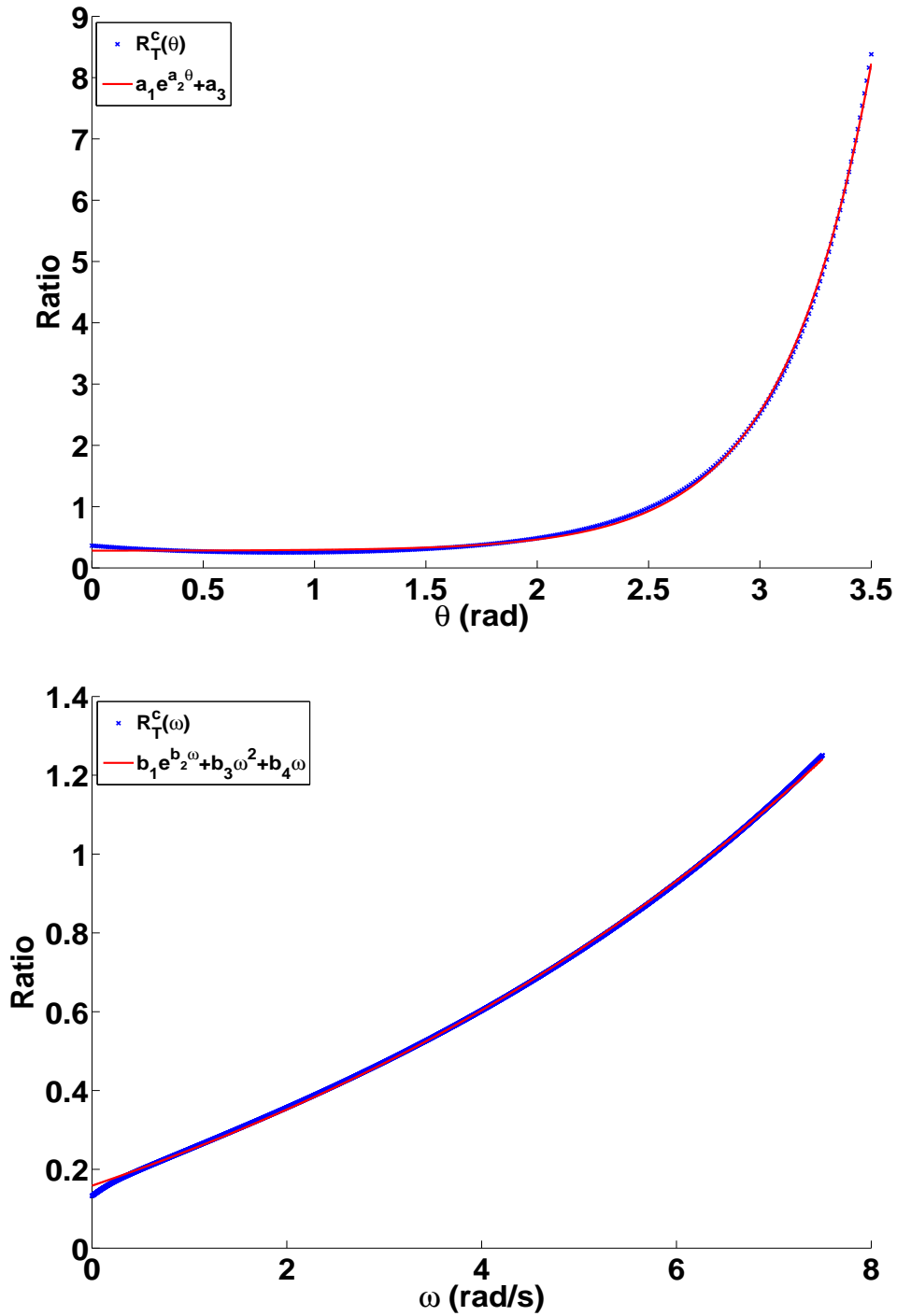


Figure 3.5: Derivation of  $R_E(\theta)$  and  $R_E(\omega)$  by fitting 3- and 4-parameter functions on the plane curves  $R_T(c, \theta)$  and  $R_T(\omega, c)$  of the  $R_T(\omega, \theta)$  function

$$R_E^c(\theta) = a_1 e^{a_2 \theta} + a_3 \quad (3.6)$$

and

$$R_E^c(\omega) = b_1 e^{b_2 \omega} + b_3 \omega^2 + b_4 \omega \quad (3.7)$$

as those produced the best fits for all values of  $c$  (Table 3.1).

Table 3.1:  $R^2$  and RMSE values for the fit of equations (3.5), (3.6) on  $R_T^c(\theta)$  and  $R_T^c(\omega)$  respectively

$c$ ( $^\circ/\text{s}$ )	$R_T^c(\theta)$		$c$ $^\circ$	$R_T^c(\omega)$	
	$R^2$	RMSE		$R^2$	RMSE
0	0.999	0.024	0	0.999	0.006
60	0.999	0.038	30	0.999	0.005
180	0.999	0.074	60	0.999	0.005
400	0.999	0.18	75	0.999	0.004

Next, various linear and non-linear combinations of  $R_T^c(\theta)$  and  $R_T^c(\omega)$  were fitted on the  $R_T(\omega, \theta)$  surface in order to determine  $R_E(\omega, \theta)$ . The best fit was obtained by the 6-parameter exponential function

$$R_E(\omega, \theta) = a \exp(b\omega^n + c\theta^m) - d\omega^{1/2}\theta^2 \quad (3.8)$$

which was subsequently fitted to all 11  $R_T(\omega, \theta)$  surfaces. To test the robustness of the  $R_E(\omega, \theta)$  function 17  $(\omega, \theta, R_T(\omega, \theta))$  points from each theoretical ratio surface were chosen and  $R_E(\omega, \theta)$  was fitted to those points and compared to the whole surface fits. Goodness of fit was assessed via the  $R^2$  and root mean square error (RMSE). All surface fits were performed in MATLAB using least squares. All coefficients were given a lower bound of zero when  $R_E(\omega, \theta)$  was fitted to the  $R_T(\omega, \theta)$  surface however, coefficients  $b$  and  $c$  were allowed to obtain negative values during the raw data fits.

### 3.2.3 Testing the $R_E(\omega, \theta)$ function on raw ratio values

However, fitting equation (3.7) on  $R_T(\omega, \theta)$  is not a conclusive enough test as it is an analytically defined function and therefore there is no “noise” in the data used for the fit unlike what would be encountered in an actual experimental or testing environment.

Therefore it was necessary to test the goodness of fit and robustness of  $R_E(\omega, \theta)$  when fitted on raw experimental data. To achieve this a new set of torque–angular velocity–angle datasets from 14 subjects was obtained. The datasets were produced during a comparative study on the functional H:Q ratios of footballers and control subjects. The measurement protocol followed is described in Evangelidis *et al.* (2015) and is very similar to the experimental protocol of the previous study outlined in the preceding sections (Pain *et al.*, 2013) with the difference that eccentric–concentric contractions were performed at six (instead of ten) different angular velocities,  $\pm 60, 240, 400^\circ/\text{s}$ .

Again the aim was to determine how close the  $R_E(\omega, \theta)$  function would be able to reproduce experimental H:Q<sub>fun</sub> values and to assess its sensitivity to the number of points used for the fit. This was done in two stages. During the first stage the experimental, raw, H:Q functional ratios,  $R_{exp}$ , at 11, 14, and 17  $(\omega, \theta)$  points were calculated for every one of the 14 subjects and  $R_E(\omega, \theta)$  was fitted on every  $(\omega, \theta, R_{exp})$  set of points (Figure 3.6). Additionally,  $R_T(\omega, \theta)$  surfaces were calculated for three of the subjects, chosen at random, and  $R_E(\omega, \theta)$  was fitted on those surfaces in order to ascertain that the goodness of the fit on the theoretical surfaces was not group–dependent.

Having established the levels of accuracy and robustness of the  $R_E(\omega, \theta)$  function the next stage was to determine whether it would be possible a) to further reduce the number of raw ratio points used in the fit and b) to determine how sensitive  $R_E(\omega, \theta)$  would be to discrepancies in the values of the knee joint angle  $\theta$  where torque is measured during contractions of hamstrings and quadriceps. To achieve this  $R_E(\omega, \theta)$  was fitted on the following sets of raw,  $R_{exp}$  points.

- An 8 raw ratio point set  $(\omega, \theta, R_{exp})$  consisting of 5 ratio points calculated during isometric contraction ( $\omega = 0, \theta, R_{exp}$ ) and three  $(\omega, \theta, R_{exp})$  points calculated at the maximum value of knee joint angle ( $\theta_{max}$ ) for each of the isovelocities ( $\omega, \theta_{max}, R_{exp}$ ).
- An 8 raw ratio point set  $(\omega_{max}, \theta, R_{exp})$  consisting of 5  $(\omega = 0, \theta, R_{exp})$  ratio points and three  $(\omega, \theta, R_{exp})$  points calculated at the maximum isovelocity  $400^\circ/\text{s}$ .
- A “varied”, 17 raw ratio point set  $(\omega, \theta_{varied}, R_{exp})$  consisting of 5  $(\omega = 0, \theta, R_{exp})$  ratio points and twelve  $(\omega, \theta, R_{exp})$  points where the hamstring  $\theta$  values were 5 degrees lower than the respective values for quadriceps.

Table 3.2 summarizes the 6 different fits that were performed to test the accuracy and robustness of the  $R_E(\omega, \theta)$  function. In general the number of points selected for each fit followed a  $\kappa n + 5$  sequence where  $\kappa$  was the number of different isovelocities ( $\omega \neq 0$ ) at which ratio points,  $R_{exp}$ , were calculated,  $n$  was the number of different joint angles,  $\theta$ , where  $R_{exp}$  was calculated per isovelocity and 5 was the number of  $R_{exp}$  points calculated during isometric contractions. The values of  $\theta$  were determined as follows. The common knee joint ROM was determined for each isovelocity for both extension and flexion. If one  $R_{exp}$  point was used per isovelocity then it was calculated at the angle of full extension,  $\theta_{max}$ . If two points were used then the full flexion angle was also used,  $\theta_{min}$ . A third angle point was added by dividing the ROM into two parts and using the midrange angle and for four  $R_{exp}$  points per isovelocity the angles at 33% and 66% of ROM were used so that the ROM was always divided into equidistant parts.

Table 3.2: Synopsis of the different  $R_{exp}$  ratio points used in the 6 fits. Number of  $R_{exp}$  points calculated during isometric ( $\omega = 0$ ) and isovelocity trials ( $\omega \neq 0$ ), number of different isovelocities employed,  $\kappa$ , and number of different joint angles per isovelocity,  $n$

Number of points fitted	Number of points per isovelocity $\omega$				Value of $\kappa$	Value of $n$
	0°/s	60°/s	240°/s	400°/s		
	<b>8</b> ( $\omega_{max}, \theta, R_{exp}$ )	5	0	0		
<b>8</b> ( $\omega, \theta_{max}, R_{exp}$ )	5	1	1	1	3	1
<b>11</b> ( $\omega, \theta, R_{exp}$ )	5	2	2	2	3	2
<b>14</b> ( $\omega, \theta, R_{exp}$ )	5	3	3	3	3	3
<b>17</b> ( $\omega, \theta, R_{exp}$ )	5	4	4	4	3	4
<b>17</b> ( $\omega, \theta_{varied}, R_{exp}$ )	5	4	4	4	3	4

Again, the  $R^2$  and RMSE values were used to assess the accuracy of the fit. Furthermore, to assess the error between different fits the normalised RMSE scores (NRMSE) were calculated by dividing the respective RMSE scores by the range values. All al-

gebraic calculations were performed using MAPLE 16 (Maplesoft Inc., Waterloo, ON, Canada).

### 3.3 Results

#### 3.3.1 Fit of $R_E(\omega, \theta)$ function on $R_T(\omega, \theta)$

The 6-parameter  $R_E(\omega, \theta)$  function was first fitted to 17  $(\omega, \theta, R_T(\omega, \theta))$  ratio points and the whole  $R_T(\omega, \theta)$  surface for each of the 11 subjects and the goodness of the fits were assessed using the  $R^2$ , RMSE and NRMSE values that are summarized in Table 3.3. The 17-points fit produced mean  $R^2$  and RMSE values of 0.998 and 0.059

Table 3.3:  $R^2$  and RMSE values for the fit of the  $R_E(\omega, \theta)$  function on the theoretical ratio surface and on 17 points of that surface

	17 points fit		Whole surface fit	
	$R^2$	RMSE	$R^2$	RMSE
<sup>a</sup> Subject <sub>1</sub>	0.999	0.012	0.999	0.014
<sup>a</sup> Subject <sub>2</sub>	0.999	0.015	0.999	0.024
<sup>a</sup> Subject <sub>3</sub>	0.998	0.061	0.992	0.274
<sup>a</sup> Subject <sub>4</sub>	0.999	0.016	0.999	0.039
<sup>a</sup> Subject <sub>5</sub>	0.999	0.032	0.999	0.021
<sup>a</sup> Subject <sub>6</sub>	0.997	0.049	0.999	0.047
<sup>a</sup> Subject <sub>7</sub>	0.999	0.044	0.999	0.015
<sup>a</sup> Subject <sub>8</sub>	0.999	0.015	0.999	0.019
<sup>a</sup> Subject <sub>9</sub>	0.996	0.168	0.989	0.151
<sup>a</sup> Subject <sub>10</sub>	0.999	0.008	0.999	0.007
<sup>a</sup> Subject <sub>11</sub>	0.996	0.129	0.998	0.042
<sup>b</sup> Subject <sub>7</sub>	0.999	0.006	0.997	0.019
<sup>b</sup> Subject <sub>10</sub>	0.994	0.026	0.992	0.056
<sup>b</sup> Subject <sub>11</sub>	0.982	0.053	0.962	0.118

<sup>a</sup> Datasets from Pain *et al.* (2013)

<sup>b</sup> Datasets from Evangelidis *et al.* (2015)

respectively that were very similar to the  $R^2$  and RMSE values exhibited by the whole

surface fit of the  $R_E(\omega, \theta)$  function on the theoretical  $R_T(\omega, \theta)$  surface of 0.999 and 0.049. The fits were repeated for three of the second group participants in order to ascertain that the fits were not group-dependent. The respective  $R^2$  and RMSE for the whole surface and 17-points fits respectively were 0.991–0.028 and 0.984–0.64 that compared well with the fits from the first dataset.

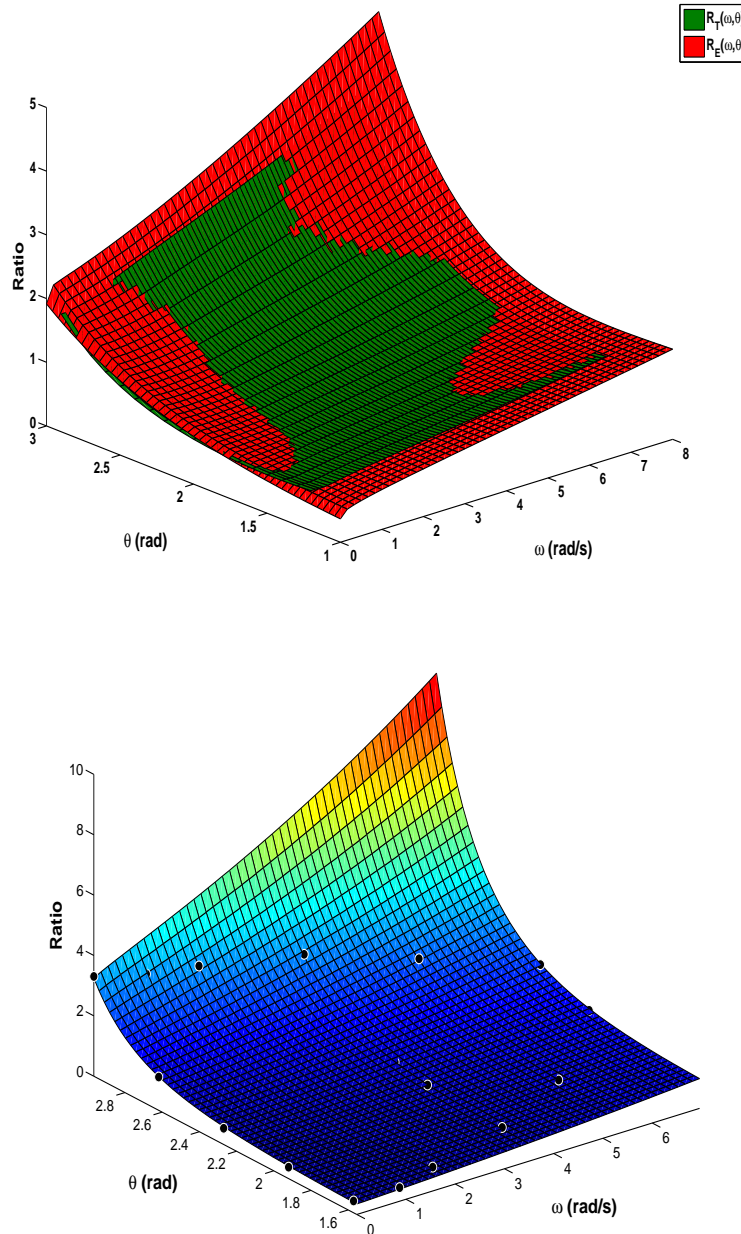


Figure 3.6: Example of fitting  $R_E(\omega, \theta)$  on the whole  $R_T(\omega, \theta)$  surface and on 17  $(\omega, \theta, R_T(\omega, \theta))$  points.

### 3.3.2 Fit of $R_E(\omega, \theta)$ function on raw H:Q<sub>fun</sub> points

#### 3.3.2.1 11, 14, and 17 point fits

The fit of the  $R_E(\omega, \theta)$  function on 11, 14, and 17  $(\omega, \theta, R_{\text{exp}})$  points of the second T- $\omega$ - $\theta$  data set produced, in turn, mean  $R^2$  values of 0.91, 0.87 and 0.84 whereas the respective mean RMSE values were 0.23, 0.25 and 0.24, Table 3.4. The mean

Table 3.4:  $R^2$  and RMSE values for the fit of the  $R_E(\omega, \theta)$  function on 11, 14, and 17  $(\omega, \theta, R_{\text{exp}})$  points of the raw H:Q surface

	11 points fit		14 points fit		17 points fit	
	$R^2$	RMSE	$R^2$	RMSE	$R^2$	RMSE
<b>Subject</b> <sub>1</sub>	0.957	0.142	0.786	0.348	0.862	0.266
<b>Subject</b> <sub>2</sub>	0.963	0.259	0.857	0.410	0.906	0.293
<b>Subject</b> <sub>3</sub>	0.973	0.128	0.931	0.166	0.890	0.183
<b>Subject</b> <sub>4</sub>	0.979	0.111	0.938	0.158	0.935	0.155
<b>Subject</b> <sub>5</sub>	0.940	0.113	0.906	0.115	0.887	0.107
<b>Subject</b> <sub>6</sub>	0.967	0.136	0.866	0.225	0.902	0.174
<b>Subject</b> <sub>7</sub>	0.943	0.186	0.936	0.169	0.923	0.167
<b>Subject</b> <sub>8</sub>	0.724	0.463	0.773	0.338	0.762	0.302
<b>Subject</b> <sub>9</sub>	0.750	0.565	0.888	0.303	0.637	0.473
<b>Subject</b> <sub>10</sub>	0.736	0.520	0.738	0.466	0.575	0.526
<b>Subject</b> <sub>11</sub>	0.992	0.057	0.946	0.127	0.940	0.123
<b>Subject</b> <sub>12</sub>	0.958	0.186	0.828	0.311	0.814	0.281
<b>Subject</b> <sub>13</sub>	0.931	0.242	0.845	0.289	0.842	0.256
<b>Subject</b> <sub>14</sub>	0.932	0.151	0.948	0.125	0.909	0.148

normalised (NRMSE) values for the 3 datasets were respectively, 0.12, 0.13 and 0.13, Table 3.5.

Table 3.5: Normalised RMSE values for the fit of the  $R_E(\omega, \theta)$  function on 11, 14, and 17  $(\omega, \theta, R_{\text{exp}})$  points of the raw H:Q surface

	11 points fit	14 points fit	17 points fit
<b>Subject</b> <sub>1</sub>	0.064	0.156	0.119
<b>Subject</b> <sub>2</sub>	0.090	0.143	0.102
<b>Subject</b> <sub>3</sub>	0.072	0.093	0.102
<b>Subject</b> <sub>4</sub>	0.074	0.105	0.103
<b>Subject</b> <sub>5</sub>	0.103	0.105	0.098
<b>Subject</b> <sub>6</sub>	0.089	0.149	0.115
<b>Subject</b> <sub>7</sub>	0.140	0.128	0.126
<b>Subject</b> <sub>8</sub>	0.219	0.160	0.143
<b>Subject</b> <sub>9</sub>	0.239	0.128	0.201
<b>Subject</b> <sub>10</sub>	0.193	0.173	0.196
<b>Subject</b> <sub>11</sub>	0.047	0.105	0.101
<b>Subject</b> <sub>12</sub>	0.086	0.144	0.130
<b>Subject</b> <sub>13</sub>	0.149	0.178	0.158
<b>Subject</b> <sub>14</sub>	0.121	0.099	0.118

### 3.3.2.2 8 point fits

The fits of the  $R_E(\omega, \theta)$  on 8  $(\omega, \theta_{\text{max}}, R_{\text{exp}})$  and 8  $(\omega_{\text{max}}, \theta, R_{\text{exp}})$  ratio points gave mean  $R^2$  values of 0.96 and 0.97 and RMSE values of 0.21 and 0.15 respectively. The 17 points fit with varied  $\theta$  values produced mean  $R^2$  value of 0.89 and mean RMSE of 0.15, Table 3.6. The mean NRMSE values for the 8 point  $(\omega, \theta_{\text{max}}, R_{\text{exp}})$ ,  $(\omega_{\text{max}}, \theta, R_{\text{exp}})$  and the 17 point  $(\omega, \theta_{\text{varied}}, R_{\text{exp}})$  fits were 0.23, 0.27, 0.15 respectively, Table 3.7.

Table 3.6:  $R^2$ , RMSE and NRMSE values for the fit of the  $R_E(\omega, \theta)$  function on 8  $(\omega, \theta_{max}, R_{exp})$ ,  $(\omega_{max}, \theta, R_{exp})$  and 17  $(\omega, \theta_{varied}, R_{exp})$  points of the raw H:Q surface

	<b>8 <math>(\omega, \theta_{max}, R_{exp})</math></b>		<b>8 <math>(\omega_{max}, \theta, R_{exp})</math></b>		<b>17 <math>(\omega, \theta_{varied}, R_{exp})</math></b>	
	<b>points fit</b>		<b>points fit</b>		<b>points fit varied</b>	
	<b><math>R^2</math></b>	<b>RMSE</b>	<b><math>R^2</math></b>	<b>RMSE</b>	<b><math>R^2</math></b>	<b>RMSE</b>
<b>Subject<sub>1</sub></b>	0.979	0.092	0.904	0.45	0.846	0.143
<b>Subject<sub>2</sub></b>	0.998	0.034	0.955	0.427	0.926	0.152
<b>Subject<sub>3</sub></b>	0.976	0.189	0.995	0.051	0.887	0.142
<b>Subject<sub>4</sub></b>	0.999	0.034	0.996	0.061	0.906	0.131
<b>Subject<sub>5</sub></b>	0.902	0.183	0.975	0.078	0.855	0.23
<b>Subject<sub>6</sub></b>	0.999	0.029	0.993	0.087	0.936	0.153
<b>Subject<sub>7</sub></b>	0.999	0.015	0.989	0.12	0.948	0.10
<b>Subject<sub>8</sub></b>	0.991	0.075	0.97	0.24	0.88	0.178
<b>Subject<sub>9</sub></b>	0.767	0.792	0.905	0.368	0.872	0.174
<b>Subject<sub>10</sub></b>	0.962	0.127	0.982	0.231	0.857	0.134
<b>Subject<sub>11</sub></b>	0.989	0.086	0.943	0.231	0.92	0.12
<b>Subject<sub>12</sub></b>	0.962	0.127	0.992	0.079	0.80	0.155
<b>Subject<sub>13</sub></b>	0.967	0.213	0.902	0.384	0.936	0.11
<b>Subject<sub>14</sub></b>	0.987	0.072	0.969	0.173	0.92	0.106

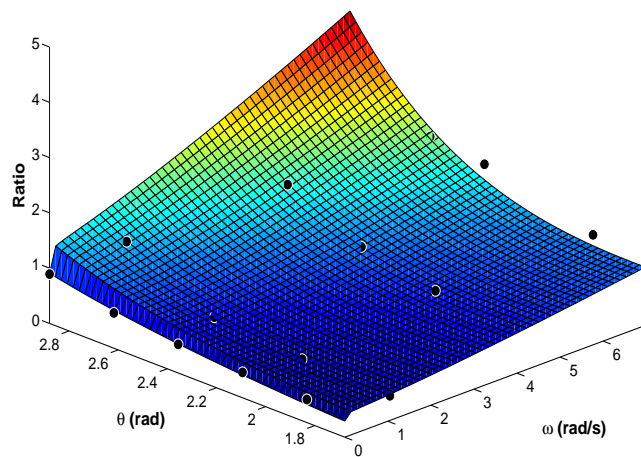
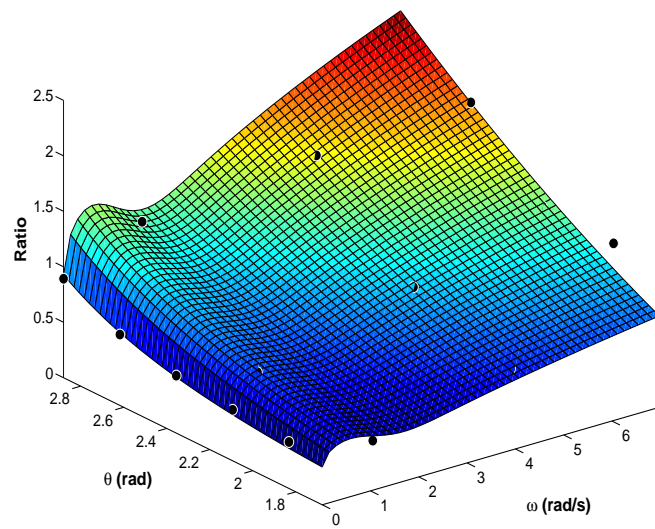
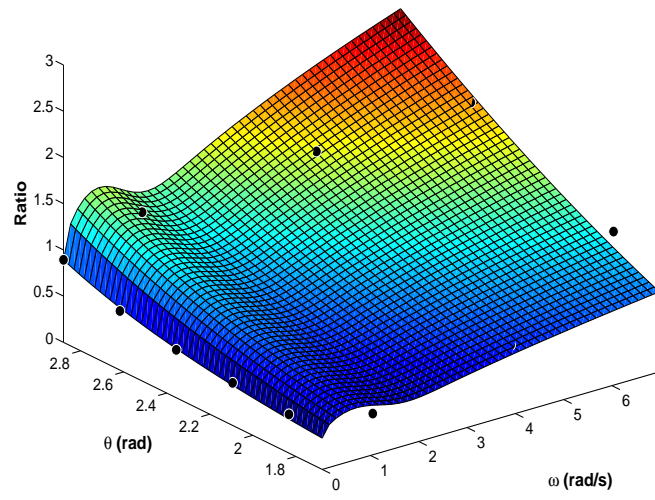


Figure 3.7: Fit of the  $R_E(\omega, \theta)$  function on 11, 14 and 17  $(\omega, \theta, R_{\text{exp}})$  points of the raw H:Q surface for Subject 4

Table 3.7: Normalised RMSE values for the fit of the  $R_E(\omega, \theta)$  function on 11, 14, and 17  $(\omega, \theta_{max}, R_{exp})$  points of the experimental H:Q surface

	<b>8</b> $(\omega, \theta_{max}, R_{exp})$	<b>8</b> $(\omega_{max}, \theta, R_{exp})$	<b>17</b> $(\omega, \theta_{varied}, R_{exp})$
	<b>points fit</b>	<b>points fit</b>	<b>points fit varied</b>
<b>Subject</b> <sub>1</sub>	0.136	0.348	0.143
<b>Subject</b> <sub>2</sub>	0.045	0.29	0.152
<b>Subject</b> <sub>3</sub>	0.284	0.12	0.142
<b>Subject</b> <sub>4</sub>	0.065	0.096	0.131
<b>Subject</b> <sub>5</sub>	0.302	0.253	0.23
<b>Subject</b> <sub>6</sub>	0.204	0.165	0.153
<b>Subject</b> <sub>7</sub>	0.026	0.44	0.10
<b>Subject</b> <sub>8</sub>	0.156	0.19	0.178
<b>Subject</b> <sub>9</sub>	0.721	0.47	0.174
<b>Subject</b> <sub>10</sub>	0.424	0.115	0.134
<b>Subject</b> <sub>11</sub>	0.093	0.54	0.12
<b>Subject</b> <sub>12</sub>	0.118	0.11	0.155
<b>Subject</b> <sub>13</sub>	0.621	0.443	0.11
<b>Subject</b> <sub>14</sub>	0.13	0.247	0.106

Table 3.8: Mean  $R^2$ , RMSE and NRMSE values for all fits with Subjects 2, 8, 9, 10 excluded

	<b><math>R^2</math></b>	<b>RMSE</b>	<b>NRMSE</b>
<b>11</b> $(\omega, \theta, R_{exp})$ <b>points</b>	0.952	0.145	0.09
<b>14</b> $(\omega, \theta, R_{exp})$ <b>points</b>	0.893	0.20	0.126
<b>17</b> $(\omega, \theta, R_{exp})$ <b>points</b>	0.89	0.185	0.117
<b>8</b> $(\omega, \theta_{max}, R_{exp})$ <b>points</b>	0.976	0.106	0.198
<b>8</b> $(\omega_{max}, \theta, R_{exp})$ <b>points</b>	0.965	0.171	0.276
<b>17</b> $(\omega, \theta_{varied}, R_{exp})$ <b>points</b>	0.894	0.146	0.139

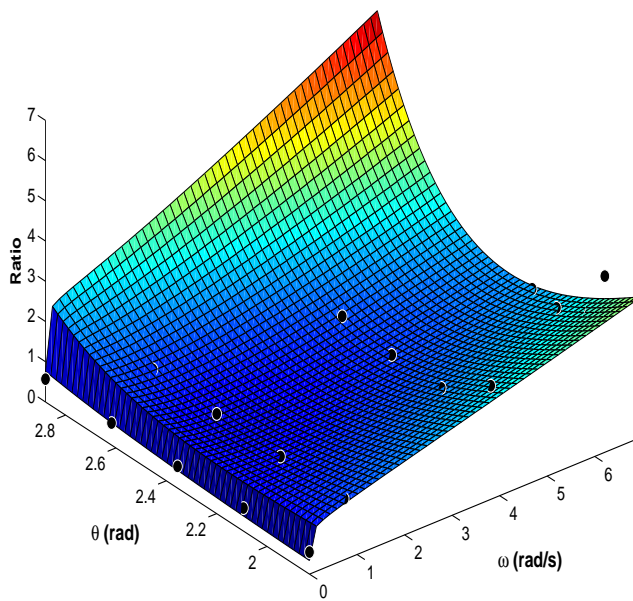
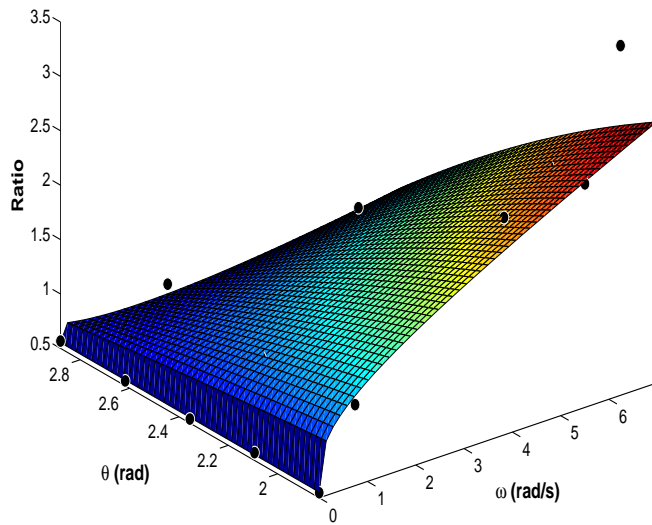


Figure 3.8: Fit of the  $R_E(\omega, \theta)$  function on 14 and 17  $(\omega, \theta, R_{\text{exp}})$  points of the experimental H:Q surface for Subject 2. The ratio values of the 14–point fit fail to increase with increasing  $\omega$  and  $\theta$  values due to an abnormally high ratio value at  $(400^\circ/s, 107^\circ) \equiv (6.98 \text{ rad/s}, 1.87 \text{ rad})$  indicating a possible sub–maximal effort and increasing the likelihood of underestimating the ratio value near full extension of the knee joint. Adding 3 extra points eliminates the skewness of the graph

Table 3.9:  $R_E(\omega, \theta)$  values evaluated at  $(400^\circ/s, 172^\circ)$  for the 17  $(\omega, \theta, R_{\text{exp}})$  points fit.  
 Mean value was 2.73

	$R_E(400, 172)$
<b>Subject<sub>1</sub></b>	1.58
<b>Subject<sub>2</sub></b>	2.11
<b>Subject<sub>3</sub></b>	1.9
<b>Subject<sub>4</sub></b>	4.52
<b>Subject<sub>5</sub></b>	1.73
<b>Subject<sub>6</sub></b>	3.96
<b>Subject<sub>7</sub></b>	2.52
<b>Subject<sub>8</sub></b>	1.78
<b>Subject<sub>9</sub></b>	3.37
<b>Subject<sub>10</sub></b>	0.98
<b>Subject<sub>11</sub></b>	2.78
<b>Subject<sub>12</sub></b>	2.17
<b>Subject<sub>13</sub></b>	5.8
<b>Subject<sub>14</sub></b>	2.72
<b>mean</b>	2.73

### 3.4 Discussion

This study aimed to derive a model equation for the H:Q functional torque ratio in terms of  $\omega$  and  $\theta$ . First a 17-parameter function  $R_T(\omega, \theta)$  was derived that defined the H:Q<sub>fun</sub> ratio in terms of angular velocity  $\omega$  and angle  $\theta$  and the H:Q<sub>fun</sub> ratio values were calculated for eleven T- $\omega$ - $\theta$  datasets. Subsequently, a six parameter function,  $R_E(\omega, \theta)$  was determined and fitted on:

- the whole  $R_T(\omega, \theta)$  surfaces and 17  $(\omega, \theta, R_T)$  points of the original eleven-subject T- $\omega$ - $\theta$  dataset.
- 11, 14 and 17  $(\omega, \theta, R_{\text{exp}})$  points that were calculated using a second, fourteen-subject T- $\omega$ - $\theta$  dataset.
- 8  $(\omega_{\text{max}}, \theta, R_{\text{exp}})$ ,  $(\omega, \theta_{\text{max}}, R_{\text{exp}})$  and 17  $(\omega, \theta_{\text{varied}}, R_{\text{exp}})$  points calculated again from the second dataset in order to test the robustness of  $R_E(\omega, \theta)$  to different ratio points and its sensitivity to small perturbations to the locations of those points on the T( $\omega, \theta$ ) surface.

The fits produced high determination coefficient,  $R^2$ , and low root mean square error, RMSE, values for all three different fits indicating that  $R_E(\omega, \theta)$  behaves consistently irrespectively of the number of points that it has been fitted on, is capable of producing a sufficient qualitative and quantitative description of the H:Q<sub>fun</sub> ratio with as few as 8 experimental points and does not appear to be sensitive to small perturbations in the values of  $\theta$ . It should be noted that with a single exception all three fits were qualitatively consistent i.e. if the 11-points fit predicted that an increase in H:Q<sub>fun</sub> values with increasing angular velocity then that trend was repeated in the other two fits (Figure 3.7). The only exception was the 14-point fit for Subject 2 that extrapolated to a low value of H:Q<sub>fun</sub> contrary to the 17-point fit that predicted a high H:Q<sub>fun</sub> value for large  $\omega$  and  $\theta$  (Figure 3.8). The possible causes of this discrepancy will be discussed later in this section.

### 3.4.1 Co-activation of quadriceps and hamstrings

In theory the  $H:Q_{fun}$  ratio is a better descriptor of the hamstrings strength relative to the quadriceps than the  $H:Q_{con}$  ratio as it takes into account the fact that during a functional movement the two muscles cannot attain their peak torques simultaneously as they exhibit different  $T-\theta$  relationships (Osternig *et al.*, 1986; Coombs & Garbutt, 2002). Indeed, as the knee joint moves from flexion to extension the quadriceps torque output decreases whereas the hamstrings torque output increases and consequently the  $H:Q_{fun}$  values increase irrespectively of the angular velocity of contraction (Aagard *et al.*, 1995, 1998; Coombs *et al.*, 2002; Coombs & Garbutt, 2002; Croisier, 2004; Evangelidis *et al.*, 2015).

This increase in the values of  $H:Q_{fun}$  was evident in all the fits of the theoretical 17-parameter function  $R_T(\omega, \theta)$  as is illustrated in Figures 3.4, 3.6, showing the good qualitative agreement of the function with experimental results, indicating that it could be used as a basis for the derivation of  $R_E(\omega, \theta)$ . When the latter was subsequently fitted on the whole  $R_T$  surfaces and on 17 points of them it was very successful in reproducing the original surfaces both qualitatively and quantitatively as is shown by the high correlation between the  $R_T(\omega, \theta)$  and  $R_E(\omega, \theta)$  functions and the low RMSE and (Table 3.3). This is evident in Figure (3.6) that shows the fit of the  $R_E(\omega, \theta)$  function on the respective  $R_T(\omega, \theta)$  surface and on 17 individual points on it for a single subject.

When  $R_E(\omega, \theta)$  was fitted on the second dataset its quantitative accuracy for the 11, 14 and 17-point fits was also good as is shown by the  $R^2$ , RMSE and NRMSE values (Tables 3.4–3.5) and Figure 3.7. The function also appeared to be robust to the different number of points included in the fit as there was very little difference between the results of the 11  $(\omega, \theta_{max}, R_{exp})$  points fit and those of the 14 and 17  $(\omega, \theta, R_{exp})$  points fits as shown by mean RMSE scores of 0.23, 0.25, 0.24 and mean NRMSE scores of 0.12, 0.13 and 0.13 respectively. The robustness of the function did not seem to be affected by further reducing the number of points used in the fit as shown by the results of the fit on 8  $(\omega_{max}, \theta, R_{exp})$  and  $(\omega, \theta_{max}, R_{exp})$  points. Indeed, the mean RMSE and NRMSE values were 0.21, 0.15 and 0.23, 0.27 respectively that compare very well with the previously obtained values (Tables 3.6–3.7). Finally, the function was shown to

behave reasonably well when the  $\theta$  values were perturbed as the mean RMSE and NRMSE values of the 17 ( $\omega$ ,  $\theta_{varied}$ ,  $R_{exp}$ ) fit were both 0.15 (Tables 3.6–3.7).

Despite the consistency across fits in the values of RMSE and NRMSE, the mean  $R^2$  scores appear to decrease with increased number of points used in the fit (mean 0.96, 0.96, 0.89, 0.84 for 8, 11, 14 and 17–point fits respectively). It was hypothesized, that this was due to the increased “noise” (error) in the data a consequence of the increase in the number of raw ratio points used in the fit. To test that the values corresponding to subjects 2, 8, 9 and 10 that achieved the worst  $R^2$  scores were excluded and new mean  $R^2$ , RMSE and NRMSE were calculated for all fits for this reduced dataset (Table 3.8).

The new  $R^2$ , RMSE and NRMS were lower as were the differences between the scores of the different fits (Table 3.8) suggesting a correlation between goodness of fit and quality of experimental data. Closer inspection of the datasets from the excluded 4 subjects revealed that they attained maximum ratio scores (3.4, 2.5, 2.9 and 3.1) at respective ( $\omega$ ,  $\theta$ ) values of ( $400^\circ/s$ ,  $113^\circ$ ), ( $400^\circ/s$ ,  $107^\circ$ ), ( $60^\circ/s$ ,  $159^\circ$ ) and ( $400^\circ/s$ ,  $108^\circ$ ) i.e. either at slow isovelocities or at low angles of extension whereas both experimental studies (Aagard *et al.*, 1995, 1998; Croisier *et al.*, 2008; Coombs *et al.*, 2002) and the theoretical ratio function  $R_T(\omega, \theta)$  have shown that the ratio value should increase with increasing  $\omega$  and  $\theta$  (Figure 3.6) as a consequence of the T– $\omega$  and T– $\theta$  relationships. This discrepancy may have increased the error in the dataset and consequently lead to the lower  $R^2$  values. The cause of this discrepancy however is not clear.

For example, a poor  $R^2$  score may be indicative of the hamstring’s weakness to produce maximal torque output during its eccentric contraction or of sub–maximal effort on the part of the subject during quadriceps concentric contraction that might lead to erroneous results (Figure 3.8). Both causes can be important in the case of a prospective study such as in (Orchard *et al.*, 1997; Cameron *et al.*, 2003; Croisier *et al.*, 2008; Yeung *et al.*, 2009) where the H:Q<sub>fun</sub> ratio is used as a predictor for possible future hamstrings injuries. The former because it would allow the identification of injury susceptible athletes and the latter because sub–maximal quadriceps contractions at an angle where those muscles are stronger than the hamstrings might artificially increase the value of the H:Q<sub>fun</sub> ratio above the 0.96–1.05 cut–off range (Aagard *et al.*, 1998; Croisier, 2004; Croisier *et al.*, 2008; Yeung *et al.*, 2009) thus underestimating the potential for a future

hamstring injury. Fitting  $R_E(\omega, \theta)$  function on the isovelocity data can provide an early indication of any such issue thus reducing that risk (Figure 3.8).

The main advantage of the  $R_E(\omega, \theta)$  function however is that it provides angle-specific estimates of the H:Q<sub>fun</sub> ratio value at obtuse angles of extension. As it was discussed earlier, hamstring strain injuries are among the most common injuries in a variety of sports such as Australian football (Orchard *et al.*, 1997; Bennel *et al.*, 1998; Orchard & Stewart, 2002), soccer (Woods *et al.*, 2004; Ekstrand *et al.*, 2011a) and sprinting (Drezner *et al.*, 2005; Alonso *et al.*, 2012; Opar *et al.*, 2012). Despite extensive research on the issue the mechanisms of these injuries remain unclear. As it was discussed in preceding sessions, Thelen *et al.* (2005b); Chumanov *et al.* (2007), among others, proposed that acute hamstring injuries may be related to excessive stretch of the hamstring during the late swing phase of the gait cycle whereas Yu *et al.* (2008) hypothesized that the magnitude of eccentric force is maximum during the stance phase. However, the majority of those studies agree that the injuries take place at extremely obtuse angles of knee joint extension. Unfortunately, obtaining reliable torque data at those angles is very difficult as they often fall outside the experimental isovelocity region especially at high isovelocities. For that reason is important to have both a good qualitative and quantitative description of the H:Q<sub>fun</sub> ratio at those ranges and this can be provided by the  $R_E(\omega, \theta)$  function (Figure 3.7). It is worth noting that 5 of the total number of points used in the fit correspond to isometric measurements ( $\omega = 0$ ). These points are the easiest to obtain experimentally and offer the added benefit of a high test-retest reliability (Maffiuletti *et al.*, 2007). Six further ratio points,  $R_{exp}$ , were used (in the case of the 11-point fit) to obtain the  $R_E(\omega, \theta)$  values, two each from isokinetic measurements at 60, 240 and 400°/s. Obtaining the  $R_{exp}$  ratio values is a relatively simple process that can be performed as soon as the isovelocity data has been collected. This makes it possible for the  $R_E(\omega, \theta)$  values to be calculated in a single testing session by the researcher or even a team tester that may not be an expert in the field. Considering that the alternative would be to follow the multi-step process described in equations (3.1) through (3.3) employing the  $R_E(\omega, \theta)$  function not only significantly reduces the need for extensive isokinetic testing protocols but also the time needed for data processing.

### 3.4.2 Implications of the $R_E(\omega, \theta)$ fit

To obtain a picture about the  $H:Q_{fun}$  values near full knee extension the  $R_E(\omega, \theta)$  function was evaluated at  $(400^\circ/s, 172^\circ)$ , a point which is outside the isovelocity range of an isokinetic dynamometer, for the 14 subjects that participated in Evangelidis *et al.* (2015) (Table 3.9). The mean  $R_E$  value for the 14 subjects was 2.73 which compares well with the reported value of approximately 1.6 at  $145^\circ$  in this study considering that  $H:Q_{fun}$  was shown to increase with angle.

Thirteen out of fourteen subjects exhibited  $H:Q_{fun}$  values that were notably higher than any of the cut-off values that have been reported in the literature as possible injury predictors. Since those values were calculated at a greater extension angle than those usually used in experimental studies on the  $H:Q_{fun}$  ratio it is logical to assume that the muscle would be more susceptible to injury at such an angle of extension. However, this is not reflected on the  $R_E(\omega, \theta)$  values which show that hamstrings are comfortably stronger than quadriceps at this angle. This observation may imply that physiologically the hamstrings are capable of acting antagonistically to the quadriceps at those angles and contraction velocities and that the underlying cause of the hamstrings' strain injury can not be explained in terms of a '*strong quadriceps vs weak hamstrings*' scenario. Hill's model  $T-\omega$  relationship shows that near full extension the quadriceps have all but lost their ability to contract concentrically and it is not their action as agonists that the hamstrings are contracting eccentrically to counteract. Therefore, the  $H:Q_{fun}$  ratio is not mechanical threshold but rather a correlation between the torque that has been developed during the course of the extension and the capacity of the hamstrings muscles to counteract it with the joint near, or at, full extension. A further complication is that there are more than one factors that contribute to the torque vector at the knee other than the concentric action of the quadriceps such as the hip flexion angle and the mass of the shank + foot segment (Guex *et al.*, 2012)

However, the quadriceps concentric torque is the biggest component of the total knee torque vector and therefore there will be a direct correlation between its magnitude and the magnitude of the total torque vector. It is possible that it is for that reason that the  $H:Q_{con}$  ratio has been successful as a future hamstring injury predictor as it gives an indirect estimate of the absolute quadriceps strength. Indeed, a low conventional

ratio may not necessarily mean weak hamstrings muscles but strong quadriceps muscles (Cameron *et al.*, 2003; Freckleton & Pizzari, 2013). This is something that the H:Q<sub>fun</sub> ratio can not easily detect as it is estimated at angles where quadriceps are at their weakest and their potential for torque production can be obscured by the more powerful (due to angle and mode of contraction) hamstrings.

Consequently, a new mixed H:Q<sub>fun</sub> ratio could be introduced and tested where the peak torque during hamstrings eccentric contraction at an angle near full extension is divided by quadriceps peak torque obtained at or near 60° of knee extension where the quadriceps are at their strongest. Such a ratio would express not only the relative strength of the hamstrings with respect to the quadriceps but also the relative peak strength of the two muscle groups a measure which has also been shown to be a potential risk indicator in HSIs (Cameron *et al.*, 2003; Freckleton & Pizzari, 2013; Opar *et al.*, 2012).

### 3.4.3 Conclusions

In this study the functional H:Q<sub>fun</sub> ratio was described as a function of  $\omega$  and  $\theta$ ,  $R_E(\omega, \theta)$ . The function was fitted to a variety of experimentally obtained ratio points and its accuracy was assessed by means of  $R^2$ , RMSE and NRMSE values. The function was robust to changes in the number of points used in the fit and exhibited consistent results across all fits. Those results showed that the  $R_E(\omega, \theta)$  function can provide a fast and accurate enough description of the 3-dimensional H:Q<sub>fun</sub> ratio profile of a test subject without them having to undergo extensive and time consuming isovelocity tests. Indeed, only a minimal dataset per subject is needed to obtain reliable results which makes  $R_E(\omega, \theta)$  suitable for use in studies or physical assessments involving a large number of subjects or athletes that have to be tested and their results evaluated in a short time frame. Moreover in the case where the  $R^2$  score of the fit is low or the fit deviates from the theoretical shape it is likely that those discrepancies were caused either by weak hamstrings muscles or from potential abnormalities in the measurements. If that is the case the latter should be re-evaluated and possibly repeated to ensure that a potential hamstrings weakness did not go unnoticed.

The evaluation of the function requires a single MATLAB or EXCEL script which

allows its use by non-specialist staff during the testing session. It would be possible to apply  $R_E(\omega, \theta)$  even in the case where the use of specially written script is not possible during a testing session and a more rudimentary approach such as manually recording and dividing torque values has to be employed as the function was shown to be robust when there was a five degree differential in the joint angle where torque was obtained for hamstrings and quadriceps.

### 3.4.4 Limitations and future work

The  $R_E(\omega, \theta)$  function's accuracy is limited by the characteristics of the experimental data that is fitted upon. The closer to the theoretical profile the experimental data is the better the fit will be and the more accurate the prediction of the H:Q<sub>fun</sub> ratio values. However, extreme care has to be taken when those values are within 12 – 13% of the injury cut-off range (0.96–1.05) and the NRMSE scores must be assessed and factored in carefully in order to avoid erroneously over- or underestimating the cut-off value.

The aim of future work should be to employ the  $R_E(\omega, \theta)$  function in large prospective studies, such as those of Orchard *et al.* (1997) or Croisier *et al.* (2008) in order to assess its efficiency in recognizing athletes in higher risk of HSIs compared to the H:Q<sub>fun</sub> or H:Q<sub>con</sub> ratios. It can also be used in studies such as that of Evangelidis *et al.* (2015) where the H:Q<sub>fun</sub> ratio is explicitly calculated for a wide range of joint angles as this will offer a measure of its ability to reproduce the raw data and will help improve its accuracy.

# 4 Introduction to computer simulation of a sporting activity

It is very difficult to discern the elements that make for a successful Snatch lift by only studying lifters performing it as no matter how successful a lifter may be it is always likely that they are using sub-optimal technique or they had to adapt their technique to account for joint mobility issues, segment asymmetries, old or current injuries etc. Experimental data of snatch kinetics and kinematics provides useful information on the techniques employed by lifters but that method of investigation cannot be used to predict what technique an athlete should employ in order to maximise the weight lifted and how technique varies with different athlete body types and biomechanical characteristics.

However, as stated by Yeadon & King (2008) (pg 197) “it is possible to use a simulation model to gain insight into the mechanics of sports techniques”. Indeed, a number of sports techniques has been, studied, analysed and, in some cases optimised using computer generated models that simulate the specific sport activity. The majority of computer simulation models used in sports biomechanics are rigid-segment models that represent the basic structure of the whole human system as a whole or a part of it (Whittlesey & Hamill, 2014). The level of complexity of the model i.e. the number of segments used, the dimensionality of the model (one-, two- or three-dimensional) etc. depend on the activity being studied and the aim of the study itself (Yeadon & King, 2008). However, even seemingly simple models can provide good representations of various sporting activities. An often quoted example is the 2-dimensional, two segment model of Alexander (1990) used to predict take-off velocities for the high and long jumps that were remarkably close to literature values. King *et al.* (1999) also used a 2-segment model to simulate the pre-flight phase of the Hecht vault. The predicted vertical and angular velocities of the model showed good agreement with respective real competition values. In a 2-dimensional model each segment is usually defined by four parameters, specifically: Segment length, mass, center of mass (henceforth COM) location and its moment of inertia. The segments are usually joined together using some type of frictionless joint such as “hinge” or “pin” joints that only allow one

degree of freedom (rotation) however, more complex configurations involving linear springs have been used for the representation of the shoulder joint (Hiley & Yeadon, 2003a).

On the other hand, Yeadon (1990b) employed an 11-segment, 3-dimensional model in order to simulate and analyze techniques used in twisting somersaults. Despite a number of assumptions such as negligible air resistance, symmetry with respect to the sagittal plane and immobility of the head, wrist and ankles the model exhibited maximum deviations of 0.04 revolutions for somersaults,  $7^\circ$  for tilt and 0.12 revolutions for twists. Rigid-body models have also been used in simulations of the squat jump (Domire & Challis, 2007), high bar dismounts (Hiley & Yeadon, 2003b), tumbling (Yeadon & King, 2002), long jump (Hatze, 1981), speed skating (Bobbert *et al.*, 2002) e.t.c.

## 4.1 Model actuation

Simulation models can be either kinematically or kinetically driven. In kinematically driven models the angle time histories of the model's joints are commonly input to the model and used to calculate the COM position and the kinetics of the model whereas in kinetically driven models the joint torque or muscle time histories combined with the muscle activation timings are input into the model in order to calculate its kinematics.

### 4.1.1 Angle driven models

Angle driven models are mainly used to model activities where the strength capacity of an athlete is not important, such as the aerial phase of trampolining (Yeadon, 1990b) or of a high bar routine (Hiley & Yeadon, 2003b; Yeadon & King, 2008). They are usually complex models with a high number of degrees of freedom due to the fact that is easier to record the joint time histories of an athletic performance than it is to determine the muscle parameters of the athlete that performed the exercise (Yeadon & King, 2008). Unfortunately this advantage is also a limiting factor when the joint angle time histories are manipulated to optimise the movement as the resulting forces may be physically impossible and thus unrealistic. This is a significant disadvantage

as most simulated movements are strength dependent and if there are no strength parameters to be optimised it becomes very difficult to find new motion patterns or optimise technique characteristics. Hiley & Yeadon (2003b) accounted for this by using surface fits similar to those of Figure 3.1 for the three joints of their model. The force produced at the joints during optimisation at a specific angle and angular velocity was compared to the respective value from the surface fit and if it exceeded it the simulation was given a penalty to avoid arriving at a physically impossible optimized state.

### 4.1.2 Muscle driven models

Another way to avoid the pitfalls of angle driven models during optimisation is to avoid using joint angle histories in the first place and instead actuate the model using the subject's strength characteristics. There are two options as to how this can be achieved.

The first is to model the muscles around the joint whose motion is simulated by including mathematical representations of individual muscles (Pandy *et al.*, 1990; Pandy, 2003). This approach is based on a Hill-type model (Caldwell, 2014) which consists of three components. A contractile element, a series elastic element and a parallel elastic element. The contractile element's role is to turn active signal into force. The magnitude of the produced force depends on three different relationships that define its mechanical characteristics. The force-length relationship, the force-contraction velocity relationship and the force-activation relationship (Caldwell, 2014).

The series elastic component represents the elasticity of passive connective tissues in the musculo-tendon complex and more specifically of the tendon and the aponeurosis (Kawakami *et al.*, 2002). At maximum isometric force the series elastic component stretches by approximately 5–6% (Muramatsu *et al.*, 2001). The parallel elastic component represents the fascia that surrounds the muscle and the individual muscle fibres that produce a non-linear force response even when the musculo-tendon complex is passively stretched (Caldwell, 2014). However, the produced force is very small for normal working ranges of joints and for that reason is often omitted from models (Yeadon & King, 2008).

As it was stated earlier the use of muscle driven models ensures that the model's force output remains physiologically plausible (as long as the parameter input values are chosen accurately). Moreover, models based on individual muscle representations can represent the actual muscle architecture and model the function of biarticular muscles such as the rectus femoris or biceps femoris. This allows the evaluation of contributions of individual muscles during activities such as walking (Pandy, 2003). The downside of such a model, however, is that muscle parameters such as peak isometric force, length and pennation angles of the muscle fibres cannot be determined for each subject individually and they must be estimated from generic literature values which may severely affect their relevance to those of the subject. Consequently, it is not possible to customise the model to the individual subject which precludes its quantitative evaluation (King & Yeadon, 2002). Additionally, the number of parameters that have to be optimized is often so high that requires the use of a supercomputer which may not be widely available Anderson & Pandy (2001).

### 4.1.3 Torque driven models

In torque driven models the cumulative effect of the individual muscles around a joint is represented by a single torque generator function for extensor and another one for flexors. This approach is also based on Hill's muscle model but instead of relying on animal or cadaver data for the derivation of the force-length, force-velocity and force-activation relationships, those can be determined using an isovelocity dynamometer. The net torque is measured over a range of angles and angular velocities and a 3-dimensional torque profile (Figure 3.1) is obtained for the subject using the 9-parameter function defined by equations (1.14), (1.16) and (1.17) (King & Yeadon, 2002; Yeadon *et al.*, 2006; Forrester *et al.*, 2011). The series elastic element parameters are still literature based however, Yeadon & King (2002) showed that its inclusion in the model had minimal effect provided that the simulated activity did not involve muscle stretching under high loads. Since a torque driven model is customized to individual subjects is possible to evaluate the performance of the model by comparing its output against performance data of the subject (Yeadon, 1990b; Yeadon & King, 2002; Yeadon *et al.*, 2006).

Representing the net effect of muscle group action via a torque generator is not without disadvantages however. Perhaps the most significant one is the inability of equations (1.14), (1.16) and (1.17) to account for changes in the length and contraction velocity of biarticular muscles during whole body movements as it is implicitly assumed that all muscles are mono-articular. Lewis *et al.* (2012) used a 19-parameter, two-joint torque generator function of the ankle joint that incorporated the effects of the change in knee angle on the torque output. They found that the single joint representation of (1.14), (1.16) and (1.17) greatly overestimated ( $\approx 20\%$ ) the ankle torque values when the knee joint was flexed by more than approximately  $40^\circ$ . They also found that overall the two-joint torque generator was able to match the measured ankle torques much better than the single joint description (RMS range: 2–7% vs 4.4–20% respectively) suggesting that the former offered more accuracy especially for knee flexion angles of more than  $40^\circ$ .

## 4.2 Model activation and control

A torque generator function essentially determines the maximum amount of net torque,  $T_{max}$ , available at the joint depending on the joint angle and the angular velocity of contraction. The assumption is that this torque is produced by the muscles that actuate the particular joint whilst contracting at their full capacity (Yeadon *et al.*, 2006; Forrester *et al.*, 2011). However, muscles are rarely maximally activated, even under dynamic conditions therefore it would be unrealistic to utilize the full amount of torque available by the torque generators in the model. Consequently the torque input must be regulated to match the actual performance and this is achieved through a single variable activation function, with respect to time,  $t$ , that takes values between 0 and 1, ACT (Neptune & Hull, 1999). The joint torque,  $T_{joint}$ , is then defined as

$$T_{joint} = T_{max} \times ACT$$

In its simplest form ACT takes one of two possible values, 0 or 1, i.e. the torque generator is either off or maximally activated. This is known as the “bang-bang” method and its main advantage is that there are no parameters to optimise (other than time of activation) during a simulation which in turns saves a lot of computer power

and time (Alexander, 1990; Pandy *et al.*, 1990; van Soest *et al.*, 1993; Chowdhary & Challis, 2001). The downside of that approach is that it implies that all motor units in a muscle are activated at the same time which contradicts the “size principle” (Yeadon & Challis, 1994; Enoka, 2008).

With advancements in computer power more complex forms of model control have been implemented. Yeadon & King (2002) used an S-shaped three-parameter activation function that allowed torque at each joint to ramp up from an initial level to maximum activation and remained maximally activated until the end of simulation. The minimum ramp up time was set at 50 ms and the initial activation levels were less than 0.5. Mills *et al.* (2008, 2009) used a four-parameter S-shape activation function with variable activation levels for extensors and flexors. The activation levels were not allowed to ramp down from maximal activation, probably due to the fact that these models studied maximal and short in duration muscle contractions.

In a slightly different representation Domire & Challis (2007) modelled the activation function as a series of nodes separated by 0.05 and used linear interpolation to determine the activation levels between the nodes, producing a linear activation time-series. A similar approach had been previously followed by Spägle *et al.* (1999) who modelled activation levels as the elements of a column vector corresponding to different moments in times. In both methods the activation levels were allowed to decrease once they reached maximum values. The downside of the former approach is that it may cause the activation profile to oscillate between nodes and this oscillatory behaviour is mirrored by the torque profile.

### **4.2.1 Ground contact**

Perhaps the simplest way to model the interaction between the simulation model and the ground surface is via a hinge joint. This type of joint has been used in muscle models that simulate jumping movements (van Soest *et al.*, 1993; Bobbert *et al.*, 2002) however because it only allows one degree of freedom (rotation) it cannot be used to model translational motion of the contact point, or movements where the initial contact velocity is not zero. Consequently, it is not suitable for models that simulate walking, running, landing or any activities that include impacts (Yeadon & King, 2008).

In order to model the interaction between the model and ground during the aforementioned activities one or more viscoelastic elements are used (usually springs). Depending on the type of contact simulated the number of springs used may vary from two (Yeadon & King, 2002) up to sixty-six (Wright *et al.*, 1998), located at one or more contact points (Hase *et al.*, 2003; Mills *et al.*, 2008). The complexity of the springs used ranges from simple linear springs with damping of the form (King & Yeadon, 2004)

$$F = -\kappa\Delta x - b\dot{x}\Delta x$$

to highly non-linear spring-damper systems (Pain & Challis, 2001b).

The viscoelastic parameters, such as the stiffness,  $\kappa$ , and damping,  $b$ , coefficients of the above equation, either are obtained experimentally (Pain & Challis, 2001a) or can be optimised by choosing initial values that are subsequently allowed to vary within bounds until the simulation optimally matches the actual subject performance (Yeadon & King, 2008; Mills *et al.*, 2006).

## 4.3 Model optimisation and evaluation

### 4.3.1 Optimisation

Optimisation can be described as “the process of search for the solution that is more useful than several others” (Venkataraman, 2009) (pg: 3). During the optimisation process a number of *design variables* will systematically vary subject to certain *constraints* until a specified *cost* or *objective* function is maximized or minimized. The constraints are imposed either via specific constraint functions or via upper and lower bounds on the values of the design variables. Optimisation problems with constraints are called *constrained* problems whereas those without constrained are called *unconstrained*. In the sports biomechanics context the objective function may describe the relation between the performance of a simulation model and the actual task that it simulates. In this case the objective function may be the root mean square difference between the time histories of the model’s and subject’s joint angles which must be minimized in order for the performance of the model to resemble as much as possible the actual one. Alternatively, if the aim of the simulation is to maximise performance

the objective function may simply be a specific performance criterion such as jump height (Yeadon & King, 2008).

The two main optimisation approaches used in sports biomechanics are *static* and *dynamic* optimisation procedures. In the static optimisation approach the net moments at joints are calculated with the inverse dynamics method and numerical optimisation is then used to find which combination of muscle forces best reproduces these moments by minimizing the objective function at each time step. The downside of this approach is that the algorithm may come up with a different combination of muscle groups that reproduce the net moments at successive time steps and also a single muscle may be picked to balance the joint torques which is physiologically unrealistic (Caldwell, 2014; Crowninshield & Brand, 1981).

On the other hand the dynamic approach is used with forward dynamics models where the muscle forces are input to the muscle model to simulate motion. In this case the design variables in the optimisation are the parameters that define the necessary muscle stimulation patterns (e.g. activation function parameters) to achieve the optimal solution (Caldwell, 2014). It could be argued that the dynamic approach is able to “synthesize” and analyse body motion, whereas the static approach can only perform the latter, and therefore it allows researchers to create and study performances for which no experimental data has been collected i.e. in studies where optimal performance is sought (Hiley & Yeadon, 2003b,a; Allen *et al.*, 2010). Unfortunately, the greater versatility of the dynamic approach comes with an increased computational cost since the complete movement must be simulated in every iteration in order to obtain the objective function. Depending on the optimisation algorithm used it may take days or even weeks for an optimal solution to be reached.

There are various methods that can be employed to minimise the objective function. The two main factors that must be considered when an optimisation algorithm is chosen are:

1. How fast the algorithm can find an optimum
2. How capable the algorithm is of finding the global optimum solution and not getting stuck at a local optimum

Unfortunately there is a trade off between speed and accuracy as “fast” algorithms such as the Simplex method (Venkataraman, 2009) tend to find local optima whereas more accurate algorithms such as the Simulated Annealing (Corana *et al.*, 1987) and Genetic algorithm methods (Holland, 1975) are better at finding the global optimum but take longer to arrive there as they are largely heuristic methods and generally involve large amounts of computation. Simulated Annealing is based on cooling of metals to obtain defined crystalline structures based on minimum potential energy whereas Genetic Algorithm is based on the combination and recombination of genes in a biological system leading to improved DNA sequences (Venkataraman, 2009).

### 4.3.2 Evaluation

Before a model can be employed in the analysis of optimal performance it is advisable to quantify the accuracy with which it reproduces the experimental data. This is usually done by comparing a simulation, run with a specific set of initial conditions, against the actual performance from which the initial conditions were derived. For example, Yeadon & King (2002) evaluated a torque driven simulation model of the take off phase in tumbling by comparing simulations against the actual take off performances of the athlete the model was based on. This was done by deriving a function that expressed the difference in joint angles and take off kinematics between model and athlete which was subsequently minimised using the Simulated Annealing algorithm . A similar function that also included the difference in ground reaction forces was used in (King *et al.*, 2006)

# 5 The Snatch

## 5.1 Literature Review

The snatch is one of the two lifts contested in the sport of Olympic weightlifting. It requires the athlete to lift a barbell from the floor to an overhead position in one continuous movement. The movement itself can be broken down in 6 different phases (Baumann *et al.*, 1988; Bartonietz, 1996; Gourgoulis *et al.*, 2000).

1. The first pull. During this phase the movement of the bar off the ground is initiated predominantly through extension of the lifters knees and to a much lesser extent of the hip. The phase is completed when the bar reaches approximately knee level, Figures 2a & 2b.
2. The transition phase which is characterised by the flexion of the knees and extension of the hip which leads to a body configuration akin to the bottom position during a countermovement jump, known as the power position (Everett, 2009), Figure 2c.
3. The second pull. The violent extension of the knee, hip and ankle (plantar flexion) that generates and transfers power to the bar to displace it overhead. During this phase the bar reaches maximum vertical velocity prior to peak displacement, Figure 2e.
4. The turn over under the bar (third pull) where the lifter moves rapidly under the bar to adopt the catch position, Figure 5.3a.
5. The catch phase where the athlete receives the bar overhead at a squat position with arms locked at full extension, Figure 5.3b.
6. The return to a standing position by performing an overhead squat, Figure 5.4.

Various kinematic studies have been performed on the bar trajectory during the lift and the consensus seems to be that there is very little variation in the technique employed by lifters during the first two phases (Gourgoulis *et al.*, 2002; Schilling *et al.*,



(a) Start of the Snatch lift



(b) End of first pull

Figure 5.1: First pull



(a) Transition phase



(b) Second pull

Figure 5.2: Transition phase and second pull



(a) Turn over



(b) Catch

Figure 5.3: Turn over and catch



Figure 5.4: Recovery

2002; Isaka *et al.*, 1996; Akkus, 2012; Kipp *et al.*, 2012). The bar is pulled towards the lifter during the first pull and until the end of the 2nd (transition) phase (Appendix L). The 3rd (2nd pull) phase of the snatch is initiated at approximately mid-thigh and is

a combination of several joint rotations. The ankle, knee and hip extensors contribute to the 2nd pull in a sequence that progresses from the hip to the ankle (Burdett, 1982; Isaka *et al.*, 1996; Ikeda *et al.*, 2012; Gourgoulis *et al.*, 2000; Ho *et al.*, 2014). These actions cause the bar to follow an S-shape trajectory that exhibits a small horizontal displacement as well as vertical (Garhammer, 1985; Baumann *et al.*, 1988; Bartonietz, 1996; Garhammer, 2001). However, the degree and manner in which each extensor muscle group is employed varies significantly between lifters as, for example, the degree of ankle plantar flexion, the angle of hip and knee extension at the beginning of the second pull and their respective values at its end. It has been hypothesized that those differences may explain, partially at least, observed variations in the horizontal displacement of the bar during the lift (Isaka *et al.*, 1996; Schilling *et al.*, 2002; Garhammer, 1985; Burdett, 1982). Consequently, the lift biomechanics depend on the physical characteristics of the individual lifter and as such they must be factored into technique training at, preferably, an early stage of a lifter's career so that the optimum lifting pattern is ingrained through repetition (Garhammer, 1985; Winchester *et al.*, 2009; Gourgoulis *et al.*, 2009; Ho *et al.*, 2014).

### 5.1.1 Quantitative analysis

Snatch technique analysis has been mainly used to study the technique of a lifter, identify and correct technical faults by providing individually targeted feedback (Gourgoulis *et al.*, 2000, 2002; Garhammer, 1991; Schilling *et al.*, 2002).

Most technique studies have employed the two-dimensional (2-D) kinematic analysis method using a single camera and capturing motion on a single (sagittal) plane (selected references: (Chen & Chiu, 2011; Chiu *et al.*, 2010; Enoka, 1988; Garhammer, 1980, 1985, 2001)). The main advantage of the method is that it requires only one camera which makes it easy to use especially during competitions. It is limited however, to a single plane of motion and thus cannot account for rotations or translations that may occur in the transverse and frontal planes and also cannot account for the knee joint angle as the knees are obstructed by the weights (Baumann *et al.*, 1988). These issues are addressed by using three-dimensional (3-D) kinematic analysis either with the use of minimum 2 phase-locked cameras placed diagonally at 45° angles (Baumann *et al.*,

1988; Gourgoulis *et al.*, 2002; Harbili & Alpteking, 2014) or, more recently by means of 3-D motion capture involving a multitude of infra-red cameras (Hadi12, Ho11, Kipp12, Kipp15).

These techniques allow for the capture and analysis of a large number of variables that affect directly or indirectly the success or failure of the lift (Isaka *et al.*, 1996; Campos *et al.*, 2006; Gourgoulis *et al.*, 2002; Hoover *et al.*, 2006; Stone *et al.*, 2006). These variables can be broadly classified into two categories; Bar and joint kinematics. A brief synopsis of the most important variables from each category will next be given.

## **5.1.2 Bar Kinematics**

### **5.1.2.1 Vertical displacement of the bar**

The vertical displacement of the bar is a key aspect of the lift. The higher the bar reaches at the end of the second pull the more time the lifter will have to drop under it and achieve a more advantageous receiving position which in turn will make the recovery easier. Peak displacement in successful lifts varies between  $1.15 \pm 0.07$  and  $1.27 \pm 0.07$  m (Campos *et al.*, 2006; Baumann *et al.*, 1988; Gourgoulis *et al.*, 2000, 2002) or approximately 70% of the lifters height (Medvedyev, 1986; Campos *et al.*, 2006). There is also evidence that the vertical drop of the bar from maximum height attained to catch position is a strong indicator of effective technique (fast turn over) with a mean value of 11.3% of maximum height reported by Gourgoulis *et al.* (2000) in agreement with previous observation from Isaka *et al.* (1996) and Baumann *et al.* (1988).

### **5.1.2.2 Bar Trajectory**

It is usually described in reference to a line in the sagittal plane which is vertical to the transverse plane and passes through the edge of the bar at its starting position. As it was mentioned earlier, in general the trajectory resembles the shape of the letter S however there are two distinct variations depending on whether the bar travels both outside and inside the vertical line or only inside (Baumann *et al.*, 1988; Chen & Chiu, 2011; Bartonietz, 1996; Hoover *et al.*, 2006; Ho *et al.*, 2014). Whichever trajec-

tory is produced seems to depend on the training history and the morphology of the weightlifter. It is important that there is as little anterior-posterior movement of the bar as possible (i.e. small loops in the S-curve) particularly during the second pull, as a big outwards curve means that the bar travels away from the centre of mass (COM) of the lifter increasing the likelihood of failure (Garhammer, 1985; Baumann *et al.*, 1988; Schilling *et al.*, 2002; Chen & Chiu, 2011; Ikeda *et al.*, 2012).

### 5.1.2.3 Bar Velocity

The peak vertical velocity of the bar is an important dimension in coaching and as such it has been researched extensively (selected examples: Garhammer *et al.*, 1980, 1985; Baumann *et al.*, 1988, Campos *et al.*, 2006; Gourgoulis *et al.*, 2000; Isaka *et al.*, 1996; Hoover *et al.*, 2006; Schilling *et al.*, 2002). It has been established that bar velocity increases during the lift (Garhammer, 1985; Baumann *et al.*, 1988; Isaka *et al.*, 1996; Gourgoulis *et al.*, 2000) however, what differentiates elite lifters is their ability to keep accelerating the bar (or not decelerating it) during the transition phase (Baumann *et al.*, 1988; Bartonietz *et al.*, 1996; Stone *et al.*, 2006). Peak bar velocity in successful lifts at the end of the second pull phase has been reported to range between  $1.68 \pm 0.03$  and  $1.98 \pm 0.09$  m/s whereas the respective values during the first pull range from  $1.13 \pm 0.07$  to  $1.26 \pm 0.17$  m/s emphasizing the power development during the second pull (Burdett, 1982; Medvedyev, 1986; Akkus, 2012; Ho *et al.*, 2014)

### 5.1.3 Joint Kinematics

Joint kinematics are usually expressed as angular displacement and/or velocity of the ankle, knee and hip joints and the joint actions during the 6 phases are well understood. During the first pull knees extend to lift the bar off the floor with very little hip extension until the bar reaches the knees when the hip starts to extend and the transition phase begins. At the end of transition the knees flex and the ankles dorsi-flex to allow the lifter to adopt the power position prior to the second pull. During the second pull a triple extension of the three limb joints from distal to proximal takes place followed by fast flexion that allows the lifter to move under the bar (turnover). The joints continue to flex so that the lifter can adopt the catch position and finally

they extend again during recovery (Baumann *et al.*, 1988; Bartonietz, 1996; Campos *et al.*, 2006; Hadi *et al.*, 2012; Gourgoulis *et al.*, 2000, 2002; Stone *et al.*, 2006).

### **5.1.3.1 The double knee bend**

Although the sequence of joint motion is well studied and understood, little research has been done on the optimal timing strategy for the initiation of each phase and how this relates to body configuration expressed in terms of joint angles (Kipp *et al.*, 2012; Murphy *et al.*, 2014; Ho *et al.*, 2014). An example of this is the double knee bend action which is a popular term in weightlifting literature used to describe the sequence knee-extension-flexion-extension which takes place during the first pull, transition phase and second pull respectively. This joint action is often considered as evidence of the lifter utilizing the stretch-shortening cycle of the knee extensors in order to propel the bar upwards (Isaka *et al.*, 1996; Gourgoulis *et al.*, 2000; Stone *et al.*, 2006). However, the timing of the second knee extension with respect to the positions of the hip and the bar and the effect it might have on the bar kinematics has not been explored.

### **5.1.3.2 The Barbell-Cervical-Hip Angle (BCH)**

This is the angle defined on the sagittal plane by the following three points: the edge on the bar, the seventh cervical vertebra (C7) and a point on the hip placed at the greater trochanter. This variable has been introduced recently (Chiu *et al.*, 2010; Chen & Chiu, 2011) and is a measure of the lifters ability to maintain the barbell at close proximity to their body during the lift reducing its horizontal displacement. Although it is not clear whether there is a correlation between values of BCH and success in the Snatch it provides a means of correlating barbell and joint kinematics and it may be worth examining in future studies.

## **5.2 Data Collection**

In this section the experimental protocol used to collect kinematic, kinetic and anthropometric data from a, male, amateur competitive weightlifter (age: 28 years, height:

1.69 m, weight: 69 kg, personal best in Snatch: 95 kg) is outlined. The subject gave written, informed consent and the study was conducted in accordance with the approval given by the Loughborough University Ethical Advisory Committee. Kinematic and kinetic data was collected over a total of five testing sessions, each spaced a week apart.

### 5.2.1 Motion Capture

The analysis of human movement requires information on kinematics of motion. Such information is usually obtained either via video-based or semi and fully automatic data collection methods (Elliott *et al.*, 2007). Video-based motion capture is, in general a lot cheaper than other methods to perform as it can be used in various environments, e.g. underwater or outdoors, and does not require the attachment of markers or sensors on the performer which can be a disturbing factor and excludes the use of marker-based systems during competitions (Payton, 2008). The downside of the video-based approach is that the quantitative analysis of the captured data is time-consuming as it usually requires the manual digitisation of a large number of body landmarks for every frame of the captured video. For a 50 Hz camera that would require the digitization of 50 frames for every second of the recorded trial. The large number of frames that need to be digitised and the manual character of the analysis make the consistent identification of body landmarks difficult and the analysis susceptible to human (operator) error (Challis, 2008)

Semi-automatic and automatic motion capture methods are based on the use of retro-reflective markers (optical-passive methods) that are tracked by infrared cameras (VICON T) or LED markers that are connected through wires to a unit attached on the subject and emit light in a predetermined sequence that allows each marker to be identified by the motion analysis unit of the system (e.g. VisualEyez, Phoenix Technologies). The advantage of the automated systems is that motion analysis can be performed much quicker and without the operator induced errors in landmark identification as there is no manual digitization involved (Yeadon & Challis, 1994). Consequently, they exhibit better accuracy than video-based systems. For example, Elliott *et al.* (2007) measured the inherent error of VICON-612 (optical-passive) and Peak Motus (video-based) systems during the flexion-extension of the elbow angle in cricket bowling. They found

that the latter had an RMSE error of  $2.3^\circ$  almost four times larger than the RMSE of the VICON system's  $0.6^\circ$ . Richards (1999) also reported lower RMSE values for the VICON system compared to Peak Motus when measuring the distance between two fully visible markers (0.062 vs 0.091 cm) and the angle between the markers on a rotating plane ( $1.421^\circ$  vs  $3.772^\circ$ ).

However, despite the improved accuracy and speed of analysis automatic systems are not without shortcomings. The first is that their use is precluded in competition as it not possible to attach markers to competing athletes (Yeadon & Challis, 1994). Secondly, there is a discrepancy between the relative movement of the skeleton and the markers due to the interposition of passive and active soft tissues (Cappozzo *et al.*, 1996). For example, a marker attached on the lateral epicondyle of the femur may move back up to 4 cm relative to the bone during knee flexion with obvious implications on the accuracy of the knee joint centre calculation. Additionally, depending on the activity captured, some of the markers may become obscured from camera view during part of the activity. If that happens then reconstruction of the marker's trajectory is problematic as it will have to be estimated either by the operator or by the software which again introduces error into the calculation (Challis, 2008).

One way to eliminate the problem of marker loss is to use electromagnetic tracker systems that utilize an electromagnetic dipole field that is emitted by a source. The electromagnetic field is sensed by specialized receptor units and based on the strength of the field that varies with the receptor-source distance calculate the position and orientation of each marker in 6 degrees of freedom. Since no cameras are used the points being tracked cannot go out view or be obscured and they can produce data in real time. Unfortunately, those systems tend to be susceptible to magnetic distortions from metal objects in the environment (Richards, 1999) and they may require the performer to carry the power supply of the source emitter which makes its use cumbersome (Yeadon & Challis, 1994)

Since the Snatch is a very dynamic activity where the athlete, ideally, should not be encumbered from wiring and cables a wireless passive-reflective marker system, such as VICON T, is probably best suited for kinematic data collection. VICON T is a system of interlinked cameras that emit infra-red (IR) radiation through arrays of IR LEDs. The IR radiation is then reflected on the reflective markers attached on the

athlete, captured by IR sensors located on the cameras and the position of the markers is determined in a three-dimensional  $x$ - $y$ - $z$  coordinate system.

### 5.2.1.1 Kinematic Data collection

Kinematic data collection took place during the first testing session. Ten VICON T cameras (Vicon Motion Systems LTD, Oxford, UK) were used to collect 3-D joint coordinates of the subject performing the Snatch. All cameras were mounted at various heights on a metal frame surrounding the volume area. The calibrated volume was approximately 4 m long, 4 m wide and 3 m high, to simulate the dimensions of competition platforms as those are defined by the International Weightlifting Federation (IWF). Cameras were set to record at 250 Hz.

Subject preparation begun by instructing the athlete to thoroughly warm-up using their preferred warm-up routine. When the athlete indicated that he was ready fifty-one, 14 mm, retro-reflective markers were positioned at locations of the subjects body in order that the positions of joint centres could subsequently be estimated (Figure 5.5 and Appendix E). Two additional retro-reflective markers were positioned on the



Figure 5.5: Marker placement on the athlete

edges of the barbell in order to define its centre of mass. Markers were applied using double-sided tape and, if necessary, spray-on glue. Reflective parts of the athletes

shoe, bar and collars were covered in black electrical tape to prevent interference with the camera system.

Five successful lifts were recorded at 70 kg (approximately 75% of 1RM) as required by the testing protocol and the 3-D marker data were collected and stored for subsequent reconstruction and analysis. There were no missed lifts. For each lift the athlete was asked to start with each foot on a force platform. The athlete was allowed to rest until he had sufficiently recovered from the previous effort. However, no rest interval exceeded the two minute mark.

### **5.2.1.2 Marker reconstruction**

Once all the trials were recorded the marker positions were reconstructed using the VICON NEXUS suite. A minimum of two cameras were used in marker reconstruction in order to keep track as much as possible of the two ASIS markers that were obscured when the athlete flexed his hip. A basic “marker model” was then created by using suitable groups of markers to define its segments (Figure 5.6). Once the model was created its markers were given suitable names and labelled and marker trajectories were reconstructed. Some of the trajectories were broken at positions where the markers had been obscured during the lift and those gaps were filled either by using cubic splines to estimate the trajectory of the marker within the gap or by estimating its position from the relative position of a second, reference marker. The latter was the preferred method with gaps of 5 frames or more. Care had to be exercised in selecting a reference marker as its trajectory should be as similar as possible to that of the missing marker so that there was no, or very little, relative movement between the reference and the reconstructed markers. For example, the left ASIS marker was used to reconstruct the trajectory of the right ASIS marker. Once all trajectories had been reconstructed the marker positions  $x$ - $y$ - $z$  coordinates were exported and used to determine the joint centres and, subsequently the athlete kinematics for input into the simulation model. Since the data were collected in three dimensions and the simulation model was two-dimensional the coordinates of the  $y$  axis were disregarded and the  $x$  and  $z$  coordinates were kept that defined the sagittal plane in the VICON coordinate system. The joint centres for ankle, knee, hip, shoulder, elbow and wrist joints were

Table 5.1: Joint centre locations

<b>Joint</b>	<b><math>x</math> marker coordinate</b>	<b><math>z</math> marker coordinate</b>
<b>Ankle</b>	Average $x$ coordinates of lateral & medial maleoli markers	Average $z$ coordinates of lateral & medial maleoli markers
<b>Knee</b>	Average $x$ coordinates of lateral & medial knee joint markers	& Average $z$ coordinates of lateral & medial knee joint markers
<b>Hip</b>	Average $x$ coordinates of ASIS & PSIS markers	Greater trochanter markers $z$ coordinates
<b>Shoulder</b>	Acromion process marker $x$ coordinate	Average $z$ coordinates of anterior & posterior shoulder markers
<b>Elbow</b>	Average $x$ coordinates of lateral & medial elbow joint markers	Average $z$ coordinates of lateral & medial elbow joint markers
<b>Ankle</b>	Average $x$ coordinates of ulna & radius styloid processes markers	Average $z$ coordinates of ulna & radius styloid processes markers

determined as described in Table 5.1.

### 5.2.1.3 Kinetic Data collection

Kinetic data collected consisted of anterior-posterior, medio-lateral and vertical ground reaction forces recorded during the first session and joint torques recorded in sessions 2 to 5. Force data were obtained using two Kistler force plates (model 9281E, Kistler LTD, Winterthur, Switzerland) placed parallel to each other. The athlete was instructed to set up and initiate the lift with each foot on either of the force plates. The force platforms had been set up to be operated through the VICON Nexus software and as such they were synchronized with the VICON kinematic data capture system. Force data was recorded at 1000 Hz and later was re-sampled at 250 Hz in order to coincide with the VICON capture frequency. A series of joint torque measurements at the ankle, knee, hip and shoulder joints, were collected using a Contrex isokinetic dynamometer with built-in gravitational torque correction (Con-Trex, CMV AG, Switzerland) over 4 sessions. A series of isometric (ISOM) and maximum concentric-eccentric

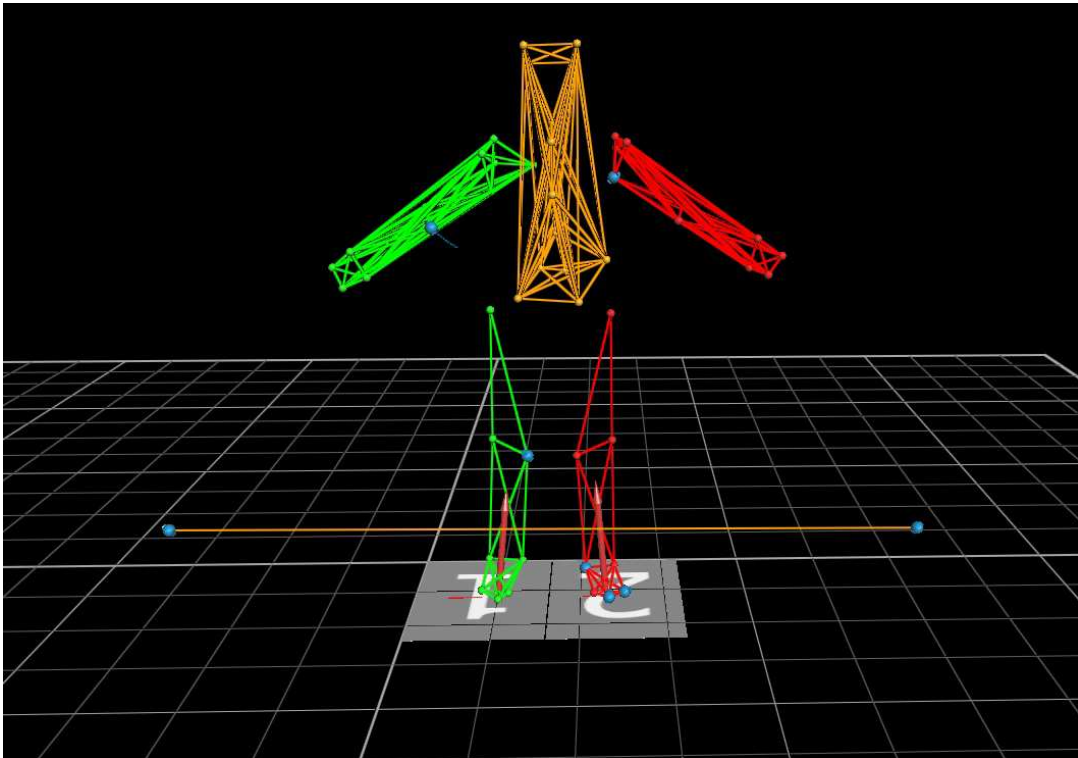


Figure 5.6: Five-segment marker model consisting of foot, shank, thigh, trunk and arms



Figure 5.7: Dynamometer set up for ankle plantar flexion measurement



Figure 5.8: Dynamometer set up for hip flexion measurement

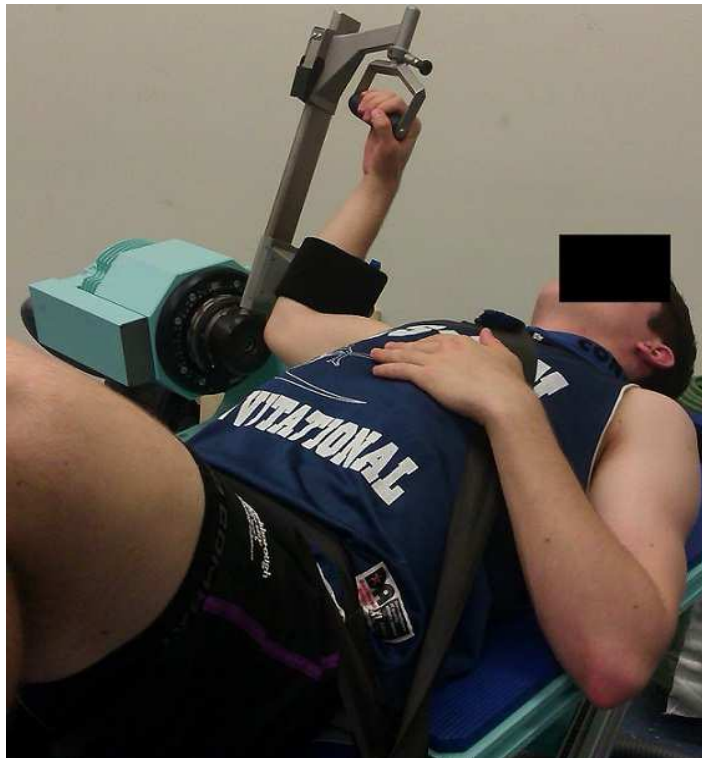


Figure 5.9: Dynamometer set up for shoulder flexion/external rotation measurement

(CON-ECC) isovelocity joint torques were measured for the following joint actions: i) ankle dorsi-flexion, ii) hip extension, iii) hip flexion, iv) knee extension, v) knee flexion,

vi) shoulder flexion with external rotation, Figures 5.7–5.9. Data was collected at 512 Hz. The isometric contractions were performed at 4 (5 in the case of the ankle joint) different crank angles per joint. The values of those angles depended on the range of motion (ROM) of the particular joint and were such as to represent as much of the ROM as possible especially near its limits (Table 5.2). The maximum CON-ECC isoveLOCITY contractions were performed according to the protocol of Yeadon *et al.* (2006) for every joint however, the range and number of angular velocities employed depended on the ROM and the particular joint. This variation was introduced to account for a number of issues concerning the use of isokinetic dynamometers such as the reduction in the time period where the crank arm travels with constant velocity (isoveLOCITY region) that is proportional to the value of angular velocity Chow *et al.* (1997). The angular velocities of contraction and contraction cycles per joint are reported in Table 5.2. During the testing sessions a warm up consisting of three to five isometric con-

Table 5.2: ROM, angles where isometric contractions took place, angular velocities of CON-ECC contractions and number of cycles for CON-ECC contractions. Angles are in degrees ( $^{\circ}$ ) and angular velocities in ( $^{\circ}/s$ ).

<b>Joint</b>	<b>ROM(<math>^{\circ}</math>)</b>	<b>Angle(<math>^{\circ}</math>)</b>	<b>Angular Velocity(<math>^{\circ}/s</math>)</b>	<b>Cycles</b>
<b>Ankle</b>	55.6	7, 17, 28, 42, 53	50, 100, 150, 200	2, 2, 3, 4
<b>Hip-Flexion</b>	78.6	7, 30, 53, 76	60, 180, 300, 400	2, 3, 5, 5
<b>Hip-Extension</b>	77	7, 30, 53, 75	60, 180, 300, 400	2, 3, 5, 5
<b>Knee-Flexion</b>	87	10, 31, 57, 83	60, 180, 300, 400	2, 3, 5, 5
<b>Knee-Extension</b>	85.7	10, 31, 57, 82	60, 180, 300, 400	2, 3, 5, 5
<b>Shoulder-Flexion</b>	128.4	10, 50, 90, 120	60, 120, 180, 240, 320	2, 2, 3, 4, 5

tractions and three separate isovelocity CON–ECC, of two cycles each, at the lowest angular velocity for that joint was performed at sub-maxima levels. This was followed by the testing protocol that consisted of maximal voluntary isometric and CON–ECC contractions (MVC). For the isometric MVC contractions the athlete was given 5 seconds to achieve and maintain maximal torque. For the isovelocity MVC contractions, a varying number of CON-ECC contraction cycles were performed per angular velocity and the maximum concentric-eccentric torque values were subsequently selected for processing from the cycle with the larger torques. Due to time restrictions only one maximal set per angle or angular velocity was performed unless it was deemed that the subject underperformed in which case the trial was repeated.

To account for possible differences between the crank arm and joint angles a mechanical goniometer was used to manually measure joint angles whilst the subject was applying maximal torque on the crank arm during isometric trials. A linear relationship, of the form  $\theta = a\phi + b$ , between the crank arm angles,  $\phi$ , and the joint angles,  $\theta$ , were established via linear regression and this allowed the joint angles to be calculated from the crank data for every angle (Appendix C).

## 5.3 Anthropometry

### 5.3.1 Inertia parameters

Simulation of human motion requires accurate segmental inertia values of the segments that represent the human body in the model. For a rigid segment the inertia parameters that have to be determined are (Yeadon & King, 2008):

- Mass of segment,  $m_s$
- Segment length,  $l_s$
- Segment centre of mass,  $COM_s$
- Moment of inertia,  $I_s$

Those parameters can be determined using a variety of methods that range from experimental techniques such as water immersion, reaction board measurements and oscillation techniques to obtain segment volumes,  $COM_s$  and  $I_s$  values respectively (Plagen-

hoef *et al.*, 1983; Hatze, 1975). However, these methods are time consuming and fail to provide  $I_s$  values for the pelvis segment (Yeadon & Challis, 1994). Other methods that provide rigid segmental inertia parameters include geometric models (Jensen, 1978; Hatze, 1980; Yeadon, 1990a) and linear and non-linear regression equations (Hinrichs, 1985; Yeadon, 1990a) that give inertia parameters using anthropometric data from the athlete or subject and inertia measurements from cadaver data (Dempster, 1955). According to Yeadon & Challis (1994) however the latter should be viewed with caution as the health and small number of the individuals in the cadaver samples make the morphological correlation with healthy, live athletes questionable.

On the other hand geometric models use only density values from cadaver data that are input into geometrical solid models and although there is still a degree of uncertainty regarding the correlation of those values with those from healthy populations and the small sample size of the datasets they are, in general, preferred over regression equation methods.

Yeadon (1990a) compared his inertia model to those of Jensen (1978) and Hatze (1980) by estimating the total body mass of three subjects with each of the three methods. The maximum error results were comparable (2.3% vs 1.8% and 0.5% for Jensen's and Hatze's models respectively) however, he argued that the accuracy by which a model estimates segmental masses and inertias should be evaluated by comparing the performance of a simulation model whose segmental parameters have been derived using the inertia model against the actual performance. Indeed, he evaluated his model using an eleven-segment computer simulation model of aerial movement (Yeadon, 1990b). He reported maximum deviations between simulations and film of 0.04 revolutions for somersault, seven degrees for tilt and 0.12 revolutions for tilt. Since the model was based on subject specific inertia parameters, the small difference between simulated and actual performances showed that anthropometric measurement errors have a small effect on the accuracy of simulations. Moreover, the number of measurements required by the model, 95, make it more suitable for use in a testing environment, where both subject and researcher may operate under time restrictions, than the model of Hatze (1980) that requires 242 measurements.

### 5.3.1.1 Anthropometric measurements

Fifty-seven anthropometric measurements were taken to be used as input to the inertia model of Yeadon (1990a), comprising of 20 lengths, 24 perimeters, 11 widths and 2 depths. It is noted that this is not the full number of measurements as the full Yeadon protocol requires ninety-five. However, one of the assumptions of the model is that the subjects anthropometrics are symmetrical between the left and right sides therefore measurements were taken unilaterally.

The model provided data for 14 segments that reduced to 8 when bilateral symmetry was assumed, namely: Head, trunk, upper and lower arm, hand, thigh, shank and foot. The simulation model of the Snatch requires 6 segments therefore the hand and forearm and head and trunk segments were considered together and their inertia parameters were found using regression equations for the former and the parallel axis theorem for the latter.

### 5.3.2 Derivation of *torso* segmental inertia parameters

The segmental inertia parameters for the head and trunk segments derived by Yeadon's (1990) model are shown in Tables 5.3 and 5.4. The first step in the derivation of the inertial parameters of the head+trunk segment (henceforth referred to as "*Torso*" for brevity) was to establish the segmental COM position of the new segment using the relation

$$\langle x_{tor}, z_{tor} \rangle = \frac{\sum_{i=1}^2 P_s \langle x_{com}, z_{com} \rangle}{P_T} \quad (5.1)$$

where  $x_{tor}, z_{tor}$  are the x, z coordinates of the torso COM,  $x_{com}, z_{com}$  the x, z coordinates of the head and trunk segments,  $P_s$  is the normalized segmental mass of each segment and  $P_T$  the combined normalized mass of the two segments. It is noted that the trunk length was adjusted to equal the distance between the hip and sternum marker so as to better agree with the VICON data. The trunk COM was also adjusted by multiplying the segment length by its relative position derived from the inertia model. Since the COM position is expressed as distance from the proximal joint, the x-coordinate can

be set to zero for all segments and equation (5.1) is solved for  $z_{tor}$  giving

$$z_{tor} = \frac{0.3673 \times (0.14 + 0.46) + 0.084 \times 0.233}{0.4512} = 0.301$$

i.e. the torso COM was at 0.301 m from the proximal (hip) joint.

Table 5.3: Segment, mass, length, centre of mass (COM) measured from proximal joint for the head and trunk of the athlete

Segment	Mass (kg)	Segment COM from proximal joint (m)	Segment length (m)
<b>Head</b>	5.807	0.14	0.276
<b>Trunk</b>	25.418	0.233	0.46

Having established the torso COM the next stage was to calculate the moments of inertia for the new segment using the parallel axis theorem

$$I_{tor}(x, y, z) = \sum I_s(x, y, z) + \sum m_s r_s^2 \quad (5.2)$$

where  $I_s(x, y, z)$  are the head and trunk moments of inertia obtained from Yeadon's (1990) inertia model and  $r_s$  are the distances between the COMs of trunk and torso and head and torso.

Table 5.4: Moments of inertia expressed in  $\text{kg} \times \text{m}^2$  for the head and trunk of the athlete written in simmechanics convention where  $x$  is the frontal axis,  $y$  the longitudinal axis and  $z$  the transverse axis

Segment	$I_x$	$I_y$	$I_z$
<b>Head</b>	0.037	0.019	0.037
<b>Trunk</b>	0.832	0.244	0.706

Using the data from Table 5.4 and equation (5.2) the inertia matrix for the torso

segment is derived

$$I_{tor}(x, y, z) = \begin{bmatrix} 1.506 & 0 & 0 \\ 0 & 0.263 & 0 \\ 0 & 0 & 1.38 \end{bmatrix} \quad (5.3)$$

### 5.3.3 Derivation of the moments of inertia for the barbell & weights system

The barbell and weight plates were modelled as a metal rod of length  $L = 0.1$  m and diameter  $d = 0.028$  m. In the simulation model the rod was connected to the forearm segment of the athlete at its COM (i.e. 0.05 m) along the frontal plane. The moment of inertia along the length of the rod (y-axis) was obtained from the equation

$$I_y = \frac{1}{3}MR^2 = \frac{1}{3}M\frac{d^2}{2} = \frac{1}{3} \times 70 \times 0.014^2 = 0.00457 \text{ kgm}^2$$

where  $M = 70$  kg was the total mass of the barbell & weights system. Since the rod is symmetrical along the x and z axis its moment of inertia along both axes is given by the equation

$$I_{x,z} = \int r^2 dm \quad (5.4)$$

where  $r$  is the distance of the volume element  $dm$  from the axis. For a rod of uniform cross-sectional area  $A$  its density  $\lambda$  can be expressed as a function of its mass,  $m$  and length,  $l$ .

$$\lambda = \frac{m}{l}$$

$$\text{Rearranging, } m = \lambda l$$

$$\Rightarrow dm = \lambda dl$$

$$= \lambda dx$$

$$= \frac{m}{l} dx \quad (5.5)$$

Due to (5.5), (5.4) becomes

$$\begin{aligned}
I_{x,z} &= \int r^2 dm = \int_{-\frac{L}{2}}^{\frac{L}{2}} r^2 \frac{m}{l} dx \\
&\stackrel{\substack{m=M \\ l=L}}{\longrightarrow} = \int_{-\frac{L}{2}}^{\frac{L}{2}} r^2 \frac{M}{L} dx \\
&= \int_{-\frac{L}{2}}^{\frac{L}{2}} x^2 \frac{M}{L} dx \\
&= \frac{M}{L} \int_{-\frac{L}{2}}^{\frac{L}{2}} x^2 dx \\
&= \frac{M}{L} \left[ \frac{x^3}{3} \right]_{-\frac{L}{2}}^{\frac{L}{2}} \\
&= \frac{ML^2}{12} = 0.0583 \text{ kgm}^2
\end{aligned}$$

Therefore the inertia matrix for the barbell segment is

$$I_{bar}(x, y, z) = \begin{bmatrix} 0.0583 & 0 & 0 \\ 0 & 0.00457 & 0 \\ 0 & 0 & 0.0583 \end{bmatrix} \quad (5.6)$$

## 5.4 Data Analysis

Since the simulation model was bilaterally symmetrical with respect to the sagittal plane the joint centre (JC) coordinates corresponding to the right and left side joints were averaged and the segment lengths,  $l$ , of the athlete were calculated using the equation

$$l = \sqrt{(x_{JC}^d - x_{JC}^p)^2 + (z_{JC}^d - z_{JC}^p)^2} \quad (5.7)$$

where  $x^d, z^d$  and  $x^p, z^p$  are the JC( $x, z$ ) coordinates for distal and proximal joint centres respectively. Next the centre of mass (COM) for each segment was calculated using the equation

$$\langle x_{COM}, z_{COM} \rangle = (\%S \times \langle x_{JC}^d - x_{JC}^p, z_{JC}^d - z_{JC}^p \rangle) + \langle x_{JC}^p, z_{JC}^p \rangle \quad (5.8)$$

%S is the COM location expressed as a percentage of the segment length. The %S values were derived from the inertia parameters (Table 5.5)

Table 5.5: Centre of mass locations, %S, expressed as percentage of segment lengths from the proximal joint centre. Values were derived from inertia parameters with the exception of the value for the forearm that was taken from the Dempster dataset (Dempster, 1955)

Segment	%S	Reference Joint
Foot	37.9%	Ankle
Shank	43.2%	Knee
Thigh	43.5%	Hip
Torso	41%	Hip
Arm	41.1%	Shoulder
Forearm	67.7%	Elbow

Having established the COM position for each segment the next step was to calculate the segmental linear and angular kinematics, specifically: linear and angular velocities and accelerations per segment.

### Linear Velocity

$$\langle v_x^i, v_z^i \rangle = \left\langle \frac{x_{COM}^{i+1} - x_{COM}^i}{\Delta t}, \frac{z_{COM}^{i+1} - z_{COM}^i}{\Delta t} \right\rangle \quad (5.9)$$

where  $v_x^i, v_z^i$  are the horizontal and vertical linear velocities at time  $i$  and  $\Delta t$  is the time interval between two successive frames. Using equation (5.9) the horizontal and vertical accelerations,  $a_x^i, a_z^i$ , were calculated

### Linear Acceleration

$$\langle a_x^i, a_z^i \rangle = \left\langle \frac{v_x^{i+1} - v_x^i}{\Delta t}, \frac{v_z^{i+1} - v_z^i}{\Delta t} \right\rangle \quad (5.10)$$

In order to calculate the angular kinematics of the athlete the segment angles relative to the horizontal axis were first derived using the  $arctan2$  function. This is a variant of the inverse tangent function,  $\tan^{-1}x$ , that is defined in the interval  $[-\pi, \pi]$ .

$$\theta = arctan2(z_{JC}^d - z_{JC}^p, x_{JC}^d - x_{JC}^p) \quad (5.11)$$

Working in a similar fashion to equations (5.9) and (5.10) the angular velocities and accelerations,  $\omega$  and  $\alpha$  respectively, are obtained

## Angular Velocity

$$\omega^i = \frac{\theta^{i+1} - \theta^i}{\Delta t} \quad (5.12)$$

## Angular Acceleration

$$\alpha^i = \frac{\omega^{i+1} - \omega^i}{\Delta t} \quad (5.13)$$

### 5.4.1 Filtering Kinematic data

Upon visual inspection of the linear and angular velocities and accelerations it became apparent that there was noise in the position data obtained from VICON probably due to the reconstruction of marker trajectories that for some markers was quite extensive. To account for this the marker data was filtered using a Butterworth low pass filter at 10 Hz. The frequency was chosen through visual inspection of the segments linear and angular acceleration plots (Figures 5.10–5.13).

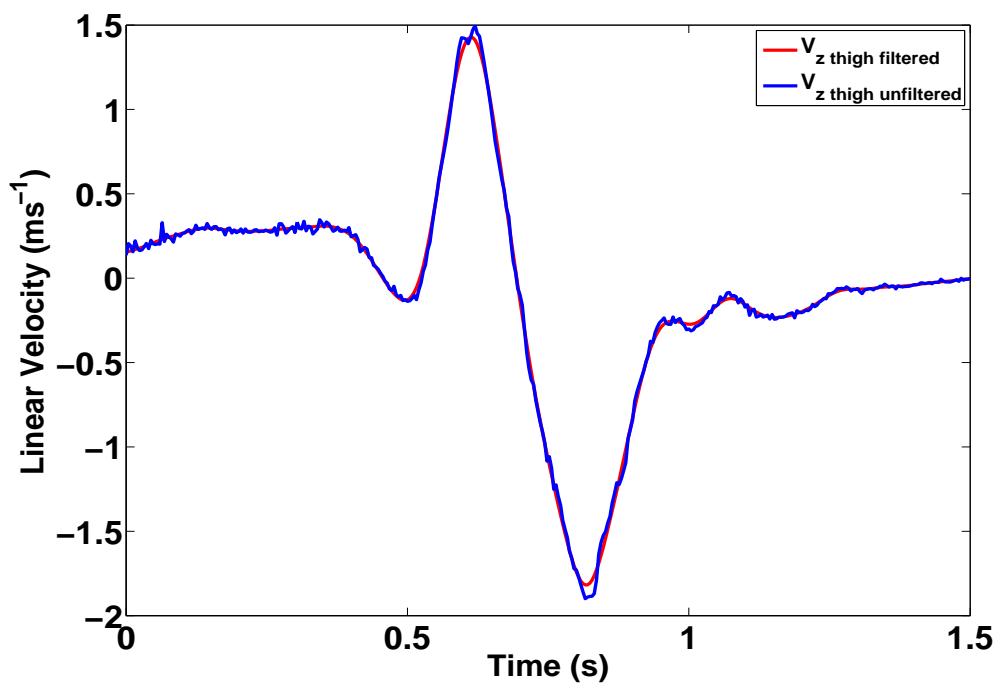


Figure 5.10: Filtered vs unfiltered linear velocity plots of the thigh

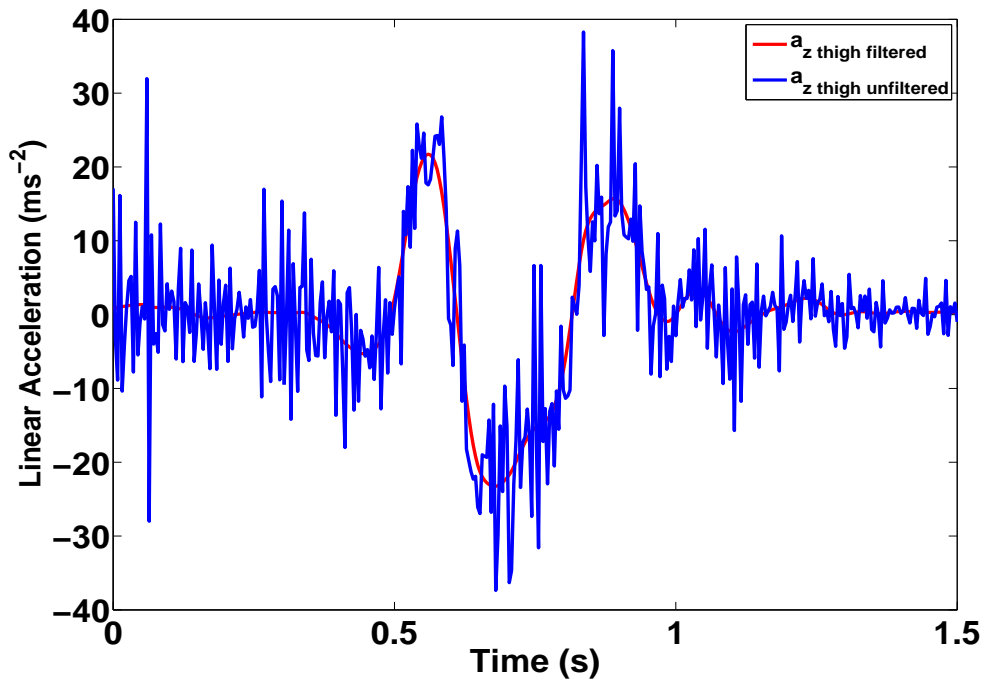


Figure 5.11: Filtered vs unfiltered linear acceleration plots of the thigh

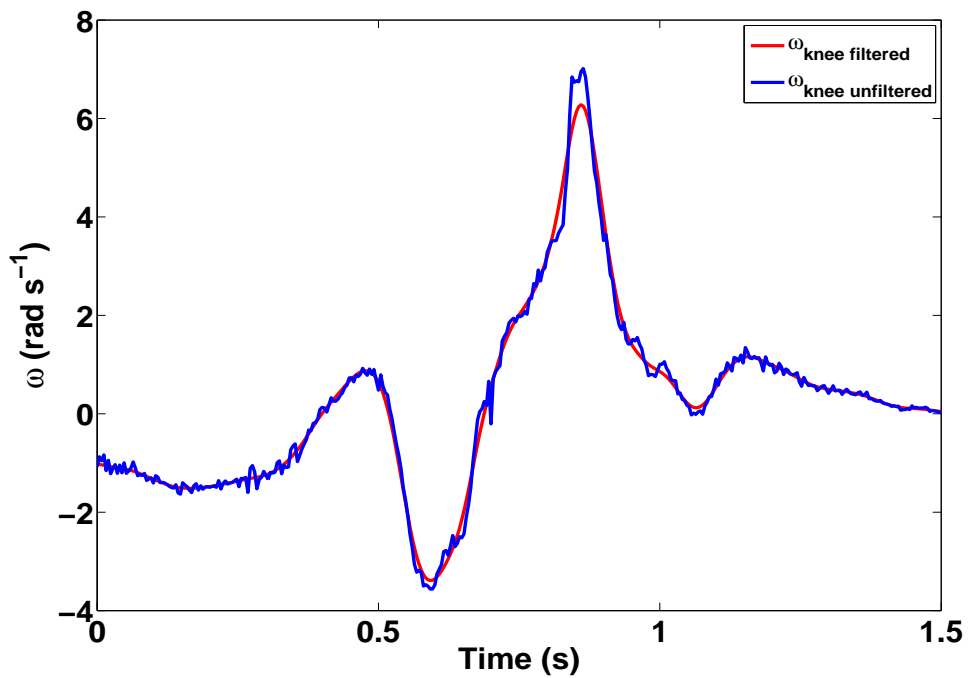


Figure 5.12: Filtered vs unfiltered angular velocity plots of the knee joint

### 5.4.2 Torque–angular velocity–angle profiles

The simulation model would be driven using torque generator functions at the ankle, knee, hip and shoulder joints. Consequently, respective torque generator functions had

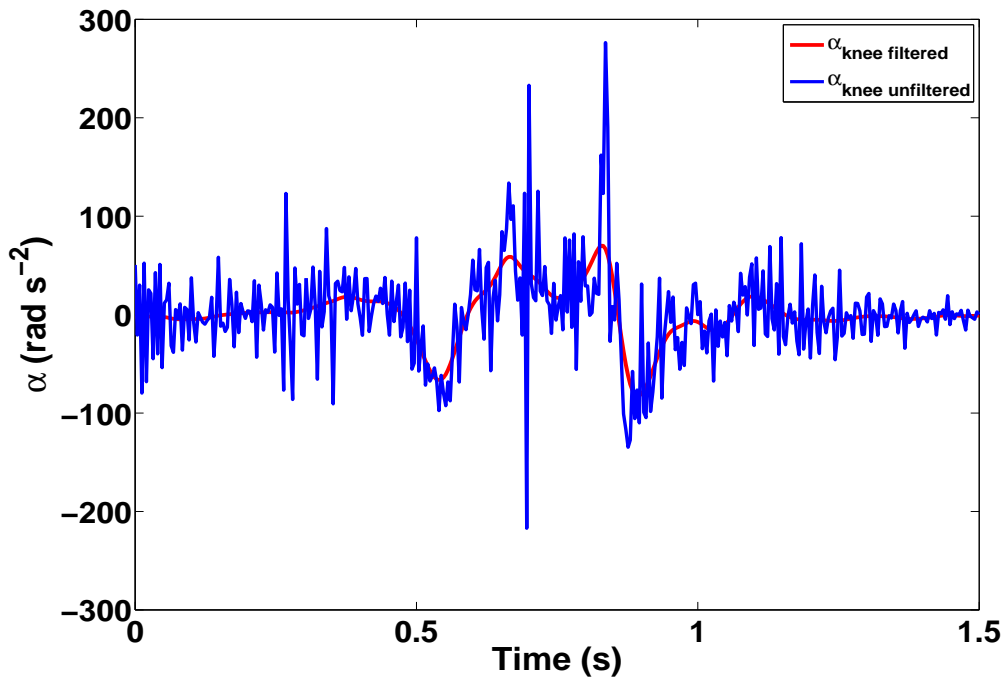


Figure 5.13: Filtered vs unfiltered angular acceleration plots of the knee joint

to be defined to represent the cumulative effect of the muscles around each joint. Nine-parameter,  $T-\omega-\theta$ , functions were derived for the hip and knee extensors (Figure 5.14) and flexors, ankle plantar flexors and shoulder flexors, by fitting equations (1.14), (1.16) and (1.17) to the  $T-\omega-\theta$  datasets obtained from the isokinetic dynamometer measurements as was described in previous chapters (Appendix D). The torque parameters for all the muscle groups are summarized in Table 5.6

Table 5.6: Torque parameters. Ext. = Extension, Flex.= Flexion

Parameter	Ankle	Hip		Knee		Shouler
	Plantar Flex.	Ext.	Flex.	Ext.	Flex.	Flex.
$T_{\max}$	244	594	214	318	175	67
$T_0$	188	312	144	245	135	51
$\omega_{\max}$ (rad s <sup>-1</sup> )	29.1	31.9	19.5	24.9	19.3	31.9
$\omega_c$ (rad s <sup>-1</sup> )	9.3	15.9	9.5	12.5	9.6	15.9
$W$	0.88	1.8	0.77	0.44	0.99	1.4
$\theta_{\text{opt}}$ (rad)	1.1	1.23	2.53	2.12	2.44	1.8
$\alpha_{\min}$	0.67	0.72	0.65	0.73	0.66	0.68
$\omega_r$ (rad s <sup>-1</sup> )	1.03	0.91	0.72	0.66	0.67	1.05
$\omega_1$ (rad s <sup>-1</sup> )	1.23	0.31	1.04	0.3	0.66	0.9

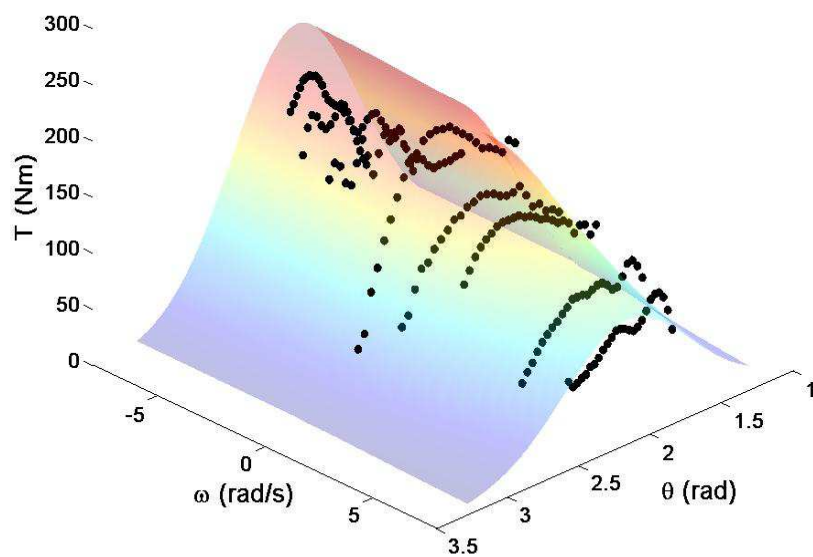


Figure 5.14: 3-d  $T$ - $\omega$ - $\theta$  surface plot for knee extension

# 6 A simulation model for the Snatch

Hubbard (1993) argued that the most fundamental understanding of an activity often comes from the simplest simulation models as an overly complex model may hide the true essence of the phenomenon. He summarized this assertion with the quote “*Always begin with the simplest possible model which captures the essence of the task being studied*”. An example of such a model was Alexander’s two–segment model of jumping (Alexander, 1990) that was successful in identifying the basic principles of long and high jumps despite having no foot segment and only a single muscle representing the knee extensors. Therefore, the aim was to build a model that would be as simple as possible, whilst being complex enough to reproduce realistically the Snatch lift.

## 6.1 Construction of the six segment model

### 6.1.1 Structure

The Snatch is a bilaterally symmetrical activity, i.e. the left side of the athlete mirrors the right side with respect to the sagittal plane. Therefore, it was reasonable to assume that the movement could be simulated in two–dimensions (on the sagittal plane) without loss of its fundamental biomechanical elements, thus greatly reducing both complexity and computational cost of simulation compared to a three–dimensional model. Since the activity studied has a lot of similarities to a counter–movement jump (Roman & Shakirzyanov, 1978) it should include foot, shank, thigh, hip and trunk segments to simulate the extension of the ankle, knee and hip joints during the first 3 phases of the lift (Allen *et al.*, 2010). Because the arms flex at the elbow to allow the bar to remain close to the COM of the lifter during the pull the arm was represented by two segments consisting of the upper arm and forearm. Since the hands are used to grip the bar they were deemed to have a negligible effect on the performance of the model and were included in the forearm segment. The head was, likewise, included in a head and trunk segment (henceforth referred to as “torso”), as discussed in Section 5.3.2, as it was assumed that its individual contribution to the lift was insignificant. Each segment was given subject–specific inertia parameters that were doubled for the

segments representing the limbs to account for the fact that those were represented by a single segment each, Figure 6.1.

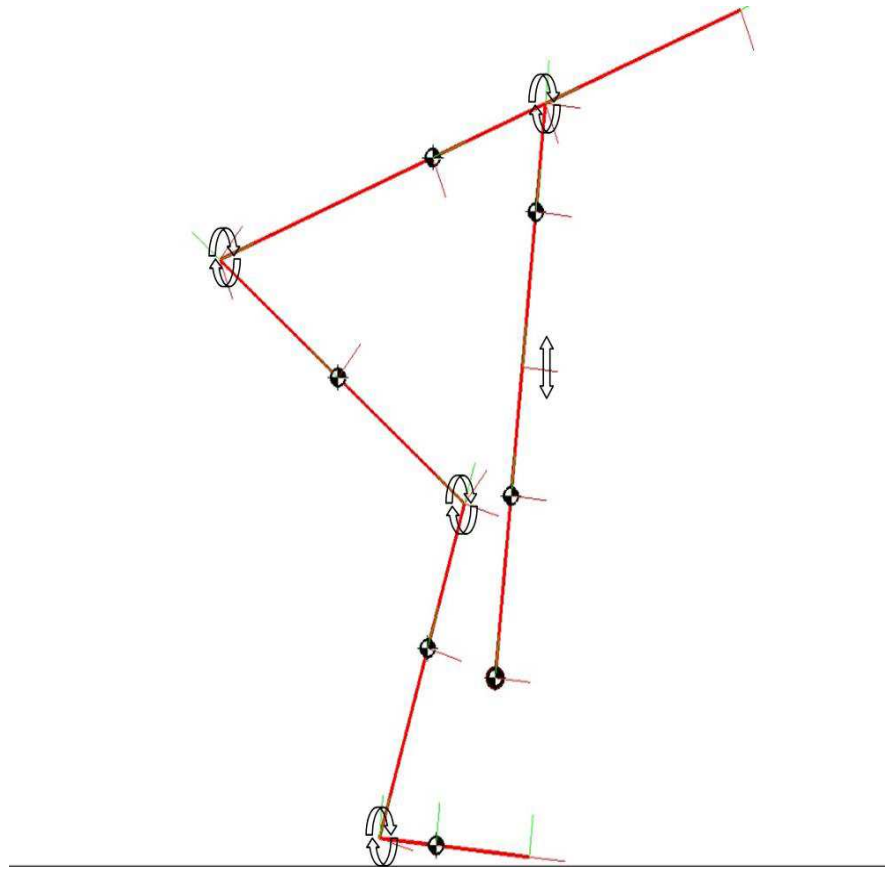


Figure 6.1: Stick model figure, showing the model configuration at the start of the lift. The circular arrows indicate rotating joints with angle drivers and the double arrow the sliding angle driven elbow joint

### 6.1.2 Building a model in SimMechanics

To construct the simulation model in the SimMechanics environment the Simulink block architecture was used where the mass and inertia properties as well as the position of orientation of each segment in space and relative to its neighbouring segments are defined through a *body* block. Each body block was connected to its neighbours (segments) via *joint* blocks that represent one or more degrees of freedom (henceforth DOF) between two bodies. All joint blocks of the model allowed for a single degree of freedom (rotation around the medio-lateral axis) between the segments with the exception of the elbow joint block that allowed translation of the forearm with respect

to the arm segment. The floor surface was represented by a *ground* block that also defines the local coordinate system of the model inside a global coordinate system of SimMechanics. The foot segment of the model was connected to the ground via another joint block that allowed for 3 DOFs, namely translation in the horizontal and vertical directions and rotation around the medio-lateral axis of the model, Figure 6.2. Once the inertia parameters, initial conditions and forces acting on the model have

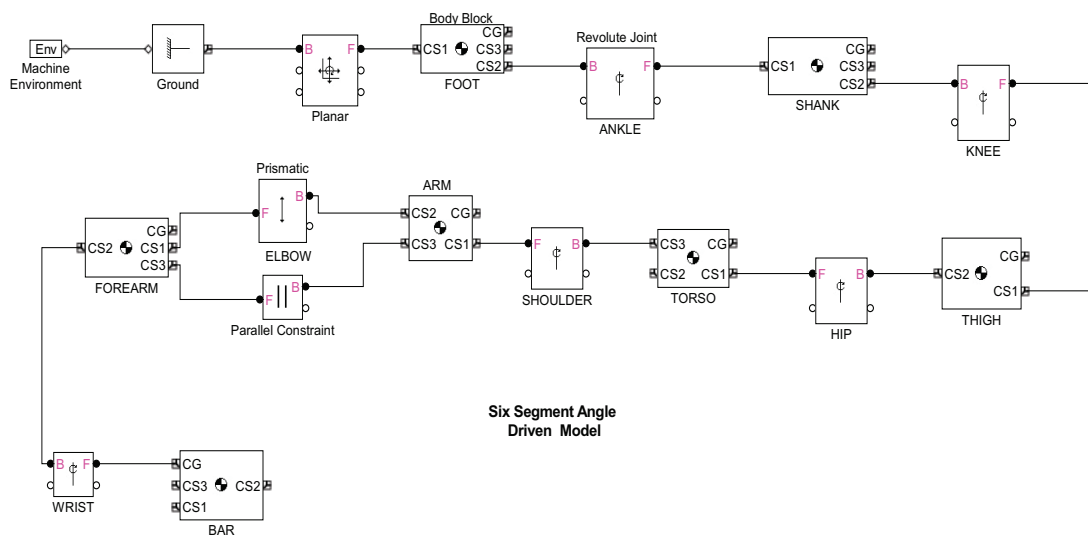


Figure 6.2: Structure of the six segment model of a Snatch athlete in the SimMechanics notation. Joint, body and ground blocks are illustrated

been input into the model, SimMechanics formulates and solves Newton's equations of motion as a system of first degree ordinary differential equations. The advantage of this approach is that it dispenses with the need to use specialised software packages where the model input has to be written in Fortran or C code.

## 6.2 Angle driven model

### 6.2.1 Actuating the model

Having defined the model segments, their inertia parameters and orientation in space the next step was to add motion to the model and this was achieved by actuating the model's joints using the angular kinematics of the athlete that had been obtained from the VICON model. Those were input into the “*joint actuator*” SimMechanics block that converted them into a motion signal which, in turn, actuated the joint. Actuating all 5 joints with the angular kinematics of a trial reproduced that particular trial. It is noted that the elbow joint was actuated using linear kinematics as the elbow joint only allowed translational movement of the forearm relative to the arm. This let the length of the upper limb (arm + forearm) to vary with time in order to simulate both its orientation and motion in the frontal plane during the Snatch that make it appear shorter when viewed in the sagittal plane. The kinematics of the upper limb were obtained by calculating  $\Delta S$ ,

$$\Delta S = S_I - S_H$$

which was the difference between the length of the upper limb as given by the inertia model,  $S_I$ , and its length in the sagittal plane when the bar was at the hip,  $S_H$ . Assuming that at the start of the lift the upper limb length was  $S_I$  the time interval between the start of the lift and the moment the bar was at the hip was calculated from the frame count. Subsequently, the velocity and acceleration of the forearm's motion relative to the arm were calculated and input in the elbow joint actuator.

The model-ground interaction was simulated using the angular and linear kinematics of the VICON model's foot segment that were input into the joint actuator. The fully angle driven model was then run in order to establish how well it was able to reproduce the original trial and to obtain a benchmark against which subsequent model versions could be compared. The combined athlete + bar COMs (henceforth CCOM) were obtained for both VICON and SimMechanics models and compared (Figure 6.3)

The SimMechanics model reproduced the trajectory of the CCOM very well in both the vertical and horizontal directions. As is illustrated in Figure 6.3 the angle driven model

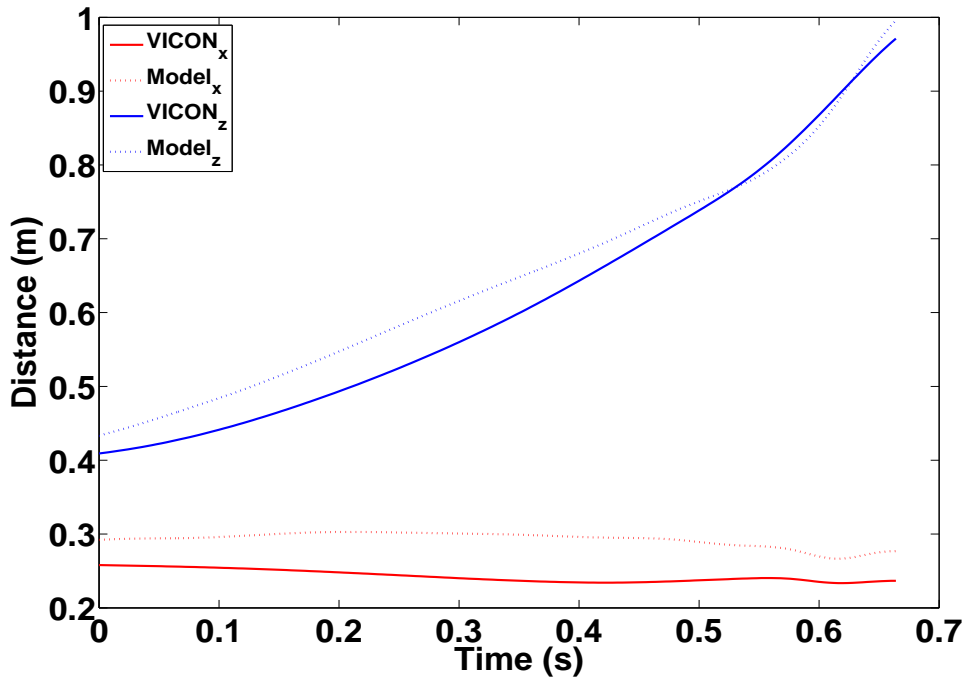


Figure 6.3: Combined athlete + barbell COM trajectories in the horizontal (x) and vertical (z) directions from VICON and full angle driven models for the first 3 phases of the lift

slightly overestimates both the x and z components of the CCOM by approximately 4 cm. This can be attributed, partly at least, to frontal plane movements of the athlete during the lift, such as external rotation of the femur at the hip joint, abduction and retraction of the humerus or compression of the joints and the spine, that cannot be reproduced by a 2-dimensional model. However, the qualitative agreement of the two models is good as the two trajectories run almost parallel in both directions. The SimMechanics schematic of the angle driven model is illustrated in Appendix F.

## 6.2.2 Ground contact

Having obtained a benchmark for the fully angle driven SimMechanics model the next step was to allow the model to simulate lifts where the joint angular kinematics would not be previously known. The first step was to define the interaction between the model and the ground in terms of the ground reaction force (henceforth GRF) i.e. the opposite of the force applied by the athlete during the lift. The GRF has a vertical and

a horizontal component,  $GRF_z$  and  $GRF_x$  respectively, and was modelled using four non-linear springs, located at the toe, centre of pressure (henceforth COP) and heel of the foot respectively. Three springs were used to model the  $GRF_z$  forces (located at toe, COP and heel) and one to simulate the  $GRF_x$  force (at toe). The springs are described by the non-linear relationship

$$F = -\kappa\Delta x^2 - b\frac{dx}{dt}\Delta x^2 \quad (6.1)$$

where

$\kappa$  is the spring stiffness coefficient

$\Delta x$  is the displacement of the spring from the equilibrium position,  $x - x_0$

$b$  is the spring damping coefficient

as such a relationship was found to better represent the interaction between foot and ground for high force activities such as running or drop landings (Gerritsen *et al.*, 1995; Pain & Challis, 2001b; Gittoes *et al.*, 2006). The horizontal spring released as soon as the foot left the platform as did the vertical spring at the toe whereas the vertical springs at the heel and COP were acting only when the whole foot was on the platform.

Table 6.1: Stiffness and damping coefficients for vertical (z) and horizontal (x) springs

	<b>z spring at toe</b>	<b>z spring at COP</b>	<b>z spring at heel</b>	<b>x spring at toe</b>
$\kappa$ ( $\mathbf{Nm}^{-2}$ )	698,859	3,452,879	4.0007	100,000
$b$ ( $\mathbf{Nsm}^{-1}$ )	8,048,592	250,000	20,000,003	10,000,000

It follows that in order to simulate the GRF forces using equation (6.1) the coefficients,  $\kappa$  and  $b$  must first be determined. This was achieved by minimising a score function that was defined as the RMS difference between the spring forces obtained from the angle driven model and the measured ones using the simulated annealing algorithm (Corana *et al.*, 1987), equation (6.2).

$$RMS_{score} = \sqrt{\frac{\sum_{i=1}^N \left[ \left( F_i(z)^{fp} - F_i(z)^{spring} \right)^2 + \left( F_i(x)^{fp} - F_i(x)^{spring} \right)^2 \right]}{N}} \quad (6.2)$$

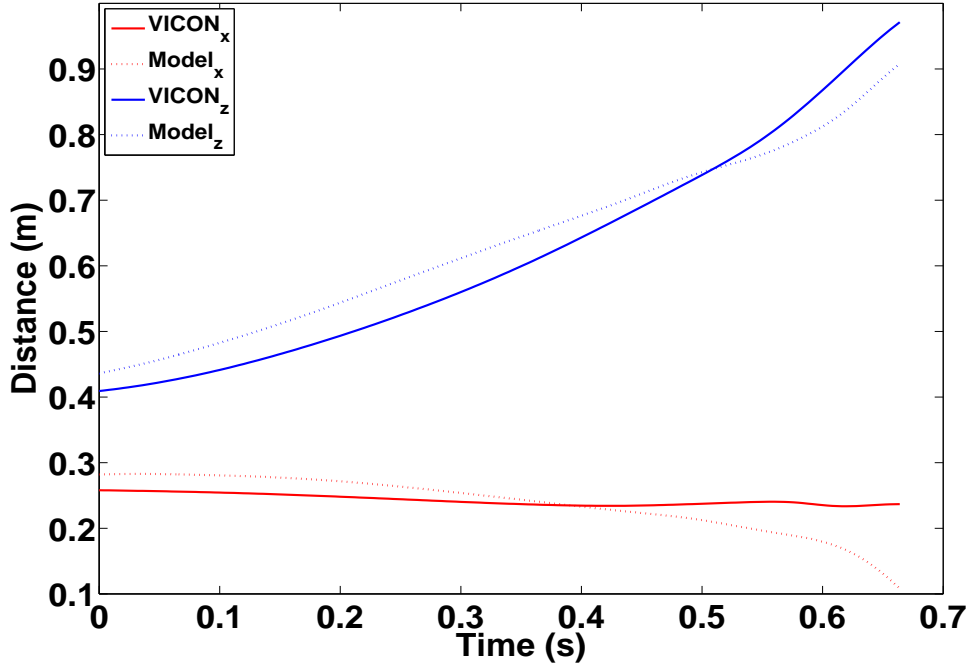


Figure 6.4: Combined athlete + barbell COM trajectories in the horizontal (x) and vertical (z) directions from VICON and angle driven with springs models for the first 3 phases of the lift

where  $F_i(x)^{fp}$ ,  $F_i(z)^{fp}$  and  $F_i(x)^{spring}$ ,  $F_i(z)^{spring}$  are the horizontal and vertical measured and spring GRFs respectively.

Initial bounds for the stiffness and damping coefficients were set and were allowed to be large as there was no existing data on their value. The initial estimates for the upper bounds of the coefficients were obtained through experimentation with the model. In order to help the optimisation process penalties were imposed on the score function if the model failed to take off. The optimised values are summarized in Table 6.1.

The optimised values of the spring coefficient were input into the SimMechanics model and the simulation was repeated with the angle driven model with springs. As is illustrated in Figure 6.4 the agreement between the VICON and the angle driven with springs models is also good and the output of the springs model is very similar to that of the fully angle driven model, Figure 6.5. The z component of the springs model becomes slightly smaller than that of the fully driven one towards the end of the lift ( $t = 0.6$  s). At that moment the second pull phase begins and the athlete pushes violently off the floor to elevate the bar. Consequently, the vertical springs compress

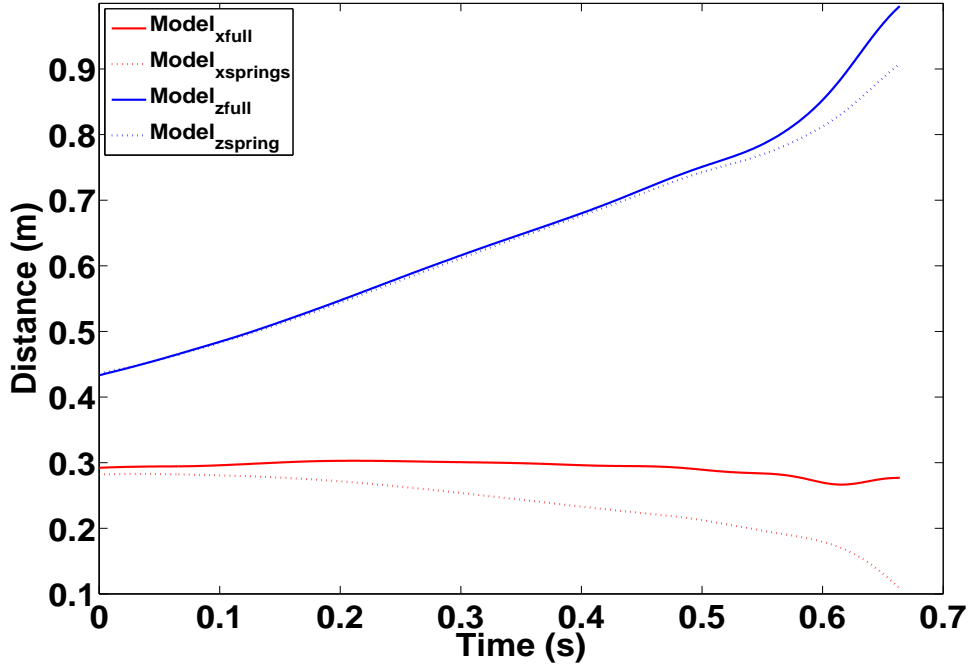


Figure 6.5: Combined athlete + barbell COM trajectories in the horizontal (x) and vertical (z) directions from full angle driven and angle driven with springs models for the first 3 phases of the lift

and the CCOM of the springs model is lowered. This can be counteracted by increasing the stiffness of the springs, when this was tried however, it induced oscillations of the model along the z axis while the model was at rest. The springs model also exhibits larger horizontal displacement than both the VICON and fully angle driven models as evidenced by a lower x component throughout the lift. It is likely that this is due to the number of ground contacts, i.e. the number of vertical springs. Since the heel and COP springs cease to exert force early on in the lift the model tends to fall slightly backwards compared to the actual lift, since the GRF vector is further forward due to the placement of the toe spring, and consequently this increases the horizontal displacement of the model CCOM. To prevent the model from jumping backwards the x-spring had to have a very high stiffness coefficient and this caused high horizontal force values  $F(x)^{spring}$  during the second pull phase that increased the  $RMS_{score}$  of the matching simulation to 1,922 N mainly due to the large RMS error of the x-spring component in (6.2). Specifically, the individual RMS scores were 1807 N and 656 N for the x- and z-springs respectively. Despite the poor RMS score of the x-spring

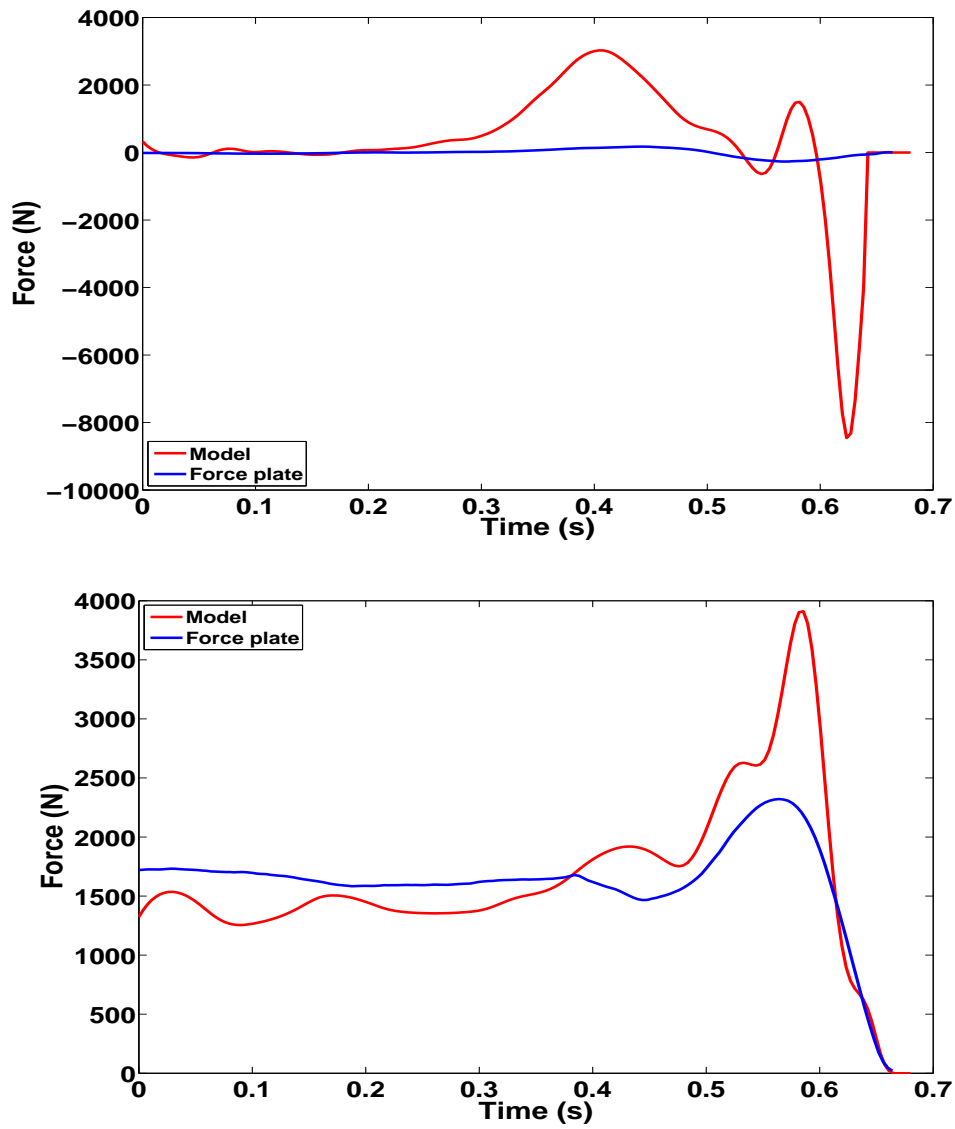


Figure 6.6: Horizontal (top) and vertical GRFs for a simulation of the initial 0.7 s of the Snatch

overall the model matched well the kinematics of the lift and since the main focus of the model was performance analysis it was decided that force would not be included in the objective function for the evaluation of the torque-driven model.

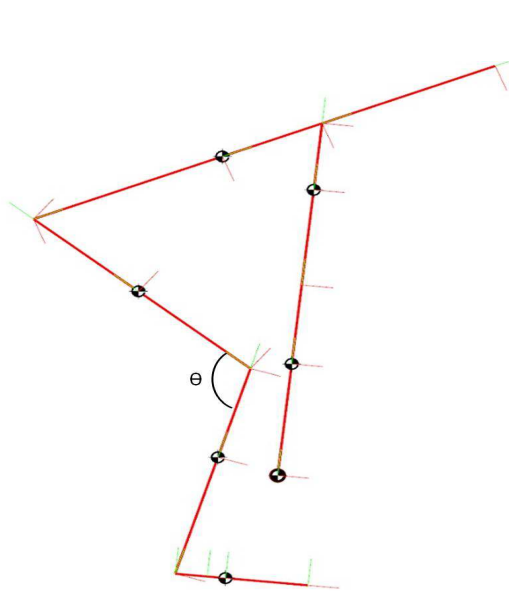
## 6.3 Torque driven model

### 6.3.1 Torque generators

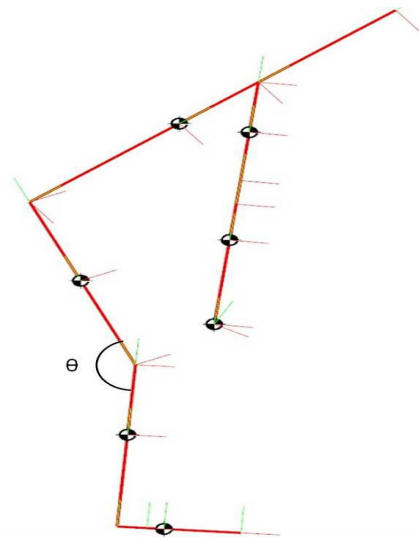
It is intuitive that performance in weightlifting is dependent on the strength of the athlete (Roman & Shakirzyanov, 1978; Garhammer, 1985). Since strength is a limiting factor of the activity it was necessary to actuate the model with the strength characteristics of the athlete. Torque generators were chosen as the means by which the simulation model was actuated. As was discussed in section 4.1 this approach allowed the derivation of subject specific  $T-\omega$  and  $T-\theta$  relations that would be subsequently used as inputs in the simulation model which in turn would make possible its evaluation against the performance data of the subject (Yeadon, 1990a; Yeadon & King, 2002; Yeadon *et al.*, 2006). Hence, torque generators were located at the ankle, knee, hip and shoulder joints. The torque generators at the knee and hip joints had both extensor and flexor profiles allowing co-contraction of extensors and flexors. On the other hand the torque generators at the ankle and shoulder joints had only plantar flexion and flexion profiles respectively as it was assumed that very little active ankle dorsiflexion or shoulder extension takes place during the lift. A torque generator,  $F$ , can be defined mathematically as a function of three variables

$$F(\omega, \theta, t) = T(\omega, \theta) \times ACT(t) \quad (6.3)$$

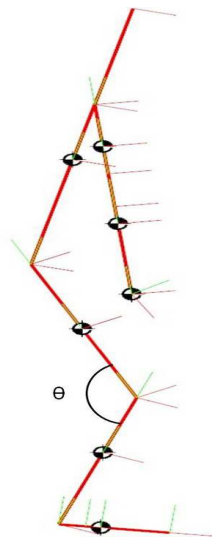
where  $T(\omega, \theta)$  is the 9-parameter function, given by equation (3.1), that expresses the maximum voluntary muscle torque as a function of  $\omega$  and  $\theta$  and  $ACT(t)$  is a time-dependent function that represents the muscle activation and “exists” between two asymptotes,  $ACT = 0$  and  $ACT = 1$ . Since the  $T(\omega, \theta)$  functions had been established from the dynamometer force measurements of the athlete a suitable activation function had to be chosen that would allow for different activation timings and levels of activation for both extensor and flexor muscle groups. This posed a challenge as those levels may vary during a snatch lift. For example, the knee joint successively extends, flexes and then violently extends again during the first three phases of the lift suggesting that the activation function of the knee extensors should have the ability to initially ramp up, then down (or remain constant) and then increase again during the simulation of the first three phases, Figures 6.7a–6.7d.



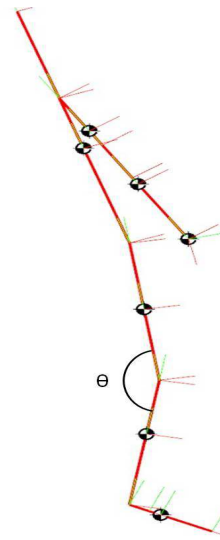
(a) Start of the Snatch lift,  $\theta = 112.2^\circ$



(b) End of first pull/start of transition,  $\theta = 150.1^\circ$



(c) End of transition,  $\theta = 131.8^\circ$



(d) End of second pull,  $\theta = 164.8^\circ$

Figure 6.7: Change in the value of the knee joint angle,  $\theta$ , during the first 3 phases (1st pull, transition and 2nd pull) of the snatch lift

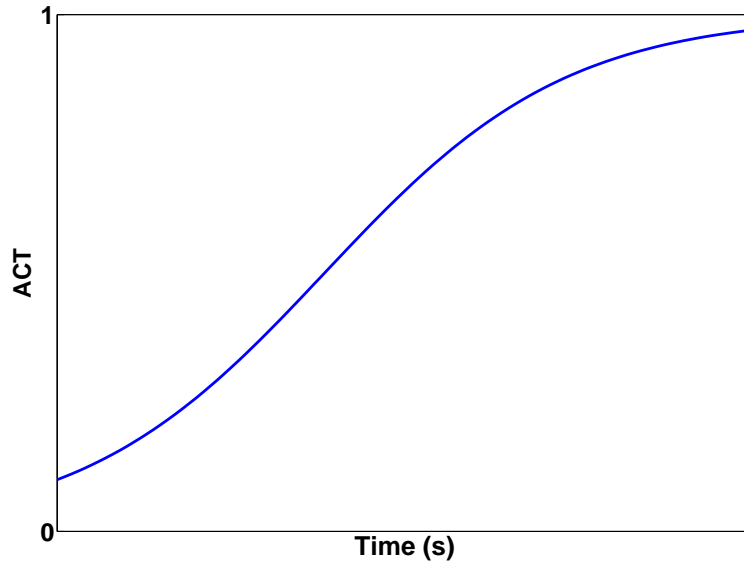


Figure 6.8: Example of activation function  $a(t)$

### 6.3.2 Activation functions

Depending on the muscle and the phase of the lift that was being simulated the complexity of the muscle activation profiles varied from simple ramp up functions to functions with both upward and downward slopes. The upward slope and downward parts of the activation function were replicated by means of a sigmoid function with the general form expressed with respect to time  $t$

$$a(t) = \frac{maxact}{1 + e^{-\frac{t}{s}}} \quad (6.4)$$

where  $maxact$  represented the maximum possible activation and  $s$  was the steepness of the curve, i.e. how fast the activation increased. The simplest activation profile curve consisted of a single upward slope illustrated in Figure 6.8. In this example the muscle activation was assumed to start at  $t = 0$ , had an initial value of 0.1 and a maximum activation value of 0.99. In reality, however, the initial activation level (or pre-activation) of the muscle at the start of the simulation ( $t = 0$ ) is not known and neither are both the start of activation (when muscle activation starts to increase from its initial state) and the final maximum level of activation that may be lower than the asymptote of equation (6.4). In order to include those parameters in the activation profile this was expressed in the form of a piecewise function with respect to time

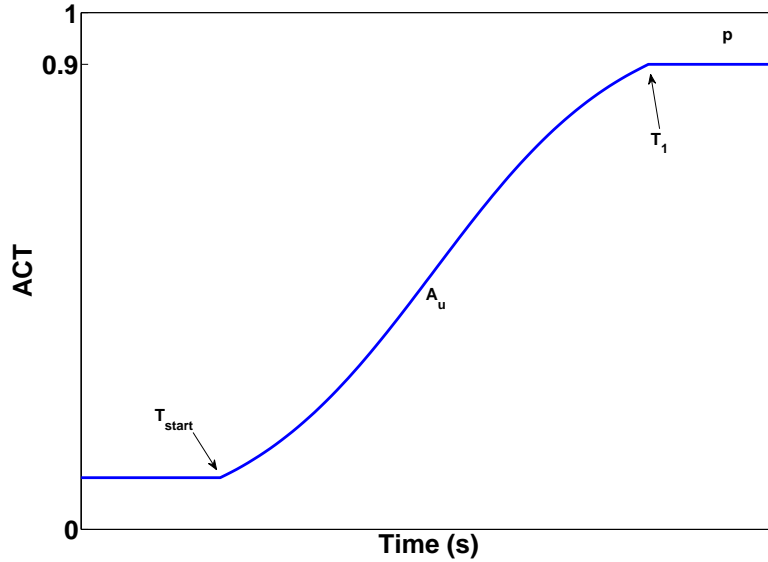


Figure 6.9: Example of a single upward activation profile  $ACT_u(t)$  of equation (6.5),  $n = 0.1$ ,  $p = 0.9$

(Figure 6.9)

$$ACT_u(t) = \begin{cases} n, & t \leq T_{start} \\ A_u(t), & T_{start} < t < T_1 \\ p, & t \geq T_1 \end{cases} \quad (6.5)$$

where

- $n$  is the level of pre-activation of the muscle
- $A_u(t)$  is the upward slope of the activation profile
- $p$  is the peak activation attained by the muscle during the simulated contraction and is always lower than  $maxact$
- $T_{start}$  is the start of the activation that corresponds to the moment when the activation ramps up
- $T_1$  is the time when peak activation is attained by the muscle

The time parameter  $T_1$  of equation (6.5) was defined as follows

$$T_1 = T_{start} + T_u^p - t_i \quad (6.6)$$

where the term  $(T_u^p - t_i)$  defined by

$$T_u^p = -\ln\left(\frac{1-p}{n}\right) s_u \quad (6.7)$$

and

$$t_i = -\ln\left(\frac{maxact - n}{n}\right) s_u \quad (6.8)$$

was the time interval between  $T_{start}$  and  $T_1$  where the ramp up of the activation takes place (Figure 6.9). The newly defined time parameters for the muscle activation were then input into equation (6.4) to obtain  $A_u(t)$

$$A_u(t) = \frac{maxact}{1 + e^{-\frac{t - T_{start} + t_i}{s_u}}} \quad (6.9)$$

The activation profile of equation (6.5) represents the simplest case of muscle activation, where the muscle attains a peak activation level and remains there for the duration of the activity. During the Snatch, however, the muscles may have to attain different levels of activation for different phases of the lift and it follows that the activation function should also be able to represent the reduction in muscle activation. This was obtained with the introduction of second sigmoid function of the form of equation (6.4) that brought the activation levels down to a lower value. The combined upward and downward parts of the activation profiles were defined via another sigmoid function

$$ACT_d(t) = \begin{cases} n, & t \leq T_{start} \\ A_u(t), & T_{start} < t \leq T_1 \\ A_d(t), & T_1 < t \leq T_2 \\ n2, & t > T_2 \end{cases} \quad (6.10)$$

where

- $n2$  is the level of activation where the muscle ramps down to from  $p$
- $A_d(t)$  is the downward slope of the activation profile
- $T_2$  is the time when the lower level of activation,  $n2$ , is attained by the muscle

The time parameter,  $T_2$ , was defined in a similar fashion to  $T_1$  by the equation

$$T_2 = T_1 - (T_d^p + t_{end}) \quad (6.11)$$

where this time the term  $(T_d^p + t_{end})$  was the time interval that corresponds to the downward part of the activation profile and was defined respectively by

$$T_d^p = -\ln\left(\frac{1 - p}{n}\right) s_d \quad (6.12)$$

and

$$t_{end} = -\ln\left(\frac{maxact - n2}{n2}\right) s_d \quad (6.13)$$

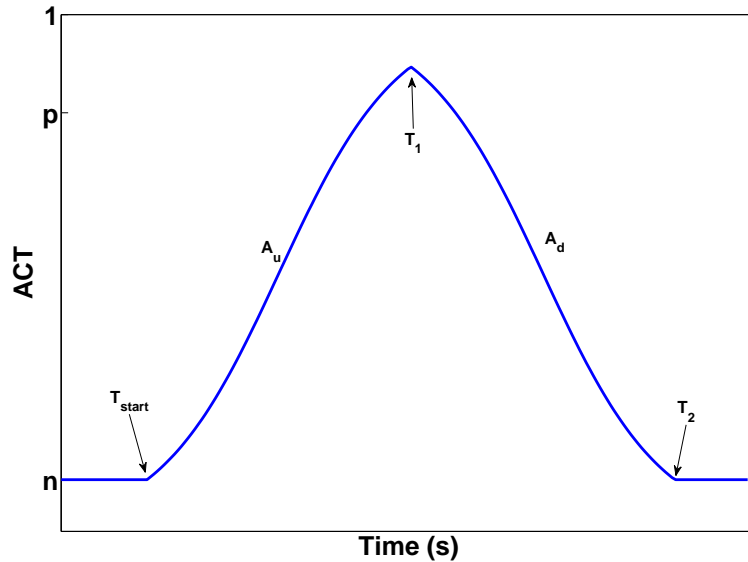


Figure 6.10: Example of an activation profile  $ACT_d(t)$  of equation (6.10) with upward and downward slopes,  $n = 0.1$ ,  $p = 0.9$ ,  $n2 = 0.1$

where  $s_d$  was the slope of the downward curve,  $A_d$

$$A_d(t) = \frac{maxact}{1 + e^{-\frac{t-T_1+T_d^p}{s_d}}} \quad (6.14)$$

A total of six parameters were needed to define the curve of equation (6.10) namely,  $tstart$ ,  $n$ ,  $n2$ ,  $p$ ,  $s_u$  and  $s_d$ . Once those were known the torque generator function for a particular muscle group can be determined and used to actuate a joint of the model. Working in the same manner more complicated activation functions could be constructed that allow for multiple activations of a single muscle. Such an example is illustrated in Figure 6.11

## 6.4 Model Evaluation

### 6.4.1 Matching optimisation

Thus far the simulation model has been actuated using angular kinematics at the ankle, knee, hip and shoulder joints and linear kinematics at the elbow joint. The next stage was to actuate the model using torque generators at all joints except the

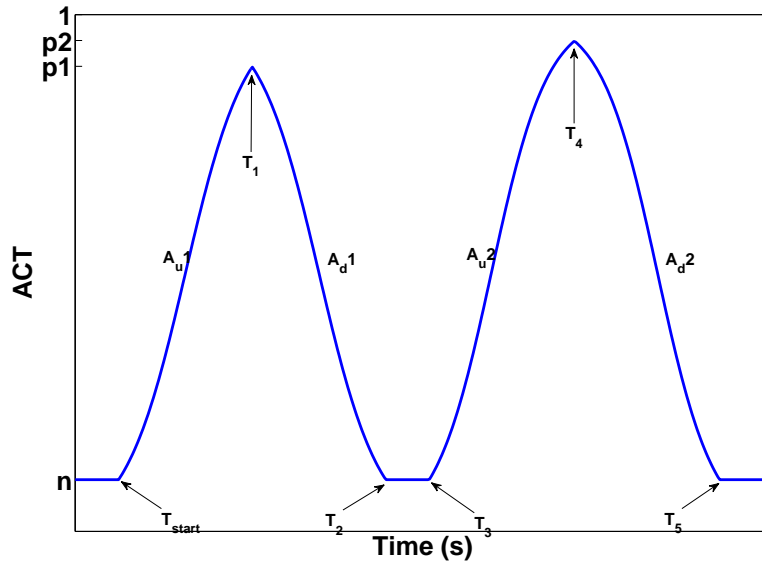


Figure 6.11: Example of an activation profile with two full activation curves both of which have an upward and downward slope. The second profile ramps up to a higher peak activation value,  $p1 = 0.9$ ,  $p2 = 0.95$

elbow joint. As was discussed earlier the knee and hip joints were actuated by both extension and flexion torque generator functions of equation (6.3) whereas the ankle and shoulder joints were actuated by a single function each representing plantar and shoulder flexion respectively. Since no EMG data were collected the number of slopes in the activation profiles during the lift (the muscle activation profiles) were not known and would have to be determined through trial and error. This posed a problem since for each activation profile  $ACT_d(t)$  six parameters had to be optimised and that meant a minimum of 36 parameters per optimisation. To simplify the process it was decided that:

1. Only the first three phases of the lift (first pull, transition and second pull) would be simulated by the torque-driven model. This would reduce the simulation time approximately by 75%, as the total lift lasted approximately 3 s whereas the first 3 phases 0.67 s, without negatively affecting the ability of the model to analyse technique since success or failure in the Snatch largely depends on the successful execution of the second pull (Garhammer, 1985; Baumann *et al.*, 1988; Gourgoulis *et al.*, 2002).
2. Each phase would be simulated separately in order to determine which activation

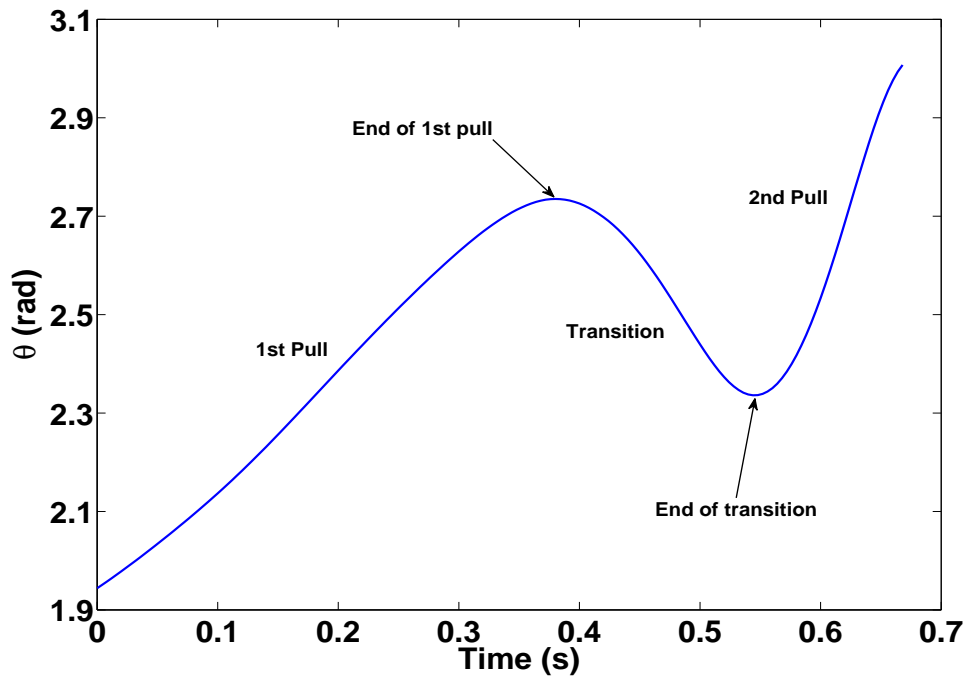


Figure 6.12: Knee joint angle from the start of the lift until the end of the second pull. The three phases of the lift are defined in terms of knee extension and flexion of the joint and marked on the graph

profile was most suitable. This would in turn allow the use of a single activation profile per muscle group keeping the number of parameters to be optimised at the minimum 36.

3. The duration of each of the three phases was determined from the knee joint angle as shown in Figure 6.12. The relevant angle and angular velocity initial conditions for each joint were determined from the actual performance and were input into the model to obtain the respective joint torque values.

The six parameters that had to be optimised per torque generator were  $t_{start}$ ,  $n$ ,  $n2$ ,  $p$ ,  $s_u$  and  $s_d$ . Since  $s_u$  and  $s_d$  represented how fast activation ramped up and down it was necessary to be given bounds that would represent the muscle's physiological activation characteristics. Specifically, they were given a lower limit that would allow a ramp up or down time interval of no more than 60 ms (Winter & Brookes, 1991).

### 6.4.1.1 Objective function

In order to obtain a measure of how well the simulation of each phase matched the actual performance the following score function was introduced that measured the RMS difference between the joint angle time histories of the model and the actual simulation.

$$RMS_{matching} = \sqrt{\frac{\sum_{i=1}^N \left[ \left( \theta_a^p - \theta_a^s \right)^2 + \left( \theta_k^p - \theta_k^s \right)^2 + \left( \theta_h^p - \theta_h^s \right)^2 + \left( \theta_s^p - \theta_s^s \right)^2 \right]}{N}} \quad (6.15)$$

where  $\theta$  is the joint angle measured during the actual performance  $p$  and simulation  $s$  and  $a, k, h, s$  refer to the ankle, knee, hip and shoulder joints respectively.

Penalties were imposed when the difference between model and athlete maximum joint angle was greater than  $6^\circ$  as this value ensured that all model joints stayed within realistic physiological bounds.

Table 6.2: Maximum joint angles

	Angle value ( $^\circ$ )
<b>Ankle</b>	107.7
<b>Knee</b>	164.8
<b>Hip (anterior)</b>	194.8
<b>Shoulder</b>	62.5

## 6.4.2 The first pull phase

### Joint angles

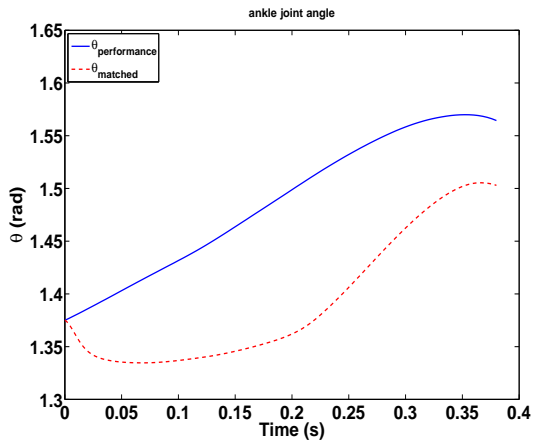
The duration of the first pull was 0.38 s, from the start of the lift until the beginning of the transition phase. The simulation matched performance well both quantitatively and qualitatively as shown in Figure 6.13 and Table 6.3. The total RMS difference score was  $12.7^\circ$  whereas the joint RMS scores ranged between  $5.7^\circ$  (ankle) and  $0.9^\circ$  (hip). The normalised RMS (NRMS) scores were also calculated by dividing the RMS scores with the total angle range of each joint during the first three phases of the lift in order to obtain an estimate for the size of error in the matching simulation with respect to the actual performance (range, 0.7%–13%). The ankle joint appears to dorsi-flex initially and subsequently to extend slower compared to performance (Figure 6.13).

Table 6.3: RMS and normalized difference scores between matched and performance angle time histories per joint for the first pull phase

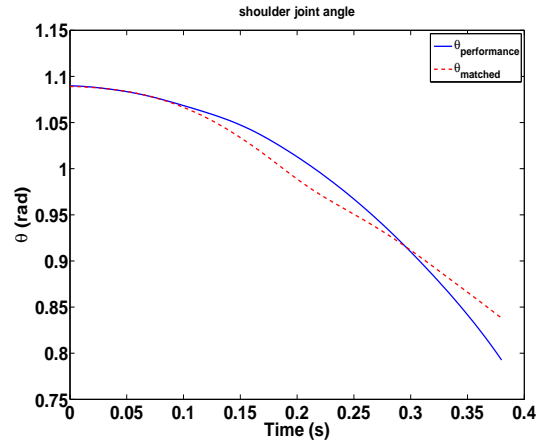
Joint	RMS ( $^\circ$ )	NRMS
Ankle	5.7	0.13
Knee	5.2	0.09
Hip	0.9	0.007
Shoulder	0.9	0.02

### Joint torques

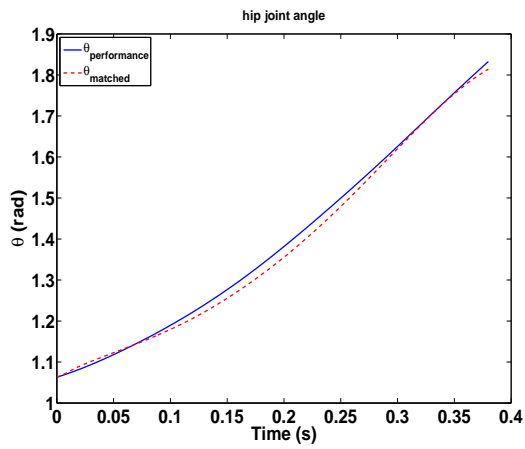
The torque time histories from performance,  $T_{\text{per}}$ , were calculated using inverse dynamics for the ankle, knee and hip joints and are illustrated with the respective torque time histories from the matched simulation,  $T_{\text{sim}}$ , in Figure 6.14. There is a significant difference in the torque values between performance and simulation for the ankle and knee joints with the  $T_{\text{per}}$  values being higher in both joints. In the case of the hip joint the simulation torque starts lower than performance, increases to a higher value at approximately 0.15 s and then dips lower again. In general the hip, knee and ankle



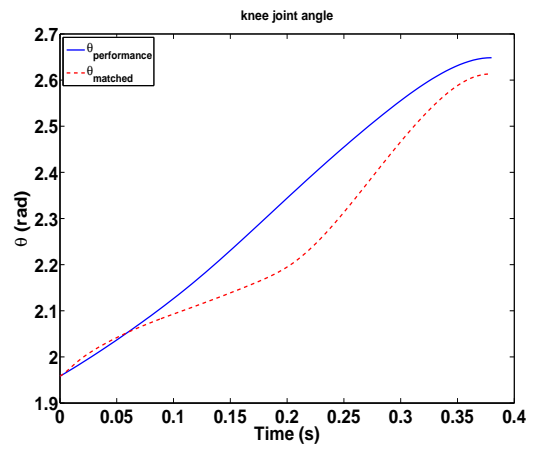
(a) Ankle joint angle time histories



(b) Shoulder joint angle time histories

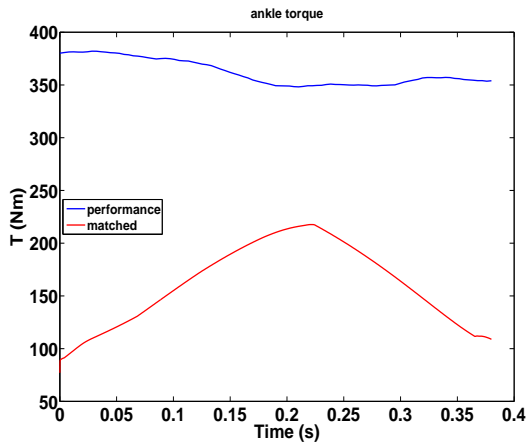


(c) Hip joint angle time histories

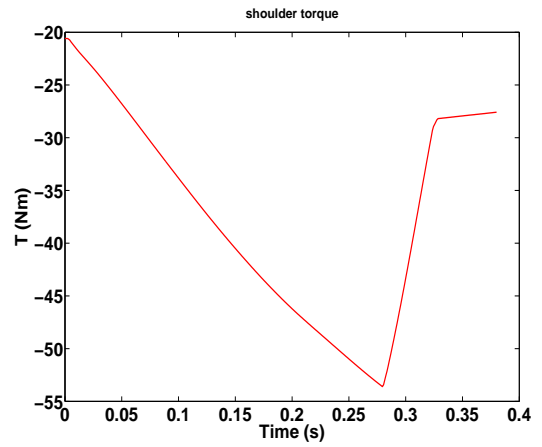


(d) Knee joint angle time histories

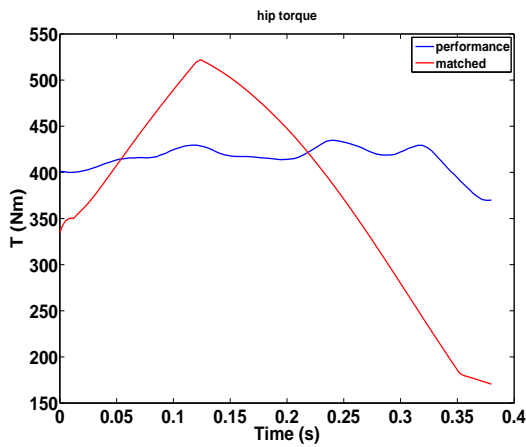
Figure 6.13: Joint angle time histories from performance (solid line) and matched simulation (dashed line) for the first pull phase



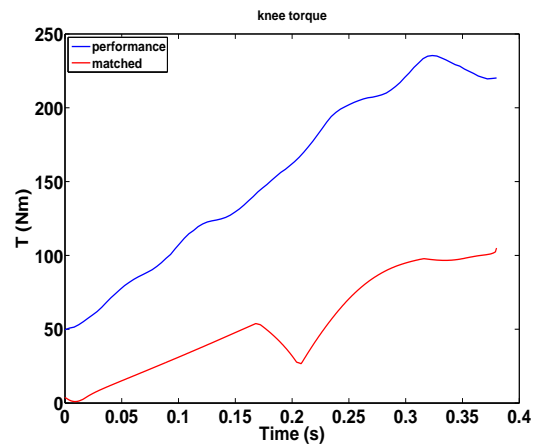
(a) Ankle joint torque time histories



(b) Shoulder joint torque time histories



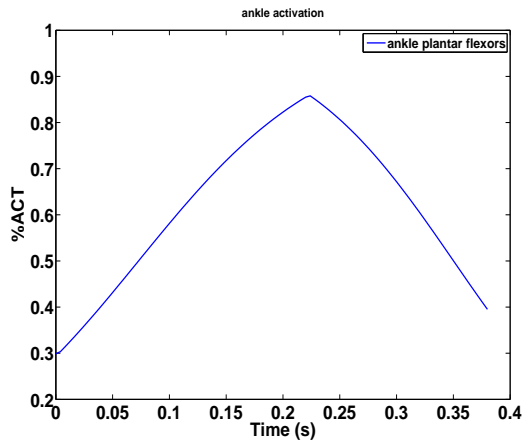
(c) Hip joint torque time histories



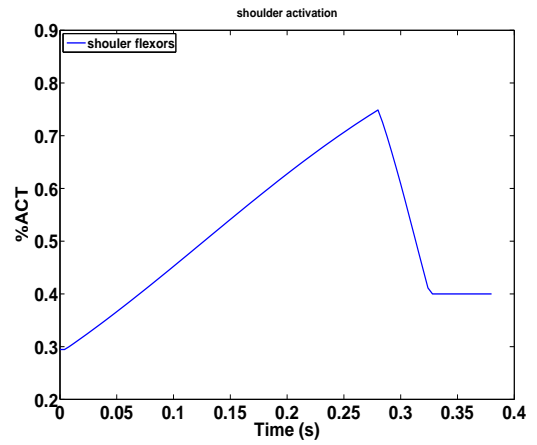
(d) Knee joint torque time histories

Figure 6.14: Joint torque time histories from performance,  $T_{\text{per}}$ , (blue) and matched simulation,  $T_{\text{sim}}$ , (red) for the first pull phase

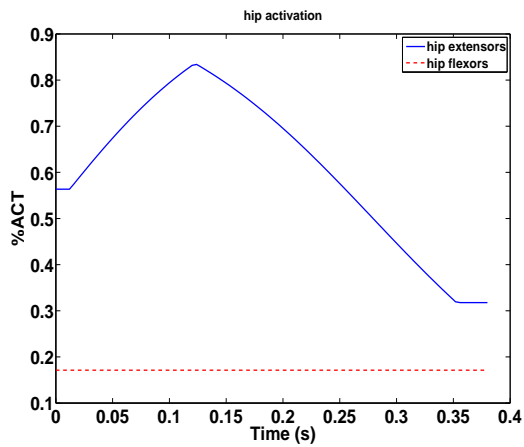
simulation joint torques follow the general pattern of the performance torques but tend to dip earlier and much deeper than  $T_{\text{per}}$  probably due to the ramping down of their activation functions, Figure 6.15. The knee  $T_{\text{sim}}$  appears to have a dip approximately 0.18 s into the lift. This was likely due to the activation of the knee flexors (Figure 6.14d) that co-contrast in order to prevent the knee from overextending. The shoulder torque values are negative, indicating that the athlete is lightly extending the shoulders in order to keep the bar close to the body.



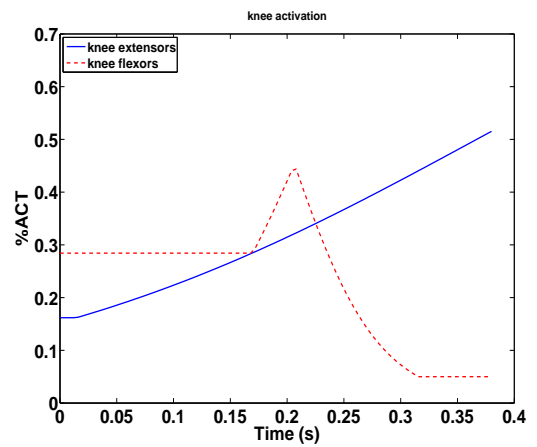
(a) Ankle joint activation time histories



(b) Shoulder joint activation time histories



(c) Hip joint torque activation histories



(d) Knee joint torque activation histories

Figure 6.15: Joint activation time histories from performance (solid line) and matched simulation (dashed line) for the first pull phase

### Activation timings

The activation time histories showed low levels of co-contraction at the hip joint with the extensors activation profile showing a similar pattern to the torque one as did the ankle and shoulder profiles. In the case of the knee joint there was strong co-contraction between knee extensors and flexors as the latter act eccentrically to prevent the overextension of the joint (Figure 6.15d).

### 6.4.3 The transition and second pull phase

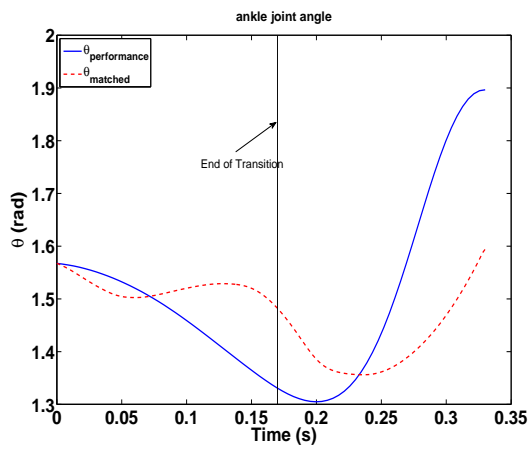
#### Joint angles

The transition phase started at 0.38 s after the initiation of the lift and lasted approximately 0.17–0.18 s. The duration of the combined transition and second pull phases for the simulated trial was approximately 0.03 s longer than performance possibly due to the prolonged knee flexion. As was the case with the first pull the qualitative agreement between simulation and performance was good as the model was able to reproduce the joint motion characteristics of the actual performance especially that of the knee joint that changes from flexion to extension mid-phase (Figure 6.16).

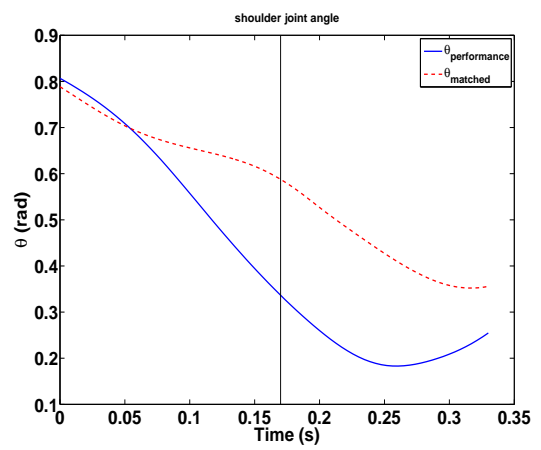
Table 6.4: RMS and normalized difference scores between matched and performance angle time histories per joint for the transition and second pull phases

<b>Joint</b>	<b>RMS (°)</b>	<b>NRMS</b>
<b>Ankle</b>	11.4	0.25
<b>Knee</b>	6.4	0.12
<b>Hip</b>	24	0.18
<b>Shoulder</b>	11	0.21

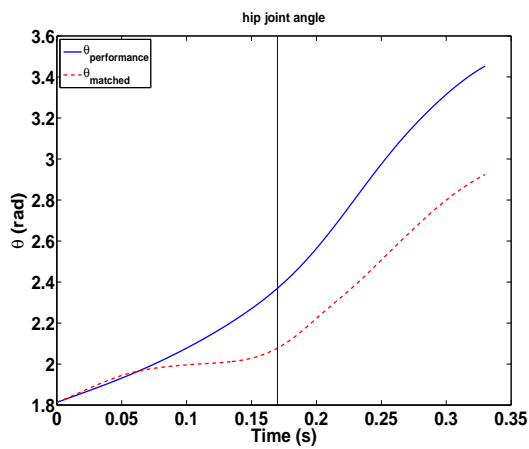
The quantitative agreement between simulation and performance is noticeably worse, however, in this case as the total RMS difference score was 52.9° with 24° of that being due to the inability of the model’s hip joint to extend as fast as the athlete’s (Table 6.4 and Figure 6.16). The simulated ankle plantar flexion and knee extension appear again to be weaker than the actual performance. It is possible that the ankle torque generator may not be always capable of providing the requisite torque to match the simulation performance. The simulated knee joint flexion during the transition phase matched qualitatively very well the performance curve but with a slightly lower degree of flexion (20° vs 31°) however, the second pull knee extension matched performance well. The shoulder joint extension during simulation was somewhat limited compared to the performance value possible as a consequence of the incomplete hip extension that resulted in a larger torso–arm angle.



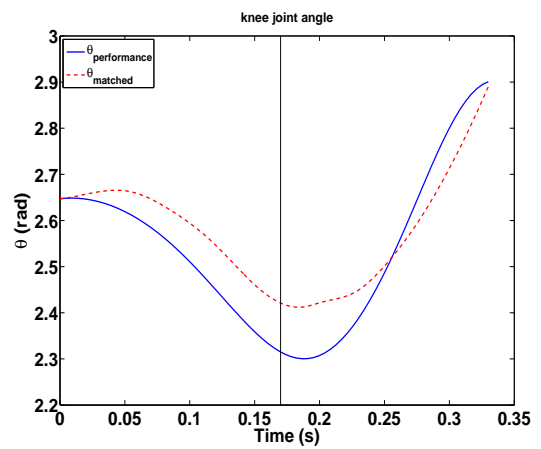
(a) Ankle joint angle time histories



(b) Shoulder joint angle time histories



(c) Hip joint angle time histories



(d) Knee joint angle time histories

Figure 6.16: Joint angle time histories from performance (solid line) and matched simulation (dashed line) for the transition and second pull phases

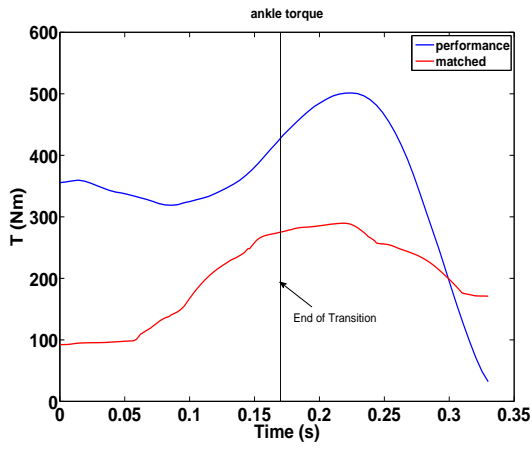
Overall, the results of the matching simulation were encouraging as the model was able to qualitatively reproduce the actual performance despite the complexity of the interactions between hip and knee extensors and flexors. Quantitatively the model did not perform as well as in the case of the first pull simulation indicating that the optimum solution may not have been found however, given the limited time available for optimisation it is likely that this can be achieved in the future.

### **Joint torques**

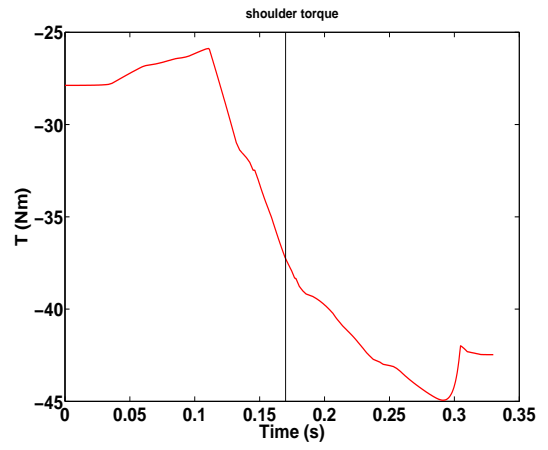
The torque time histories from the matched simulation and inverse dynamics for the four and three joints respectively are illustrated in Figure 6.17. The simulation extension torques of the hip and knee joints start to increase rapidly approximately 0.05s into transition phase in order to accelerate the bar upwards and then start to fall becoming negative at end of the second pull as a result of the their antagonist groups' action. On the other hand the inverse dynamics torques attain their highest value at the start of the phase and they decrease as the lift progresses. That difference is rather expected as the  $T_{sim}$  torques first had to ramp up close to the maximum  $T_{per}$ , following their activation profiles, and then ramped down to lower levels as did the  $T_{per}$  values. However, both ankle and knee maximum  $T_{sim}$  values remained lower than the respective  $T_{per}$  values despite the fact that the former attained almost full activation, Figure 6.18a.

### **Activation timings**

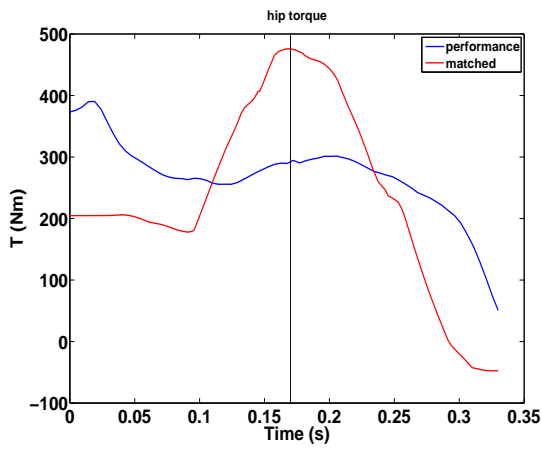
The starting activation levels of the four joints were initially set to match the final activations of the first pull solution and allowed to vary within limits. As it is shown in Figure 6.18 the starting activations for the ankle, hip and shoulder joints were very close to their respective activation levels at the end of the first pull (Figure 6.15) however, this was not the case for the knee joint that had to adopt a higher starting activation value for both extensors and flexors (0.68 vs 0.52 and 0.23 vs 0.05 respectively). Although qualitatively the strategy appears to be the same (high extensor, low flexor activation) the difference in the activation values between the two phases is notable. This is not unexpected, however, as the knee joint motion (and therefore activation pattern) is



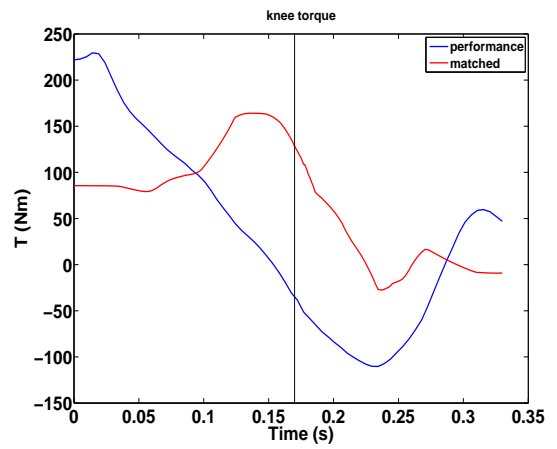
(a) Ankle joint torque time histories



(b) Shoulder joint torque time histories

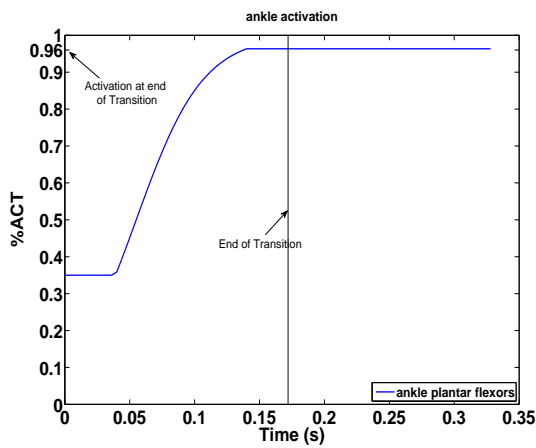


(c) Hip joint torque time histories

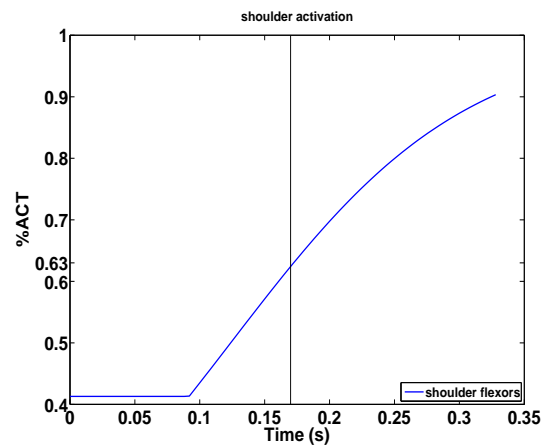


(d) Knee joint torque time histories

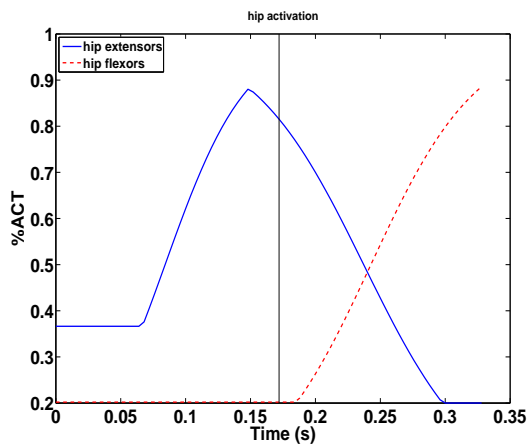
Figure 6.17: Joint torque time histories from performance,  $T_{\text{per}}$ , (blue) and matched simulation,  $T_{\text{sim}}$ , (red) for the transition and second pull phases



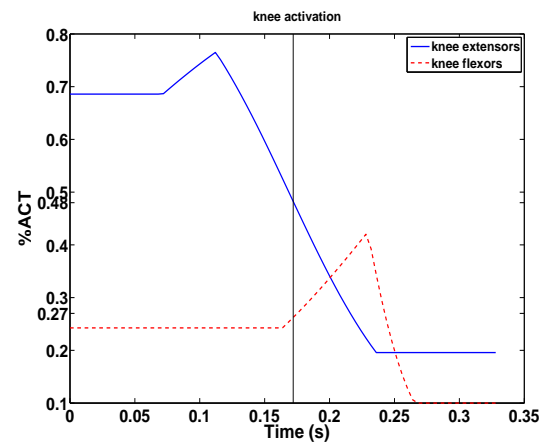
(a) Ankle joint activation time histories



(b) Shoulder joint activation time histories



(c) Hip joint torque activation histories



(d) Knee joint torque activation histories

Figure 6.18: Joint activation time histories from performance (solid line) and matched simulation (dashed line) for the transition and second pull phases

significantly more complex during the transition and second pull phase compared to the first pull phase, however, by modelling each phase separately each solution fails to take into account the complexities of the subsequent phases as it was optimised for that particular lift segment only. Moreover, the initial conditions at the beginning of each phase were set equal to the performance values and may (and do) differ slightly from the model kinematics of the previous phase. For example, the athlete's knee joint at the beginning of the second phase was extending at  $11^\circ/\text{s}$  whereas the respective model velocity at the end of the first was  $2^\circ/\text{s}$ . It is possible that the model had to adopt a higher starting activation value for the second phase to account for that difference.

As illustrated in Figure 6.18 the activation of the ankle started rising early in the

transition phase and achieved its maximum value approximately at the start of the second pull. Again there was co-contraction of the knee extensors and flexors during both phases with the flexors activation ramping up during the second pull part of the phase in order to prevent the over-extension of the knee joint (Figure 6.18d). The same activation pattern was observed for the hip joint.

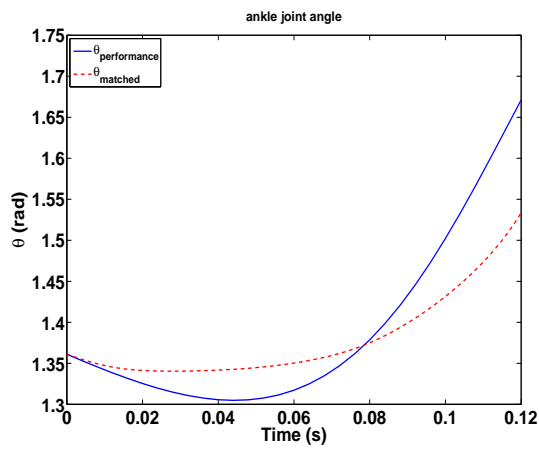
#### 6.4.4 The second pull phase

##### Joint angles

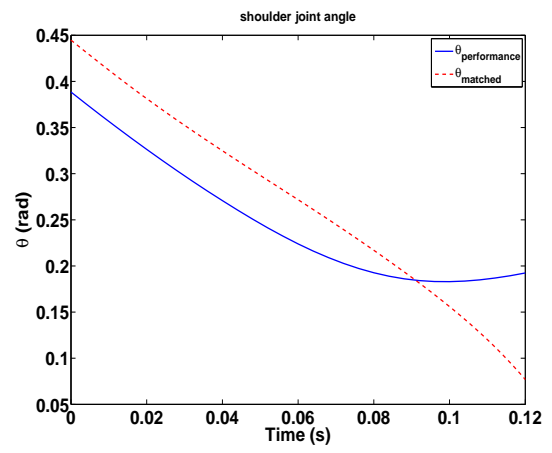
The second pull phase started at 0.544 s after the initiation of the lift and its duration was approximately 0.12 s. Figure 6.19 shows the joint angle time histories from the athlete's performance during the second pull and the respective matched simulation for that phase. The qualitative agreement between simulation and performance was good as the latter matched the joint function well especially for the ankle and knee joints. With respect to the quantitative agreement between simulation and performance the total RMS difference score between performance and simulation was  $10.1^\circ$  whereas the individual RMS scores per joint ranged from  $1.7^\circ$  to  $3.1^\circ$  (Table 6.5). The greatest deviation between simulation and performance, both qualitatively and quantitatively, was observed for the ankle joint in agreement with the results of the previous simulations.

Table 6.5: RMS and normalized difference scores between matched and performance angle time histories per joint for the second pull

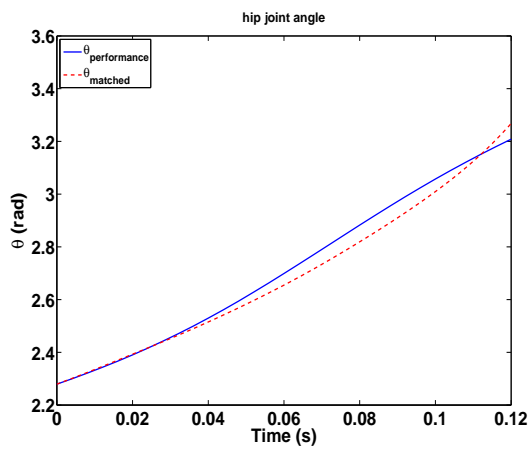
<b>Joint</b>	<b>RMS (<math>^\circ</math>)</b>	<b>NRMS</b>
<b>Ankle</b>	3.1	0.07
<b>Knee</b>	1.7	0.03
<b>Hip</b>	2.2	0.02
<b>Shoulder</b>	3.1	0.06



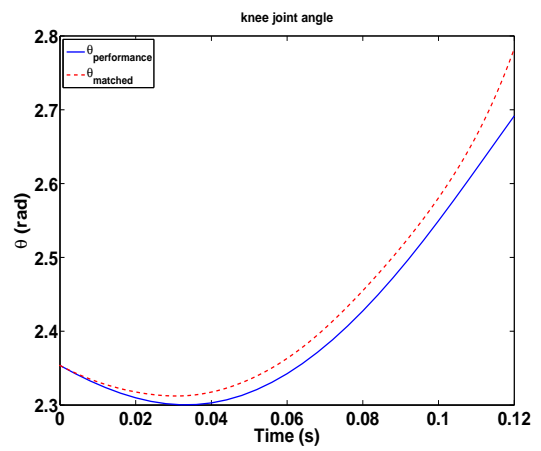
(a) Ankle joint angle time histories



(b) Shoulder joint angle time histories

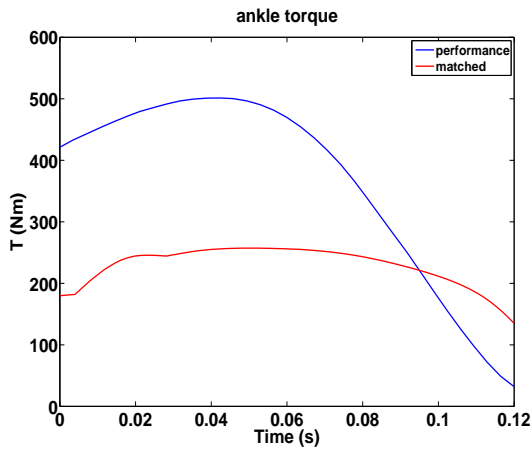


(c) Hip joint angle time histories

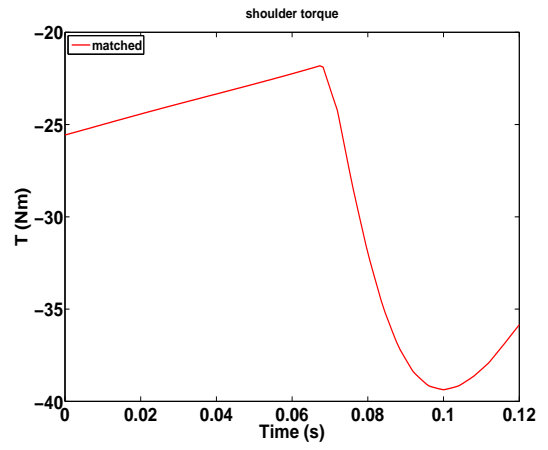


(d) Knee joint angle time histories

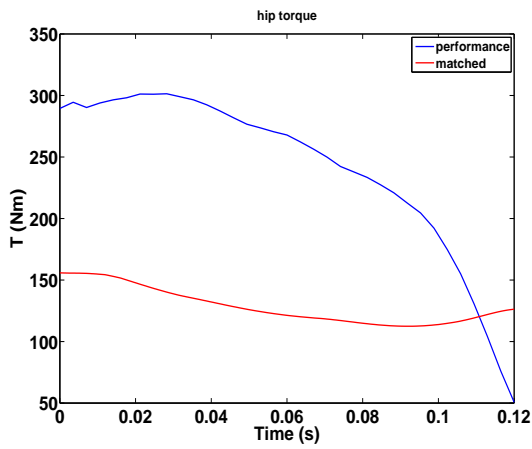
Figure 6.19: Joint angle time histories from performance (solid line) and matched simulation (dashed line) for the second pull



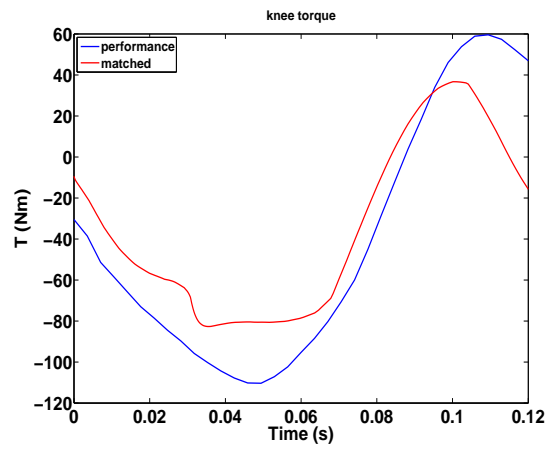
(a) Ankle joint torque time histories



(b) Shoulder joint torque time histories



(c) Hip joint torque time histories



(d) Knee joint torque time histories

Figure 6.20: Joint torque time histories from performance,  $T_{\text{per}}$ , (blue) and matched simulation,  $T_{\text{sim}}$ , (red) for the second pull phase

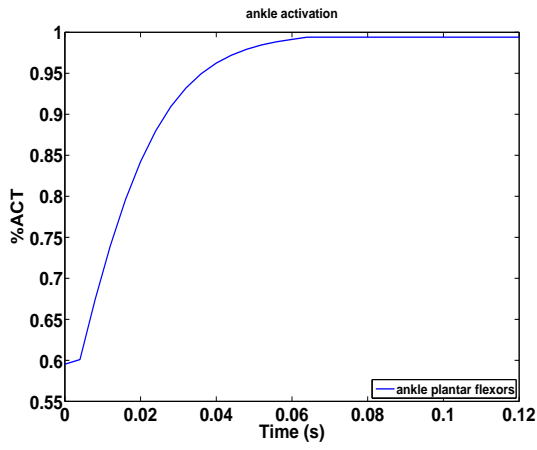
## Joint torques

Figure 6.20 shows the torque time histories from the matched simulation and inverse dynamics for the second pull. In general there is qualitative agreement between performance and inverse dynamics torques with the latter being larger for the knee and hip joints and larger for the ankle. As observed in the previous simulation the values of both  $T_{\text{per}}$  and  $T_{\text{sim}}$  for the knee joint decrease at the end of the lift implying that the knee flexors are strongly co-contracting with the extensors in order to prevent overextension of the knee joint. The ankle torque drops from mid-phase onwards likely because as the ankle joint extends, the plantar-flexors go on into the downward curve of the force-length relationship and their ability to produce force decreases as do the hip extensors. The negative value of the torque at the shoulder joint indicates that the model is trying to prevent the barbell from moving horizontally.

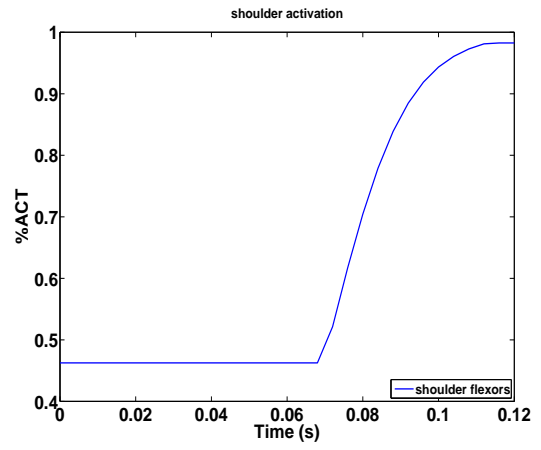
## Activation timings

The starting activation levels of the four joints were again set to match the final activations at the end of the transition phase and allowed to vary within limits that were progressively increased until an optimal solution was obtained. This time only the shoulder, knee extensors and hip flexors activation levels at the start of the second pull were close to the respective values at the end of the transition phase whereas the ankle, knee flexors and hip extensors activation levels varied significantly (Figures 6.18 and 6.21). The starting activation level of the ankle was low compared to the end of the transition (0.6 vs 0.96). This is likely another indication of a weak torque generator at the ankle as at the end of the transition phase the model ankle joint is dorsi-flexing (Figure 6.16) and consequently the torque actuator is nearly maximally activated in order to match the athlete's plantar-flexion. In the second pull simulation the initial conditions have the ankle plantar-flexing at  $6^\circ/\text{s}$  and therefore the starting activation levels need not be as high though they quickly reach their maximum value, Figure 6.21a.

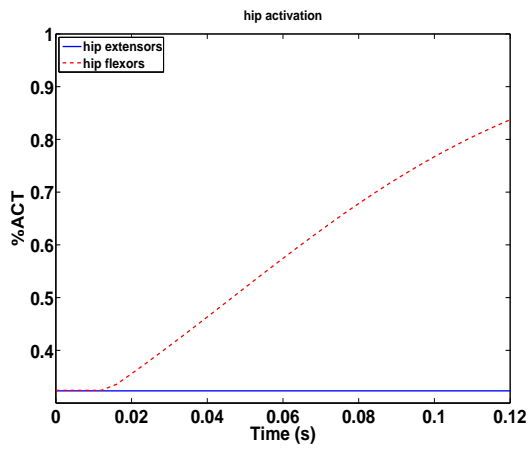
There was co-contraction of the knee extensors and flexors, particularly from mid-phase onwards, in order to prevent hyperextension of the knee joint during the final moments of the pull, Figure 6.21d. This was also observed during the combined transi-



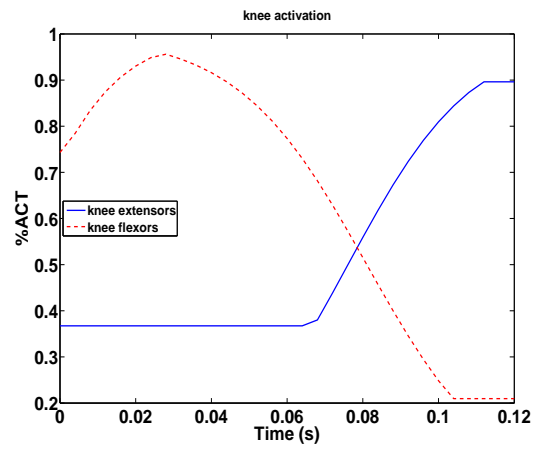
(a) Ankle joint activation time histories



(b) Shoulder joint activation time histories



(c) Hip joint torque activation histories



(d) Knee joint torque activation histories

Figure 6.21: Joint activation time histories from performance (solid line) and matched simulation (dashed line) for the second pull

tion phase and second pull simulation however, the activation levels of the knee flexors were lower compared to the starting activation levels of the second pull (0.3 vs 0.73 respectively). The higher flexors activation can be, partially at least, attributed again to the difference between the angular velocity of knee extension at the start of the second pull between the two simulations ( $4.5^\circ/\text{s}$  vs  $36^\circ/\text{s}$  for the combined and second pull only simulations respectively) as a higher extension velocity might have induced higher co-contraction of extensors and flexors and, hence, higher activation for the latter.

On the other hand, the hip extensors activation values at the start of the second pull were lower (0.34) compared to the respective value during the combined simulation (0.78). A possible explanation for this discrepancy may be given by the difference in the value of the hip joint angle between the two simulations. Indeed, as Figure 6.16 illustrates the model hip joint angle at the start of the second pull during the combined simulation was, approximately,  $16^\circ$  lower than the performance value used as initial condition for the second pull simulation. The longer moment arm at the hip joint puts the model at more disadvantageous position compared to the performance values and increases the flexion torque at the joint which is likely to induce higher hip extensors activation in order for the joint to match the athlete's hip extension during the combined simulation. It is noted that while the hip flexors activation approached its maximum value at the end of the pull the extensors activation did not ramp up likely due to the extensors being significantly stronger than the flexors as is shown in Table 5.6. The shoulder activation remained low during the pull as the bar was approximately in line with the shoulder joint centre (Figure 6.7c).

## 6.5 Optimisation of the second pull

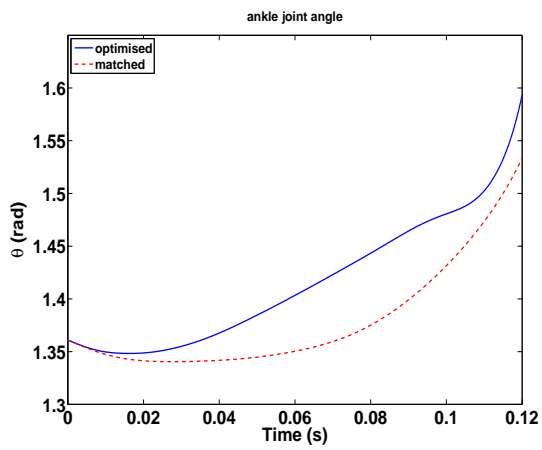
For a lift to be successful the peak displacement of the barbell must be no less than 70% of the lifter's height. Since no upwards force is exerted on to the barbell by the lifter after the end of the second pull (Garhammer, 1980, 1985; Gourgoulis *et al.*, 2002) the higher the barbell vertical velocity is at the end of this phase, the larger the peak vertical displacement of the barbell will be. Therefore, the model was optimised for the vertical velocity,  $v_z$ , of the barbell at the end of the second pull. The method of optimisation of the second pull phase was the same as in the matching simulation with the starting activation levels of the four joints set equal to their respective values obtained at the end of the transition phase during the matching simulation. As in the case of the latter penalties were imposed if the difference between model and athlete maximum joint angle was greater than  $6^\circ$ .

### 6.5.1 Joint angles

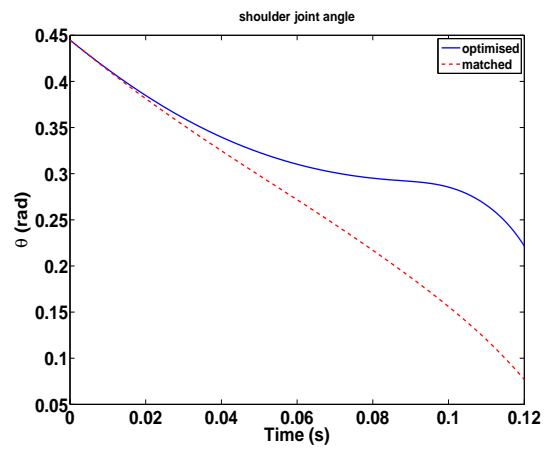
With the exception of the hip joint all the other joint angles increased during the optimised simulation. Significantly, the maximum ankle and knee joint angle values increased by approximately  $4^\circ$  and  $11^\circ$  respectively as the model attempted to maximise extension in order to increase the vertical velocity of the bar. This strategy is very similar to real performances where athletes are instructed to “finish the pull” i.e. to maximise the extension of the ankle, knee and hip joints in order to maximise the vertical acceleration of the barbell (Everett, 2009; Medvedyev, 1986).

### 6.5.2 Joint torques

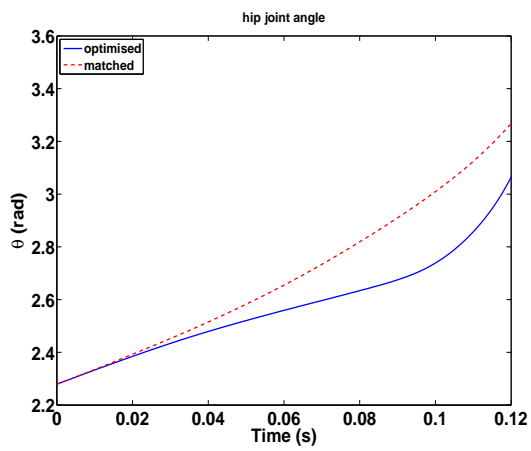
The main difference in the joint torque time histories between optimised and matched performances were in the hip joint where the maximum extension torque values were significantly (323 N) higher in the former, Figure 6.23c. At the knee joint a strong flexion torque was produced during the optimised performance instead of the weak extension torque that was obtained during the matching simulation (Figure 6.24d) possibly to prevent the overextension of the joint due to the strong hip extension.



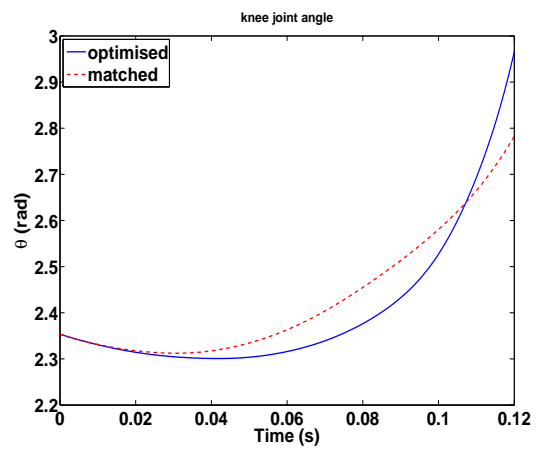
(a) Ankle joint angle time histories



(b) Shoulder joint angle time histories

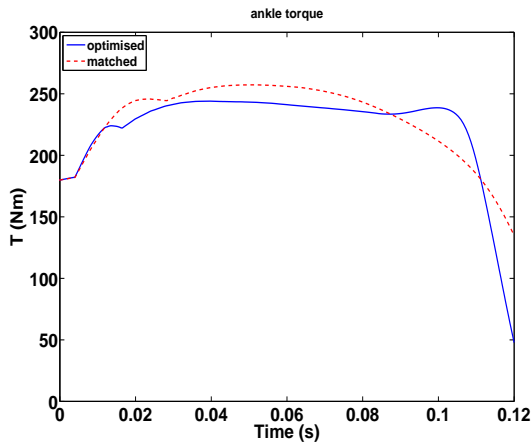


(c) Hip joint angle time histories

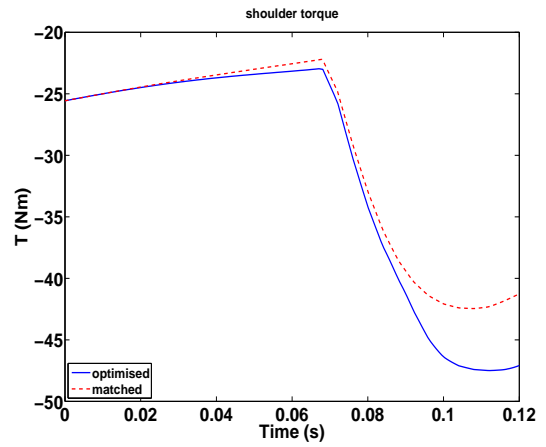


(d) Knee joint angle time histories

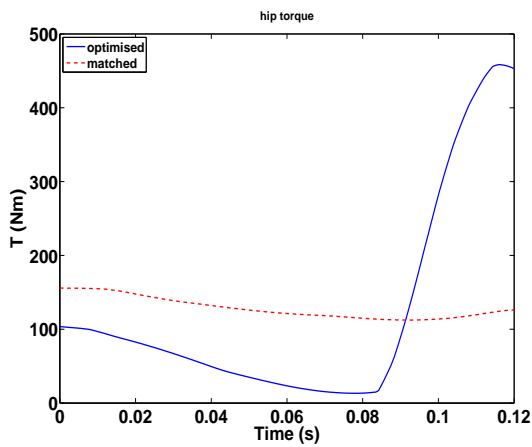
Figure 6.22: Joint angle time histories from optimised (solid line) and matched simulation (dashed line)



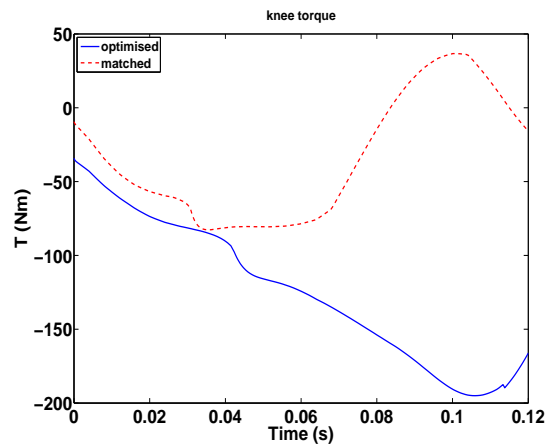
(a) Ankle joint torque time histories



(b) Shoulder joint torque time histories



(c) Hip joint torque time histories



(d) Knee joint torque time histories

Figure 6.23: Joint torque time histories from optimised (solid line) and matched simulation (dashed line)

The ankle and shoulder joint torque time histories were very similar to the matched performance with the ankle torque demonstrating weaker plantar–flexion at the end of the lift and the should slightly stronger extension (Figures 6.24a, b).

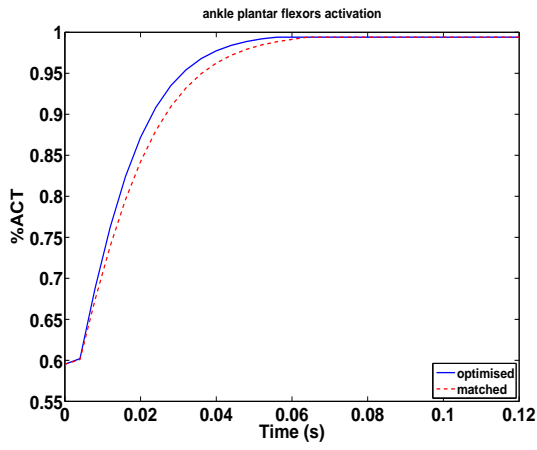
### 6.5.3 Activation timings

Although the starting activation values at the four joints were set equal to the respective values from the combined transition pull and second pull matching simulation, the optimal solution converged to initial activation levels that were very close to the second pull matching simulation with the exception of the hip flexors activation values

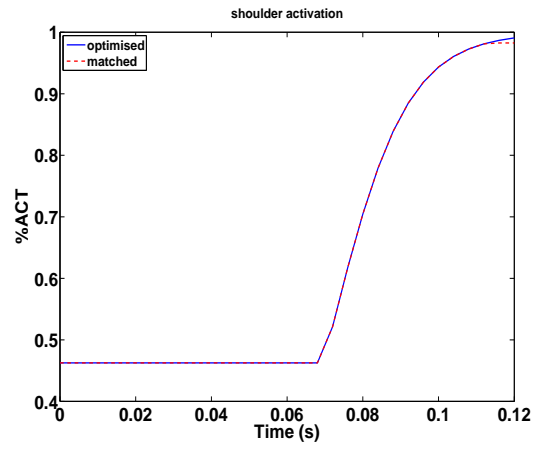
(Figure 6.24). The ankle and shoulder activation time histories were very close to the matching simulation values (Figure 6.24a, b). The hip activation time histories, however, deviated significantly from the matching simulation as there was a significant ramp up of the hip extension activation after the first 0.08s of the lift which explains the significant increase in the hip extension torque discussed earlier (Figure 6.24c). The hip flexor initial activation value was significantly higher than that of the matching simulation and ramped up slowly towards its maximum. As a result of this strategy the hip was slowly extended during the first 0.08s of the lift and fast during the last 0.04s (Figures 6.22c & 6.23c) leading to a significant increase in the bar vertical velocity (Figure 6.25). The activation time histories of the knee extensors were similar to those of the matching simulation, however, the ramp up of the activation took place later in the lift (Figure 6.24e). Combined with the slow ramp down of the knee flexors activation (Figure 6.24f) this resulted in the observed flexion torque for the knee joint.

Table 6.6: Maximum (MAX) and minimum (MIN) torque values from inverse dynamics and matching simulations for the shoulder, hip, knee and ankle joints

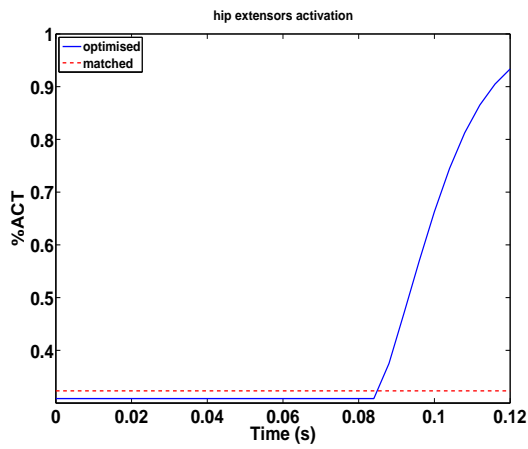
<b>Joint</b>	<b>Simulation</b>		<b>Inverse dynamics</b>	
	<b>MAX (N)</b>	<b>MIN (N)</b>	<b>MAX (N)</b>	<b>MIN (N)</b>
<b>Ankle</b>	292	49	501	2.9
<b>Knee</b>	159	-195	235	-110
<b>Hip</b>	525	-42	435	6
<b>Shoulder</b>	-23	-48	–	–



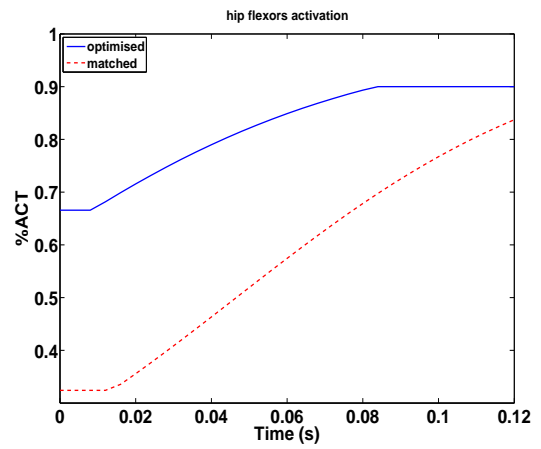
(a) Ankle joint activation time histories



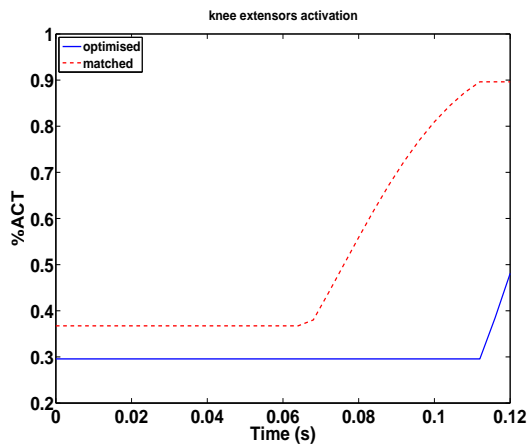
(b) Shoulder joint activation time histories



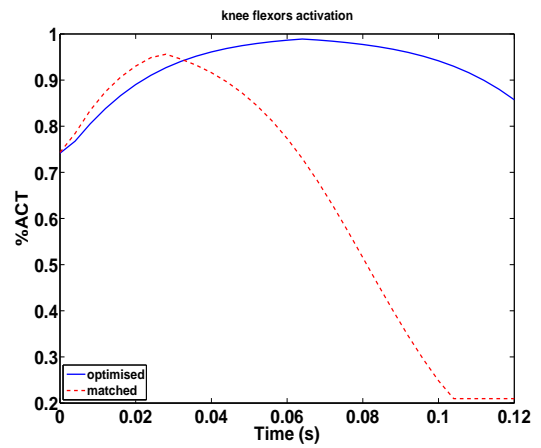
(c) Hip joint extensors activation histories



(d) Hip joint flexors activation histories



(e) Knee joint extensors activation histories



(f) Knee joint flexors activation histories

Figure 6.24: Joint activation time histories from optimised (solid line) and matched simulation (dashed line)

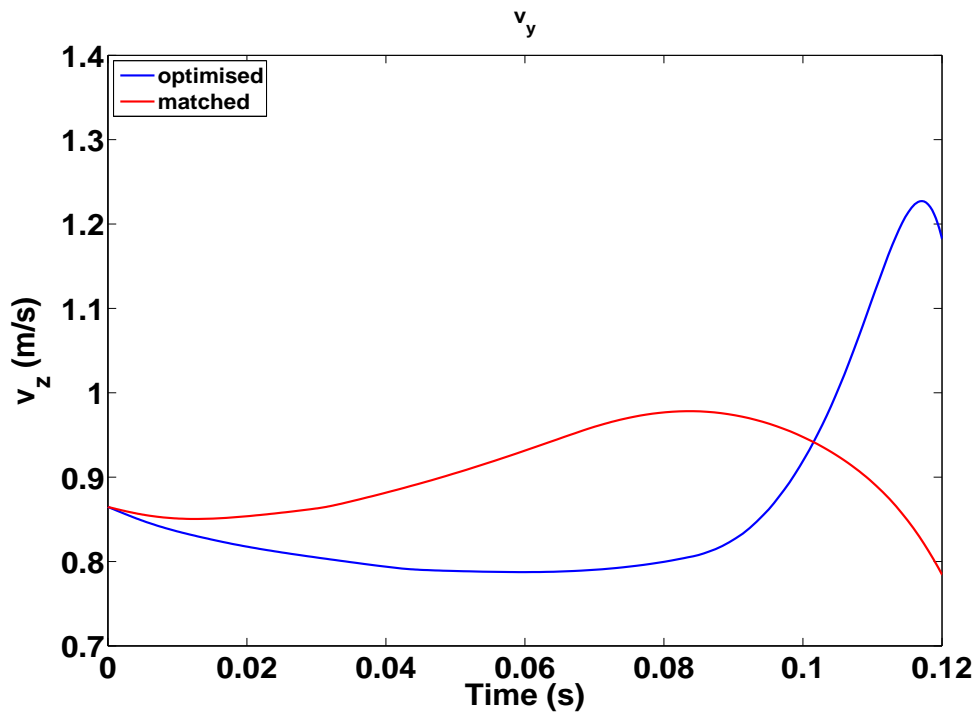


Figure 6.25: Vertical velocity,  $v_z$ , from optimised and matched simulations during the second pull phase

#### 6.5.4 Barbell velocity

The vertical barbell velocity at end of the second pull was 0.88 m/s for the matching simulation and 1.23 m/s for the optimised performance ( Table 6.7 and Figure 6.25) a 39% increase in the value of  $v_z$  as a result of the significant increase in the activation and torque output of the hip extensors during the optimised simulation.

Table 6.7: Vertical velocity at the end of the second pull for performance, matching simulation and optimised simulation

Simulation type	Velocity (m/s)
Matched	0.88
Optimised	1.23

## 6.6 Discussion

Good agreement has been demonstrated between simulation and performance for the first and second pull phases of the lift. In the former the % error in the RMS difference scores (expressed by the NRMS values) was low for the shoulder, knee and hip joints (range 0.7–9% respectively, Table 6.3) and moderate for the ankle joint (13%). In the case of the second pull phase the % error RMS difference was lower than 10% for all four joints. The low NRMS values in the matching simulations of the first and second pull phases indicate that the accuracy of the model is sufficient enough to be employed in optimisation simulations such as the maximisation of barbell velocity at the end of the second pull, Table 6.5.

On the other hand the quantitative agreement between the matching simulation and performance for the combined and second pull phases was moderate as indicated by the high NRMS values (range: 12–25%, Table 6.4). This was likely caused by the complexity of the phase which involved an initial knee flexion during the transition phase followed by a knee extension for the second pull whereas the hip joint was extending in both phases. The model also failed to match the actual joint torque values for the ankle joint, obtained via inverse dynamics, in all three simulations (Figures 6.14, 6.17, 6.20) indicating a possible inability of the ankle torque generator to match the *in vivo* torque values particularly during fast plantar flexions. If this was indeed the case, then it was likely due to the inability of the athlete to perform maximal plantar flexions during dynamometer testing that resulted in sub-maximal torque values at the descending limb of the force-length curve, Figure 6.26. This produced, in turn, sub-maximal  $T(\omega, \theta)$  torque generator function values when the 9-parameter function of equations (1.14), (1.16) and (1.17) was fitted on the ankle  $T-\omega-\theta$  dataset, Table 5.6. The knee joint torque generator also failed to match the inverse dynamics joint torques in the first pull and transition phase + second pull simulations however it did so during the third simulation of the second pull. Although it is possible that an insufficient torque generator was again the cause of the discrepancy in torque outputs the fact that this was not observed in all simulations and the low angle time histories RMS for the knee joint, may suggest that there might have been other causes. For example, in order to compensate for the weak ankle extension the model may have had

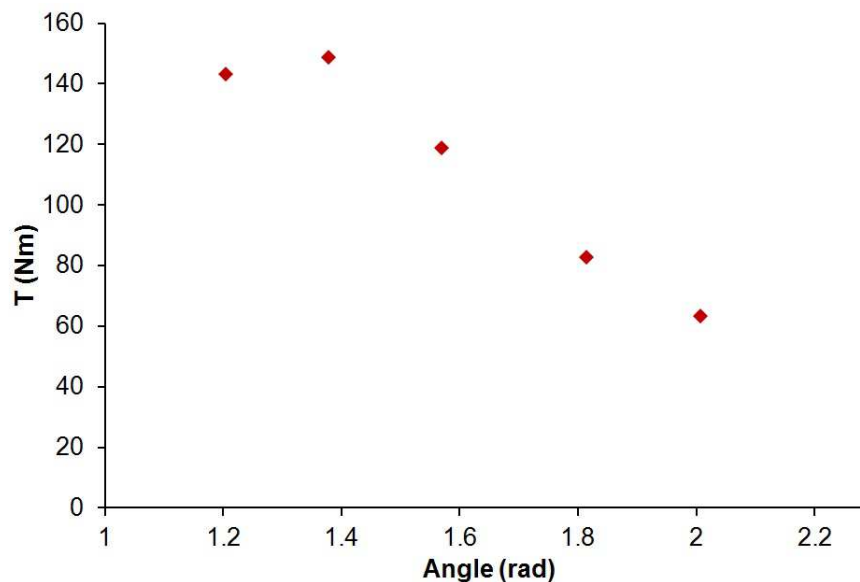


Figure 6.26: Torque vs angle values for ankle plantar flexion obtained from the study participant during dynamometer testing

to produce high torque output at the hip joint. This in turn may have caused a higher degree of passive stretch at the knee and hence reduced the amount of torque needed to actuate the joint (Jessop, 2011). Despite the moderate quantitative agreement, the simulation was successful in reproducing the joint movement patterns. Given the limited time available to obtain an optimum solution it is likely that the simulation accuracy can be further improved.

Baumann *et al.* (1988) used inverse dynamics to calculate the muscle moments in the ankle, knee, and hip joints from 9 different lifters that competed in the 1985 World Championships in Sweden. They found that during the first pull the knee and ankle moments increased just prior and after barbell lift-off from the floor and subsequently decreased with the knee moment becoming negative in some cases towards the end of the phase. The hip moment varied little during this phase with a slightly downwards trend. During the transition phase the knee and ankle joints increased reaching a second maximum before declining again during the second pull. The hip moments on the other hand steadily decreased as the joint extended and reached their minimum value at the end of the second pull. Those results are in good qualitative agreement with the results of the matching simulations, particularly with the first pull and the combined transition + second pull simulations that showed similar moment patterns

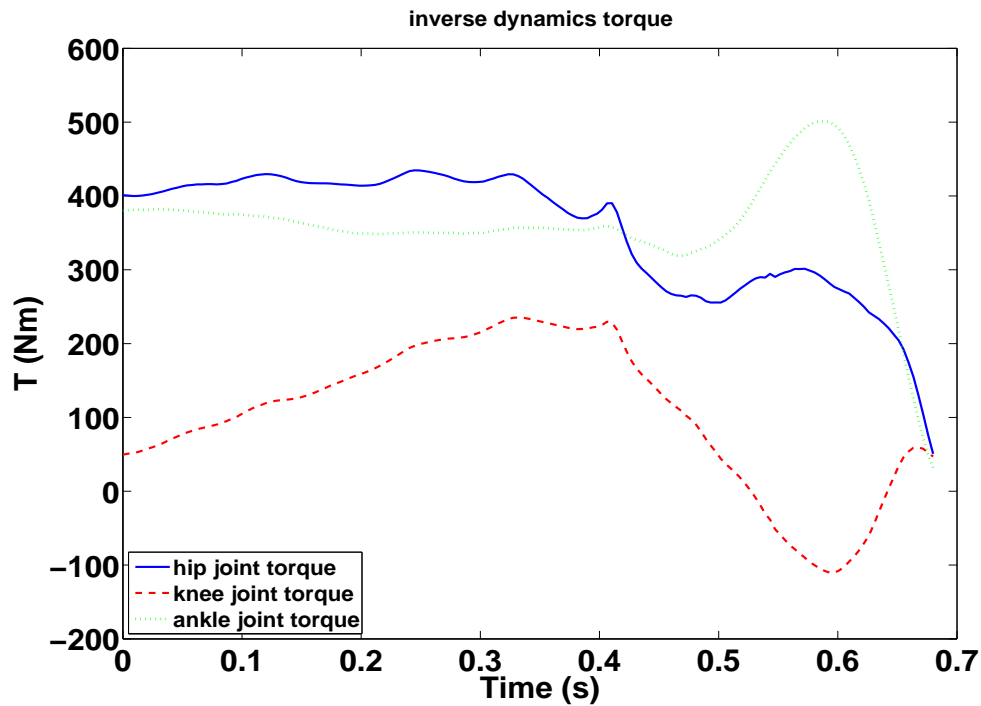


Figure 6.27: Ankle, knee and hip joint torques for the first three phases of the Snatch calculated using inverse dynamics for a single lift

(Figures 6.14, 6.17). They also compare well with the respective inverse dynamics calculations of the current study (Figure 6.27). Baumann *et al.* (1988) noted that the highest moments occurred at the hip joint and were 4–6 times higher than the moments recorded at the knee joint which were the lowest of the three. The results of the matching simulations are in good agreement with these findings as the maximum hip joint torque was approximately 3.3 and 1.8 times higher than the maximum knee and ankle torque values respectively, Table 6.6. The inverse dynamics results showed a similar pattern with the maximum hip joint torques being 1.9 times higher than the respective knee joint values though they failed to exceed the maximum ankle joint torque values (Table 6.6). However, Baumann *et al.* presented mean maximum joint torque values from 15 different lifts and consequently a quantitative comparison with the respective results of the current study cannot be made.

Baumann *et al.* (1988) observed that the low knee moments were unexpected and could not be reconciled with the number of problems reported from the overloading of the knee joint. They mentioned, that a positive moment value is indicative of higher extensors muscle action whereas a negative one indicates that the flexors' action is

dominant. If however, there exists co-contraction of extensors and flexors the degree of activation of both muscle groups may be high, potentially overloading the joint, whereas the net joint torque may be low. Indeed the activation profiles of the knee joint showed co-contraction of the knee extensors and flexors during all three phases and particularly during the second pull where the flexors are significantly activated in order to stop the knee joint from overextending (Figures 6.15d, 6.18d, 6.21d). An additional factor that needs to be considered is the biarticular nature of the semitendinosus, semimembranosus and biceps femoris (long head) that act both as knee flexors and hip extensors. Since the hip joint is actively extending throughout the first three phases of the Snatch those muscles will be continuously activated explaining the observed co-contraction at the knee joint even at high flexion angles such as in the start of the first pull. Wu *et al.* (2013) also calculated the ankle, knee and hip joint moments for the Snatch, using a 21-segment, inverse dynamics model. Their results closely matched those of Baumann *et al.* and were similar to those of the current study particularly for the knee joint moments during the second pull.

The results of the matching optimisations indicated that the model was able to reproduce some important kinematic and kinetic characteristics of the first three phases of the Snatch despite the fact that these phases were modelled individually however the scope of a model is not only to identify relationships and important features in a sporting activity but also to help optimise the athlete's performance. Consequently, the model was optimised with respect to the vertical velocity,  $v_z$ , at the end of the second pull in order to examine which lift parameters would help the athlete improve his performance during that phase.

The model predicted that by increasing the ROM at the ankle and knee joints, activation and torque outputs at the hip joint, the value of  $v_z$  could be increased by approximately 39%. Considering that the athlete lifted approximately 75% of his competition maximum during testing it is likely that he did not need to perform maximally to successfully complete the lift. Therefore the model appeared to choose the correct strategy in order to increase performance during that phase. This was also in agreement with the optimum technique characteristics of the second pull which require the athlete to fully extend at the ankle, knee and hip joints in order to maximise the upwards acceleration of the barbell Bartonietz (1996); Baumann *et al.* (1988); Gourgoulis

*et al.* (2002, 2009); Ho *et al.* (2011).

It has to be noted, however, that despite the good match between the angle time histories of performance and simulation in the second pull the model underestimated the magnitude of  $v_z$  at the end of the phase. A number of reasons may have been the cause of this discrepancy the most likely of which was the weak ankle torque generators discussed earlier in this section.

### 6.6.1 Limitations and future work

During the Snatch motion occurs outside the sagittal plane that cannot be represented by a planar model such as this. For example, there is external and internal rotation of the femur at the hip joint during the first pull and the recovery phases respectively, horizontal abduction of the shoulder during the second pull, diagonal abduction during the catch phase and adduction of the shoulder girdle during the first three phases. Full biarticular symmetry of the lift was also assumed whereas in reality there will always be small perturbations between the left and right sides of the athlete due to inherent musculoskeletal imbalances. However, the results of the model evaluation showed that the model was able to reproduce, to a high degree, all the important features of the first three phases of the lift indicating that these motions did not have a significant effect on performance.

The foot was modelled as a one part segment for simplicity with three initial ground contact points (heel, COP, toe). The downside of this approach was that as soon as the heel was lifted a single contact was left at the toe to propel the foot up. A two-part representation of the foot would have allowed for a second contact point after heel lift-off however, due to time constraints this was not possible.

Data for this study was collected at the Loughborough University Biomechanics laboratory. Consequently the lift had to take place on two uncovered force plates and not on a lifting platform where the athlete was accustomed to lift and the weight lifted was limited to 75–80% of the athlete's competition best due to safety precautions. This may have affected the technique of the athlete during the lift however, if that did happen the effect was likely minimal and did not significantly alter the kinematic

characteristics of the lift (Ho *et al.*, 2011)

It must also be noted that, as discussed in Chapter 4 and the previous section, the torque-driven model did not incorporate the effects on joint torque due to changes in the length and contraction velocity of biarticular muscles (e.g. the gastrocnemius) as the torque generator functions only account for length and velocity changes about a single-joint. This might have significantly affected the torque generator output as shown by Lewis *et al.* (2012) who found that a single joint representation of ankle plantar flexion overestimated the ankle plantar flexor torques by approximately 20% for knee flexion greater than 40°. However, in this case the torque generator of the ankle appeared to lack the strength capacity to match the actual performance therefore it is unlikely that the exclusion of the secondary joint effects negatively affected the simulation of the ankle plantar flexion. It cannot be known however, how this exclusion affected the torque outputs at the other joints.

These limitations should be addressed in future work. Moreover, the medium term objective is to include all three phases, that were individually simulated, in a single simulation with a unique set of initial conditions. Successful completion of this optimisation will likely provide a better understanding of the interdependence of the three phases such as the effect of initial body position on the maximal value of  $v_z$  or the horizontal displacement of the bar during the lift and how those may vary with different athlete body types and could potentially help address a number of research questions such as:

- What are the optimum knee and hip angles at the start of the second pull for maximised power production on the bar?
- How do those angles change as the body dimensions (anthropometry) of the lifter changes?
- What is the optimal timing of the double knee bend (initiation of the second pull)?
- What is the optimal starting position from the floor and how does it change with body dimensions?
- Is there a correlation between BCH angle and optimal bar kinematics?

# 7 Summary and Conclusion

## 7.1 Summary

The aim of the current work was to investigate different aspects of muscle function using mathematical techniques that originated from the work of Hill (1938). Those included the effects of isokinetic training on the tension-limiting mechanism of the knee extensors, the expression of the hamstrings:quadriceps functional strength ratio with respect to both angle and angular velocity and the construction of a torque-driven simulation model of the Snatch. All three studies were based on equations (1.14), (1.16) and (1.17) that are re-written below for reference in the form of equations (3.2) and (3.3)

- $\omega \geq 0$

$$T_{conc}^{tet}(\omega, \theta) = \left[ \frac{T_0 w_c (w_{max} + w_c)}{w_{max} (w_c + w)} - \frac{T_0 w_c}{w_{max}} \right] \times \left( \alpha_{min} + \frac{\alpha_{max} - \alpha_{min}}{1 + e^{\left(-\frac{\omega - \omega_1}{\omega_r}\right)}} \right) e^{\left(-\frac{1}{2}\right) \left[ \frac{(\theta - \theta_{opt})^2}{w^2} \right]} \quad (7.1)$$

- $\omega < 0$

$$T_{ecc}^{tet}(\omega, \theta) = - \left[ \frac{(T_{max} - T_0)^2 \omega_{max} \omega_c}{\kappa T_0 (\omega_{max} + \omega_c) \left[ \frac{(T_{max} - T_0) \omega_{max} + \omega_c}{\kappa T_0 (\omega_{max} + \omega_c)} - \omega \right]} + T_{max} \right] \times \left( \alpha_{min} + \frac{\alpha_{max} - \alpha_{min}}{1 + e^{\left(-\frac{\omega - \omega_1}{\omega_r}\right)}} \right) e^{\left(-\frac{1}{2}\right) \left[ \frac{(\theta - \theta_{opt})^2}{w^2} \right]} \quad (7.2)$$

In this section the methods used within the study will be summarized, the research questions raised in the beginning of the thesis will be addressed and possible future directions will be discussed.

### 7.1.1 Quadriceps activation obtained by theoretical and experimental means

This study aimed to investigate the effects a training-intervention, consisting on of performing high velocity concentric-eccentric contractions on an isovelocity dynamometer,

on the neural activation of the quadriceps and to establish the accuracy and robustness of the DIFACT function for different levels of maximal activation. Participants underwent a three-week training protocol consisting of eccentric/concentric knee extension cycles at velocities ranging between 50 and 400° /s. In order to assess the effects of training two testing sessions were performed, pre- and post-training respectively. Those included MVC and supra-maximally electrically stimulated isometric and isovelocity contractions using the ITT technique. %VA- $\omega$  and T- $\omega$  datasets were obtained from both sessions and statistically compared both group-wise and individually in order to establish whether or not the training intervention had increased the neural activation and torque output of participants. Furthermore, the neural activation levels were theoretically modelled via the DIFACT function (1.16) using three different upper bounds for the maximal activation,  $\alpha_{max}$ , (90%, 95% and 100%) and then were statistically compared to establish the degree of accuracy and robustness of the function.

### 7.1.2 The H:Q ratio as a function of $\omega$ and $\theta$

The aim of this study was to derive a mathematical expression for the functional, H:Q<sub>fun</sub>, ratio that would allow it to be determined as a function of both angular velocity,  $\omega$  and joint angle  $\theta$  and not as a single variable function as has been the case thus far. First a theoretical description of the ratio was derived, in the form of a 17-parameter function  $R_T(\omega, \theta)$ , using equations (7.1)–(7.2). Using  $R_T(\omega, \theta)$  as a benchmark a simpler, 6-parameter function was derived.

$$R_E(\omega, \theta) = a \exp(b\omega^n + c\theta^m) - d\omega^{1/2}\theta^2 \quad (7.3)$$

$R_E(\omega, \theta)$  was assessed in two stages. First its capacity to reproduce  $R_T(\omega, \theta)$  was assessed by fitting it to 11  $R_T(\omega, \theta)$  whole surfaces and then to 17 individual points from each surface. Goodness of fit was assessed via the  $R^2$  and root mean square error (RMSE). Having ascertained the ability of  $R_E(\omega, \theta)$  to reproduce the theoretical surface it was next fitted to 8, 11, 14 and 17 raw, H:Q<sub>fun</sub> points from a second, larger, dataset that had been obtained from a 14-participant study. The accuracy and robustness of  $R_E(\omega, \theta)$  were established using the  $R^2$ , RMSE and normalised RMSE values from the different fits.

### **7.1.3 A six–segment, torque–driven simulation model of the Snatch**

The purpose of this study was to develop a torque-driven, two-dimensional, simulation model of the Snatch lift to be employed in analysis and optimization of the lift mechanics. The model was developed in the SimMechanics suite of Matlab. The athlete's body was simulated by 6 segments (foot, shank, thigh, torso, upper arm and forearm) and the bar + weights system by a metal rod 0.1 m in length. Torque generators were located at the ankle, knee, hip and shoulder joints with those at knee and hip having both flexion and extension profiles and the remaining two flexion profiles only. The elbow joint was kinematically driven using linear kinematics data in order to represent the movement of the upper limb in the frontal plane during the lift. The model development stages are summarized next.

#### **7.1.3.1 Collection and analysis of kinematic data**

Kinematic data from the Snatch lift were collected using ten VICON T cameras at a sample frequency of 250 Hz. Fifty-one markers were placed on the athlete and traced. Marker positions were reconstructed using the VICON Nexus suite and subsequently filtered using a low pass Butterworth filter with a cut-off frequency of 10 Hz. Joint centres, segment length and COM locations, linear velocities and accelerations were derived and projected onto the sagittal plane. Finally, the joint angles and angular velocities accelerations were calculated, concluding the kinematic analysis of the lift.

#### **7.1.3.2 Collection and analysis of kinetic data**

Force data was captured using two Kistler, piezoelectric, force plates at 1000 Hz and subsequently re-sampled to 250 Hz in order to synchronize it with the kinematic data. Joint torque data from the ankle, knee, hip and shoulder joints was recorded using a Con-Trex isovelocity dynamometer at 512 Hz. The crank angles were converted to joint angles through linear regression using joint angle values that had been measured with a mechanical goniometer during isometric trials.

### 7.1.3.3 Anthropometric measurements

Anthropometric data were collected using the geometric inertia model of Yeadon (1990a). Due to the bilaterally symmetric nature of the model fifty-seven measurements were taken instead of the ninety-five required by the full bilateral model. The trunk length was adjusted to better agree with the kinematic data. Since the trunk and head segments were combined into a single torso segment the inertia parameters and the COM of the combined segment were calculated using equation (5.1) and the parallel axis theorem.

### 7.1.3.4 Ground contact

The interaction between the model and ground was modelled via 3 vertical and 1 horizontal springs (equation (6.1)). The spring parameters were obtained by minimising the RMS difference between their force output and the force trace recorded from the force plates (equation (6.2)) using a simulated annealing algorithm (Corana *et al.*, 1987).

### 7.1.3.5 Model evaluation

Only the first three phases of the lift were simulated as this significantly decreased simulation time without negatively affecting the ability of the model to optimise lifting technique. Each phase was simulated separately in order to keep the number of torque generator activation parameters as low as possible and avoid the use of overly complex activation functions. A total of 36 activation parameters were optimized by minimising the RMS score between the sum of the joint angles of the model and that of the athlete during the lift.

## 7.2 Research questions

*Is it possible to reduce the neural inhibition during fast eccentric contractions and increase torque output by means of eccentric strength training?*

Statistical comparisons between group pre- and post-training torque datasets using both the Student's t-test and the extra-sum-of-squares F-test showed a significant,  $p < 0.05$ , increase in torque outputs post-training for both eccentric and concentric contractions. Individual pre- and post-training comparisons found that three out of the six subjects also demonstrated a significant,  $p < 0.05$ , increase in the torque output indicating, thus, that the training protocol was successful in improving the torque output of the subjects during MVC contractions. Regarding the effect of training protocol on neural activation and the action of the tension-limiting mechanism, a significant increase,  $p < 0.05$ , in the %VA post-training was achieved as well as in the peak torque outputs during eccentric contractions at  $350^\circ/\text{s}$  with respect to torque outputs from  $150^\circ/\text{s}$ . Those results, though not definitive, are indicative of increased neural activation post-training and a possible reduction in the inhibitive action of the tension limiting mechanism.

*How well does the sigmoid DIFACT function of (1.16) represent the in vivo neural activation profile during voluntary contractions and can it cope with perturbed levels of maximum activation?*

Two different non-linear regression fits were performed in order to establish the accuracy and robustness of the sigmoid DIFACT function. Specifically, a non-linear regression fit of the seven parameter MVC torque function, the product of (1.14) and (1.16), was performed to each of the T- $\omega$  datasets with the DIFACT upper bound,  $\alpha_{\max}$ , set at three different values, 100%, 95% and 90% and the  $R^2$  and RMS scores of the fits were determined. Likewise, the DIFACT function was fitted to the %VA- $\omega$  datasets. Results from the first fit showed that the MVC torque function was very successful in reproducing the raw T- $\omega$  datasets for all values of  $\alpha_{\max}$ . The DIFACT function was moderately accurate in reproducing the %VA- $\omega$  datasets especially those from the pre-training testing session. It was hypothesized that the difference in the goodness of fits between the two datasets (pre- and post-training) could be attributed, partly at least, to inconsistent participant performance or variations in the onset of stimuli due to experimental limitations. Overall however, the DIFACT function remained robust for all the  $\alpha_{\max}$  values and successfully represented the neural inhibition of knee extensors.

*Is it possible to obtain a mathematical description of the functional H:Q ratio with*

*respect to both angle,  $\theta$  and angular velocity  $\omega$  of contraction?*

A six parameter function,  $R_E(\omega, \theta)$ , was derived capable of producing sufficient qualitative and quantitative descriptions of the H:Q<sub>fun</sub> ratio with as few as 8 experimental points that also appears to be insensitive to small perturbations in the values of  $\theta$ . To arrive at  $R_E(\omega, \theta)$  17-parameter function  $R_T(\omega, \theta)$  was first derived that described the H:Q<sub>fun</sub> ratio in terms of  $\omega$  and  $\theta$  and was used to obtain H:Q<sub>fun</sub> ratio values for 11 datasets of knee extension–flexion.  $R_E(\omega, \theta)$  is the non-linear combination of the plane curves  $R_T(c, \theta)$  and  $R_T(\omega, c)$  that best reproduced the  $R_T(\omega, \theta)$  surfaces. Its robustness and accuracy were tested by fitting it successively first on the whole  $R_T(\omega, \theta)$  surfaces, on 17 points of each  $R_T(\omega, \theta)$  surface and on 8, 11, 14 and 17 raw ratio points calculated from a second knee extension–flexion dataset. The fits produced mean NRMSE of as low as 0.12 and high  $R^2$  values (mean 0.91) and provided angle-specific estimates of the H:Q<sub>fun</sub> ratio near full knee extension where hamstrings' injuries are more likely to occur.

*How close to optimum was the technique of the Olympic weightlifter that performed the Snatch lift?*

The optimisation of the of the barbell vertical velocity,  $v_z$ , in the second pull showed that the athlete was operating sub-maximally during this phase. The optimisation of second phase produced an increase of 0.35 m/s (a 39% increase) in the value of  $v_z$ , achieved by increasing the extension of the ankle and knee joints and the respective activation and torque values. Since the model did not match the torque output of the athlete at the ankle and knee joints it is not possible to conclude that the value of  $v_z$  would have been increased by the same amount had the athlete performed optimally however, it can be inferred that the model was able to identify and use the correct strategy in order to optimise the vertical velocity of the barbell and therefore successfully detect the sub-optimal performance of the lifter during that phase.

# References

- Aagaard, P., Simonsen, E. B., Andersen, J. L., Magnusson, P., & Dyhre-Poulsen, P. 2002. Neural adaptation to resistance training: changes in evoked V-wave and H-reflex responses. *Journal of Applied Physiology*, **92**, 2309–2318.
- Aagard, P., Trolle, E., & Bangsbo, J. 1995. Isokinetic hamstring/ quadriceps strength ratio : influence from joint angular velocity, gravity correction and contraction mode. *Acta Physiologica Scandinavica*, **154**, 421–427.
- Aagard, P., Simonsen, E.B., Magnusson, S.P., Larsson, S.P., & Dyhre-Poulsen, P. 1998. A new concept for isokinetic Hamstring:Quadricep muscle strength ratio. *American Journal of Sports Medicine*, **26**, 231–237.
- Aagard, P., Simonsen, E.B., Magnusson, S.P., Andersen, J.L, Halkjaer-Kristensen, J., & Dyhre-Poulsen, P. 2000. Neural inhibition during maximal eccentric and concentricquadriceps contraction: effects of resistance training. *Journal of Applied Physiology*, **89**, 2249–2257.
- Aagard, P., Leffers, A.M., Magnusson, S.P., Andersen, J.L, Halkjaer-Kristensen, J., & Dyhre-Poulsen, P. 2001. A mechanism for increased contractile strength of human pennate muscle in response to strength training: changes in muscle architecture. *European Journal of Applied Physiology Occup Physiol.*, **73**, 149–156.
- Akkus, H. 2012. Kinematic analysis of the snatch lift with elite female weightlifters during the 2010 World Weightlifting Championship. *The Journal of Strength and Conditioning Research*, **26**, 897—905.
- Alexander, R. M. 1990. Optimum take-off techniques for high and long jumps. *Philosophical Transactions of the Royal Society of London–Series B*, **329**, 3–10.
- Allen, S.J., King, M.A., & Yeadon, M.R. 2010. Is a single or double arm technique more advantageous in triple jumping? *Journal of Biomechanics*, **43**, 3156–3161.
- Alonso, J. M., Tscholl, P. M., Engebretsen, L., Mountjoy, M., Dvorak, J., & Junge, A. 2010. Occurrence of injuries and illnesses during the 2009 IAAF World Athletics Championships. *British Journal of Sports Medicine*, **44**, 1100–1105.

- Alonso, J. M., Edouard, P., Fischetto, G., Adams, B., Depiesse, F., & Mountjoy, M. 2012. Determination of future prevention strategies in elite track and field: analysis of Daegu 2011 IAAF Championships injuries and illnesses surveillance. *British Journal of Sports Medicine*, **46**, 505–514.
- Amiridis, I.G. 1996. Co-activation and tension-regulating phenomena during isokinetic knee extension in sedentary and highly skilled humans. *Journal of Physiology*, **534**, 613–623.
- Anderson, F. C., & Pandy, M. G. 2001. Dynamic optimization of human walking. *Journal of Biomechanical Engineering*, **123**, 381–390.
- Babault, N., Pousson, M., Ballay, Y., & Hoecke, J. Van. 2001. Activation of human quadriceps femoris during isometric, concentric, and eccentric contractions. *Journal of Applied Physiology*, **91**, 2628–2634.
- Babault, N., Pousson, M., Michaut, A., Ballay, Y., & Hoecke, J. 2002. EMG activity and voluntary activation during knee-extensor concentric torque generation. *European Journal of Applied Physiology*, **86**, 541–547.
- Bahr, R., & Holme, I. 2003. Risk factors for sports injuries: a methodological approach. *British journal of sports medicine*, **37**, 384–392.
- Baratta, R., Solomonow, M., Zhou, B.H., Letson, D., Chuinard, R., & D’ambrosia, R. 1988. Muscular coactivation: The role of the antagonist musculature in maintaining knee stability. *The American journal of sports medicine*, **16**, 113–122.
- Baroni, B. M., Rodrigues, R., Franke, R. A., Geremia, J. M., Rassier, D. E., & Vaz, M. A. 2013. Time Course of Neuromuscular Adaptations to Knee Extensor Eccentric Training. *International Journal of Sports Medicine*, **34**, 904–911.
- Bartonietz, K. 1996. Biomechanics of the Snatch: Toward a Higher Training Efficiency. *Strength and Conditioning Journal*, **18**, 24–31.
- Batzopoulos, V., & Brodie, D. A. 1989. Isokinetic Dynamometry: Applications and Limitations. *Sports Medicine*, **8**, 101–116.

- Baumann, W., Gross, V., Quade, K., Galbierz, P., & Schwirtz, A. 1988. The snatch technique of world class weightlifters at the 1985 world championships. *International Journal of Sport Biomechanics*, **4**, 68–89.
- Beltman, J.G.M. 2004. Voluntary activation level and muscle fiber recruitment of human quadriceps during lengthening contractions. *Journal of Applied Physiology*, **97**, 619–626.
- Bennel, K., Wajswelner, H., Lew, P., Schall-Riauour, A., Leslie, S., Plant, D., & Cirone, J. 1998. Isokinetic strength testing does not predict hamstring injury in Australian Rules Footballers. *British Journal of Sports Medicine*, **32**, 309–314.
- Bobbert, M. F., Houdijk, H., de Koning, J. J., & de Groot, G. 2002. From a One-Legged Vertical Jump to the Speed-Skating Push-off: A Simulation Study. *Journal of Applied Biomechanics*, **18**, 28–45.
- Brooks, J. H. M., Fuller, C.W., Kemp, S. P. T., & Reddin, D. B. 2005. Epidemiology of injuries in English professional rugby union: part 1 match injuries. *British Journal of Sports Medicine*, **39**, 757–766.
- Brooks, J. H. M., Fuller, C.W., Kemp, S. P. T., & Reddin, D. B. 2006. Incidence, risk, and prevention of hamstring muscle injuries in professional rugby union. *The American journal of sports medicine*, **34**, 1297–1306.
- Burdett, R. 1982. Biomechanics of the snatch technique of highly skilled and skilled weightlifters. *Research Quarterly for Exercise and Sport*, **53**, 193–197.
- Burkett, L. E. 1969. Causative factors in hamstring strains. *Medicine and science in sports*, **2**, 39–42.
- Caiozzo, V.J., Perrine, J.J., & Edgerton, V.R. 1981. Training-induced alterations of the in vivo force-velocity relationship of human muscle. *British Journal of Sports Medicine*, **51**, 750–754.
- Caldwell, G. E. 2014. *Muscle modelling*. In: D. G. E. Robertson et al. *Research methods in Biomechanics*. Second edn. Champaign, Il, USA: Human Kinetics.

- Cameron, M., Adams, R., & Maher, C. 2003. Motor control and strength as predictors of hamstring injury in elite players of Australian football. *Physical Therapy in Sport*, **4**, 159–166.
- Campos, J., Poletaev, P., Cuesta, A., Pablos, C., & Carratala, V. 2006. Kinematical analysis of the snatch in elite male junior weightlifters of different weight categories. *The Journal of Strength and Conditioning Research*, **20**, 843–850.
- Cappozzo, A., Catani, F., Leardini, A., Benedetti, M. G., & Croce, U. Della. 1996. Position and orientation in space of bones during movement; experimental artefacts. *Clinical Biomechanics*, **11**, 90–100.
- Challis, H. C. 2008. *Data processing and error estimation*. In: C. J. Payton and R. M. Bartlett (ed). *Biomechanical evaluation of movement in sport and exercise*. First edn. 270 Madison Ave, New York, USA: Routledge.
- Chen, Y. H., & Chiu, H. T. 2011. The relationship between the barbell trajectories of snatch and BCH angles. *Portuguese Journal of Sport Sciences*, **11**, 171–173.
- Chiu, H. T., Wang, C. H., & Cheng, K. B. 2010. The three-dimensional kinematics of a barbell during the snatch of Taiwanese weightlifters. *The Journal of Strength and Conditioning Research*, **24**, 1520–1526.
- Chow, J. W., Darling, W. G., & Hay, J. G. 1997. Mechanical characteristics of knee extension exercises performed on an isokinetic dynamometer. *Medicine and Science in Sports and Exercise*, **29**, 794–803.
- Chowdhary, A. G., & Challis, J. H. 2001. The Biomechanics of an Overarm Throwing Task: a Simulation Model Examination of Optimal Timing of Muscle Activations. *Journal of Theoretical Biology*, **211**, 39–53.
- Chumanov, E.S., Heiderscheit, B. C., & Thelen, D.G. 2007. The effect of speed and influence of individual muscles on hamstring mechanics during the swing phase of sprinting. *Journal of Biomechanics*, **40**, 3555–3562.
- Chumanov, E.S., Heiderscheit, B. C., & Thelen, D.G. 2011. Hamstring musculotendon dynamics during stance and swing phases of high-speed running. *Med Sci Sports Exerc*, **43**, 525–532.

- Cohen, J. 1992. Statistical power analysis. *Current Directions in Psychological Science*, **1**, 98–101.
- Coombs, R., & Garbutt, G. 2002. Developments in the use of the Hamstring/Quadriceps ratio for the assessment of muscle balance. *Journal of Sports Science and Medicine*, **1**, 56–62.
- Coombs, R., Garbutt, G., & Cramp, M. 2002. Comparison of conventional and functional hamstring quadriceps moment ratios through a 90 range of leg motion. *Journal of Sports Sciences*, **20**, 3–4.
- Corana, A., Marchesi, M., Martini, C., & Ridella, S. 1987. Minimising multimodal functions of continuous variables with the simulated annealing algorithm. *ACM Transactions on Mathematical Software*, **13**, 262–280.
- Corriander, E.B., & Tesch, P.A. 1990. Effects of eccentric and concentric muscle actions in resistance training. *Act Physiologica Scandinavica*, **140**, 31–39.
- Coyle, E.F., Feiring, D.C., Rotkis, T.C., 3rd, R.W. Cote, Roby, F.B., Lee, W., & J.H.Wilmore. 1981. Specificity of power improvements through slow and fast isokinetic training. *Journal of Applied Physiology*, **51**, 1437–1442.
- Croisier, J.L. 2004. Factors Associated with Recurrent Hamstring Injuries. *Sports Medicine*, **10**, 681–695.
- Croisier, J.L., Ganteaume, S., Binet, J., Genty, M., & Ferret, J-M. 2008. Strength imbalances and prevention of hamstring injury in professional soccer players. A prospective study. *The American Journal of Sports Medicine*, **36**, 1469–1475.
- Crowninshield, R. D., & Brand, R. A. 1981. The prediction of forces in structures: Distribution of intersegmental resultants. *Exercise and Sport Sciences Reviews*, **9**, 159–182.
- Dempster, W. T. 1955. Space requirements of the seated operator: geometrical, kinematic, and mechanical aspects of the body, with special reference to the limbs. *WADC Technical Report*.
- Domire, Z. J., & Challis, J. H. 2007. The influence of squat depth on maximal vertical jump performance. *Journal of Sport Sciences*, **25**, 193–200.

- Drezner, J., Ulager, J., & Sennett, M. D. 2005. Hamstring muscle injuries in track and field athletes: a 3-year study at the Penn Relay Carnival. *Clinical Journal of Sports Medicine*, **15**, 386.
- Dudley, G.A., Harris, R.T., Duvoisin, M.R., Hather, B.M., & Buchanan, P. 1990. Effect of voluntary vs. artificial activation on the relationship of muscle torque to speed. *Journal of Applied Physiology*, **69**, 2215–2221.
- Edman, K. A. 1988. Double hyperbolic force-velocity relation in frog muscle fibers. *Journal of Physiology*, **404**, 301–321.
- Edman, K. A., Elzinga, G., & Noble, M. I. 1978. Enhancement of mechanical performance by stretch during tetanic contractions of vertebrate skeletal muscle fibers. *Journal of Physiology*, **281**, 139–155.
- Ekstrand, J., Hägglund, M., & Wálden, M. 2011a. Epidemiology of Muscle Injuries in Professional Football (Soccer). *The American Journal of Sports Medicine*, **39**, 1226–1232.
- Ekstrand, J., Wálden, M., & Hägglund, M. 2011b. Injury incidence and injury patterns in professional football: the UEFA injury study. *British journal of sports medicine*, **45**, 553–558.
- Elliott, B. C., Alderson, Jacqueline A., & Denver, Eliot R. 2007. System and modelling errors in motion analysis: Implications for the measurement of the elbow angle in cricket bowling. *Journal of Biomechanics*, **40**, 2679–2685.
- Elliott, M. C. C. W., Zarins, B., Powell, J. W., & Kenyon, C. D. 2011. Hamstring Muscle Strains in Professional Football Players. A 10-Year Review. *The American Journal of Sports Medicine*, **39**, 843–850.
- Enoka, R. M. 1988. Load and skill related changes in segmental contributions to weightlifting movement. *Medicine and Science in Sports and Exercise*, **20**, 178–187.
- Enoka, R. M. 1996a. Eccentric contractions require unique activation strategies by the nervous system. *Journal of Applied Physiology*, **81**, 2339–2346.
- Enoka, R. M. 1996b. Neural adaptations with chronic physical activity. *Journal of Biomechanics*, **30**, 447–455.

- Enoka, R. M. 2008. *Neuromechanics of human movement*. Fourth edn. Champaign, IL, USA: Human Kinetics.
- Ergun, M., Igen, ., & E, Takran. 2004. A cross-sectional analysis of sagittal knee laxity and isokinetic muscle strength in soccer players. *International Journal of Sports Medicine*, **25**, 594–598.
- Evangelidis, P. E., Pain, M. T.G., & Folland, J. P. 2015. Angle-specific hamstring-to-quadriceps ratio. A comparison of football players and recreationally active males. *Journal of Sport Sciences*, **33**, 309–319.
- Everett, G. 2009. *Olympic Weightlifting: A complete guide for athletes and coaches*. Second edn. USA: Catalyst Athletics, LLC.
- Feeley, B. T., Kennelly, S., Barnes, R. P., Muller, M. S., Kelly, B. T., Rodeo, S. A., & Warren, R. F. 2008. Epidemiology of National Football League training camp injuries from 1998 to 2007. *The American journal of sports medicine*, **36**, 1597–1603.
- Folland, J. P., & Williams, A. G. 2007a. The Adaptations to Strength Training: Morphological and Neurological Contributions to Increased Strength. *Sports Medicine*, **37**, 145–168.
- Folland, J. P., & Williams, A. G. 2007b. Methodological issues with the interpolated twitch technique. *Journal of Electromyography and Kinesiology*, **17**, 317–327.
- Foreman, T.K., Addy, T., Baker, S., Burns, J., Hill, N., & Madden, T. 2006. Prospective studies into the causation of hamstring injuries in sport: A systematic review. *Physical Therapy in Sport*, **7**, 101–109.
- Forrester, S. E., Yeadon, M. R., King, M. A., & Pain, M.T.G. 2011. Comparing different approaches for determining joint torque parameters from isovelocity dynamometer measurements. *Journal of Biomechanics*, **44**, 955–961.
- Freckleton, G., & Pizzari, T. 2013. Risk factors for hamstring muscle strain injury in sport: a systematic review and meta-analysis. *British journal of sports medicine*, **47**, 351–358.
- Fukunaga, T. 1997. Determination of fascicle length and pennation in a contracting human muscle in vivo. *Journal of Applied Physiology*, **82**, 354–358.

- Garhammer, J. 1980. Power production by Olympic Weightlifters. *Medicine and Science in Sports and Exercise*, **12**, 54–60.
- Garhammer, J. 1985. Biomechanics Profiles of Olympic Weightlifters. *International Journal of Sports Biomechanics*, **1**, 122–130.
- Garhammer, J. 1991. A comparison of maximal power output between elite male and female weightlifters in competition. *International Journal of Sports Biomechanics*, **7**, 3–11.
- Garhammer, J. 2001. Barbell trajectory, velocity and power changes: Six attempt and four world records. *Weightlifting USA*, **19**, 27–30.
- Garrett, W. E. 1990. Muscle strain injuries: clinical and basic aspects. *Medicine and science in sports and exercise*, **22**, 436–443.
- Gerritsen, K. G. M., van den Bogert, A. J., & Nigg, B. M. 1995. Direct dynamics simulation of the impact phase in heel–toe running. *Journal of Biomechanics*, **28**, 661–668.
- Gittoes, M. J.R., Brewin, M. A., & Kerwin, D. G. 2006. Soft tissue contributions to impact forces simulated using a four-segment wobbling mass model of forefoot heel landings. *Human Movement Science*, **25**, 775–787.
- Gourgoulis, V., Aggelousis, N., Mavromatis, G., & Garas, A. 2000. Three–dimensional kinematic analysis of the snatch of elite Greek weightlifters. *Journal of Sport Sciences*, **18**, 643–652.
- Gourgoulis, V., Aggelousis, N., Antoniou, P., Mavromatis, G., Christoforidis, C., & Garas, A. 2002. Comparative 3-dimensional kinematic analysis of the snatch technique in elite male and female greek weightlifters. *The Journal of Strength and Conditioning Research*, **16**, 359–366.
- Gourgoulis, V., Aggelousis, N., Garas, A., & Mavromatis, G. 2009. Unsuccessful vs. successful performance in snatch lifts: a kinematic approach. *The Journal of Strength and Conditioning Research*, **23**, 486–494.

- Guex, K., Gojanovic, B., & Millet, G. P. 2012. Influence of Hip-Flexion Angle on Hamstrings Isokinetic Activity in Sprinters. *Journal of Athletic Training*, **47**, 390–395.
- Hadi, G., AkkuS, H., & Harbili, E. 2012. Three-dimensional kinematic analysis of the snatch technique for lifting different barbell weights. *The Journal of Strength and Conditioning Research*, **26**, 1568–1576.
- Harbili, E., & Alpteking, A. 2014. Comparative Kinematic Analysis of the Snatch Lifts in Elite Male Adolescent Weightlifters. *Journal of Sports Science and Medicine*, **13**, 417–422.
- Harry, J. D., Ward, A. W., Heglund, N. C., Morgan, D. L., & McMahon, Thomas A. 1990. Cross-bridge cycling theories cannot explain high-speed lengthening behavior in frog muscle. *Biophysical Journal*, **57**, 201–208.
- Hase, K., Miyashita, K., Ok, S., & Arakawa, Y. 2003. Human gait simulation with a neuromusculoskeletal model and evolutionary computation. *The Journal of Visualization and Computer Animation*, **14**, 73–92.
- Hatze, H. 1975. A new method for the simultaneous measurement of the moment of inertia, the damping coefficient and the location of the centre of mass of a body segment in situ. *European Journal of Applied Physiology and Occupational Physiology*, **34**, 217–226.
- Hatze, H. 1980. A mathematical model for the computational determination of parameter values of anthropomorphic segments. *Journal of Biomechanics*, **13**, 833–844.
- Hatze, H. 1981. A comprehensive model for human motion simulation and its application to the take-off phase of the long jump. *Journal of Biomechanics*, **14**, 135–142.
- Heiderscheit, B. C., Hoerth, D. M., Chumanov, E. S., Swanson, S. C., Thelen, B. J., & Thelen, D. G. 2005. Identifying the time of occurrence of a hamstring strain injury during treadmill running: A case study. *Clinical Biomechanics*, **20**, 1072–1078.
- Heiser, T. M., Weber, J., Sullivan, G., Clare, P., & Jacobs, R. R. 1984. Prophylaxis and management of hamstring muscle injuries in intercollegiate football players. *The American Journal of Sports Medicine*, **12**, 368–370.

- Higashihara, A., Ono, T., Kubota, J., Okuwaki, T., & Fukubayashi, T. 2010. Functional differences in the activity of the hamstring muscles with increasing running speed. *Journal of Sports Sciences*, **28**, 1085–1092.
- Higashihara, A., Nagano, Y., Ono, T., & Fukubayashi, T. 2014. Relationship between the peak time of hamstring stretch and activation during sprinting. *European Journal of Sport Science*, **ahead of print**, 1–6.
- Higbie, E. J., Cureton, K. J., Warren, G. L., & Prior, B. M. 1996. Effects of concentric and eccentric training on muscle strength, cross-sectional area, and neural activation. *Journal of Applied Physiology*, **81**, 2173–2181.
- Hiley, M. J., & Yeadon, M. R. 2003a. The margin for error when releasing the high bar for dismounts. *Journal of Biomechanics*, **36**, 313–319.
- Hiley, M. J., & Yeadon, M. R. 2003b. Optimum Technique for Generating Angular Momentum in Accelerated Backward Giant Circles Prior to a Dismount. *Journal of Applied Biomechanics*, **19**, 119–130.
- Hill, A. V. 1938. The Heat of Shortening and the Dynamic Constants of Muscle. *Proceedings of the Royal Society of Londodn, Series B*, **126**, 136–195.
- Hinrichs, R. N. 1985. Regression equations to predict segmental moments of inertia from anthropometric measurements: an extension of the data of Chandler et al.(1975). *Journal of Biomechanics*, **18**, 621–624.
- Ho, L. K. W., Williams, M. D., Wilson, C. J., & Meehan, D. L. 2011. Using three-dimensional kinematics to identify feedback for the Snatch: A case study. *The Journal of Strength and Conditioning Research*, **25**, 2773–2780.
- Ho, L. K. W., Lorenzen, C., Wilson, C., Saunders, J., & Williams, M. D. 2014. Reviewing current Knowledge in snatch performance and technique: the Need for Future directions in applied research. *The Journal of Strength and Conditioning Research*, **28**, 574–586.
- Holland, J. H. 1975. *Adaptation in natural and artificial systems*. First edn. Ann Arbor, USA: University of Michigan Press.

- Hoover, D. L., Carlson, K. M., Christensen, B. K., & Zebas, C.J. 2006. Biomechanical analysis of women weightlifters during the snatch. *The Journal of Strength and Conditioning Research*, **20**, 627–633.
- Hortobagyi, T., Hill, J. P., Houmard, J. A., Fraser, D. D., Lambert, N. J., & Israel, R. G. 1996. Adaptive responses to muscle lengthening and shortening in humans. *Journal of Applied Physiology*, **80**, 765–772.
- Hubbard, M. 1993. Computer simulation in sport and industry. *Journal of Biomechanics*, **26**, 53–61.
- Huxley, A. F. 1957. Muscle structure and theories of contraction. *Progress in Biophysics and Biophysical Chemistry*, **7**, 225–318.
- Iga, J., George, K., Lees, A., & Reilly, T. 2009. Crosssectional investigation of indices of isokinetic leg strength in youth soccer players and untrained individuals. *Scandinavian Journal of Medicine and Science in Sports*, **19**, 714–719.
- Ikedo, Y., Jinji, T., Matsubayashi, T., Matsuo, A., Inagaki, E., Takemata, T., & Kikuta, M. 2012. Comparison of the snatch technique for female weightlifters at the 2008 Asian championships. *The Journal of Strength and Conditioning Research*, **26**, 1281–1295.
- Isaka, T., Okada, J., & Funato, K. 1996. Kinematic Analysis of the Barbell During the Snatch Movement of Elite Asian Weight Lifters. *Journal of Applied Biomechanics*, **12**, 508–516.
- Jensen, R. K. 1978. Estimation of the biomechanical properties of three body types using a photogrammetric method. *Journal of Biomechanics*, **11**, 349–358.
- Jessop, D. 2011. *Computer simulation of the sprint start*. Ph.D. thesis, Loughborough University.
- Katz, B. 1939. The relation between force and speed in muscular contraction. *Journal of Physiology*, **96**, 45–64.
- Kawakami, Y., Muraoka, T., Ito, S., Kanehisa, H., & Fukunaga, T. 2002. In vivo muscle fibre behaviour during counter-movement exercise in humans reveals a significant role for tendon elasticity. *The Journal of Physiology*, **540**, 635–646.

- Kellis, E., & Katis, A. 2007. Biomechanical characteristics and determinants of instep soccer kick. *Journal of Sports Science and Medicine*, **6**, 154–165.
- King, M. A., & Yeadon, M. R. 2002. Determining subject specific torque parameters for use in a torque-driven simulation model of dynamic jumping. *Journal of Applied Biomechanics*, **18**, 207–217.
- King, M. A., & Yeadon, M. R. 2004. Maximising somersault rotation in tumbling. *Journal of Biomechanics*, **37**, 471–477.
- King, M. A., Yeadon, M. R., & Kerwin, D. G. 1999. A two-segment simulation model of long horse vaulting. *Journal of Sports Sciences*, **17**, 313–324.
- King, M. A., Wilson, C., & Yeadon, M. R. 2006. Evaluation of a Torque-Driven Model of Jumping for Height. *Journal of Applied Biomechanics*, **22**, 264–274.
- Kipp, K., Redden, J., Sabick, M. B., & Harris, C. 2012. Weightlifting performance is related to kinematic and kinetic patterns of the hip and knee joints. *The Journal of Strength and Conditioning Research*, **26**, 1838–1844.
- Komi, P. V. 1984. Physiological and biomechanical correlates of muscle function: effects of muscle structure and stretch-shortening cycle on force and speed. *Exercise and sport sciences reviews*, **12**, 81–122.
- Krentz, J. R., & Farthing, J. P. 2010. Neural and morphological changes in response to a 20-day intense eccentric training protocol. *European Journal of Applied Physiology*, **110**, 333–340.
- Krylow, A. M., & Sandercock, T. G. 1997. Dynamic responses of muscle involving eccentric contraction. *Journal of Biomechanics*, **30**, 27–33.
- Lee, H. D., & Herzog, W. 2002. Force enhancement following muscle stretch of electrically stimulated and voluntarily activated human adductor pollicis. *Journal of Physiology*, **545**, 321–330.
- Lewis, M. G.C., King, M. A., Yeadon, M. R., & Conceição, Filipe. 2012. Are Joint Torque Models Limited by an Assumption of Monoarticularity? *Journal of Applied Biomechanics*, **28**, 520–529.

- Lieber, R. L., & Fridén, J. 1993. Muscle damage is not a function of muscle force but active muscle strain. *Journal of Applied Physiology*, **74**, 520–526.
- Lombardi, V., & Piazzesi, G. 1990. The Contractile Response During Steady Lengthening of Stimulated Frog Muscle Fibres. *Journal of Physiology*, **431**, 141–171.
- Lund, H., Søndergaard, K., Zachariassen, T., Christensen, R., Bülow, P., Henriksen, M., Bartels, E. M., B. Danneskiold-Samsøe, B., & Bliddal, H. 2005. Learning effect of isokinetic measurements in healthy subjects and reliability and comparability of Biodex and Lido dynamometers. *Clinical Physiology and functional Imaging*, **25**, 75–82.
- Madsen, O. R. 1996. Torque, total work, power, torque acceleration energy and acceleration time assessed on dynamometer: reliability of knee and elbow extensor and flexor strength measurements. *European Journal of Applied Physiology and Occupational Physiology*, **74**, 206–210.
- Maffiuletti, N. A., Bizzini, M., K. Desbrosses, N. Babault, & Munzinger, U. 2007. Reliability of knee extension and flexion measurements using the Con-Trex isokinetic dynamometer. *Clinical Physiology and Functional Imaging*, **27**, 346–353.
- Mann, R. V. 1981. A kinetic analysis of sprinting. *Medicine and Science in Sports and Exercise*, **13**, 325–328.
- Medvedyev, A. S. 1986. *A system of multi-year training in weightlifting*. First edn. Moscow: Fizkultura i Sport.
- Merton, P. A. 1954. Voluntary strength and muscle fatigue. *Journal of Physiology*, **123**, 553–564.
- Mills, C., Pain, M. T. G., & Yeadon, M. R. 2006. Modelling a viscoelastic gymnastics landing mat during impact. *Journal of Applied Biomechanics*, **22**, 103–111.
- Mills, C., Pain, M. T. G., & Yeadon, M. R. 2008. The influence of simulation model complexity on the estimation of the internal loading in gymnastics landings. *Journal of Biomechanics*, **41**, 620–628.

- Mills, C., Pain, M. T. G., & Yeadon, M. R. 2009. Reducing ground reaction forces in gymnastics landings may increase internal loading. *Journal of Biomechanics*, **42**, 671–678.
- Motulski, H., & Christopoulos, A. 2004. *Fitting Models to Biological Data using Linear and Nonlinear Regression*. First edn. 198 Madison Avenue, New York, USA: Oxford University Press.
- Muramatsu, T., Muraoka, T., Takeshita, D., Kawakami, Y., Hirano, Y., & Fukunaga, T. 2001. Mechanical properties of tendon and aponeurosis of human gastrocnemius muscle in vivo. *Journal of Applied Physiology*, **90**, 1671–1678.
- Murphy, D. F., Connolly, D. A. J., & Beynnon, B. D. 2003. Risk factors for lower extremity injury: a review of the literature. *British journal of sports medicine*, **37**, 13–29.
- Murphy, D. F., Connolly, D. A. J., & Beynnon, B. D. 2014. Anthropometry and barbell trajectory in the snatch lift for elite women weightlifters. *The Journal of Strength and Conditioning Research*, **28**, 1636–1648.
- Neptune, R.R., & Hull, M.L. 1999. A theoretical analysis of preferred pedaling rate selection in endurance cycling. *Journal of Biomechanics*, **32**, 409–415.
- Novacheck, T. F. 1998. The biomechanics of running. *Gait and Posture*, **7**, 77–95.
- Opar, D. A., Williams, M. D., & Shield, A. J. 2012. Hamstring Strain Injuries. *Sports Medicine*, **42**, 209–226.
- Orchard, J. W. 2012. Hamstrings are most susceptible to injury during the early stance phase of sprinting. *British journal of sports medicine*, **46**, 88–89.
- Orchard, J. W., & Stewart, H. 2002. Epidemiology of injuries in the Australian Football League, seasons 19972000. *The American Journal of Sports Medicine*, **36**, 39–44.
- Orchard, J. W., Marsden, J., Lord, S., & Garlick, D. 1997. Preseason hamstring muscle weakness associated with hamstring muscle injury in Australian footballers. *The American Journal of Sports Medicine*, **25**, 81–85.

- Orchard, J. W., Alcott, E., James, T., Farhart, P., Portus, M., & Waugh, S. R. 2002. Exact moment of a gastrocnemius muscle strain captured on video. *British journal of sports medicine*, **36**, 222–223.
- Osternig, L. R., Hamill, J., Lander, J. E., & Robertson, R. 1986. Co-activation of sprinter and distance runner muscles in isokinetic exercise. *Medicine and Science in Sports and Exercise*, **18**, 431–435.
- Paillard, T., Noé, F., Passelergue, P., & Dupui, P. 2005. Electrical stimulation superimposed onto voluntary muscular contraction. *Sports Medicine*, **35**, 951–966.
- Pain, M. T. G., & Challis, J. H. 2001a. High resolution determination of body segment inertial parameters and their variation due to soft tissue motion. *Journal of Applied Biomechanics*, **17**, 326–334.
- Pain, M. T. G., & Challis, J. H. 2001b. The role of the heel pad and shank soft tissue during impacts: a further resolution of a paradox. *Journal of Biomechanics*, **34**, 327–333.
- Pain, M. T. G., & Forrester, S. E. 2009. Predicting maximum eccentric strength from surface EMG measurements. *Journal of Biomechanics*, **42**, 1598–1603.
- Pain, M. T. G., Forrester, S. E., & Young, F. 2013. The torque-velocity relationship in large human muscles: maximum voluntary versus electrically stimulated behaviour. *Journal of Biomechanics*, **46**, 645–650.
- Pandy, M. G. 2003. Simple and complex models for studying muscle function in walking. *Philosophical Transactions of the Royal Society B: Biological Sciences*, **358**, 1501–1509.
- Pandy, M. G., Zajac, F. E., Sim, E., & Levine, W. S. 1990. An optimal control model for maximum-height human jumping. *Journal of Biomechanics*, **23**, 1185–1198.
- Payton, C. J. 2008. *Motion analysis using video*. In: C. J. Payton and R. M. Bartlett (ed). *Biomechanical evaluation of movement in sport and exercise*. First edn. 270 Madison Ave, New York, USA: Routledge.
- Plagenhoef, S., Evans, F. G., & Abdelnour, T. 1983. Anatomical data for analyzing human motion. *Research quarterly for Exercise and Sport*, **54**, 169–178.

- Prior, M., Guerin, M., & Grimmer, K. 2009. An evidence-based approach to hamstring strain injury: a systematic review of the literature. *Sports Health: A Multidisciplinary Approach*, **1**, 154–164.
- Richards, J. G. 1999. The measurement of human motion: A comparison of commercially available systems. *Human Movement Science*, **18**, 589–602.
- Roman, R. A., & Shakirzyanov, M. S. 1978. *The Snatch, the Clean and Jerk*. First edn. Moscow: Fizkultura i Sport.
- Ruiter, C. J. De, Didden, W. J. M., Jones, D. A., & Haan, A. De. 2000. The force-velocity relationship of human adductor pollicis muscle during stretch and the effects of fatigue. *Journal of Physiology*, **526**, 671–681.
- Schache, A. G., Wrigley, T. V., Baker, R., & Pandy, M. G. 2009. Biomechanical response to hamstring muscle strain injury. *Gait and Posture*, **29**, 332–338.
- Schache, A. G., Dorn, T. W., Wrigley, T. V., Brown, N. A. T., & Pandy, M. G. 2013. Stretch and activation of the human biarticular hamstrings across a range of running speeds. *European journal of applied physiology*, **113**, 2813–2828.
- Schilling, B. K., Stone, M. H., O'Bryant, H. S., Fry, A. C., Coglianese, R. H., & Pierce, K. C. 2002. Snatch technique of collegiate national level weightlifters. *Journal of Strength and Conditioning Research*, **16**, 551–555.
- Seger, J. Y., & Thorstensson, A. 2004. Effects of eccentric versus concentric training on thigh muscle strength and EMG. *International Journal of Sports Medicine*, **26**, 45–52.
- Shield, A., & Zhou, S. 2004. Assessing Voluntary Muscle Activation with the Twitch Interpolation Technique. *Sports Medicine*, **34**, 253–267.
- Spägle, T., Kistner, A., & Gollhofer, A. 1999. Modelling, simulation and optimisation of a human vertical jump. *Journal of Biomechanics*, **32**, 521–530.
- Staron, R. S., Karapondo, D. L., Kraemer, W. J., Fry, A. C., Gordon, S. E., Falkel, J. El, Hagerman, F. C., & Hikida, R. S. 1994. Skeletal muscle adaptations during early phase of heavy-resistance training in men and women. *Journal of Applied Physiology*, **76**, 1247–1255.

- Stone, M. H., Pierce, K. C., Sands, W. A., & Stone, M. E. 2006. Weightlifting: A Brief Overview. *Strength and Conditioning Journal*, **28**, 50–66.
- Tesch, P. A., Ekberg, A., Lindquist, D. M., & Trieschmann, J. T. 2004. Muscle hypertrophy following 5-week resistance training using a non-gravity-dependent exercise system. *Acta Physiologica Scandinavica*, **180**, 89–98.
- Thelen, D. G., Chumanov, E. S., Hoerth, D. M., Best, T., Swanson, S. C., Li, L., Young, M., & Heiderscheit, B. C. 2005a. Hamstring Muscle Kinematics during Treadmill Sprinting. *Medicine and Science in Sports and Exercise*, **37**, 108–114.
- Thelen, D. G., Chumanov, E. S., Best, T. M., Swanson, S. C., & Heiderscheit, B. C. 2005b. Simulation of biceps femoris musculotendon mechanics during the swing phase of sprinting. *Medicine and science in sports and exercise*, **37**, 100–104.
- Tillin, N. A., Pain, M. T. G., & Folland, J. P. 2012. Contraction type influences the human ability to use the available torque capacity of skeletal muscle during explosive efforts. *Proceedings of the Royal Society: B*, **279**, 2106–2115.
- Tourny-Chollet, C., & Leroy, D. 2002. Conventional vs. dynamic hamstring-quadriceps strength ratios: a comparison between players and sedentary subjects. *Isokinetics and Exercise Science*, **10**, 183–192.
- van Soest, A. J., Schwab, A. L., Bobbert, M. F., & van Ingen Schenau, G. J. 1993. The influence of the biarticularity of the gastrocnemius muscle on vertical-jumping achievement. *Journal of Biomechanics*, **26**, 1–8.
- Venkataraman, P. 2009. *Applied optimization with matlab programming*. First edn. USA: John Wiley & sons, Inc.
- Voukelatos, D., & Pain, M. T. G. 2015. Modelling suppressed muscle activation by means of an exponential sigmoid function: Validation and bounds. *Journal of Biomechanics*, **48**, 712–715.
- Weber, S., & Kriellaars, D. 1997. Neuromuscular factors contributing to in vivo eccentric moment generation. *Journal of Applied Physiology*, **83**, 40–45.
- Westing, S. H. 1988. Eccentric and concentric torque-velocity characteristics of the quadriceps femoris in man. *European Journal of Applied Physiology*, **58**, 100–104.

- Westing, S. H., Seger, J. Y., & Thorstensson, A. 1990. Effects of electrical stimulation on eccentric and concentric torque-velocity relationships during knee extension in man. *Acta Physiologica Scandinavica*, **140**, 17–22.
- Westing, S. H., Cresswell, A. G., & Thorstensson, A. 1991. Muscle activation during maximal voluntary eccentric and concentric knee extension. *European journal of applied physiology and occupational physiology*, **62**, 104–108.
- Whittlesey, S. N., & Hamill, J. 2014. *Computer Simulation of Human Movement*. In: D. G. E. Robertson et al. *Research methods in Biomechanics*. Second edn. Champaign, IL, USA: Human Kinetics.
- Winchester, J. B., Porter, J. M., & McBride, J. M. 2009. Changes in bar path kinematics and kinetics through use of summary feedback in power snatch training. *The Journal of Strength and Conditioning Research*, **23**, 444–454.
- Winter, E. M., & Brookes, F. B. C. 1991. Electromechanical response times and muscle elasticity in men and women. *European Journal of Applied Physiology*, **63**, 124–128.
- Wood, G. A., & Jennings, L. S. 1979. On the use of spline functions for data smoothing. *Journal of Biomechanics*, **12**, 477–479.
- Woods, C., Hawkins, R. D., Hulse, M., & Hodson, A. 2002. The Football Association Medical Research Programme: an audit of injuries in professional football—analysis of preseason injuries. *British journal of sports medicine*, **36**, 436–441.
- Woods, C., Hawkins, R. D., Maltby, S., Hulse, M., Thomas, A., & Hodson, A. 2004. The Football Association Medical Research Programme : an audit of hamstring injuries in professional football—analysis of hamstring injuries. *Exercise and Sport Sciences Reviews*, **38**, 36–41.
- Wright, I.C., Neptune, R.R., van den Bogert, A.J., & Nigg, B.M. 1998. Passive regulation of impact forces in heel-toe running. *Clinical Biomechanics*, **13**, 521–531.
- Wu, J. F., Liu, Y. C., & Chen, W. C. 2013. The computer simulation of one and three trunk segment model in analyzing Snatch lifting.
- Yeadon, M. R. 1990a. The simulation of aerial movement – II: A mathematical inertia model of the human body. *Journal of Biomechanics*, **23**, 67–74.

- Yeadon, M. R. 1990b. The simulation of aerial movement – IV: A computer simulation model. *Journal of Biomechanics*, **23**, 85–89.
- Yeadon, M. R., & Challis, J. H. 1994. The future of performance-related sportsbiomechanics research. *Journal of Sports Sciences*, **12**, 3–32.
- Yeadon, M. R., & King, M. A. 2002. Evaluation of a torque driven simulation model of tumbling. *Journal of Applied Biomechanics*, **18**, 195–206.
- Yeadon, M. R., & King, M. A. 2008. *Computer simulation modelling in sport*. In: C. J. Payton and R. M. Bartlett (ed). *Biomechanical evaluation of movement in sport and exercise*. First edn. 270 Madison Ave, New York, USA: Routledge.
- Yeadon, M. R., King, M. A., & Wilson, C. 2006. Modelling the maximum voluntary joint torque/angular velocity relationship in human movement. *Journal of Biomechanics*, **39**, 476–482.
- Yeung, S. S., Suen, A. M. Y., & Yeung, E. W. 2009. A prospective cohort study of hamstring injuries in competitive sprinters: preseason muscle imbalance as a possible risk factor. *British Journal of Sports Medicine*, **43**, 598–594.
- Yu, B., Queen, M., Abbey, A. N., Liu, Y., Moorman, C. T., & Garrett, W. E. 2008. Hamstring muscle kinematics and activation during overground sprinting. *Journal of Biomechanics*, **41**, 3121–3126.

# Appendices

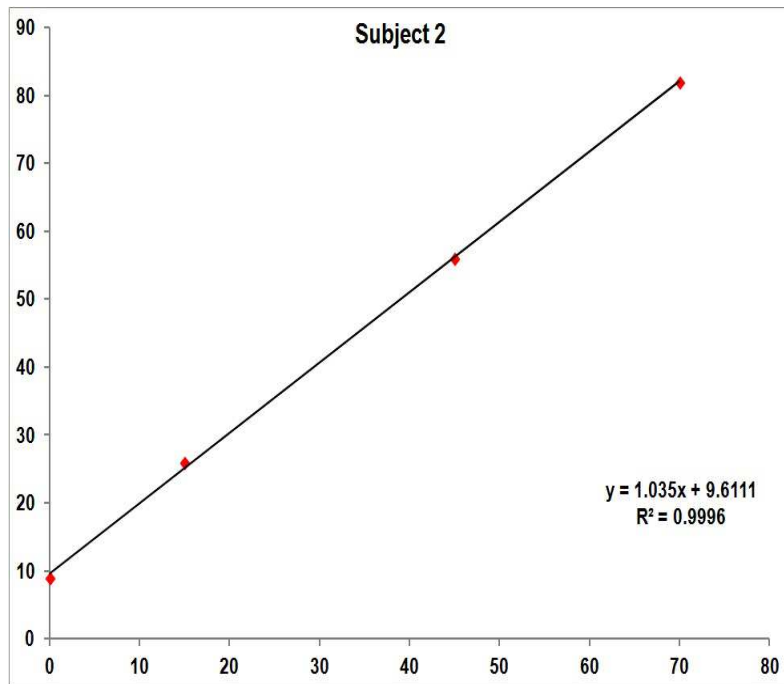
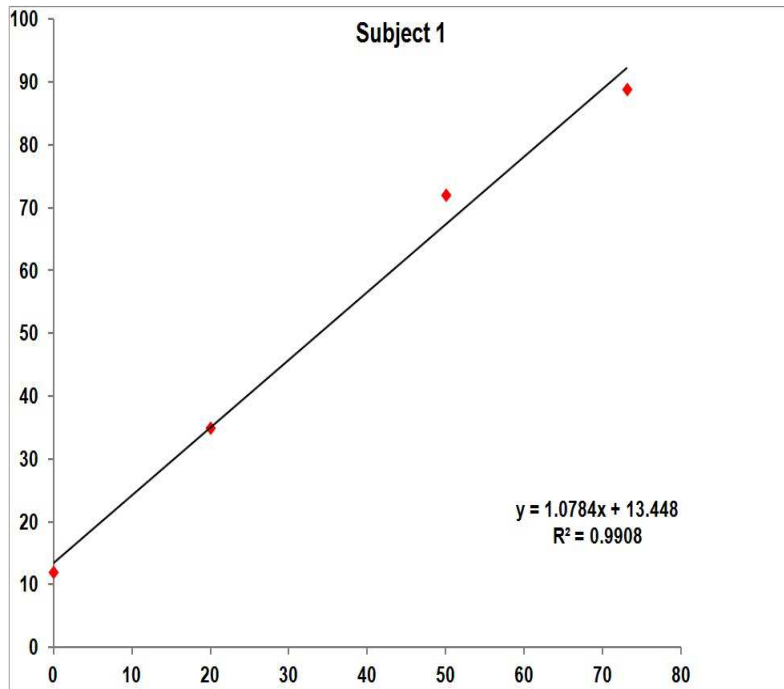
## Appendix A: Training programme

The following table contains information on every workout that took place during the training period. All subjects performed the same number of sets and repetitions on a particular training day. As is illustrated in the table the number of sets and repetitions per training session increased progressively until the 7th training day where it was reduced from 10 to 8 sets and finally to 6 on the final training session.

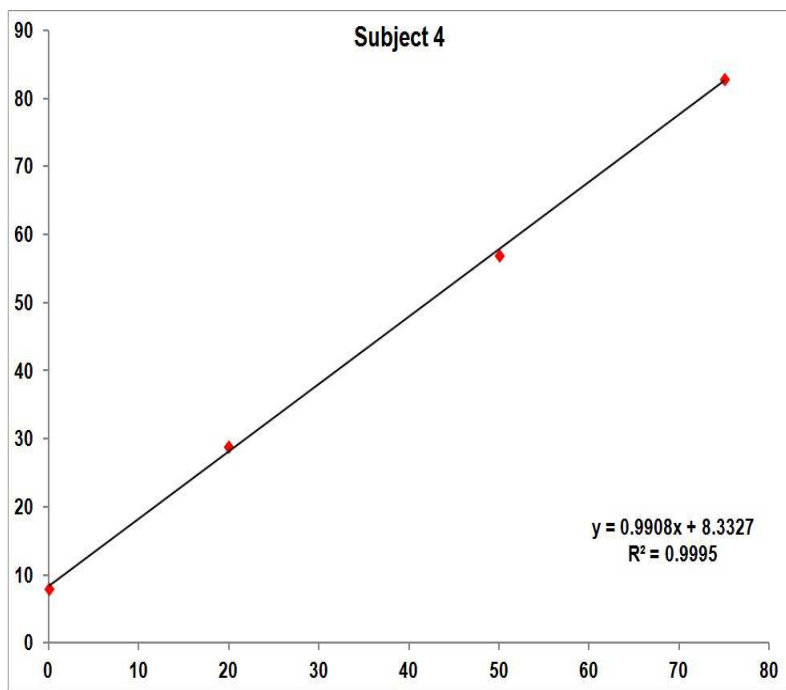
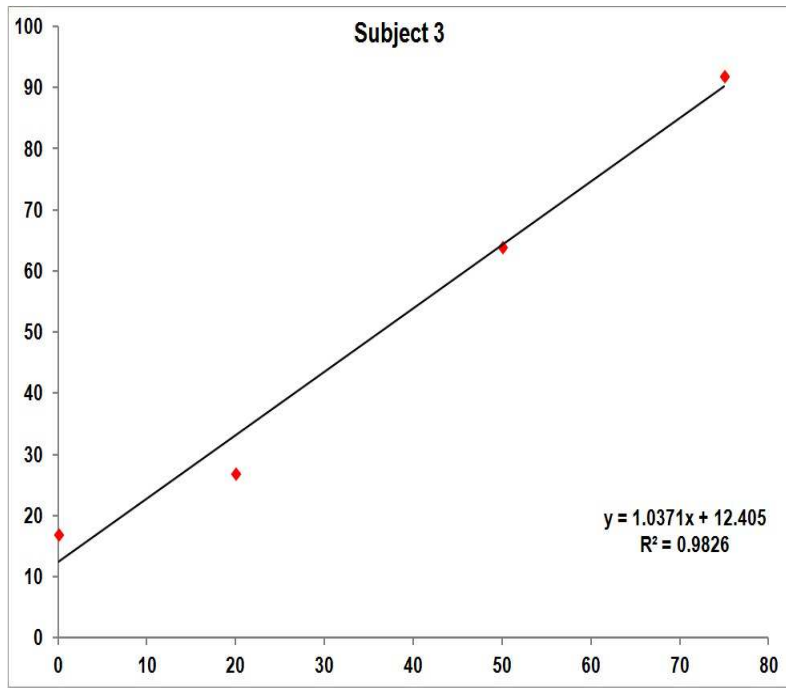
Training programme

Training Session								
	1	2	3	4	5	6	7	8
$\omega$	Number of Sets/Cycles							
<b>50</b>	2/2	1/2	–	–	–	–	–	–
<b>100</b>	2/3	2/3	2/2	–	–	–	–	–
<b>150</b>	2/4	1/4	2/3	2/3	2/3	1/3	–	–
<b>250</b>	–	1/5	2/5	2/5	2/5	1/5	1/4	–
<b>350</b>	–	1/6	2/6	3/6	3/6	4/6	3/5	2/4+1/5
<b>400</b>	–	–	–	2/6	3/6	4/7	4/6	2/4+1/5

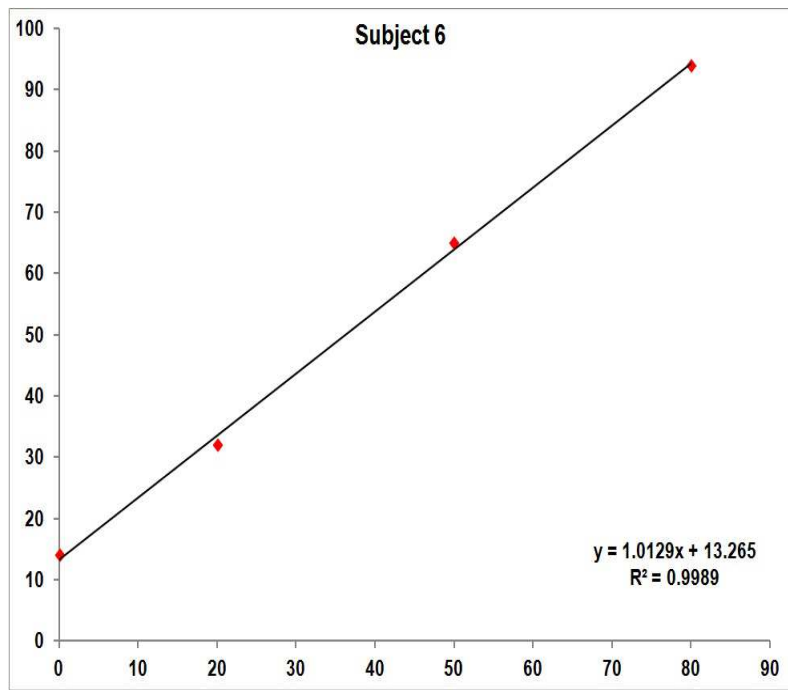
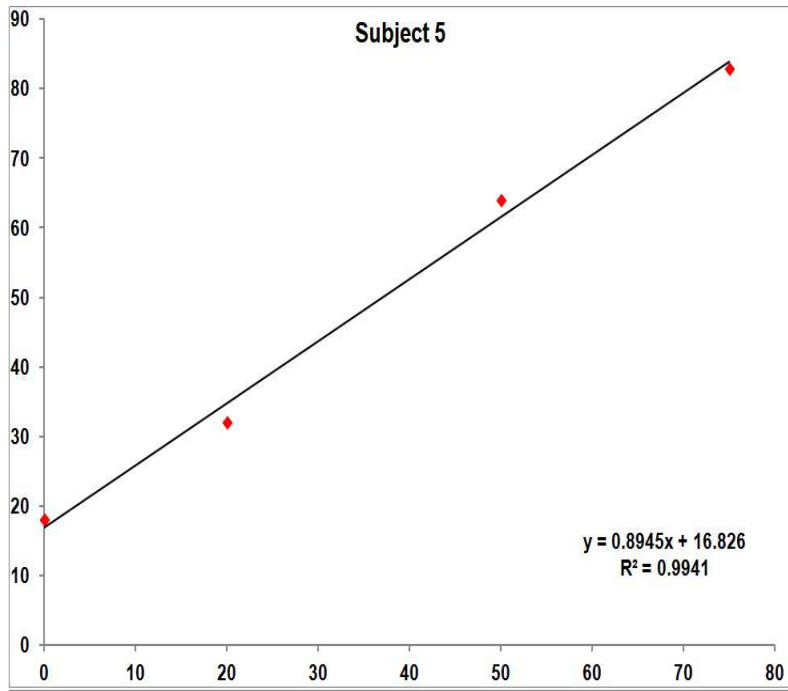
## Appendix B: Regression Relations 1



Regression equation, plot and  $R^2$  values for Subjects 1 & 2

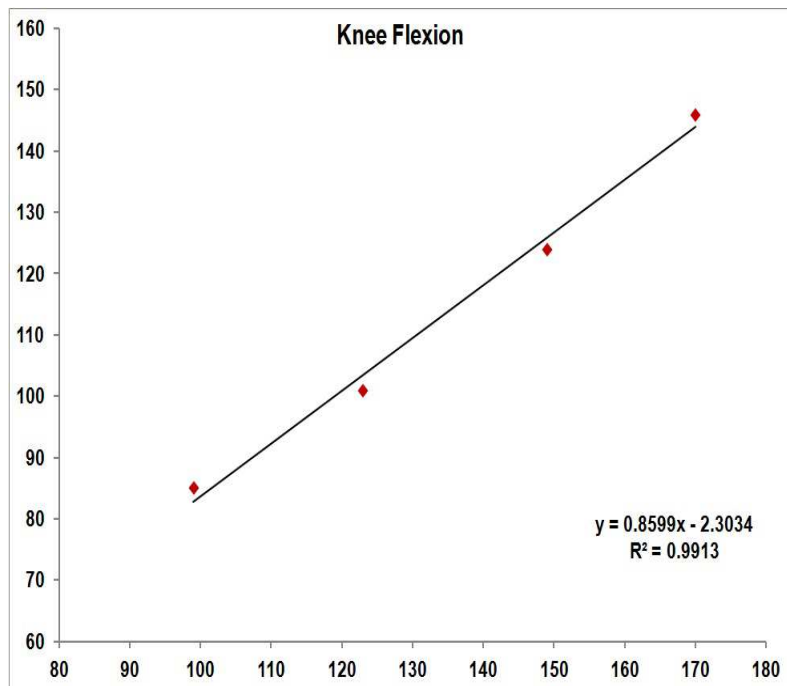
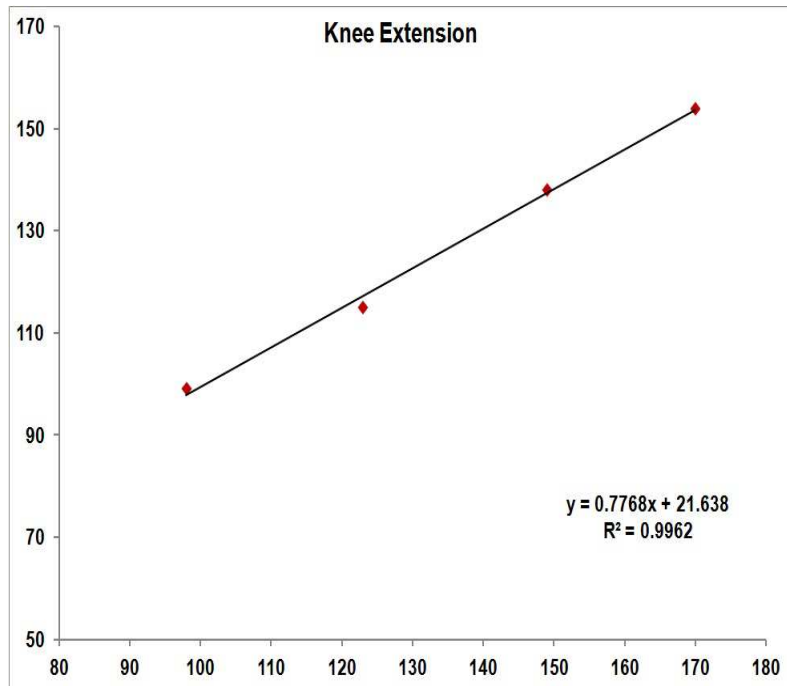


Regression equation, plot and  $R^2$  values for Subjects 3 & 4

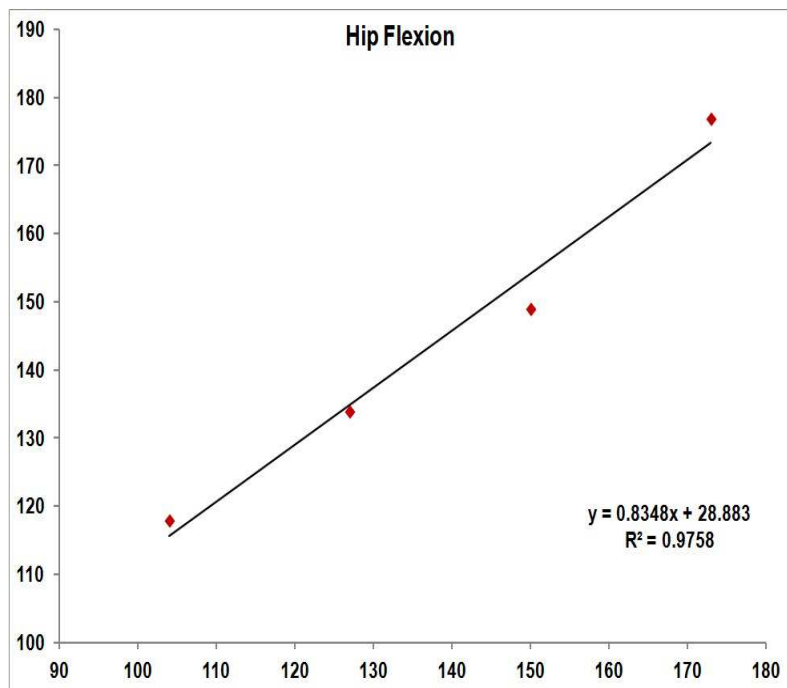
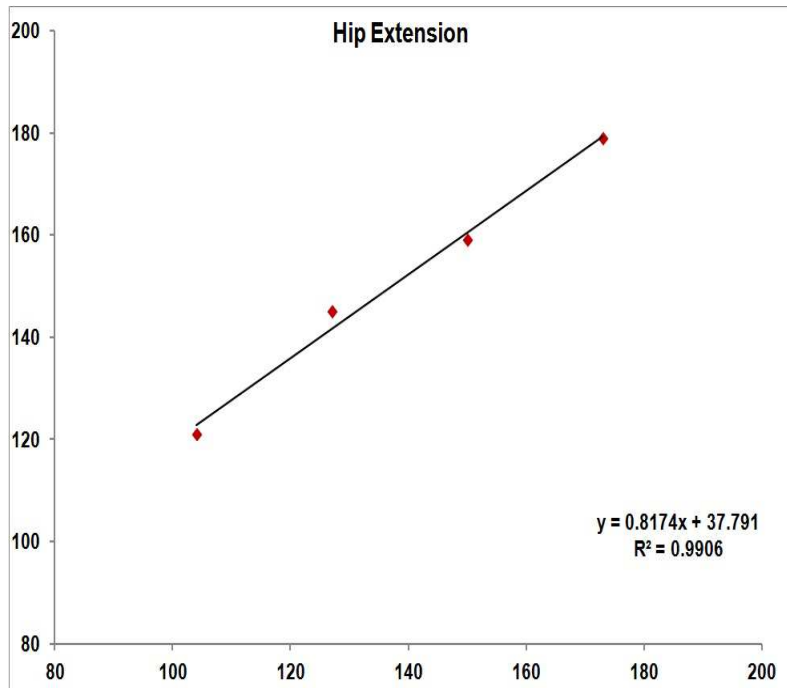


Regression equation, plot and  $R^2$  values for Subjects 5 & 6

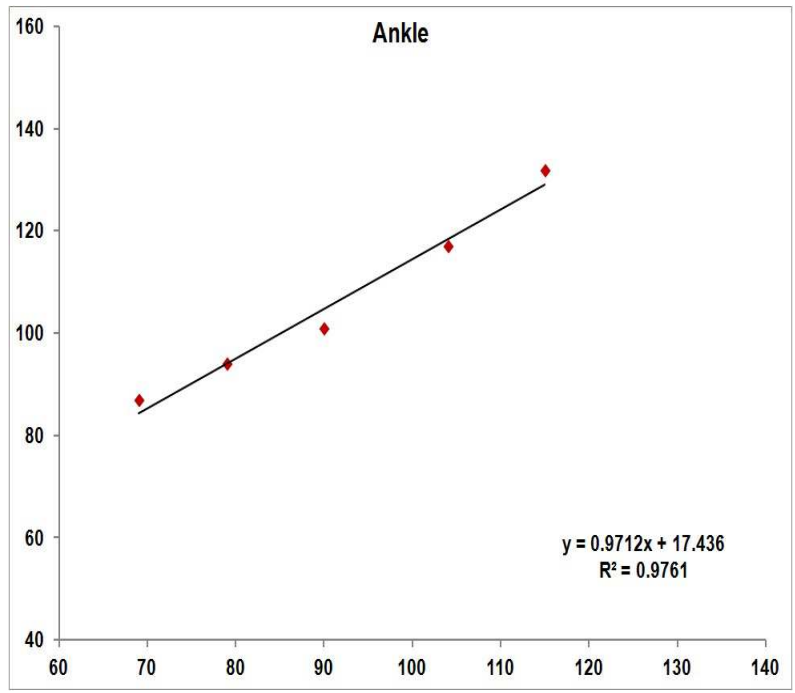
## Appendix C: Regression Relations 2



Regression equation, plot and  $R^2$  values for knee extension and flexion

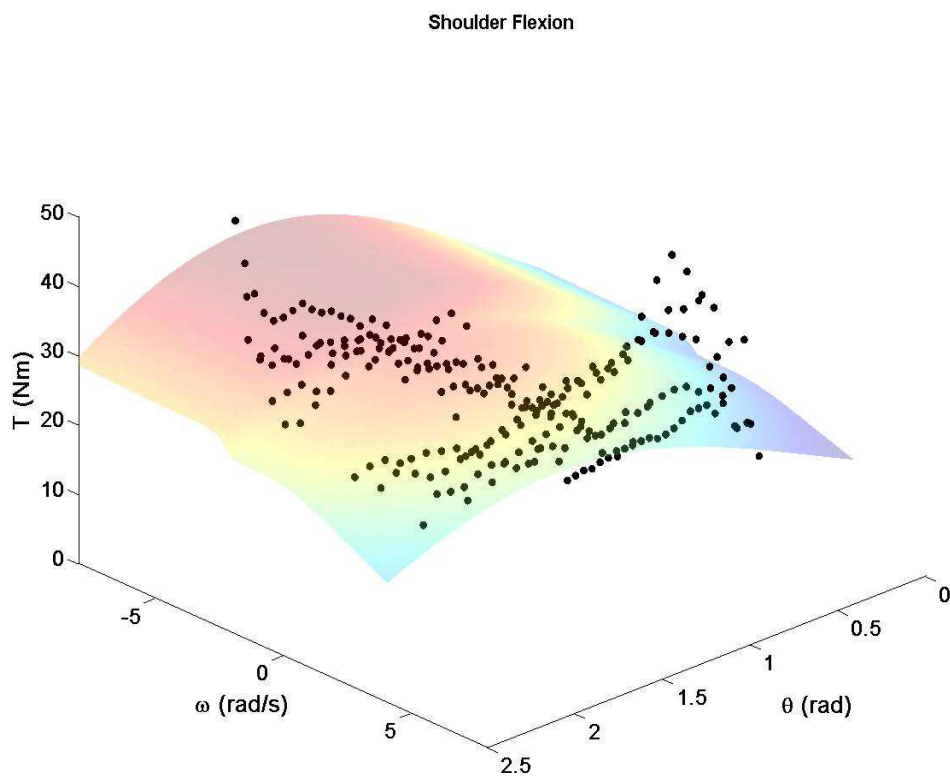
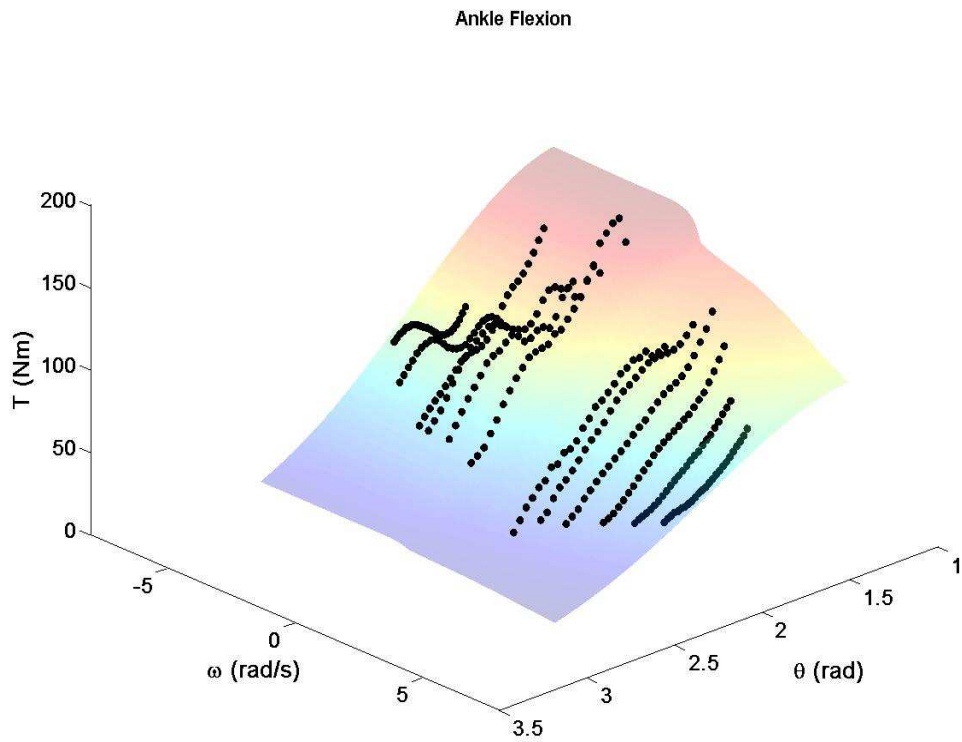


Regression equation, plot and  $R^2$  values for hip extension and flexion



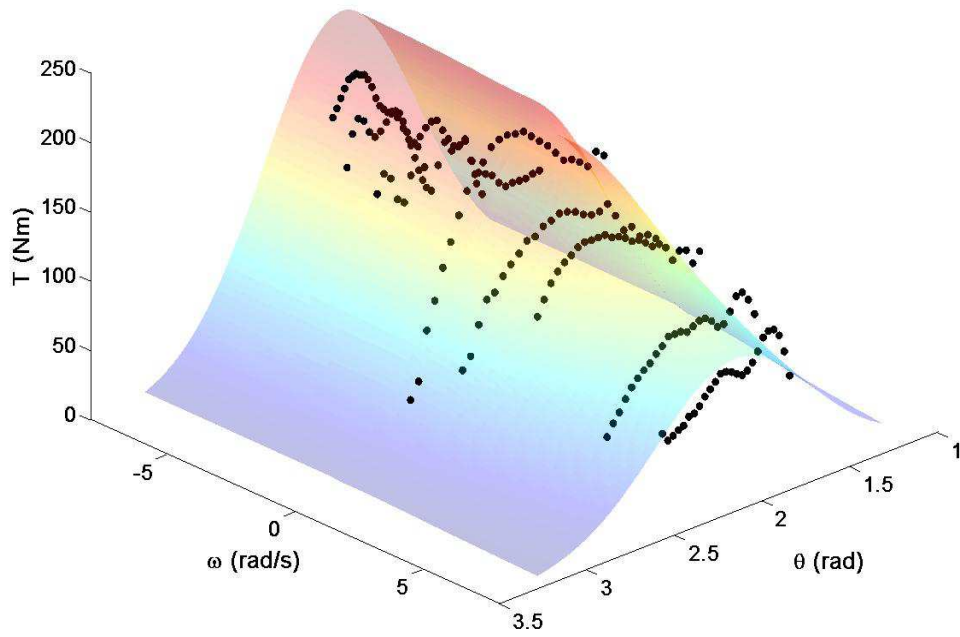
Regression equation, plot and  $R^2$  values for ankle plantar flexion

## Appendix D: Torque profiles

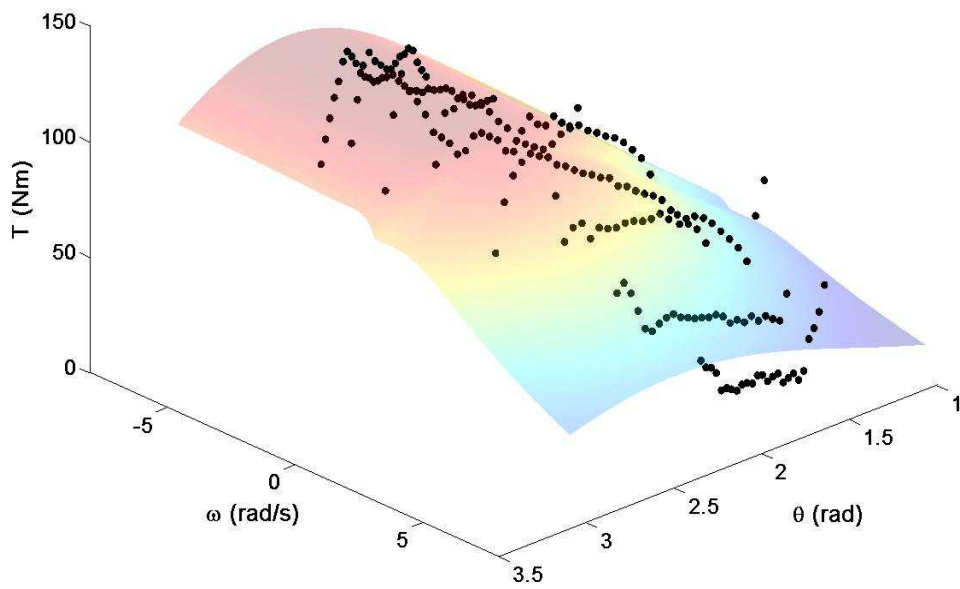


3-dimensional  $T-\omega-\theta$  plots for ankle plantar flexion and shoulder flexion

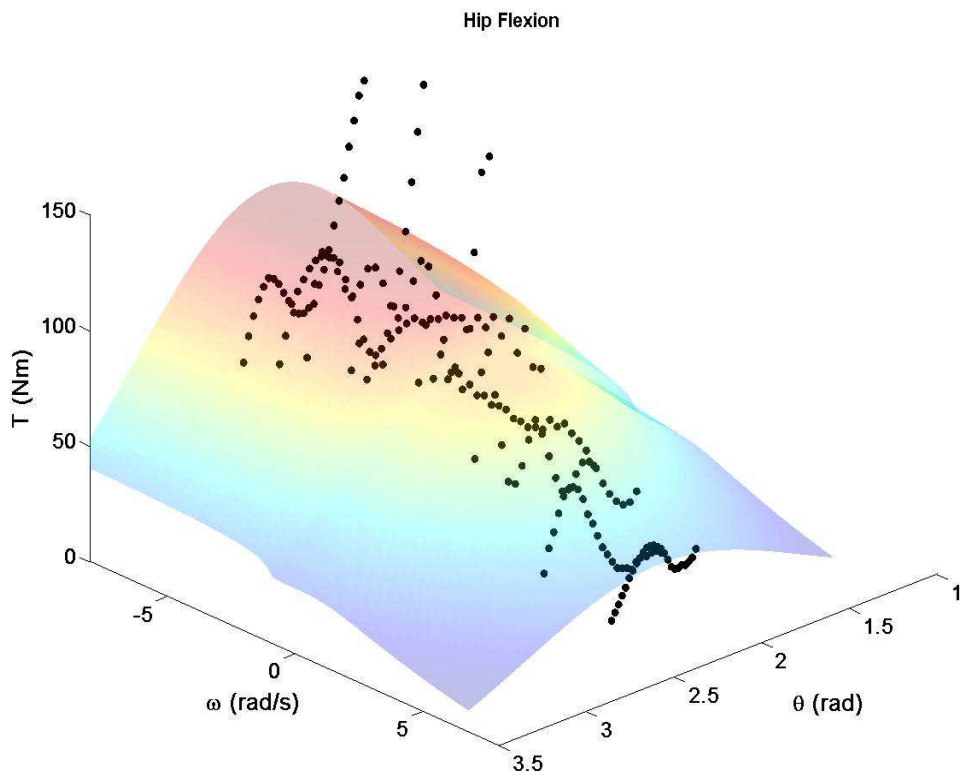
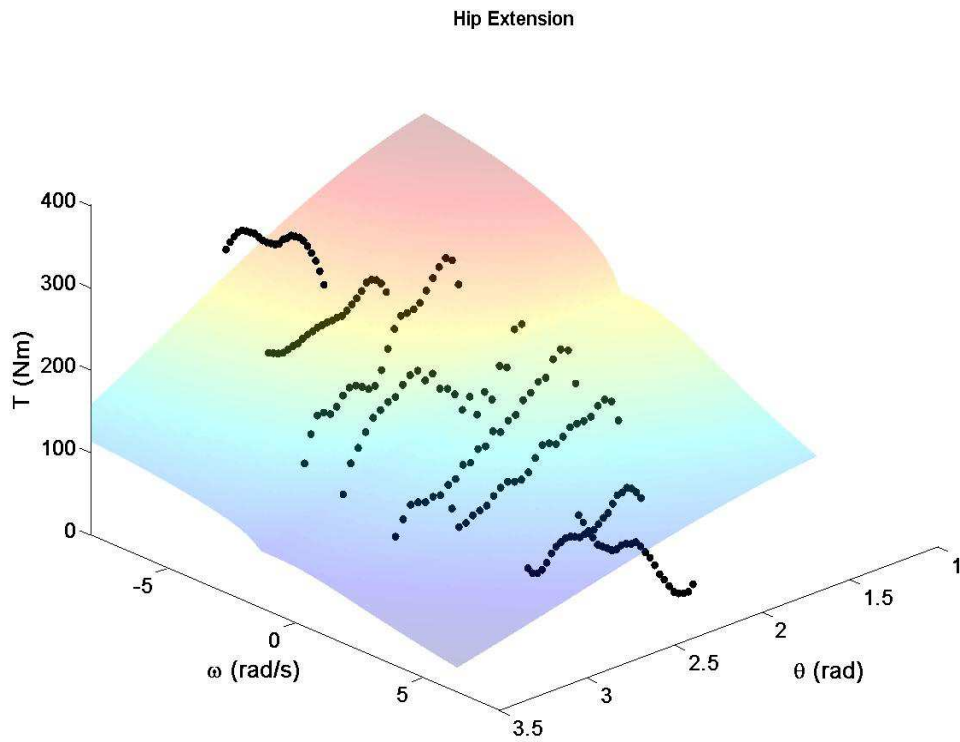
Knee Extension



Knee Flexion



3-dimensional  $T-\omega-\theta$  plots for knee extension and flexion



3-dimensional  $T$ - $\omega$ - $\theta$  plots for hip extension and flexion

## Appendix E: Marker positions

### Marker body positions

Maker Label	Marker Position	Description
<b>Finger</b>	End of third distal phalanx (finger)	Tip of middle finger
<b>5MCP (R/L)</b>	Dorsal aspect of the head of the 5th metatarsal	Medial and lateral projections of the MCP joint centre (joint centre at midpoint)
<b>2MCP (R/L)</b>	Dorsal aspect of the head of the 2nd metatarsal	As above
<b>US(R/L)</b>	Lateral aspect of the styloid process of the ulna	Medial and lateral projections of the wrist joint centre (joint centre at midpoint)
<b>RS(R/L)</b>	Lateral aspect of the styloid process of the radius	As above
<b>LE(R/L)</b>	Lateral aspect of the lateral humeral epicondyle	Medial and lateral projections of the elbow joint centre (joint centre at midpoint)
<b>ME(R/L)</b>	Lateral aspect of the medial humeral epicondyle	As above
<b>Acromion(R/L)</b>	Superior tip of the Acromion process	
<b>Shoulder(R/L)</b>	Estimated lateral projection of the glenohumeral joint centre when the arm is elevated	Approximately the belly of the posterior Deltoid when the arm is elevated
<b>Toe (R/L)</b>	End of 1st distal phalanx	Tip of big toe
<b>Head Band</b>	Four markers placed at front right–left and back left–right of the head	

<b>Maker</b>	<b>Marker Position</b>	<b>Description</b>
<b>Anterior Shoulder(R/L)</b>	Estimated anterior projection of the glenohumeral joint centre when the arm is elevated	Mid point of these two markers
<b>Posterior Shoulder(R/L)</b>	Estimated posterior projection of the glenohumeral joint centre when the arm is elevated	(AS & PS) is the shoulder joint centre
<b>R Scapula</b>	Middle of right scapula	
<b>Sternum</b>	Superior tip of the manubrium of the sternum	Suprasternal notch at top of sternum
<b>Xiphoid</b>	Centre of the xiphoid process of the sternum	Inferior tip of sternum
<b>C7</b>	7th cervical vertebra	Prominence at base of neck when neck is flexed
<b>T10</b>	10th thoracic vertebra	
<b>L1</b>	1st Lumbar vertebra	
<b>LHIP</b>	Superior border of left iliac crest	Used only for indentification of left side
<b>ASIS (R/L)</b>	Anterior superior iliac spine in line with hip joint centre	Bony landmark on the front of the pelvis
<b>PSIS (R/L)</b>	Posterior superior iliac spine	Dimple in the skin at the back of the pelvis
<b>Left Iliac</b>	Superior and lateral tip of the left iliac crest	Used for indentification of left side
<b>HIP (R/L)</b>	Greater trochanter of the femur	
<b>MK (R/L)</b>	Lateral aspect of the medial femoral epicondyle	Medial and lateral projections of the knee joint centre
<b>LK (R/L)</b>	Lateral aspect of the lateral femoral epicondyle	(at midpoint of these two markers)
<b>MM (R/L)</b>	Lateral aspect of the medial malleolus of the fibula	Medial and lateral projections of the ankle joint centre (at midpoint of these two markers)

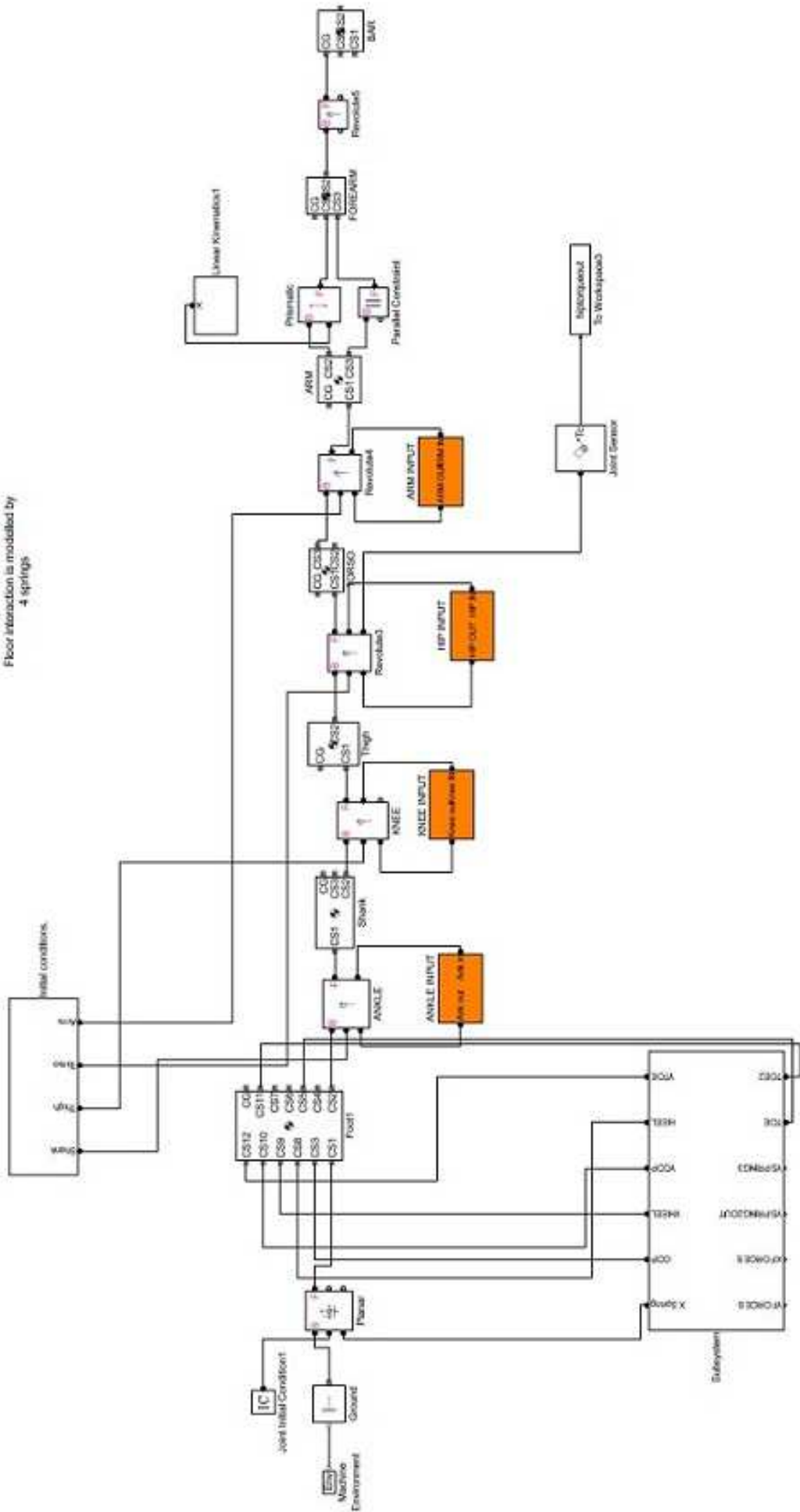
<b>Maker Label</b>	<b>Marker Position</b>	<b>Description</b>
<b>LM (R/L)</b>	Lateral aspect of the lateral malleolus of the fibula	
<b>1 MTP(R/L)</b>	Head of the 1st metatarsal	Medial and lateral projections of
<b>5 MTP (R/L)</b>	Head of the 5th metatarsal	the MTP joint centre

## Appendix F: Full Angle driven model



## Appendix G: Full Torque driven model

Torque driven model.  
Floor interaction is modelled by  
4 springs



Full Torque-driven model  
199

## Appendix H: Optimisation script for torque driven model

```
%script to start the optimization of the torque model.
%using the sigmoid function.
%Inputs:
% time-time instant
% n: preactivation
% su: slope of upward curve (exponential)
% sd: slope of downward curve
% maxact: asymptote of max activation j1
% ne: final de-activated level

global maxact time Anklejointang Ankang ankact knflexact knexact hpexact hpflexact
armact anktime t
global Kneejointang Hipjointang Armjointang
%define the timings
load Angles_ joint
load Angular_ kinematics
load Angles_ relative_ new

spring=[6.9885964e+05 8.0485927e+06 4.0007063e+04 2.0000003e+07 3.4528795e+06
2.5000021e+05 1.0000000e+05 1.0000000e+07];

ystiff=spring(1);ydamp=spring(2);ystiff2=spring(3);ydamp2=spring(4);
ystiff3=spring(5);ydamp3=spring(6);xstiff=spring(7);xdamp=spring(8);
n1=2050; t=0.35; dt=floor(t/0.004);
n2=n1+dt;
Anklejointang=Ankle_ angjoint(n1:n2,1);
Kneejointang=Knee_ angjoint(n1:n2,1);
Hipjointang=Hip_ angjoint(n1:n2,1);
Armjointang=Arm_ angjoint(n1:n2,1);
```

```
N=n2-n1+1;maxact=0.999; time=0:0.004:(n2-n1)*0.004;
time=time';
```

```
opttype = 3;
```

```
-----ANKLE-----
```

```
%tstartank-sua-----sda-----pa-----na-----nea
```

```
x1=0.02; x2=0.09; x3=0.028; x4=0.7; x5=0.2; x6=0.29;
```

```
LB1=0.01; LB2=0.05; LB3=0.0101;LB4=0.65; LB5=0.15; LB6=0.2;
```

```
UB1=0.04; UB2=0.15; UB3=0.1; UB4=0.85; UB5=0.3; UB6=0.35;
```

```
-----KNEEFLEXION-----
```

```
%tstart su-----sd-----p-----n-----ne
```

```
x8=0.15; x9=0.090; x10=0.0306; x11=0.8; x12=0.38; x13=0.27;
```

```
LB8=0.14; LB9=0.05; LB10=0.020; LB11=0.7; LB12=0.3; LB13=0.2;
```

```
UB8=0.35; UB9=0.18; UB10=0.08; UB11=0.95; UB12=0.45; UB13=0.35;
```

```
-----KNEEEXTENSION-----
```

```
%tstart su-----sd-----p-----n-----ne
```

```
x17=0.036; x18=0.195; x19=0.0177; x20=0.8; x21=0.16; x22=0.3;
```

```
LB17=0.001; LB18=0.09; LB19=0.010; LB20=0.7; LB21=0.14; LB22=0.2;
```

```
UB17=0.05; UB18=0.25; UB19=0.03; UB20=0.9; UB21=0.25; UB22=0.4;
```

```
-----HIPFLEXION-----
```

```
%tstart su-----sd-----p-----n-----ne
```

```
x28=0.15; x29=0.1152; x30=0.1187; x31=0.50; x32=0.15; x33=0.15;
```

```
LB28=0.1; LB29=0.0101; LB30=0.012; LB31=0.4; LB32=0.05; LB33=0.1;
```

```
UB28=0.35 ; UB29=0.3; UB30=0.3; UB31=0.75; UB32=0.3; UB33=0.3;
```

```
-----HIPEXTENSION-----
```

```
% tstart su-----sd-----p-----n-----ne
```

```
x37=0.0015; x38=0.12; x39=0.04; x40=0.85; x41=0.5; x42=0.25;
```

```
LB37=0.001; LB38=0.08; LB39=0.015; LB40=0.7; LB41=0.3; LB42=0.1;
```

UB37=0.05; UB38=0.25; UB39=0.2; UB40=0.99; UB41=0.7; UB42=0.32;

—————ShoulderFLEXION—————

`%tstart- su ——— sd ——— p ——— n ——— ne`

x47=0.09; x48=0.25; x49=0.0216; x50=0.65; x51=0.2; x52=0.2;

LB47=0.001; LB48=0.14; LB49=0.015; LB50=0.45; LB51=0.10; LB52=0.15;

UB47=0.15; UB48=0.35; UB49=0.03; UB50=0.75; UB51=0.3; UB52=0.3;

`%SET BOUND VECTORS`

`%initial guess`

x0 = [x1; x2; x3; x4; x5; x6;

x8; x9; x10; x11; x12; x13;

x17; x18; x19; x20; x21; x22;

x32;x37; x38; x39; x40; x41; x42;

x47; x48; x49; x50; x51; x52];

`%lower bound`

LB = [LB1; LB2; LB3; LB4; LB5; LB6;

LB8; LB9; LB10; LB11; LB12; LB13;

LB17; LB18; LB19; LB20; LB21; LB22;

LB32;LB37; LB38; LB39; LB40; LB41; LB42;

LB47; LB48; LB49; LB50; LB51; LB52];

`%upper bound`

UB = [UB1; UB2; UB3; UB4; UB5; UB6;

UB8; UB9; UB10; UB11; UB12; UB13;

UB17; UB18; UB19; UB20; UB21; UB22;

UB32;UB37; UB38; UB39; UB40; UB41; UB42;

UB47; UB48; UB49; UB50; UB51; UB52];

if opttype == 1

`%opt using fmincon`

options = optimset('LargeScale','off','Display','iter','maxIter',10000,'MaxFunEvals',20000,

```

... 'TolFun',1.0e-14,'TolCon',1.0e-12);
[x, fval, exitflag, output] = fmincon(@TorqueSCORE_1stpull, x0, [], [], [], [], LB,
UB,[],options);
%opt using SIMANN
elseif opttype == 2
scorefile = 'TorqueSCORE_1stpull';
sa_t = 5;
sa_rt = 0.55;
sa_nt = 5;
sa_ns = 20;
[xopt,fopt]=simann(scorefile, LB, UB, sa_t, sa_rt, sa_nt, sa_ns,x0);

xopt
% display solutions
fopt
% display RMS score

save xopt xopt -ascii
save fopt fopt -ascii
end

```

## Appendix I: Score script for torque driven model

```
function [scoretorque] = TorqueSCORE_1stpull (x)
global tstartank tstartknflex tstartknex tstarthpflex tstarthpex tstartar
global sua suknflex suknex suhpflex suhpex suar
global sda sdknflex sdknflex sdhpflex sdhpflex sdar
global na nknflex nknex nhpflex nhpex nar
global nea neknflex neknex nehpflex nehpflex near
global pa pknflex pknex phpflex phpex par
global maxact time t maxact1
global Ankang Kneeang Hipang Armang
global Anklejointang Kneejointang Hipjointang Armjointang
global ankact knflexact knflexact hpflexact hpflexact armact

%define the optimization vector
%ankle
tstartank=x(1);
sua=x(2);
sda=x(3);
pa=x(4);
na=x(5);
nea=x(6);

tstartknflex=x(7);
suknflex=x(8);
sdknflex=x(9);
pknflex=x(10);
nknflex=x(11);
neknflex=x(12);

tstartknex=x(13);
suknflex=x(14);
```

sdknex=x(15);  
pknex=x(16);  
nknex=x(17);  
neknex=x(18);

tstarthpflex=x(19);  
suhpflex=x(20);  
sdhpflex=x(21);  
phpflex=x(22);  
nhpflex=x(19);  
nehpflex=x(24);

tstarthpex=x(25);  
suhpex=x(26);  
sdhpex=x(27);  
phpex=x(28);  
nhpex=x(29);  
nehpex=x(30);

tstartar=x(31);  
suar=x(32);  
sdar=x(33);  
par=x(34);  
nar=x(35);  
near=x(36);

ankact=muscleACT(tstartank,sua,sda,na,nea,pa);  
knflexact=muscleACT(tstartknflex,suknflex,sdknflex,nknflex,neknflex,pknflex);  
knexact=muscleACT(tstartknex,suknex,sdknex,nknex,neknex,pknex);  
hpflexact=muscleAC(tstartknflex,suknflex,sdknflex,nknflex,neknflex,pknflex);  
hpexact=muscleACT(tstarthpex,suhpex,sdhpex,nhpex,nehpex,phpex);  
armact=muscleACT(tstartar,suar,sdar,nar,near,par);

```

%=====Now calculate the Score=====
%run the model
sim('six_seg_tordriven_3SPRINGS_1stpull1',[0,t]);

M=length(tout); N=length(time);
if (M>N)

for i=1:N
[tmp, idx]=min(abs(tout(:,1)-time(i,1)));
Ank(i,1)=Ankang(idx);
Knee(i,1)=Kneeang(idx);
Hip(i,1)=Hipang(idx);
Arm(i,1)=Armang(idx);
end
RMSankle=sqrt(sum((Anklejointang(:)-Ank(:)).^ 2/numel(Anklejointang)));
RMSknee=sqrt(sum((Kneejointang(:)-Knee(:)).^ 2/numel(Kneejointang)));
RMSHip=sqrt(sum((Hipjointang(:)-Hip(:)).^ 2/numel(Hipjointang)));
RMSarm=sqrt(sum((Armjointang(:)-Arm(:)).^ 2/numel(Armjointang)));

elseif (M<N)
for i=1:M
[tmp, idx]=min(abs(tout(i,1)-time(:,1)));
Ank(i,1)=Anklejointang(idx);
Knee(i,1)=Kneejointang(idx);
Hip(i,1)=Hipjointang(idx);
Arm(i,1)=Armjointang(idx);
t(i,1)=time(idx); end RMSankle=sqrt(sum((Ank(:)-Ankang(:)).^ 2/numel(Ankang)));
RMSknee=sqrt(sum((Knee(:)-Kneeang(:)).^ 2/numel(Kneeang)));
RMSHip=sqrt(sum((Hip(:)-Hipang(:)).^ 2/numel(Hipang)));
RMSarm=sqrt(sum((Arm(:)-Armang(:)).^ 2/numel(Armang)));

else
RMSankle=sqrt(sum((Anklejointang(:)-Ankang(:)).^ 2/numel(Ankang)));

```

```

RMSknee=sqrt(sum((Kneejointang(:)-Kneeang(:)).^ 2/numel(Kneeang)));
RMShip=sqrt(sum((Hipjointang(:)-Hipang(:)).^ 2/numel(Hipang)));
RMSarm=sqrt(sum((Armjointang(:)-Armang(:)).^ 2/numel(Armang)));
end
RMS = RMSankle+RMSknee+RMShip+RMSarm;

if (abs(max(Ankang)-max(Anklejointang))>0.1);
ankpen=500;

else
ankpen=0;
end

if (abs(max(Kneeang)-max(Kneejointang))>0.1);
kneepen=500;

else
kneepen=0;
end

if (max(Hipang)>max(Hipjointang));
hippen=1000;

else
hippen=0;
end

if (abs(max(Armang)-max(Armjointang))>0.1);
armpen=500;

else armpen=0;

%%%%%%%%%%

```

$PEN = ankpen + kneepen + hippen + armpen;$

$scoretorque = RMS + PEN;$

## Appendix J: Script of activation function

```
%function to calculate activation function for a given segment/joint
%using the sigmoid function.
%Inputs:
% time-time instant
% n: preactivation
% su: slope of upward curve (exponential)
% sd: slope of downward curve
% maxact: asymptote of max activation j1
% ne: final de-activated level
function act = muscleACT(tstart,su,sd,n,ne,p)
%define global variables

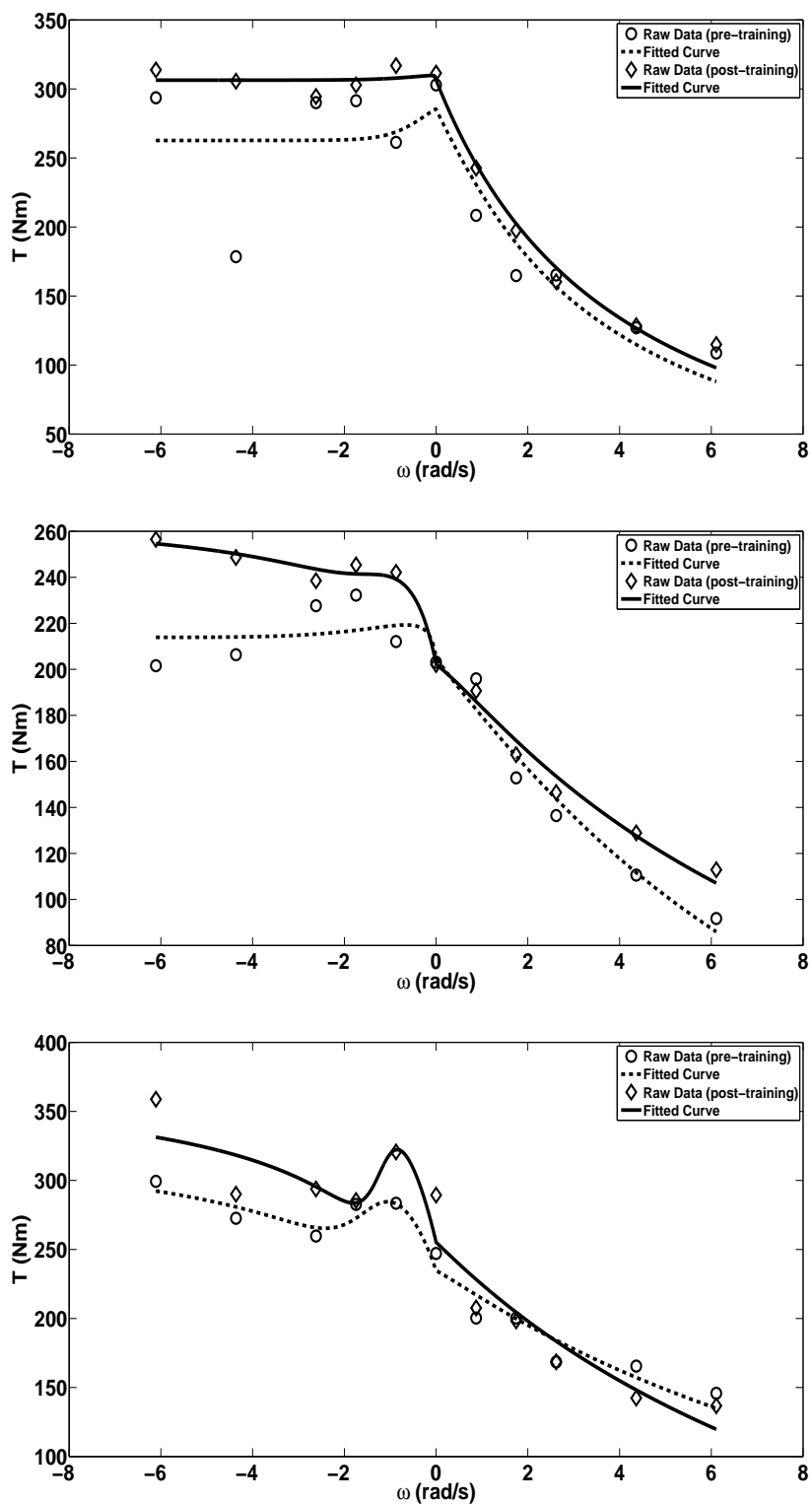
global maxact time

ti=-log((maxact-n)/n)*su; %preactivation timing
tpeaku = -(log((1-p)/p)*su); %timing of peak lvl of upward activation
tpeakd = (log((1-p)/p)*sd); %timing of peak lvl of downward activation
tend = (log((maxact-ne)/ne)*sd); %deactivation timing
ttotal = -ti+tstart+tpeaku-tpeakd+tend; %Total time
t1=tstart+tpeaku-ti;

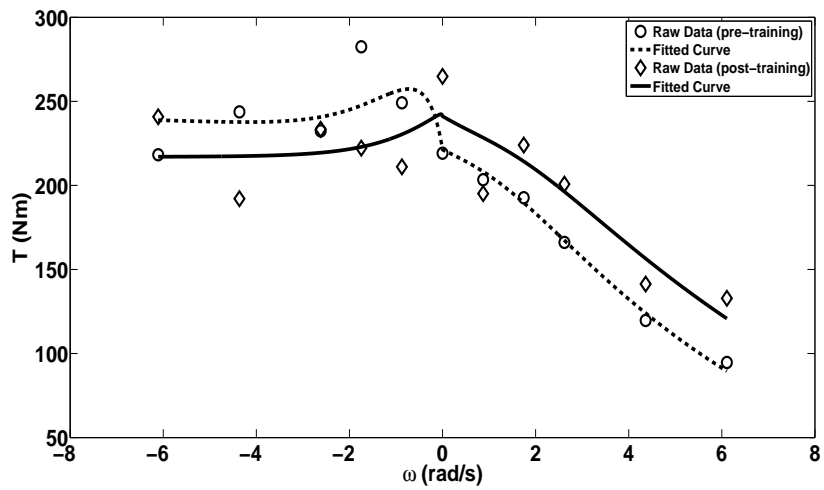
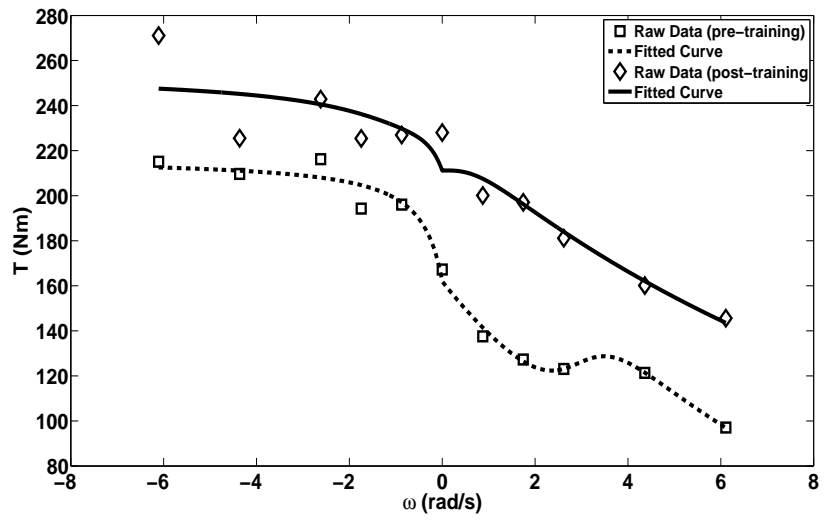
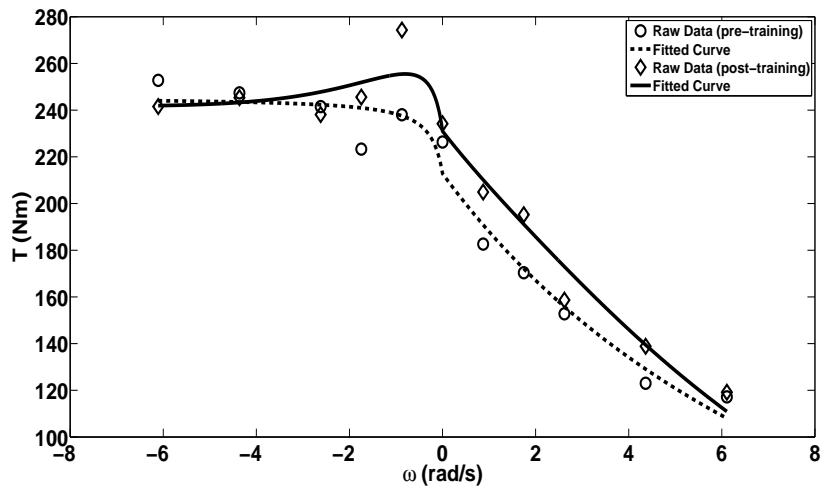
a=zeros(length(time),1);
for i=1:length(time)
Au(i)=maxact/(1+exp(-(time(i)-tstart+ti)/su));
Ad(i)=maxact/(1+exp((time(i)-tstart+ti-tpeaku+tpeakd)/sd));
if (time(i)>=0) & (time(i)<=tstart)
a(i,1)=n;
elseif (time(i)>tstart) & (time(i)<=t1)
a(i,1)=Au(i);
elseif (time(i)>t1) & (time(i)<=ttotal)
```

```
a(i,1)=Ad(i);  
else  
a(i,1)=ne;  
end  
end  
act=[time,a(:,1)];
```

# Appendix K: Fits of MVC torque function on $T-\omega$ datasets

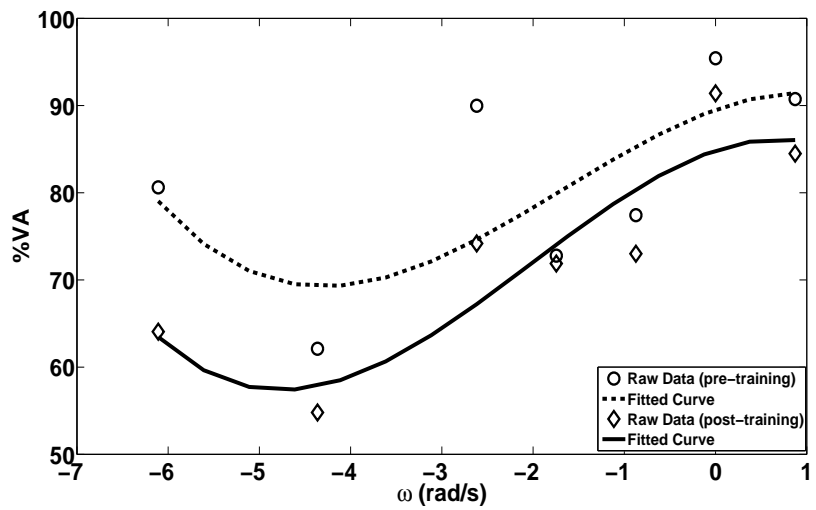
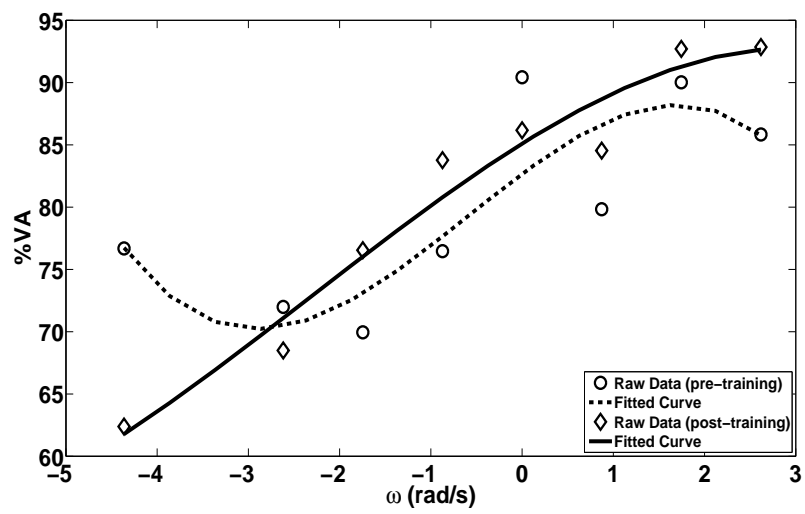
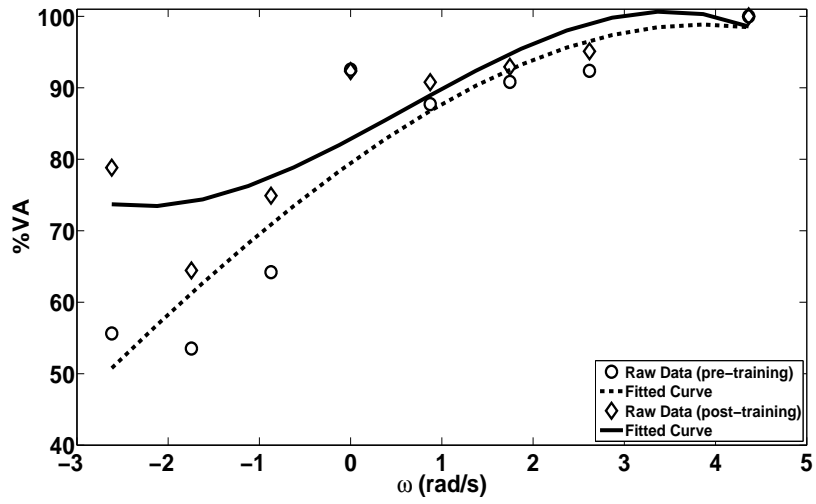


Plots of MVC torque function fits on the pre- and post-training  $T-\omega$  raw data sets for Subjects 1, 2, 3

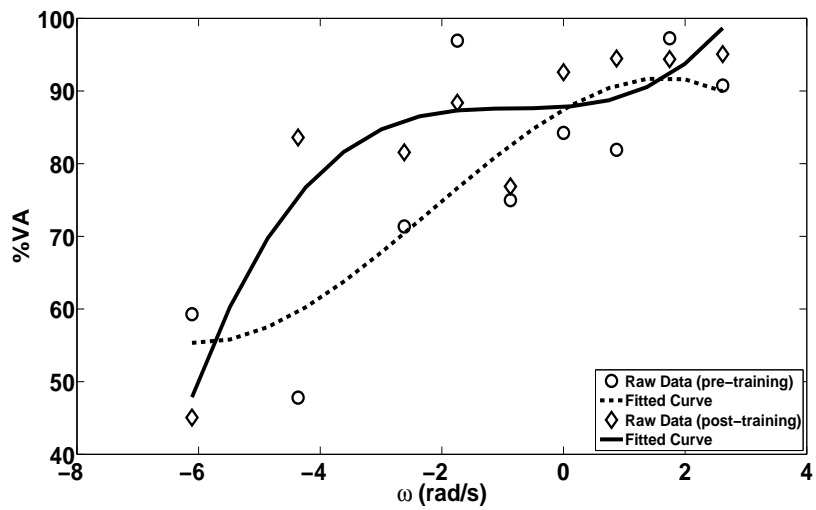
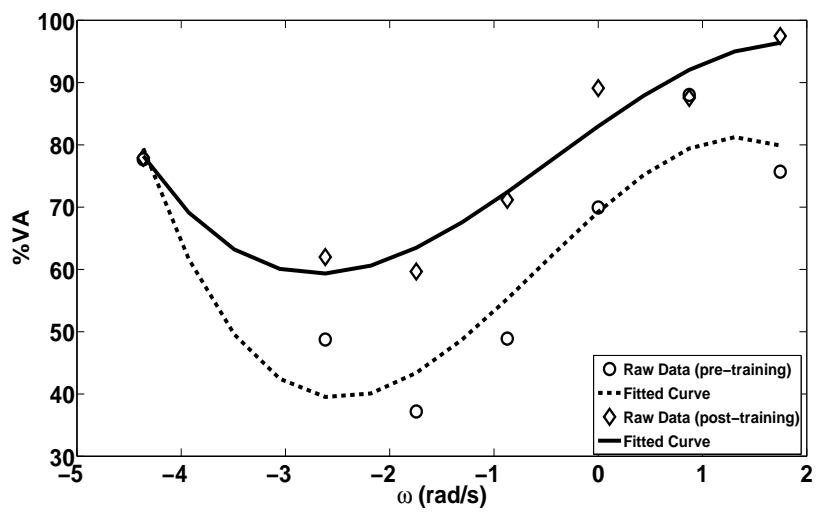
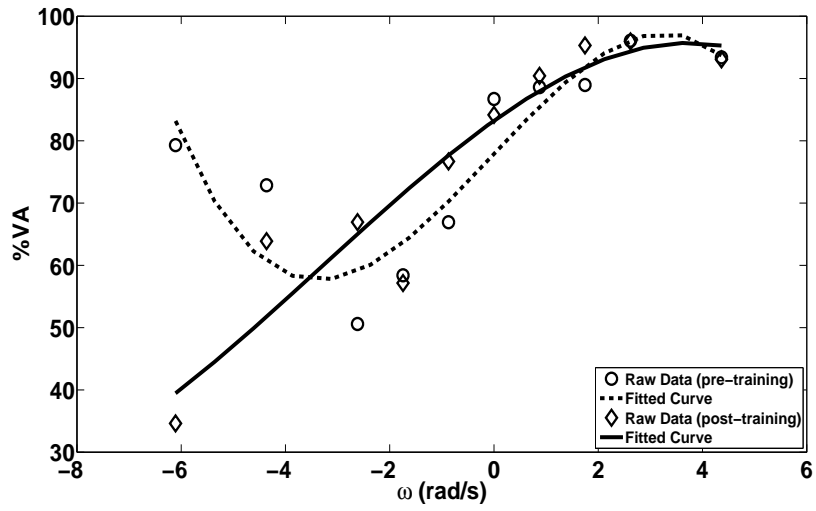


Plots of MVC torque function fits on the pre- and post-training  $T$ - $\omega$  raw data sets for Subjects 4, 5, 6

Appendix L: 3rd degree polynomial fits on the  
 $\%VA-\omega$  datasets

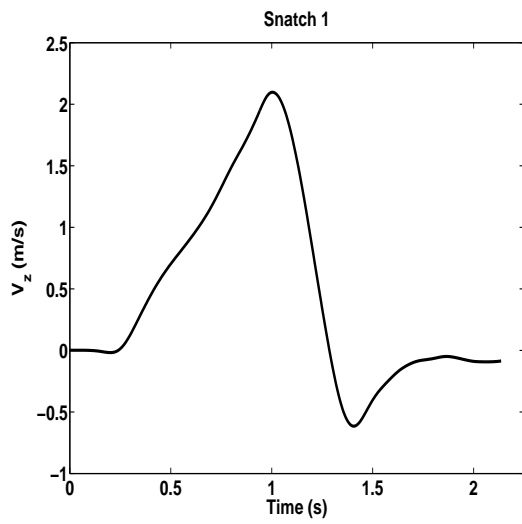


Plots of 3rd degree polynomial fits on the pre- and post-training %VA- $\omega$  raw data sets for Subjects 1, 2, 3

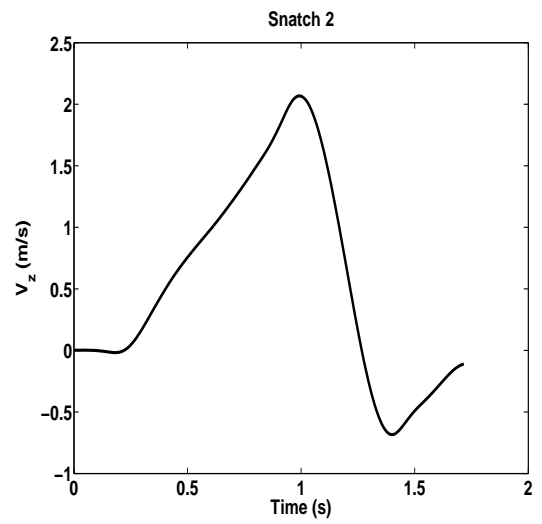


Plots of 3rd degree polynomial fits on the pre- and post-training %VA- $\omega$  raw data sets for Subjects 4, 5, 6

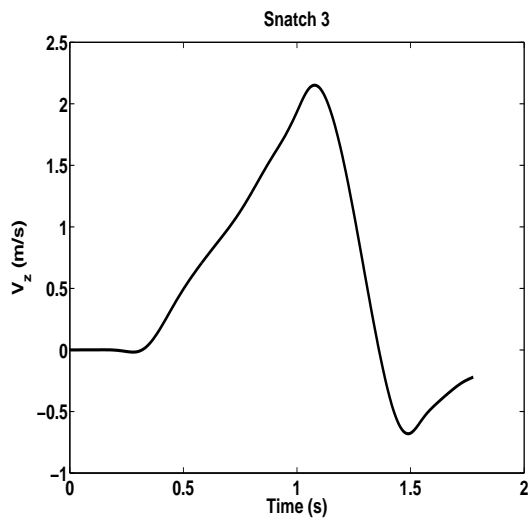
## Appendix M: Bar vertical velocity during the Snatch



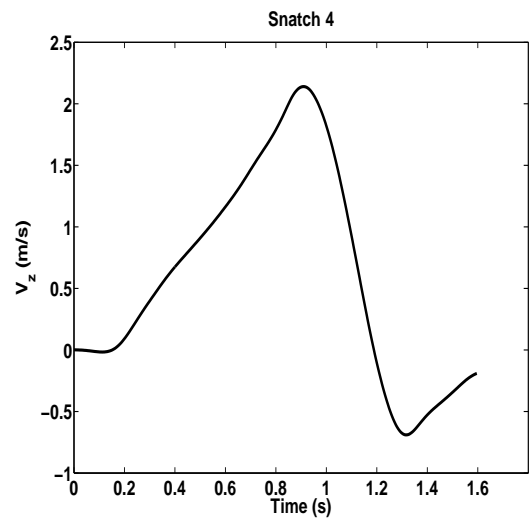
(a) Snatch 1



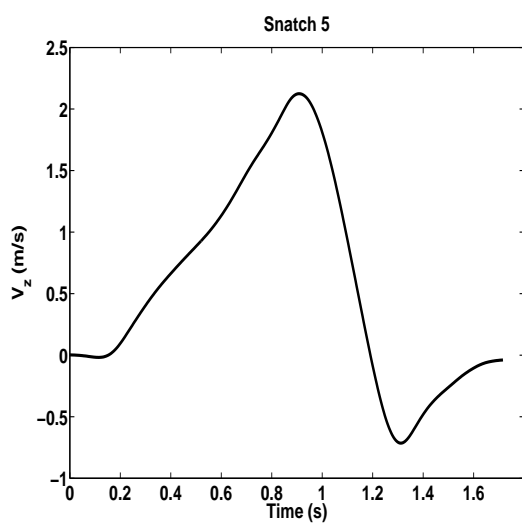
(b) Snatch 2



(c) Snatch 3



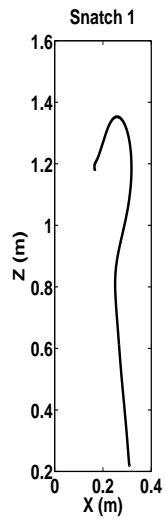
(d) Snatch 4



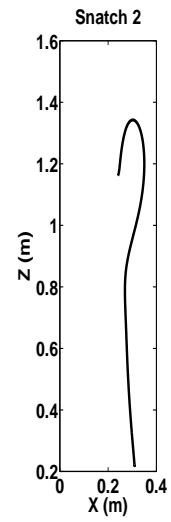
(e) Snatch 5

Barbel vertical velocity,  $v_z$ , during the 5 trial snatches.

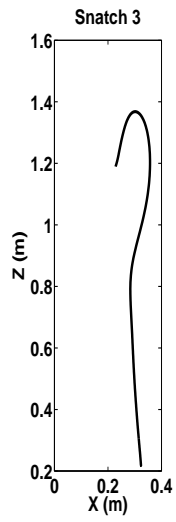
## Appendix N: Bar trajectory during the Snatch



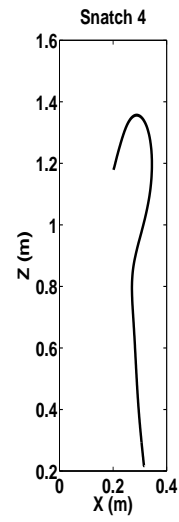
(a) Snatch 1



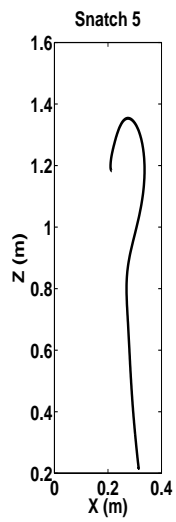
(b) Snatch 2



(c) Snatch 3



(d) Snatch 4



(e) Snatch 5

Barbel trajectory from the first three phases for each of the 5 trial snatches.